N. M. NEWMARK

CIVIL ENGINEERING STUDIES
STRUCTURAL RESEARCH SERIES NO. 231

STRENGTH AND BEHAVIOR IN SHEAR OF DEEP REINFORCED CONCRETE BEAMS UNDER STATIC AND DYNAMIC LOADING

By
H. A. R. de PAIVA
and
C. P. SIESS

Report to
RESEARCH DIRECTORATE
AIR FORCE SPECIAL WEAPONS CENTER
Air Force Systems Command
Kirtland Air Force Base
New Mexico

UNIVERSITY OF ILLINOIS
URBANA, ILLINOIS
OCTOBER 1961

THE INVESTIGATION OF DEEP REINFORCED CONCRETE BEAMS UNDER STATIC AND DYNAMIC LOADING

Vol. 2

STRENGTH AND BEHAVIOR IN SHEAR

by

H. A. R. de Paiva

approved by

C. P. Siess

University of Illinois
Department of Civil Engineering

May 1961

Research Directorate
AIR FORCE SPECIAL WEAPONS CENTER
Air Force Systems Command
Kirtland Air Force Base
New Mexico

Project No. 1080
Contract AF 29(601)-2372

TABLE OF CONTENTS

LIST OF TABLES

LIST OF FIGURES

LIST OF FIGURES (Cont'd)

LIST OF FIGURES (Cont'd)

LIST OF FIGURES (Cont'd)

LIST OF FIGURES (Cont'd)

1. INTRODUCTION

1.1 Introductory Remarks

Both theory and tests indicate that deep beams, that is, beams which have depth-to-span ratios considerably greater than those used in ordinary construction, are both suitable and frequently necessary in structures designed to withstand the high overpressures which result from blast loadings. The literature (1) reveals a number of investigations of the behavior of shallow reinforced concrete beams under rapidly applied loading. At present, only two series of tests of reinforced concrete deep beams subjected to rapidly applied loading have been reported (2,3).

1.2 Object and Scope

The general object of the investigation of which this study formed one part was to obtain information from which a rational design procedure for deep members subjected to blast type loading could be developed. Initially, the emphasis in the experimental program on reinforced concrete deep beams was directed toward the flexural behavior of simply supported deep members, subjected to either slowly or rapidly applied loading.

The primary objective of this phase of the investigation was to study the strength and behavior in shear of moderately deep reinforced concrete beams subjected to both static and dynamic loading and to determine if failure under dynamic loading is different from that under static loading. In particular the program was designed to determine whether web reinforcement would prevent shear failures, and if so, how much web steel would be required to produce a flexural failure.

---

* Numbers in parentheses refer to items in the Bibliography.

Tests were made on 35 rectangular reinforced concrete deep beams. Thirteen beams were tested to failure statically and 22 beams were tested to failure dynamically under an "infinite" duration pulse loading in which load levels ranged from 110 to 200 percent of the static yield load. Tests were carried out in various series consisting of one static test and two dynamic tests of similar beams. The static test was on a beam without web reinforcement, and the dynamic tests were on beams both with and without web reinforcement. Two static tests of beams with web reinforcement are also reported.

All beams were simply supported on a span of 24 in. and were loaded by two concentrated loads placed at the one-third points. The major variables involved were: the amount of tension reinforcement, which ranged from 0.46 to 2.58 percent; the concrete strength, which varied from 2890 to 5600 psi; the amount of web reinforcement, which ranged from 0 to 1.09 percent; and the span-depth ratios, which were 2, 3 and 4. The beam depth was varied to vary the span-depth ratio, and the beam width was also varied to keep the cross sectional area constant at 24 sq. in. Compression reinforcement equal to about one-half the tension reinforcement was used in all beams. Special end anchorages were provided for all tension reinforcement to prevent premature bond and anchorage failures.

The results of the tests are presented, discussed, and compared, and although the number of tests are somewhat limited, simple formulas are presented for computing the static shear strength of deep beams under concentrated loads. Data reported in another investigation was used to extend the use of these formula to deep beams subjected to uniform loading. Dynamic shear strengths are related to the static shear strengths as a

function of the time to failure and a simple formula is presented for computing the dynamic shear strength.

1.3 Acknowledgments

The work described in this report was carried out in the Structural Research Laboratory of the Civil Engineering Department of the University of Illinois, as part of a cooperative project between the University and the Air Force Special Weapons Center, Department of the Air Force under Contract AF 29(601)-2372, Project 1080. The project was under the general direction of N. M. Newmark, Professor and Head of the Department of Civil Engineering, and Dr. C. P. Siess, Professor of Civil Engineering. The work reported herein was under the immediate supervision of H. A. R. de Paiva, Research Assistant in Civil Engineering.

Mr. C. D. Grigg, Research Assistant in Civil Engineering, helped fabricate the test specimens and conduct the tests. Mr. V. J. McDonald, Associate Professor of Civil Engineering, and his staff were completely responsible for the dynamic instrumentation used during the investigation.

Special thanks are extended to Dr. C. P. Siess for his guidance in planning this study and his help in the preparation of the report.

1.4 Notation

Designation of Test Specimens

Each beam was designated by a series of letters and numerals; e.g. G33D-31. The letters and numerals have the following significance:

First letter (G33D-31)

Identifies this series of deep beam tests from others which have been carried out in the laboratory.

First numeral (G33D-31)

This number is equal to the L/d ratio and the width of the beam in inches.

Second numeral (G33D-31)

Identifies the nominal concrete strength at test:

3 - 3,000 psi

4 - 5,000 psi

Second letter (G33D-31)

Identifies the type of test:

D - dynamic test

S - static test

Third numeral (G33D-31)

Identifies the order of testing which can be roughly correlated to the tension reinforcement ratio for each L/d ratio. See Table 1

Fourth numeral (G33D-31)

Identifies the presence of web reinforcement:

1 - without web reinforcement

2 - with web reinforcement

Symbols:

Symbols used are defined as they are encountered in the text but are presented here for ease in reference.

A_s = total area of tension reinforcement

A'_s = total area of compression reinforcement

A_w = total area of one stirrup

a = length of shear span from the center of the load point to the center of the support.

b = width of member

C_1 = total compressive force in the concrete

C_2 = total compressive force in the compression reinforcement

d = the effective depth, the distance from the top compressive fiber to the centroid of the tension reinforcement

d' = distance from the centroid of the compression reinforcement to the centroid of the tension reinforcement.

E_c = modulus of elasticity of the concrete

E_s = modulus of elasticity of the reinforcing steel

$f = f'_s - 0.85 f'_c$

f_c = stress in the concrete

f'_c = compressive strength of concrete, as determined from standard 6 by 12-in. control cylinders

f_s = stress in the tension reinforcement

f'_s = stress in the compression reinforcement

f_u = ultimate strength of the tension reinforcement

f'_u = ultimate strength of the compression reinforcement

f_y = yield strength of the tension reinforcement

f'_y = yield strength of the compression reinforcement

j = ratio of lever arm of the internal resisting moment to the effective depth, for a fully-cracked section, Fig. A.1

k = ratio of depth of the compression zone to the effective depth, for fully-cracked elastic section, Fig. A.1

$k' = d'/d$

k_1 = ratio of area of the concrete stress block to the area of the enclosing rectangle

k_2 = fraction of the depth of the compression zone which determines the position of the centroid of the compressive force at maximum load

k_3 = ratio of the maximum compressive stress in the concrete member to the cylinder strength

k_u = ratio of the depth of the compression zone to the effective depth d

L = span length center to center of supports

M_f = theoretical ultimate bending moment

M_y = moment at flexural yielding

$n = E_s/E_c = 6 + \frac{10,000}{f'_c}$

P = applied load

P_c = theoretical load at inclined cracking

P_{dyn} = measured applied dynamic load level

P_s = theoretical load at shear failure

P'_s = computed load at failure in "shear proper", Eq. (5)

P''_s = computed shear strength by "shear proper", Eq. (6)

P_u = measured static ultimate test load

P'_u = theoretical ultimate load at flexural failure

P_{ud} = measured dynamic ultimate test load

P'_{ud} = computed dynamic ultimate load

P_y = measured static yield test load

P'_y = theoretical load at static yielding

P_{yd} = measured maximum load reached in a dynamic test

$p = A_s/bd$ = ratio of tension reinforcement

$p' = A'_s/bd$ = ratio of compression reinforcement

r = A_w/sb = ratio of web reinforcement

s = horizontal spacing of web reinforcement

t_f = time to failure for the dynamic tests

T = total tensile force in the tension reinforcement

Δ = midspan deflection

Δ_u = measured midspan deflection at ultimate load for the static tests

Δ_{ud} = measured midspan deflection at ultimate load for the dynamic tests

Δ_y = measured midspan deflection at flexural yielding for the static tests

Δ_{yd} = measured midspan deflection at flexural yielding for the dynamic tests

ϵ_c = strain in the concrete at top midspan

ϵ_{cn} = strain in the concrete as defined in Fig. 4.28

ϵ_{cs} = strain in the concrete as defined in Fig. 4.28

ϵ_o = strain in the tension reinforcement at the beginning of strain hardening

ϵ'_o = strain in the compression reinforcement at the beginning of strain hardening

ϵ_s = strain in the tension reinforcement

ϵ_{sn} = strain in the tension reinforcement as defined in Fig. 4.15

ϵ_{ss} = strain in the tension reinforcement as defined in Fig. 4.15

ϵ_u = crushing strain of the concrete

ϵ_y = yield point strain of the tension reinforcement

ϵ'_y = yield point strain of the compression reinforcement

2. DESCRIPTION OF TEST SPECIMENS

2.1 Description of Beams

Details of the dimensions and the properties of the test specimens used in this investigation are given in Table 2.1 and Fig. 2.1. All beams were 28 inches long and varied in depth from 7 in. to 13 in. Effective depths were 12, 8 and 6 in. respectively for L/d ratios of 2, 3 and 4. The beam widths were 2, 3 or 4 in. depending on the depth, to give a constant value of bd of 24 sq. in. for all beams tested. All beams were simply supported on a span of 24 in.

The length of bearing at both the load points and the supports was maintained constant at 4 in. For the narrow beams with L/d = 2 the bearing area was 8 sq. in. For the wider beams with L/d = 4, the bearing area was 16 sq. in.

All beams had both tension and compression reinforcement. The area of compression reinforcement was approximately equal to one-half the area of the tension reinforcement for all beams except those of series G33S-31, G33D-31, G33S-32 and G33D-32. In these series, the area of the compression reinforcement was equal to approximately one-third the area of the tension reinforcement.

The tension reinforcement consisted of one or two intermediate grade deformed bars placed in a single layer. Special anchorage was provided for all tension reinforcement. This consisted of a steel plate, 1/2 in. thick, 2 in. wide, and with the length equal to the width of the beam, which was welded to the ends of the tension bars, (Fig. 2.1). All tension reinforcement was straight and extended the full length of the beams.

The compression reinforcement consisted of one or two intermediate grade reinforcing bars placed in a single layer near the top of the beam. All the bars except the No. 2 bars were deformed. All the compression steel was straight and extended the full length of the beams. No special anchorage or ties were provided.

Web reinforcement consisted of No. 7 black annealed wire stirrups formed into closed loops. The number, spacing and inclination of web reinforcement is shown in Fig. 2.1.

The center of the compression reinforcement was 3/4 in. from the top surface of the beam. This gave a minimum clearance of 9/16 in. for the largest bar used. The center of the tension reinforcement was 1 in. above the bottom surface of the beam. This resulted in a minimum clearance of 11/16 in. for the largest bar used. For beams with reinforcement consisting of two bars, the centers of the bars were 3/4 in. from the sides of the beam. This resulted in a minimum side clearance of 7/16 in. for the tension steel and 9/16 in. for the compression steel.

2.2 Materials and Fabrication

Cement

Marquette Type III, high-early-strength, Portland cement was used in all beams. It was purchased in sacks from a local dealer and stored under proper conditions.

Aggregates

Wabash River sand and pea gravel were used for all mixes. The maximum size of the gravel was 3/8 in. The fineness modulus of the sand was about 3.2. The absorption in both aggregates was approximately one percent

by weight of the saturated surface dry material. Both of these aggregates have been used in the laboratory for previous investigations.

Concrete Mixes

The design of the concrete mixes was based on results obtained from previous investigations carried out in the laboratory using the same aggregates. Mixes were designed for nominal 14-day strengths of 3000 and 5000 psi. Actual strengths varied from 2890 to 3560 psi for the 3000-psi mix and from 4960 to 5600 psi for the 5000-psi mix.

Properties of the concrete mixes are given in Table 2.2. Compressive strengths are average values for at least five standard 6 by 12-in. cylinders. The modulus of rupture values are averages from tests of two 6 by 6 by 20-in. standard control beams loaded at the third points on a span of 18 in.

All beams were cast from a single batch. Since the batches were small, moisture control became a problem, especially if the mixes were batched with aggregates taken directly from the bins. To obtain better control of the moisture, the quantities of the aggregates needed for a batch were premixed on the day prior to casting and stored under polyethylene film to prevent loss of moisture to the air. This method proved satisfactory.

Reinforcement

Longitudinal tension reinforcement consisted of No. 3, 4 or 5 intermediate grade reinforcing bars. The longitudinal compression reinforcement consisted of No. 2 or 3 intermediate grade bars. The No. 2 bars were plain rounds. The No. 3 bars were deformed meeting the requirements of ASTM Designation A 305-56T. To assure approximately similar properties, the reinforcement in each series of beams was cut from the same bar.

A two-foot length was cut from one end of each bar for a standard coupon test. The stress strain curve for each coupon was obtained up to the beginning of the strain hardening range using an 8-in. microformer extensometer and an automatic recording device on a 120,000-lb. Baldwin Universal Testing Machine. Beyond the strain hardening range and up to the point of failure, the elongations were measured over an 8-in. gage length using a metal rule with graduations to 0.01 in. The complete stress-strain curves for all the longitudinal tension and compression steel are presented in Figs. B1-B9 in Appendix B. Table 2.3 lists their mechanical properties.

The web reinforcement was made from No. 7 black annealed wire having a diameter of 0.1770 in. This wire was received in the laboratory covered with a film of oil and dirt. Before using it, it was cleaned in a solution of hydrochloric acid, rinsed in water, and stored outside to rust. After the wire rusted, two coupon tests on two-foot long specimens established its yield point at 32 ksi.

Casting and Curing

All beams were cast on their sides in oiled wooden forms. The tension steel was supported and properly spaced by the anchorage plates welded to the ends of the bars. For the beams with web reinforcement the compression steel was supported and properly spaced by the stirrups; otherwise it was supported and spaced by temporary ties and spacers.

The concrete was mixed for about six minutes in a 6-cu. ft. non-tilting horizontal drum type mixer, placed in the forms, and compacted with an internal rod vibrator. Not less than six standard 6 by 12-in. control cylinders and two 6 by 6 by 20-in. control beams were cast in steel forms and also compacted with the vibrator. Generally one series

consisting of three beams, two without web reinforcement and one with web reinforcement, were cast at one time to assure similar concrete strengths for related tests. Exceptions to this casting procedure were Beams G33S-32 and G33D-32 which were cast as a pair, and Beam G33S-12 which was cast at the same time as Beams G33S-31 and G33D-31.

Immediately after casting, a 3/8-in. diameter steel rod with a 1/4-in. diameter threaded hole at each end was placed in the wet concrete at midspan of the beam at approximately the position of the neutral axis. This rod was made to the exact width of the beam cast and was flush with both surfaces. It was used to fasten a steel cross bar to the beam for the attachment of the deflection gages. Several hours after casting, the surface of the beams was trowelled smooth and the cylinders were capped with neat cement paste.

The day following casting, the specimens were removed from the forms and cured. The curing was the same for all beams. After removal from the forms, the beams and control specimens were placed in the moist room for seven days. They were then removed and stored in the laboratory until tested.

Strain Gage Application

Prior to casting, electric resistance strain gages were attached to the reinforcing bars. At the gage locations, the bar deformations were ground off and a smooth surface prepared. Two types of gages were used on the reinforcement, HE-141-B metalfilm gages having a gage length of 1/4-in. and SR-4 Type A-7 wire gages also having a gage length of 1/4-in. The HE-141-B gages were applied with GA-5 heat curing epoxy adhesive following the manufacturers instructions. The SR-4 Type A-7 gages were applied with Eastman 910 contact cement.

The gages were soldered to No. 22 plastic coated solid lead wires. They were waterproofed with successive layers of wax, GA-1 waterproofing compound, asbestos compound and epoxy resin. The leakage and electrical resistances were checked at various stages of application. Unsuitable gages were replaced. The instrumentation of the reinforcing steel will be discussed further in Section 3.2.

3. LOADING APPARATUS, INSTRUMENTATION, TESTING PROCEDURES

3.1 Loading Apparatus and Testing Equipment

A 60-kip capacity pneumatic loading device was used to apply both the static and dynamic loads. This apparatus and its associated pressurizing and control equipment have been described completely in Reference 4. Figure 3.1a is a photograph of the machine. This machine can apply a static load in tension or compression, a combination of a static load and a pulse load, or a pulse load of long or short duration, restricted only by its 60-kip capacity.

For static loads, pressurized gas was directed into the main chamber to act on the piston. For dynamic loads, the machine was operated as an "implosion" machine. This was done by storing pressurized gas in external chambers and then releasing the gas into the internal chamber through a slide valve mechanism. Commercial nitrogen gas under high pressure was used.

The rise time to maximum load for the dynamic loading was found to be approximately 0.003 sec. and seemed to be independent of the load attained. The dynamic loads used in these tests were of "infinite" duration; that is, maximum load was applied to the beam and held until the beam failed.

The load was transmitted to the test specimen through a distributing beam which applied a two-point load at points 4-in. each side of midspan. Figures 3.2 and 3.3b show the test setup. The distributing beam was equipped with load cells at each load point to measure directly the load applied to the test specimen. The sum of the outputs of the two load cells was considered to be the load applied to the beam. For the static tests, the output of a third load cell, which measured the load transferred to the

distributing beam from the loading apparatus, was used as a check on the sum of the outputs of two load cells transferring load directly into the beam. The load cells bore on 4 by 4 by 1-in. bearing blocks which in turn rested on a 1/4-in. thickness of leather belting placed on the top surface of the test specimen.

The stop beam (Fig. 3.2) which passed through the distributing beam was used to limit the vertical travel of the distributing beam. Its purpose was to stop the motion of the loading equipment and prevent possible damage to the testing apparatus after the beam had failed.

The beams were supported as shown in Figs. 3.1b and 3.2. The system provided an almost frictionless resistance to lateral motion and rotation. The design of the reaction system limited the lateral movement at each support to a maximum of one inch. This allowed the test specimen to elongate axially about two inches before lateral restraint at the supports occurred. In most cases, this amount of movement was sufficient. Uplift at the reactions was prevented by a tie rod system.

The reaction system described had no load-measuring devices. Studies of deep beams by Untrauer (2) showed that the total applied load at any instant was nearly always equal to the total reaction. This indicates that the inertia forces do not contribute significantly to the force system and can be neglected. The applied load could then be used as a measure of the resistance of the test specimens without introducing a large error.

The supporting frame for the testing equipment and the loading apparatus is shown in Fig. 3.3a. It consists of two welded rectangular structural steel bents, bolted to a base and made rigid by a system of lateral bracing. The base consists of a rectangular mat of structural shapes

partially encased in concrete. Provision was made for the attachment of measuring devices to the frame.

3.2 Instrumentation

Applied loads, deflections, and steel and concrete strains were measured in both the static and dynamic tests with electrical measuring devices. Loads were measured with load cells, the deflection with linear-variable differential transformers, and the strains with electrical-resistance strain gages. The signals from the measuring devices were recorded on photographic paper by magnetic oscillographs.

(a) Measuring Equipment

Loads

Load applied to the specimen by the distributing beam was measured at each load point by a load cell. Each load cell consisted of a hollow steel cylinder rigidly fastened to the distributing beam and threaded at the bottom end to half rounds of steel. The load cells were designed to resist one-third as much load laterally as axially without yielding in order to allow for the wedging action of the deforming test specimen. To minimize lateral deformations of the cells under load, a 1/8-in. plate spacer was fastened between the load cells at the level of the half rounds (Fig. 3.2).

Instrumentation of each load cell consisted of four SR-4 Type AD7 strain gages arranged in a Wheatstone bridge circuit. The gages were mounted at midheight of the cells in an alternating horizontal and vertical pattern at 90 degree intervals around the circumference. The vertical gages formed opposite legs of the bridge and were oriented perpendicular to the long axis of the test specimen. This arrangement resulted in a strain output

increase of about 2.6 and eliminated the effects of bending. The sensitivity of this load dynamometer was approximately 45 kip per 0.001 strain.

The load cells were calibrated by placing them in a 120,000-lb Baldwin Universal Testing machine, applying increments of load, and recording the corresponding strain output with a strain indicator. With this data a calibration curve was established. At the start of a series of tests, the strain bridge on the load cells was read with a strain indicator while selected resistors were shunted across one leg of the bridge. The measured output of the strain bridge was converted to equivalent load for each resistor and this information was then used to determine the value of the calibration steps for the oscillograph records obtained with the same resistors.

Deflections

Deflections were measured at the top of the beams at midspan with linear-variable-differential transformer deflection gages, designated hereafter as LVDT deflection gages. The fixed ends of these gages were attached to a rigid bracket mounted on 2-in. diameter pipe supports (Fig. 3.2). The movable cores were firmly attached to the ends of a cross bar which was attached to the top of the beam at midspan and cantilevered out from each side. Three deflection gages were mounted in this manner. Two gages, placed symmetrically about the midline of the beam, were designed to measure the deflections up to yielding, and were calibrated only to 0.10 in. maximum deflection. The average of the deflections measured with these two gages was considered to be the deflection at midspan. The third gage was used to measure deflections beyond yielding and up to the maximum load and was calibrated to a maximum deflection of 2.0 in. This gage was mounted at

one end of the cross bar, and it was assumed that for the large values of deflection, the errors due to twisting of the beam would be small.

The brackets to which the fixed ends of the LVDT gages were attached were equipped with a threaded device which permitted the raising and lowering of the fixed ends of the transformers for calibration purposes. Increments of displacement, controlled with dial indicators were recorded on the oscillograph records to give the required calibration steps.

The 2-in. diameter pipes were well braced to the testing frame by a series of one-half inch diameter turnbuckles and rods. This bracing reduced the tendency of the pipes to vibrate, and thus introduce secondary effects into the deflection measurements. Although a previous investigation (2) showed that these effects were small, it seemed desirable to eliminate or at least reduce them to the greatest extent possible.

Steel and Concrete Strains

Strains in the tension reinforcement were measured at midspan with HE-141 Type B, post-yield foil resistance strain gages, and SR-4 Type A-7 bonded wire resistance strain gages. The HE-141 Type B gages, were applied to the reinforcing and oriented so that they measured the strain on the side of the bar facing the bottom surface of the beams. In several tests these gages were supplemented with SR-4 Type A-7 gages attached to the adjacent bar for beams with two tension bars, or on the opposite face of the same bar for beams with a single bar. For Beams G33S-31, G33D-31, G33S-32 and G33D-32, the strain distribution along the tension steel was determined by mounting additional SR-4 Type A-7 gages eight inches each side of midspan.

Each strain gage formed one leg of a Wheatstone bridge with three dummy gages. The strain bridges were calibrated by shunting selected

resistors across one leg of the bridge and recording the equivalent strain with a strain indicator. The same resistors were used to establish the strain calibrations on the oscillograph records at the beginning of each test.

Concrete strains were measured on the top surface of the beam at midspan with a single SR-4 Type A-3 wire resistance strain gage. In Beams G33S-21, G33D-21 and G33D-22, two additional gages were mounted seven inches each side of midspan to determine the distribution of the concrete strains along the top surface. Similarly each gage formed one leg of a Wheatstone bridge with three dummy gages. The bridges were calibrated as described above.

(b) Recording Equipment

Signals from the electrical measuring devices were recorded on photographic paper with Hathaway S-14 magnetic oscillographs operating on a MCR-18 carrier measuring system. Figure 3.4 shows a block diagram of the measuring and recording system. A timing trace was put on all records by a timing trace generator.

Two oscillographs were used to record the output signals from the measuring equipment. The opening and closing of a gang switch through which the timing traces passed caused a simultaneous break in the timing trace on each oscillograph record tying together positively the records of the two oscillographs.

At intervals throughout the static tests, photographs of the beam were taken on 35-mm film to record the progress and development of major crack patterns at various stages of loading. They were tied to the oscillograph records by noting the gas pressure at the instant the pictures

were taken. This gas pressure was then related to the load recorded by the oscillograph records.

A 16-mm Wollensak high speed movie camera was used to photograph all the beams tested dynamically at a speed of 4000 frames per second. These pictures provided a continuous record of crack formation and beam behavior under load and proved to be valuable in determining the modes of failure. The film strips were tied to the oscillograph records through the same gang switch that was used to cause a break in the timing traces on the oscillograph records. The opening and closing of the switch caused a small neon light to flash simultaneous with the break in the timing traces. This lamp was strategically located so that its flash was recorded by the camera.

3.3 Test Procedure

Until the actual application of load began, the preparation of the test beams and the testing procedure was the same. The beams were usually tested in groups of three designated as a test series. Four beams were tested in pairs; G33S-31 and G33D-31, and G33S-32 and G33D-32; and one beam, G33S-12, was tested alone. All tests in one series were carried out in succession as rapidly as possible, depending on the time required to set up each beam in the testing frame. Figure 3.3b shows a photograph of a beam in position and ready to test.

Beam Preparation

Preparation of the beams for testing began with seating them on a 1/2-in. thick bearing plate at the supports with a rapid setting high-strength gypsum cement. A special jig was used to keep the beam in a vertical position while it was being seated. Slight imperfections in casting

necessitated this initial step to assure that the beams would stand vertically on the reactions.

After the beam was seated, its midspan was located, the position for the load blocks established, and the position for the concrete gage marked. The surface of the beam at the gage location was sanded smooth with coarse emery paper, and the SR-4 Type A-3 gage was mounted with Duco Cellulose cement and held in position by a light weight. After the gage dried, it was checked for serviceability by measuring its resistance and the leakage to ground. Lead wires were attached and the gage was then ready to use.

The cross bar, to which the movable cores of the LVDT deflection gages were to be fastened, was positioned on the beam with the aid of a metal square and fastened firmly by the tie rods to the 3/8-in. diameter threaded steel rod cast into the beam. The beam was placed in the testing rig, the leather pads and load blocks positioned, and the distributing beam brought to bear. The tiedowns at the supports were positioned and tightened, the cores of the deflection gages fastened to the cross bar, and the strain gage leads connected to the recording equipment. The beam was then ready for test.

Static Tests

In the static test, the calibration steps were first put onto the oscillograph records. The gain of the amplifiers had been adjusted so that the maximum trace deflection, which represents a value of load, strain or deflection, would remain on the record. The recording equipment was started and the load applied at a rate such that the beam would fail in one to two minutes. Photographs were taken at intervals throughout the test, as described previously, until the beam failed. When the beam failed, the

recording equipment was stopped, the pressure was bled off the loading device, the piston raised, and zero readings of the load cells taken.

Dynamic Tests

Before each dynamic test, a dry run was made to make sure that the solenoid on the slide valve triggering mechanism and the high speed camera were operating properly. The external chamber of the pneumatic loading device was partially pressurized before the calibration steps were put on the records. When the calibrations were completely recorded, the external chamber was pressurized to the desired value. The auxiliary chambers for operating the slide valves were then pressurized. The oscillographs were started and the load was applied by throwing a switch which energized the solenoid on the slide valve mechanism and started the high speed camera. A timing device on the switch permitted the camera to start operating 1/4 second before the solenoid was energized. After the beam failed, the oscillographs were shut off, the pressure bled from the loading device, the piston raised and the zero readings of the load cells taken.

Photographs of all beams, static and dynamic, were taken after failure.

4. RESULTS OF STATIC TESTS

4.1 Introductory Remarks

The static tests described in this section were carried out primarily as companions to the dynamic tests. Their purpose was to provide a base to which the results of the dynamic tests could be related. However, the static tests in themselves are of interest, and for that reason it seems desirable to discuss them separately.

Various investigators have studied the problem of the stress distribution in reinforced concrete deep beams, both theoretically and experimentally. A survey of the literature reported by Austin (1) outlines briefly the work that has been done. Probably the greatest value of these early studies was that they brought out the deficiencies of applying shallow beam concepts to very deep members. Notably, in very deep members the compressive stresses at the support and load points have a considerable influence on the distribution of the internal stresses and cannot be assumed to be negligible as is done in shallow beams. However, there seems to be a gradual transition from shallow beams to deep beams and a region exists where the shallow beam concepts can be applied to what is defined as moderately deep beams. The specimens tested in this investigation were considered as moderately deep members. That is, the span to depth ratio was greater than two but less than six or seven, which is considered the limit of the shallow beam range.

Thirteen static tests are discussed. Eleven specimens had no web reinforcement and the remaining two specimens had vertical stirrups. The number of variables involved precludes an independent study of these results; therefore, current shear and flexural strength concepts as applied to shallow

members are considered in relation to the strength and behavior of the test specimens. The applicability of these concepts are discussed and the differences are pointed out.

4.2 Presentation of Test Data and Results

The results of the 13 static tests are summarized in Table 4.1. The values of load and deflection at yielding are those obtained from the intersection of the primary and secondary slopes of the load-deflection curves as shown in Figs. 4.1-4.5. The values of load and deflection at ultimate capacity are those at collapse of the test specimens. The load values include live load only; the total weight of the beams was less than 70 lb.

Load-deflection curves for the static tests are presented in Figs. 4.1 through 4.5. Selected points from the oscillograph traces of load versus time and deflection versus time were combined to define the shapes of the curves. They are grouped according to similar L/d ratios and concrete strengths.

Curves of load versus steel strain and of load versus concrete strain were similarly defined from the strain-time traces and are presented in Figs. 4.8 through 4.22 and 4.23 through 4.35.which include also the load-strain curves for the dynamic tests. These latter will be discussed in Chapter 5, which is reserved for the dynamic test results. The upper set of curves in Figs. 4.8-4.22 covers the complete range of the steel strains measured; the lower set of curves shows, to a larger scale, the steel strains up to yield.

In several of the beams, additional strain gages were placed on the tension steel at midspan. Since the strains measured with these gages

were in close agreement with those from the regular gages, only the readings of the regular gages are presented in Figs. 4.8-4.22.

Sketches of the crack patterns at failure for the static tests are presented in Fig. 4.36 together with those for the dynamic tests. The widths of the lines indicates the relative size and importance of cracks. Photographs of the beams after failure are shown in Fig. 4.37.

4.3 Behavior Under Load and Mode of Failure

Load-Deflection Curves

The load deflection curve for a beam represents an over-all property which is useful for illustrating the behavior of the beam under load and for evaluating the effects of variables.

The load-deflection curves in Figs. 4.1-4.5 for the beams tested statically show two major stages of behavior. First, the "elastic" behavior of the beams up to yielding of the tension reinforcement. And second, the "inelastic" behavior after yielding and up to ultimate, where the deformations become large with respect to load.

The portion of the load-deflection curve up to yield can be approximated by a straight line. Actually, because of the formation of cracks, which reduces the stiffness of the beam and increases the tension steel stresses, the rate of deflection increases continually with load.

The shape of the load-deflection curve after yield roughly follows the shape of the stress-strain curve for the tension reinforcement. This can be seen in Figs. 4.1-4.5 for the beams having large deformations before failure. Corresponding to the yield range of the tension steel, the load deflection curve has a relatively flat slope. When the tension steel reaches the strain-hardening region, the slope increases and the load again

begins to increase. The beams with large steel percentages show this shape more distinctly than the beams with low steel percentages.

The gradual transition from the elastic to the inelastic stage of behavior was due to the progressive yielding of the tension reinforcement along the span and seems to be more noticeable for the beams with the high steel ratios. A sharp transition between the elastic and inelastic stages, as was observed for Beams G24S-21 and G33S-21 having low steel ratios, is due to more nearly simultaneous yielding of the tension reinforcement along the span.

Load-deflection curves are useful for distinguishing between flexure and shear failures. Beams failing in flexure exhibit large inelastic deformations before failure whereas beams failing in shear usually exhibit little or no inelastic deformation. This can be illustrated by considering Fig. 4.6, which shows a typical load-deflection curve for a beam exhibiting large inelastic deformations. Point A marks the beginning of inelastic behavior. The portion of the curve from A to B shows the behavior to the maximum or "ultimate" load, and the portion from B to C shows the gradual decrease in load between "ultimate" and final collapse. It was not possible in the static tests to obtain the portion of the curve from B to C because the nature of the loading did not allow the load to drop off gradually after the ultimate was reached, and the beam failed suddenly.

Ordinarily if a beam failed at a deflection corresponding to the points marked 1 and 2 on Fig. 4.6, it would be called a shear failure. If it failed at point 3, 4, or 5 it would be called a flexure failure.

Cracking Configurations and Modes of Failure

A study of the formation and development of cracks in a reinforced concrete member under load is essential to determine its behavior and mode

of failure. In deep beams, two types of cracks are considered important: flexural cracks which usually appear in the midspan region at sections of maximum moment; and inclined cracks which usually begin at the bottom of the beam near the supports and propagate upward toward midspan.

In the following paragraphs the behavior of the beams is discussed in relation to the crack patterns developed during the test. Owing to the nature of the test procedure, the first cracks became visible only near yield although the load-deflection and load-steel strain curves, Figs. 4.1-4.5 and 4.8-4.22 indicate that cracking actually began at a load equal to about one-third of the yield load. The cracks discussed are only those wide enough to appear in a photograph and thus correspond to those visible at or near yield; nevertheless, they form the major crack patterns.

In deep beams, the inclined cracks are more important than the flexural cracks, since they have a much greater influence on the behavior. The formation of inclined cracks eliminates the inclined principal tensile stresses necessary for beam action and causes a redistribution of the internal stresses which results in a tied arch action in which the reinforcement acts as the tension tie and the portions of the concrete beam outside the inclined cracks act as the arch rib.

Figure 4.7a shows the typical effect of inclined cracks on the behavior of deep beams. The solid lines represent the strain distributions which result from the formation of inclined cracks; the dashed lines represent the theoretical strain distributions if inclined cracks did not form. Once the inclined cracks have formed, the strains in the tension steel become nearly uniform along the entire length of the beam, and the concrete strains tend to concentrate at midspan over the inclined cracks.

Arch behavior in deep beams causes very high stresses in the tension reinforcement near the supports. If special provision is not made to anchor the bars at the supports, the beams may fail in anchorage or bond before reaching their "flexural" or "shear" capacity.

Arch behavior is not a phenomenon peculiar only to deep beams. It develops locally in ordinary reinforced concrete beams, when inclined cracks form at some location in the shear span away from the support and causes the strain in the tension reinforcement along the horizontal projection of the inclined crack to become uniform (Fig. 4.7b). The concrete strains become concentrated in a region near the upper end of the inclined crack. In Fig. 4.7b the solid lines represent the strain distributions for an ordinary beam with inclined cracks and the dashed lines represent the theoretical strain distributions if inclined cracks did not form.

The sketches of the crack patterns in Figs. 4.36 show that the deep beams tested statically had well developed inclined cracks at failure, and thus behaved as tied arches.

Flexure Failure

In Table 4,1 the modes of failure have been described as flexure, shear, or flexure-shear. A reinforced concrete beam fails in flexure when the bending stresses in the region of high moment cause the concrete to crush in the compression zone or cause the longitudinal tension reinforcement to rupture. Failure by crushing of the concrete in the compression zone can occur before, simultaneously with, or after yielding of the tension reinforcement. Similarly, members can fail by rupture of the longitudinal tension reinforcement before, simultaneously with, or after the concrete in the compression zone begins to crush. In deep beams, a flexure failure is

defined as a failure of the "tied arch" by a crushing of the concrete rib in compression at the "crown" or by a rupture of the tension "tie". Beams G33S-21 and G34S-21 failed by crushing of the concrete at the "crown". Beams G23S-21, G24S-11 and G24S-21 failed by rupture of the tension "tie".

For the beams which failed in flexure, the first crack to form was either a vertical crack near midspan or an inclined crack which usually started at the bottom of the beam near a support. At advanced stages of loading, both vertical and inclined cracks formed and became well developed. For Beams G24S-21, G33S-21, G34S-21 and G44S-11, the first visible crack was an inclined crack. For Beam G23S-21 the first visible crack was a vertical crack near the midspan. For Beams G24S-21 and G43S-11 the nature of the first crack could not be determined. In Beam G33S-21 the inclined cracks started away from the support, but propagated along the reinforcing to the support causing unbonding of the tension reinforcement and formation of the typical arch. For beams with L/d = 2 the inclined cracks advanced at approximately 45 degrees toward midspan and then rose almost vertically to the compression zone. For L/d = 3 or 4, the diagonal cracks propagated at approximately 45 degrees toward the load point and arched over toward midspan in the compression zone.

Shear Failure

A reinforced concrete beam of ordinary span and depth can fail in shear in various ways. Failures in such beams begin with the formation of a diagonal tension crack as a result of combined bending and shearing stresses. Once this diagonal crack has formed, the beam may fail in one of several modes. The member may collapse at the inception of the diagonal crack by crushing of the concrete in the compression zone; this mode of failure has

been referred to as "diagonal-tension". If the member can carry additional load after the formation of the diagonal crack, it may fail in one of two ways: the crack may extend into the compression zone and the member may fail by crushing of the concrete;this has been called a "shear-compression" failure. Or, the crack may advance along the tension reinforcement toward the support until failure occurs in bond and anchorage; this has been called a "shear-tension" failure. Members may also fail in a combination of shear-tension and shear-compression. Shear-compression and shear-tension failures have been observed in shallow beams both before and after yielding of the longitudinal tension reinforcement.

When the ratio of shear span to effective depth is small, as in the deep beams considered in this investigation, a shear failure must be defined somewhat differently than that observed for ordinary beams since it seems to be a modified form of "shear-compression" type of failure. Failure is preceded by the formation of a "second" inclined crack which extends from the load point to the support outside the first inclined crack and roughly parallel to it. This gives the beam a "strut-like" appearance between the load point and the support and failure occurs with the destruction of this strut, accompanied by shearing off of the unloaded portion of the beam outside the load blocks and unbonding of the tension reinforcement over the supports. Destruction of the strut may occur simultaneously with the formation of the second inclined crack, or the beam may support additional load after its formation. This type of "shear" failure can occur before, simultaneously with, or after yielding of the tension reinforcement.

For the beams which failed in shear, inclined cracks formed in all beams prior to failure. The presence of flexural cracks was not observed, although the load-steel strain curves indicated their presence. Beams

G33S-11 and G33S-12 failed in shear soon after the tension reinforcement yielded and were not able to support load after the formation of the second inclined crack. Beams G33S-31 and G33S-32 were able to support additional load after formation of the second inclined crack and failed in shear almost simultaneously with yielding of the tension reinforcement.

Flexure-Shear Failure

Beams G23S-11, G34S-11, G43S-11 and G44S-11 have been called flexure-shear failures in Table 4.1. According to the load-deflection curves of Figs. 4.1-4.5 the failure of these beams would and possibly should be called flexural failures. However, their behavior at failure was enough different from that of the flexure failures described previously that it was decided to consider them separately. The particular characteristic which separates these beams from those failing in flexure is that ultimate collapse occurred in a manner identical to that described for the shear failures. It will be shown later in this chapter that these beams reached their full flexural capacity. It will also be shown that, according to the criterion established for predicting shear strength, these same beams had also reached their full shear capacity.

For the beams which failed in flexure-shear, both flexural and inclined cracks formed and became well developed at failure. These beams failed by destruction of the inclined strut at the formation of the second inclined crack.

Steel Strains

The load-steel strain curves for the static tests of Figs. 4.8-4.22 show the two major stages in the behavior of the beams under load; the elastic behavior up to yield, and the inelastic behavior after yield. Corresponding to elastic behavior before cracking, the slope of the curves are steep. The

formation and development of cracks, which means that the concrete in the tension zone can no longer carry any stress, causes the steel strains to increase more rapidly with load and produces a change in the slope of the curve. The transition from the "uncracked" condition to the "fully-cracked" condition seems to be more sharply defined in these beams than in beams of ordinary depths. This is due to the development of inclined cracks and the formation of arch action.

Yielding marks the beginning of the inelastic stage where the strains increase rapidly with load. For the beams which failed after a large amount of deformation, the load-steel strain curves have the same general shape as the stress-strain curves for the tension reinforcement. Regardless of the type of failure, the tension steel in all beams reached yield at or before failure.

The steel strain curves for Beams G33S-31 and G33S-32 in Figs. 4.15 and 4.17 show the arching behavior that develops in deep beams at the formation of the inclined cracks. Up to the formation of the inclined cracks, the beams exhibited typical beam-type behavior with the strains being distributed along the tension reinforcement roughly in accordance to the distribution of moment. The formation of the inclined cracks and the resulting redistribution of internal stresses caused the strains in the steel near the support to increase rapidly until they became of the same order of magnitude as the strains at midspan. After inclined cracking, the strain in the bar adjacent to the support increased at a slightly greater rate than the strain at midspan and yielding occurred near the supports.

Comparison of the load-steel strain curves in Fig. 4.17 shows that the presence of the web reinforcement in Beam G33S-32 seemed to have no

effect on its behavior when compared to Beam G33S-31 without web reinforcement. Inclined cracking developed at almost the same load and strain in each case. The slight differences in maximum load and strain are due mainly to differences in the concrete strengths and properties of the tension reinforcement.

Concrete Strains

The curves of load versus concrete strain presented in Figs. 4.23 to 4.35 are similar in shape to the steel strain curves and show the two major stages of behavior; namely, elastic up to yield and inelastic after yield. The concrete strains increase with load until the concrete begins to crush. Crushing is identified by the decrease in measured strain with increase in load. The maximum recorded concrete strains for the static tests are presented in Table 4.2. These strains do not represent the true crushing strains because the strains presented were those measured at midspan and crushing was observed first near the load blocks. Although the strain should theoretically be constant throughout the midspan region since the moment is constant, it is evident that this was not the case. When crushing occurred at one section there was a relieving of strain at adjacent sections.

Concrete strain as high as 0.0091 was measured for Beam G24S-21 before it failed in flexure by rupture of the tension reinforcement with little or no visible crushing. The lowest measured midspan concrete strain for a beam failing in flexure was 0.0044, for Beam G43S-11 which failed in flexure-shear. The average measured concrete strain at observed crushing for beams failing in flexure was 0.0059. All of the beams which failed in flexure carried a maximum load greater than that observed at crushing except Beam G24S-21 for which the maximum measured strain occurred at the ultimate load.

For beams failing in shear, the measured concrete strains at midspan varied from 0.0010 at failure for Beam G33S-32 to 0.0047 at a load less than maximum for Beam G33S-11.

Figure 4.28 contains load-strain curves for Beam G33S-21 at three locations along the top surface of the beam. The typical transfer to arch action is quite noticeable. Before cracking the concrete strains are distributed roughly according to the distribution of moments. With cracking, the strain at midspan increases rapidly and becomes very large whereas the strains outside the load blocks remain small.

4.4 Discussion of Test Results

The effects of the variables on the strength and behavior of the beams tested are discussed in this section. The variables considered were the concrete strength, tension steel percentage, L/d ratio, and the presence of a nominal amount of web reinforcement.

Concrete Strength

As was expected, changing the nominal concrete strength from 3000 to 5000 psi had negligible effect on the ultimate strength of beams failing in flexure but produced an increase in strength for beams failing in shear. Comparing Beams G23S-21 and G24S-21, and G33S-21 and G34S-21, in Table 4.1 shows the negligible increase in strength for the flexure failures. Comparing Beams G23S-11 and G24S-11 shows that the measured concrete strength changed the mode of failure from flexure-shear to flexure with negligible change in strength. Comparing G33S-11 and G34S-11 shows, however, that the increase in concrete strength changed the mode of failure from shear to flexure-shear with an increase in strength of about 30 percent. The results for Beams

G43S-11 and G44S-11 both failing in flexure-shear, show a negligible increase in strength but a large increase in deflection before failure, with the increase in concrete strength.

Steel Percentage

The effect of changing the percentage of tension reinforcement can be illustrated by comparing beams in which the concrete strength and L/d ratios remain constant. As expected, increasing the amount of tension steel, increased the capacity of the beams and tended to change the mode of failure from flexure to shear. This is illustrated in Fig. 4.3 and Table 4.1. Beam G33S-21 with a low percentage of steel had a low strength, a large increase in ultimate deflection, and failed in flexure. Beams G33S-11 and G33S-12 with moderate steel percentages failed in shear shortly after yielding of the tension steel, and G33S-31 and G33S-32 with fairly high steel percentages failed in shear at yield.

L/d Ratio

Increasing the depth of a beam increased the moment capacity because of the increase in the lever arm of the internal forces. However, there is not a proportional increase in shear strength because the total cross-sectional area was kept constant in these tests. Therefore increasing the depth increased the load carrying capacity insofar as moment is concerned only if the shear capacity had not been reached. This was observed and can be illustrated using the results in Table 4.1.

For beams failing in flexure or in predominately a flexure mode, G23S-11 and G33S-21, and G24S-11 and G34S-21, showed a 60 percent increase in strength for a 50 percent increase in depth. For beams in which the

mode of failure changed sharply from predominately flexure to shear, such as G43S-11 to G33S-11, there was a negligible change in strength but a noticeable decrease in the ultimate deflection.

Web Reinforcement

The presence of web reinforcement in the form of vertical and inclined stirrups had only a relatively small effect on the strength and behavior of the beams tested statically, but this effect was not the same for all beams. The results of the tests will therefore be discussed in groups to show the effects of the presence of web reinforcement.

It was expected that web reinforcement would slow the development of inclined cracks, cause a more favorable distribution of stress, by preventing arch action, and increase the resistance to shear failure. It has already been shown in Section 4.3 that up to 1.09 percent of web reinforcement had no effect on the development of inclined cracks. In the discussion to follow it will be shown that for the beams with web reinforcement there was a small increase in the ultimate strength and a decrease in the deflection at ultimate for beams which failed in flexure and shear if the mode of failure was not changed. However, if the beam with web reinforcement failed in flexure or flexure-shear whereas its companion beam without web reinforcement failed in shear, or flexure-shear, there was an increase in both strength and deflection.

The load-deflection curves for Beams G33S-12 and G33S-32 with web reinforcement, replotted to a larger scale, are shown with similar curves for their companion beams without web reinforcement, G33S-11 and G33S-31, in Figs. 4.38 and 4.39. Similarly, the load strain curves for the two beams

with web reinforcement and for their companion beams without web reinforcement have been replotted and are presented in Figs. 4.44 and 4.45. The load-deflection curves for those of Untrauer's (3) beams for which there were companion beams without web reinforcement in this series are shown in Fig. 4.40 to 4.43, plotted to a different scale from Figs. 4.38 and 4.39. The test results for Untrauer's beams are summarized in Table 4.3.

Figure 4.38 shows that G33S-12 with web reinforcement exhibited a decrease in deflection as compared to G33S-11. Both beams failed in shear shortly after yielding. Figure 4.44 shows that the web reinforcement had virtually no effect on the concrete and steel strains at midspan, and thus indicates that the stress distribution in G33S-12 was not greatly influenced by the presence of the web steel.

Figure 4.39 shows that G33S-32 with web reinforcement exhibited a small decrease in maximum load and deflection as compared to G33S-31 without web reinforcement. Both beams failed in shear shortly after yielding. Figure 4.45 shows, that there was a large decrease in the midspan concrete strain for G33S-32 and a small increase in the midspan steel strain, which indicates that the deflection at maximum load for G33S-32 should be less than for G33S-31.

Figures 4.40 and 4.41 include load-deflection curves for the beams with and without web reinforcement which failed in flexure. Beams F3S2 and F2S1 with web reinforcement showed an increase in strength and a decrease in ductility when compared to the beams without web reinforcement G33S-21 and G24S-11. The strength increase is due mainly to the different strength properties of the tension reinforcement. The decrease in ultimate deflection reflects the influence of the web reinforcement on the stress distributions by reducing the degree of arch behavior.

Figure 4.42 includes the load-deflection curve for the beam with web reinforcement which failed in flexure and its companion beam without web reinforcement which failed in flexure-shear. Beam F4S22 with web reinforcement showed an increase in strength and deflection, and a change in the mode of failure as compared to G44S-11 without web reinforcement.

Figure 4.43 includes the load-deflection curves for Beams F3S3 and G34S-11 with and without web reinforcement, both of which failed in flexure-shear. Beam F3S3 with web reinforcement showed an increase in strength and ultimate deflection as compared to G34S-11 without web reinforcement. The increase in strength is due mainly to the different strength properties of the tension reinforcement. The increase in deflection reflects the influence of the web reinforcement on the stress distributions by reducing the degree of arch behavior and forcing the beam more toward a flexure failure.

For all beams with web reinforcement there was a very noticeable reduction in the amount of visible damage as compared to the beams without web reinforcement.

For the beams without web reinforcement, the effects of the variables are illustrated schematically in Fig. 4.46 as a plot of L/d versus percentage of tension reinforcement. On this plot regions of flexure and shear failures for the beams tested can be separated, though rather roughly, by lines which are a function of concrete strength. Briefly, this figure says that shear strength increases with concrete strength and the effect of this variable is more noticeable at low than at high L/d ratios. There is a change in the mode of failure from flexure to shear as the percentage of steel increases and the level at which this occurs increases with L/d and f'_c. These observations are qualitative in nature because of the very limited information used to develop the plot.

From the point of view of strength, the presence of a nominal amount of web reinforcement seemed to have little effect on the ultimate strength of the beams regardless of the mode of failure. However, the web reinforcement had a noticeable effect on the ultimate deflections. Its presence seemed to result in the stress distribution being forced away from arch action, reducing the deflections of the beams and tending to reduce the shear effects on those which exhibited predominantly flexural behaviors, particularly the beams failing in the flexure-shear modes.

4.5 Analysis of the Test Results

In this section it will be shown that the flexural strength of the beams tested statically can be predicted by using established formulas with some slight modifications, and that the shearing strengths can be related to cracking load and ultimate strength concepts which have been developed elsewhere. Since the few static tests reported herein are not sufficient to attempt an independent approach to the development of a shear strength concept, it was decided to approach the problem so to speak, backwards. That is, a formula which had been developed from tests on beams of somewhat similar nature was used to predict the strength of these beams in shear, and the results compared with the results of the tests.

The emphasis in this section is placed on shear strength. Flexural strength is discussed only to give continuity and completeness.

Flexural Strength

It is now well known that the moments at flexural yielding in moderately deep beams can be predicted reasonably accurately by the conventional straight line theory. The results of the static tests reported herein also support this statement. The standard formulas for computing

moments at yielding for beams reinforced in tension only or in both tension and compression are presented in Appendix A for easy reference.

In Table 4.4 the measured loads at yield and the loads corresponding to the computed yield moments are presented for the beams tested. The ratio of measured to computed yield load varies from 0.96 to 1.17 with an average of 1.08.

It was found in previous investigations (5,6) that the ultimate flexural strength of moderately deep beams could be predicted by the standard ultimate strength procedures provided an increased value of the limiting concrete strain at failure was used; the value used was 0.008. The measured maximum loads and the loads corresponding to the computed ultimate moments are presented in Table 4.4 for all the beams tested. For the beams failing in flexure, the ratio of measured to computed load varies from 0.94 to 0.97 and the average is 0.95. For the beams failing in shear, this ratio varies from 0.82 to 0.83 and the average is 0.82. For the beams which were designated as flexure-shear failures, this ratio varies from 0.99 to 1.07 and the average is 1.06. These comparisons show that although these latter beams collapsed in a mode similar to the shear failures described, they had reached, at least for practical purposes, their full flexural capacity, whereas the beams failing in shear did not.

Shear Strength

(a) Cracking Load

The complex nature of the stress distribution in beams failing in shear is well known. For this reason, investigators have had to resort to empirical approaches for interpreting test results and developing expressions for shear strength. Today the cracking load is considered to

be a measure of the useful shear capacity of a reinforced concrete beam without web reinforcement and justifiably so because, for fairly long members, the formation of the first fully developed inclined crack is synonomous with complete collapse. For medium long members, the formation of the fully developed inclined crack is well defined and the beams are able to carry some load beyond this point. However for deep members, after the development of the inclined crack, the beams can support considerable additional load before collapse. The inclined crack in a deep member is considered to be fully developed when there appears to be a marked change in the steel stresses, and arch action has developed.

The test results are correlated in terms of the cracking load. DeCossio, (7) after Viest, (8) presented an empirical relationship with which he could predict the cracking load of the beams of his investigation with reasonable accuracy, and which was in a form suitable for application to beams under either uniform or concentrated loads. The equation is written as follows:

$$\frac{V_x}{bd} = 2.14 \sqrt{f'_c} + 4600\ p\ \left(\frac{Vd}{M}\right)_x \qquad (1)$$

where V_x = shear at critical section, lb.

b = width of member, in.

d = effective depth to tension reinforcement, in.

f'_c = concrete strength of 6 x 12-in. cylinders, psi

p = A_s/bd = tensile steel ratio

$\left(\frac{Vd}{M}\right)_x$ = ratio of shear to moment multiplied by the effective depth, computed at the location where V_x is computed, always positive.

Equation 1 expresses the cracking shear V_x as a function of the concrete strength and the cross section and as a function of the shear to moment ratio at a critical location along the span. For simple spans under symmetrical concentrated loads, the applied shear is constant throughout the shear span, but the computed cracking shear varies from a minimum at the load point to a maximum at the support. Although it appears that the critical section should occur at the load point, DeCossio took the critical section at the middle of the shear span. This corresponded fairly well to the location of the inclined cracks and also gave good correlation between the predictions of equation 1 and the test results.

Equation 1 was used to calculate cracking loads for all of the beams tested. The results of the computations are tabulated in column 4 of Table 4.5. The values of cracking load can be correlated to a reasonably well defined point on the load steel strain curves. The point in question marks a change in behavior of the beams from beam action to arch action, where the strain becomes uniformly distributed along the tension reinforcement. For the two beams in which the steel strains were measured along the span, (Fig. 4.15 and 4.17) the value of cracking load computed by Eq. 1 corresponds very closely to the load at which the steel strain near one support became equal to the steel strain at midspan.

The formation of inclined cracks is reflected by a change in the slope of the plot of the midspan steel strain versus load. When the strains become distributed uniformly along the beam, the slope of the load-strain curve becomes constant and remains so up to yield of the steel. The transition to this slope marks the beginning of arch action and the formation of well developed inclined cracks and should correspond to the cracking load. The cracking load computed for each beam was found to correspond very

closely to the load at which this transition was observed on the load-strain curves. The values of the computed cracking loads have been noted on these curves by short horizontal lines and the notation CL.

The observations made in the previous paragraph were valid for all of the beams tested in this investigation. For the two beams with approximately 1.09 percent of web reinforcement, G33S-12 and G33S-32 in Figs. 4.13 and 4.17, the computed cracking load corresponded very closely to the observed transition in the load-steel strain curves. This indicates that the load at inclined cracking was not affected by the presence of a nominal amount of web reinforcement and Eq. 1 can then be used to predict the cracking load capacity for beams with or without web reinforcement.

All of the beams, however, exhibited considerable load-carrying capacity beyond cracking as defined by Eq. 1. The maximum measured load for each beam is tabulated in column 5 of Table 4.5. Values of P_u/P_c, the ratio of maximum load to computed cracking load, are presented in column 6 for all of the beams tested. It appears that this ratio varies roughly inversely as the a/d or L/d ratio for all beams failing ultimately in shear.

In Fig. 4.47 the ratios P_u/P_c are plotted against a/d for the beams without web reinforcement which failed in shear and in flexure-shear modes. In the same figure are plotted the ratios of P_u/P_c for the tests reported by DeCossio (7). The data from the flexure-shear failures were included for two reasons: first, the ultimate mode of collapse was observed to be the same as that for the shear failures, and second, the ratios P_u/P_c for these particular cases followed the trend indicated in Fig. 4.47 for shear failures. With a/d ratios less than about three there is a definite increase in the shear capacity beyond cracking load as a/d decreases. There seems to be some influence of other variables on the capacity beyond

cracking load but their significance is obscured by the interaction between them. The curve drawn on Fig. 4.47 has no particular significance except for the fact that it indicates the trend of the data and can thus be used for comparative purposes.

It was shown in Section 4.4 that when web reinforcement was included there was a small increase in strength and in some cases a change in the mode of failure from shear to flexure. The increase in strength should also be reflected as an increase in P_u, and thus in P_u/P_c, for both flexure and shear failures. The discussions of the following paragraphs indicate this.

Cracking load computations using Eq. 1 were carried out for Untrauer's (3) beams with web reinforcement. The results of the computations are tabulated in Table 4.6 along with the measured ultimate loads, the ratios of P_u/P_c, and the observed modes of failure. Of the six tests reported, four failed in flexure, one in shear and one in flexure-shear.

Figure 4.48 is a plot of P_u/P_c versus a/d for those beams with web reinforcement which failed in shear, flexure-shear or flexure and whose companion beams without web reinforcement failed in shear or flexure-shear. The two points which fall above the trend line for beams without web reinforcement are for Beams F3S3 and F4S22, in which the addition of web reinforcement resulted in an increase in strength and which changed the mode of failure from flexure-shear to flexure for F4S22. Beam F3S3 failed in flexure-shear as did its companion without web reinforcement G34S-11. For the beams failing in shear, the plotted points fall on or below the trend line. The two points below the line correspond to Beams G33S-12 and G33S-32 in which very little or no increase in shear strength was noticed with the addition of web reinforcement.

(b) Ultimate Shear Strength

The ultimate strength of beams failing in shear has been the subject of several papers (9,10,11). These studies have shown that the load at ultimate shear failure may be correlated best on the basis of the failure moment at a critical section, and empirical expressions have been developed for the moment capacity at shear failure. These expressions, however, were based on the assumption that shear failures usually occur before yielding of the tension steel; if there was considerable deformation beyond yielding, the failure was called a flexure failure. In this report, a shear failure has been defined in terms of the ultimate mode of failure of the "tied arch" even though in some cases there was a relatively large amount of deformation beyond yielding prior to collapse. Consequently, the equations developed previously should tend to underestimate the shear strength of these beams.

Laupa's (11) formula for the moment at shear failure is:

$$\frac{M_s}{bd^2 f'_c} = (k + np')\left(0.57 - \frac{4.5f'_c}{10^5}\right) \qquad (2)$$

where M_s = moment at shear failure

b = width of beam

d = effective depth

f'_c = concrete strength of 6 x 12-in. standard cylinders

k = theoretical depth of the compression zone, as given by equations A3 or A6 of Appendix A for beams with tension reinforcement only or with tension and compression reinforcement, respectively.

n = modular ratio as expressed by equation A4, Appendix A

p' = ratio of compression reinforcement

Equation 2 is based on the criterion of a limiting moment for shear failure rather than a limiting shearing stress and on the assumption that a beam fails in shear before yielding of the tension reinforcement.

For beams with web reinforcement, Laupa presented the following empirical equation which was found to be most consistent with his test results:

$$P_{sw}/P_s = 1 + \frac{2rf_{yw}}{10^3} \qquad (3)$$

where P_s = strength of beam without web reinforcement

P_{sw} = strength of beam with web reinforcement

$r = \frac{A_w}{sb}$ = ratio of web reinforcement

A_w = area of stirrup

s = spacing of stirrups

f_{yw} = yield stress of web reinforcement

This equation was based on the assumption that the shear strength of a beam with web reinforcement is affected not only by the amount and properties of the web reinforcement but also by the shear strength of the beam itself. The most important function of web reinforcement is that it resists the extension and widening of inclined cracks. It would seem logical to assume therefore, as Laupa did, that a given amount of web reinforcement will increase the shear strength in proportion to the amount provided. It has also been observed that the stirrups yield before a beam fails in shear, which indicates that the shear strength is proportional also to the yield strength of the web reinforcement.

As described previously, a shear failure in a deep beam is different from that observed by Laupa in the tests from which he developed his equations.

It was also observed that the presence of web reinforcement in the deep beams tested here and those reported by Untrauer (3) had relatively little effect on the ultimate strength of beams failing in shear. Web reinforcement, however, did affect the deformation characteristics and changed several flexure-shear failures to flexure failures but the influence on the strength was again negligible. Since the contribution of the web reinforcement is negligible, the use of Eq. 3 to evaluate its effectiveness is not recommended as a possible design procedure for beams having dimensions similar to those reported herein.

Although Eq. 3 was not considered a valid means of determining the contribution of the web reinforcement to the strength of deep beams, it was felt that Eq. 2, in light of the wide use of this type of relationship for computing shear strength of ordinary beams, might be applicable for deep beams both with and without web reinforcement.

The ultimate shear strengths were computed by Eq. 2 and the results are tabulated in Tables 4.7 and 4.8. For the beams both with and without web reinforcement which failed in shear or flexure-shear, the ratios P_u/P_s are plotted against a/d in Fig. 4.49. Also plotted in this figure are the ratios of P_u/P_s for the beams reported by Laupa (11).* It it interesting to note that for the beams tested the plotted points fall above the trend indicated by Laupa as would be expected since these beams failed in shear only after yielding of the reinforcement.

It was shown in Section 4.4 that the ultimate strength beyond the cracking load was an inverse function of the a/d ratio. Since Eq. 2 was formulated independent of a/d, the ultimate strengths computed by this equation should also show some influence of this variable. For the beams

---

* It should be noted that the computed shearing strengths P_s, for the beams reported herein are based on Eq. 2 with no allowance for the effect of web reinforcement indicated by Eq. 3, whereas Laupa's calculations were always based on Eq. 3 for beams with web reinforcement. The reason for this difference is expalined later.

reported by Laupa (11) there was, except for two series of beams which will be discussed later, no noticeable effect of a/d, He was concerned only with beams having a/d ratios greater than one, where the effect of this variable was obscured by the presence of other variables. However, when the beams which failed in shear in this report are added to Fig. 4.49, there is a sharp increase in P_u/P_s for the low avalues of a/d. Therefore, Eq. 2 tends to underestimate the shear strength of the deep beams tested, as predicted.

Among Laupa's results there were several beams with web reinforcement which failed at lower loads than predicted by Eq. 3 but at higher loads than predicted using only Eq. 2, and thus neglecting the effect of web reinforcement. These were the beams with short shear spans, a/d = 1.17 and 1.52, which were reinforced with vertical stirrups. These beams are marked as groups A and B in Fig. 4.49. These results suggest that Eq. 3 overestimates the effect of web reinforcement for small values of a/d but underestimates the effect of the a/d ratio itself. For this reason, Laupa interpreted the tests of beams having small a/d ratios in terms of failure by "shear proper", and developed an expression for their strength which was dependent on the shear span but virtually independent of the web reinforcement. The following expression was derived by Laupa for beams having "zero" shear span from tests by Graf (12) on rectangular and T-beams loaded very close to the support:

$$v_s = \frac{V}{bD} = 200 + 0.188\ f'_c + 21{,}300\ p_t \qquad (4)$$

where V = shearing force at failure in "shear proper"

v_s = nominal shearing stress

b = width of beam

D = total depth of beam

$$P_t = \frac{A_s (1 + \sin \alpha)}{bD}$$

The quantity $A_s (1 + \sin \alpha)$ refers to the "total" steel area crossing a vertical section between the load point and support and α is the angle of inclination of bent up reinforcement to the axis of the beam. The use of longitudinal steel was equally effective at any depth in the beam and the use of bent up bars was more effective than the addition of longitudinal reinforcement and its effectiveness increased as the angle of inclination increased up to a value of $\alpha = 62.7$ degrees. The use of vertical stirrups did not increase the ultimate load and therefore there seems to be a value of α which limits the usefulness of bent up bars.

Laupa computed the nominal shearing strength v_s as given by Eq. 4 for each of the beams with a/d = 1.17 and 1.52 which failed in shear and plotted the ratio v/v_s for both his and Graf's tests against x/D, the ratio of the clear distance between the load blocks to the total depth of the beam. He found that v/v_s decreased as x/D increased from zero to one (Fig. 28 of Ref. 11). Although a trend was indicated, all of his points fell at the extremes of his plot and he was not able to determine a valid relationship between v/v_s and x/D from the limited information available.

For the deep beams reported herein and by Untrauer (3), the nominal shearing stress v_s was expressed in terms of a load P'_s:

$$P'_s = 2v_s bD \qquad (5)$$

where P'_s is the computed load at failure in "shear proper" and v_s is given by Eq. 4, and the ratios of P_u/P'_s and x/D are shown in Tables 4.9 and 4.10. The data from Fig. 28 of Reference 11 were also expressed in terms of P_u/P'_s

and are presented in Fig. 4.50. The results of the tests on deep beams plot on Fig. 4.50 in the range between zero and one and follow the general trend indicated previously by Laupa. The line drawn through the data represents a lower bound to the test results, and can be represented by the expression:

$$\frac{P''_s}{P'_s} = 0.80\ (1 - 0.6\ \frac{x}{D}) \quad 0 \leq \frac{x}{D} \leq 1.0 \qquad (6)$$

where P''_s is the computed shear strength. The point x/D = 1 marks roughly the transition between the conventional shear-compression failures of beams of ordinary dimensions and the shear failures of deep beams described in this report. The use of vertical stirrups as web reinforcement in beams with x/D less than one has a small effect on the shear strength. However, on the basis of Laupa's studies the use of bent up bars should be more effective.

It is not possible to relate x/D to a/d in a general manner because many of the beams with the same a/d ratios had different x/D ratios because of variation in the widths of the load blocks and the cover beneath the tension reinforcement.

These studies suggest a design procedure based on two separate criteria with the change from one to the other being made at an x/D ratio equal to one. For x/D less than one, vertical stirrups are no longer assumed to be effective and the shear capacity can be determined by using Eqs. (4) and (6). When x/D values are greater than one, the shear moment Eqs. (2) and (3) can be used to determine the shear capacity and design the web reinforcement of simply supported beams.

Uniform Load

Up to this point the discussion has been concerned with beams subjected to concentrated loads. Since a blast load is a uniform load an extension of the criterion developed for the shear strength under concentrated loads for application to beams under uniform loads is desirable. Reference 6, which presents some information on several deep beam tests which failed in shear under a simulated uniform load, will be used to check the validity of Eqs. 2-6 with respect to uniform loading.

Three types of shear failures were observed in the uniformly-loaded deep beams of Reference 6, and they all seemed to be a function of the length to depth ratio L/d. The beam with L/d = 3 failed at the yield point in shear compression by crushing of the concrete at the head of the inclined crack near midspan. The beam with L/d = 2 failed in the shear mode described herein, by a destruction of an inclined strut which formed between the support and the top surface of the beam after the formation of a "second" inclined crack. Beams with L/d = 1.5 and 1 failed after the formation of an almost vertical crack which extended from the inside of the load block up to the top of the beam and gave the appearance of a pure shear or "shear proper" failure. This was not the case, however, because the cracks formed initially from the combination of the inclined tensile stresses due to bending and the Poisson tension stresses due to the vertical compressive forces in the region of the support. Failure occurred when the concrete at the top and bottom of these cracks was destroyed.

The problem involved in relating the concentrated load criterion to uniformly loaded beams is in determining the critical section at which the interaction of moment and shear will produce a failure condition. Beams under concentrated loads failed at a section of maximum moment in a region

of constant maximum shear and the load at failure was expressed in terms of a maximum moment or a maximum shear (Eqs. 2-6) depending upon the dimensions of the beam. For beams under uniform load, maximum moment occurs at a section of zero shear and maximum shear occurs at a section of zero moment. Consequently failure must occur at some section in between where the moment-shear ratio permits the formation of the inclined cracks necessary to a shear failure.

Laupa (11) in a study of several simply-supported uniformly loaded T-beams with web reinforcement found that Eqs. 2 and 3 expressed the ultimate shear strength of normal sized beams provided the critical section was taken at M/Vd = 4.5. Bernaert (13), in a study of 18 simply supported uniformly loaded beams without web reinforcement found that Eq. 2 could be applied to the test results of his beams only if it was multiplied by a constant equal to 1.35 at the critical section, which occurred in the tests at a distance of L/3 from a support. For the uniformly loaded deep beams of Ref. 6 which failed in shear, Laupa's equation tends to underestimate the shear strength, while Bernaert's modified formula overestimates the shear strength, and in both cases the shear failures cannot be clearly differentiated from the flexure failures. The results of these computations are presented in Tables 4.11 and 4.12.

For the deep beams under uniform load which failed in shear, the critical section at M/Vd = 4.5 determining the shear-compression moment by Equation 2 is so close to the midspan that for practical purposes the mid-span section can be assumed as the critical section. The use of an arbitrary critical section at L/3 from a support as done by Bernaert (13) is not applicable to the deep beams because at failure the inclined cracks had propagated almost to midspan, with the result that the critical section

for moment could be considered the midspan moment. On the basis that the critical section occurred at midspan, Bernaert's uniformly loaded beams were reanalyzed using Eq. 2, and taking the critical section at the midspan. The results of the computations presented in Table 4.14 are plotted in Fig. 4.51. This figure can be interpreted in two ways: one, that the shear-compression moment as defined by Eq. 2 expressed the shear strength as some function of the maximum moment at midspan and the L/d ratio; or second, the location of the critical section for computing the shear-compression moment by Eq. 2 varies from midspan for beams with L/d = 1 to about 0.2L from a support for beams with L/d = 8. For beams with L/d greater than 8 the critical section appears to remain at 0.2L from a support. It also indicates a transition from conventional beam behavior to deep beam "arch" behavior for uniformly loaded beams failing in shear and that the limit of conventional beam behavior occurs about L/d = 8.

The poor correlation of the data from the deep beam tests to the shear-compression equations of either Laupa or Bernaert suggests, on the basis of the results of the deep beams tested under concentrated loads, a correlation to the "shear proper" equation.

The shear strengths of the beams of Ref. 6 were then computed using Eqs. 4 and 5 and the results are presented in Table 4.13 as values of P_u/P'_s. The next thing to be determined was what value of x should be used for uniformly loaded beams in order to obtain results consistent with those for the beams under concentrated loads.

DeCossio (13) showed from his tests of uniformly loaded beams and frames that a/d was approximately equivalent to $l'/4d$ where l' was the simply supported span length. On this basis x/D for the uniformly loaded

beams was taken as L'/4D where L' is the clear span between supports. The ratios of P_u/P'_s for the uniformly loaded beams have been plotted against x/D in Fig. 4.50. Since the points seem to be consistent with the trends of the test results for the beams with concentrated loads, the line represented by Eq. 6 may then be used to represent a lower bound for the shear strength of uniformly loaded beams.

5. RESULTS OF DYNAMIC TESTS

5.1 Introductory Remarks

The tests described in this chapter were carried out primarily to study the dynamic strength and behavior in shear of deep beams and to compare the dynamic behavior with that observed in the static tests. Twenty-two dynamic tests are described, and the modes of failure observed and the general behavior of the beams are compared with those of the static tests on companion beams discussed in Chapter 4.

5.2 Presentation of Test Data And Results

The results of the dynamic tests are presented in graphs, tables, and photographs, Figures B.10 through B.62 of Appendix B are plots of measured loads, deflections, steel strains, and concrete strains versus time. The load is the sum of the outputs of the two load cells. The load records were plotted until the beams collapsed or until the distributing beam came into contact with the stop beam. The deflection records were plotted until the beam collapsed or until the distributing beam came into contact with the stop beam, or when the deflection exceeded the maximum calibration value of two inches.

Figures B.10-B.31 show that the loads rose rapidly to high values, then fell to a lower level which was maintained until the beams failed and the load decreased rapidly to zero. The "peak" load was always higher than the load that could be obtained from consideration of the static pressure of the gas within the cylinder of the loading device. There are two phenomena which might contribute to this "peaking" of the load: first, the "imploding" of the gas into the cylinder causes the loading device to vibrate.

If the frequency of this vibration is in phase with the rise time of the load then the maximum load would increase due to the inertia effects of the loading device. And second, "imploding" the gas into the cylinder causes the gas itself to vibrate setting up a pulsating pressure against the face of the piston. If the frequency of this pulsating pressure is in phase with the rise time of the load, it too will contribute to the "peaking". As these vibrations dampen out the load reaches a steady state at a level below the peak. The load-time curve in Fig. B.19 shows an oscillation in the load trace prior to reaching the maximum load which is probably caused by these phenomena.

Figure B.30 shows that the recorded deflection for Beam G44D-11 began to drop off while the beam was still supporting considerable load. Since this type of deflection behavior is inconsistent with the general trend of the results, a malfunction of the measuring equipment was suspected.

When referring to the figures of Appendix B, it should be noted that they were not all plotted to the same scale. This is especially to be noted in Figs. B.32-B.61 where some of the steel strain-time curves have been plotted to two strain scales. The curve marked (b) shows the complete strain-time history as recorded to one scale, while the curve marked (a) shows the strain-time history only up to yield, to a larger scale. The strain records were plotted up to the time at which the beam collapsed, the strain gages were destroyed, or the distributing beam came into contact with the stop beam.

For the beams which had additional strain gages mounted on the steel at midspan, the strain-time histories measured with these gages, marked ϵ_1 are plotted in Figs. B.32-B.61 with the strain-time histories

measured together with "the regular gages", marked ϵ_s. For the beams which had additional gages mounted on the steel near the supports, the strain-time histories for these gages, marked ϵ_{sn} and ϵ_{ss} are plotted on Figs. B.32-B.61 together with the corresponding regular midspan gage records. A sketch on the figures locates the position of gages ϵ_{sn} and ϵ_{ss}.

In several beams, the concrete strains were also measured at several points along the top surface. The strain-time histories of the additional gages marked ϵ_{cn} and ϵ_{cs} are plotted with the strain-time history of the midspan concrete gage marked ϵ_c. The sketch on the figures locates the positions of ϵ_{cn} and ϵ_{cs}.

Figures 5.1-5.11 are the load-deflection curves. Each figure has three curves corresponding to the three beams which made up a test series. Two of the curves are for the beams tested dynamically, one with and one without web reinforcement; the third curve is for the static companion beam without web reinforcement.

The curves of steel and concrete strain versus load are presented in Figs. 4.8-4.22 and 4.23-4.35 and are grouped in series with the curves for the static companion beams.

Table 5.1 summarizes the loading information for the dynamic tests. The maximum load levels, P_{dyn}, applied to the beams by the pneumatic loading device, which were obtained from those recorded by the main load cell as it rested on the stop beam after collapse of the test beam, are tabulated along with the "peak" loads, P_{yd}, and the measured yield loads of the static companion beams. The ratio of the maximum load levels to the static yield loads are given and the rise times to maximum load, which were estimated from the load-time curves of Figs. B.10-B.31, are also presented in Table 5.1. The rise times were estimated by assuming a linear rise from

zero to maximum load according to the average slope of the load-time curves (Figs. B.10-B.31) neglecting any roundoff near the top and bottom.

Table 5.2 summarizes the results of the dynamic tests. The values of maximum load and deflection, P_{yd} and Δ_{yd}, and ultimate load and deflection, P_{ud} and Δ_{ud} are tabulated. They were taken from the load-deflection curves as indicated in Figs. 5.1-5.11.

Sketches of the crack patterns at failure are presented in Fig. 4.36 along with their static companions. The crack patterns were sketched from the 16-mm Fastax movies of the dynamic tests. Photographs of the test beams after failure are presented in Fig. 5.12. Figures 5.13-5.16 present sequences of photographs showing the progress of cracking under load for Beams G24D-11, G24D-12, G33D-31, and G34D-11; these were taken from the 16-mm film strips.

5.3 Behavior Under Load and Mode of Failure

Load Deflection Curves

The load deflection curve for a beam loaded dynamically represents the resistance and behavior of the member. When compared to the load-deflection curve for the static companion beam, it represents the increase in resistance due to the dynamic load.

The load-deflection curves of Figs. 5.1-5.11 show two major stages in the behavior of the dynamically loaded beams; elastic and inelastic, corresponding to the elastic and inelastic stages of the load-deflection curves for the beams loaded statically. The dynamic stiffness was observed to be about the same as the static stiffness.

The load-deflection curves for the dynamic tests show two major configurations which are associated with two major types of failure, flexure

and shear. In Fig. 5.1 the load-deflection curve for Beam G23D-11 shows the typical shape for a beam which failed in flexure. There was a large increase in deformation with load after the peak load had been reached and the dynamic load level had stabilized. In the same figure, the curve for Beam G23D-12 shows the typical shape for a beam which failed in shear. After the peak load had been reached, the load decreased rapidly to a value less than the maximum load in the static test with only a small amount of deformation. The secondary load level indicated was caused by the beams continuing to resist deformation after failure and before the distributing beam came into contact with the stop beam.

Several of the other load-deflection curves need further explanation. In Figs. 5.3 and 5.9, the curves for Beams G24D-12, G34D-21 and G34D-22 show a second peak just before the load began to decrease. This was caused when the reaction system reached the limit of its travel and introduced a restraint at the supports. The maximum load and deflection for these beams was obtained by extrapolating that portion of the curve adjacent to the second peak to the deflection at which the "second" peak load began to decrease, as shown in Figs. 5.3 and 5.9.

Cracking Configurations and Modes of Failure

The study of the formation of the crack patterns using the 16-mm movies was very useful in helping to determine the modes of failures in the dynamic tests. The sketches of the crack patterns at failure in Fig. 4.36 and the photographs in Fig. 5.12 show that generally the cracking configurations at failure in the dynamic tests corresponded closely to those for the static tests for similar modes of failure. The "tied arch" action observed in the static tests was also observed in the dynamic tests. Nearly

all of the beams had the typical vertical and inclined cracks associated with arch action, however, several beams in which arch action developed when the tension reinforcement became unbonded between the vertical cracks and the supports failed without the formation of inclined cracks.

Table 5.2 lists three modes of failure for the dynamic tests: flexure, shear, and flexure-shear. Of the 22 beams tested dynamically, twelve were considered to have failed in flexure, five in shear, and five in flexure-shear. The mechanics of the modes of failure have been described in detail in Section 4.3 for the static tests and the same criteria were used to determine the modes of failure for the dynamic tests.

Of the twelve beams which failed in flexure, nine failed by rupture of the tension "tie", and three failed by crushing of the concrete in compression at the arch "crown". The first crack to form was either a vertical crack in the midspan region or an inclined crack which began near the support. At failure, both vertical and inclined cracks had formed in all beams except G23D-21 which had only vertical flexure cracks. Vertical cracks formed the major crack patterns for flexure failures. Figure 5.13 is a sequence of photographs showing the crack formation for Beam G24D-12.

The five beams which were classified as shear failures are G23D-12, G33D-11, G33D-12, G33D-31, and G33D-32. Inclined cracks formed the major crack patterns for all beams failing in shear and failure occurred shortly after the peak load was reached. Vertical cracks in the midspan region formed after the inclined cracks in Beams G23D-12 and G33D-12. In Beams G33D-11, G33D-31 and G33D-32 only inclined cracks were observed at failure. Beams G33D-11 and G33D-31 failed in shear in the mode observed for the static tests; that is, by destruction of the compression strut between the

load point and the support after the formation of a second inclined crack. Figure 5.14 shows the formation of the cracks under load for Beam G33D-31 failing in shear. Beams G23D-12, G33D-12, and G33D-32 seemed to show a tendency toward a "shear proper" type of failure rather than a compression failure of the "arch rib". At failure only two major inclined cracks extending from the supports to the load blocks had formed in these beams. For Beam G23D-12, the entire end block seemed to be acting as a compression strut, and failure occurred by crushing of the concrete beneath the load block as the end of the beam sheared off. Both G33D-12 and G33D-32 failed by destruction of the concrete outside the load blocks as the mid-portion of the beams moved down vertically in relation to the ends. Figures 5.12i and 5.12e shows photographs of these beams after failure.

Beams G23D-11, G24D-11, G34D-11, G43D-11 and G43D-12 were considered to have failed in the flexure-shear mode. Although several of these beams exhibited very marked flexural behavior up to failure, e.g., G23D-11 where the tension reinforcement ruptured, the 16-mm movies and the final photographs indicated that ultimate failure occurred in shear. All of these beams appeared to have reached or just about reached their full flexural capacity at failure. Correlation of the 16-mm movies and the loads measured from the individual load cells indicated that at or just before the "second" inclined cracks became visible in the movies the load measured by the load cell adjacent to the inclined crack exhibited a sudden drop. This drop occurred at the ultimate load as recorded in Table. 5.2 Figures 5.15 and 5.16 are sequences of photographs of Beams G24D-11 and G34D-11 showing the development of the crack patterns.

The flexure-shear failure is probably the most uncertain of all failures to define because it is difficult to determine whether or not a

beam has reached its full flexural capacity before failing in shear. Therefore this type of failure would almost be impossible to predict.

Steel and Concrete Strains

The load-steel strain curves of Figs. 4.8-4.22 show the two major stages of behavior, elastic and inelastic, of the beams tested dynamically. They show also that, for beams failing in flexure, the tension steel began to yield before, after, or at the peak load; if the beams failed in shear, the steel began to yield before or at the peak load. In all cases, the dynamic yield load and strain were both higher than the static yield load and strain owing to the effect of the rate of straining.

Figures 4.16 and 4.18 show that for Beams G33D-31 and G33D-32 the steel strains measured near the supports at maximum load were of the same order of magnitude as those measured at midspan, indicating that the beams behaved as arches.

Figures 4.8-4.22 also indicate that the beams cracked at a higher load dynamically than statically. The "uncracked" slopes of these curves rose to higher values of load at which the slopes changed and became roughly parallel to the slopes of the static test curves. Cracking in the dynamic tests is not reflected by the load-steel strain curves as it was for the static tests.

The load-concrete strain curves for the dynamic tests, presented in Figs. 4.23-4.35 follow the same general pattern as the steel strain curves in Figs. 4.8-4.22. As in the static tests, the concrete strains increase with load until the concrete begins to crush, and then begin to decrease as the load is still increasing. The maximum measured concrete strains for the dynamic tests are presented in Table 5.3. Again, these strains do not

represent the actual crushing strains because crushing began near the load blocks away from the position where the strain gages were located. Maximum measured strains varied from 0.0042 to 0.0090 for the beams failing in flexure, with an average of 0.0062. Those for shear failures varied from 0.0016 to 0.0074 with an average of 0.0052. For the beams failing in a flexure-shear mode, measured concrete strains varied from 0.0042 to 0.0082, with an average of 0.0053. These measured strains are of the same order of magnitude as those observed in the static tests.

5.4 Discussion of Test Results

The application of a dynamic load to a reinforced concrete beam may be considered as another variable. The effect of concrete strength, steel percentage, L/d ratio, and the presence of a nominal amount of web reinforcement has already been discussed for the static tests in Chapter 4. In this section emphasis will be placed on the effects of the dynamic load; and the test results will be discussed, first in relation to beams without web reinforcement, and second in relation to beams with web reinforcement. The other variables will be discussed briefly only where necessary to the overall discussion.

Properties of the Dynamic Load

It was mentioned previously that the type of dynamic load applied was a step pulse of "infinite" duration. Both theory and tests (2, 3) have shown that the ratio of the rise time to the natural period is an important quantity in determining the response of members to this type of loading. If this ratio is zero, the inertia forces are a maximum and the member exhibits its maximum resistance. If the ratio is greater than zero and equal to an integral number, the inertia forces are equal to zero and the member exhibits

a minimum resistance (static). Between successive integral values intermediate maximum resistances are reached which diminish as the ratio increases. For the dynamic tests reported a theoretical consideration of the rise times to the natural periods indicated that the inertia forces should be small.

For the tests reported in Reference 2 on beams of approximately the same size and stiffness as those tested herein, it was found that the reaction-time traces followed the load-time traces quite closely indicating that the inertia forces were small. Untrauer (3) showed experimentally that, for similar beams tested using the same testing equipment, the inertia forces at maximum load were less than five percent of the applied load and below maximum load they were of the order of four to five kips. This discussion shows that the inertia forces are small and no appreciable error will occur in the interpretation of the test results if they are neglected. The applied load is then a measure of the resistance of the beam.

Although the "dynamic" loads do not cause an appreciable dynamic response in the deep beams tested, the rate of loading is such that there is a "strain-rate" effect on the strength properties of both the concrete and the reinforcing steel. Reference 15 indicates that increasing the rate of straining of an intermediate grade reinforcing bar increases its yield strength. Reference 16 indicates that increasing the rate of straining increases the compressive and flexural strengths of concrete as determined by the standard control tests. Increasing the flexural strength of concrete increases the resistance of the beams to the formation of cracks which should increase the resistance to shear failure.

Beams Without Web Reinforcement

For the beams without web reinforcement the application of the dynamic load generally increased the ultimate strength and deflection of the

beams failing in flexure; changed the mode of failure from flexure-shear to flexure or vice versa, in both cases with increased strength and deflection; and increased the strength and decreased the deflection of beams which failed in shear after yielding of the tension steel, or increased the deflection if shear failure occurred at yielding of the tension steel.

Comparing Tables 4.1 and 5.2 indicates that for the beams without web reinforcement which failed in flexure statically the companion beams loaded dynamically failed in flexure or flexure-shear. The dynamically loaded beams exhibited an increase in yield and ultimate strength and deflection as compared to the static companion beams. Since the distinction between a flexure and a flexure-shear failure is a fine one, the change in the mode of failure from flexure under static load to flexure-shear under dynamic load is not to be unexpected nor considered a major change in the behavior of the beams.

Tables 4.1 and 5.2 indicate that for the beams without web reinforcement which failed in shear statically the companion beams loaded dynamically also failed in shear. Figure 5.5 and Table 5.2 show that for Beam G33D-11 there was an increase in strength and a decrease in maximum deflection when compared to G33S-11, the static companion, whereas Fig. 5.7 and Table 5.2 show for Beam G33D-31 an increase in strength and a slight increase in the maximum deflection as compared to the static companion G33S-31. The dynamic shear failures appear to be more severe when compared to the companion beams which failed in shear statically after some yielding of the tension reinforcement because the dynamically loaded beams failed in shear shortly after reaching maximum load.

Comparing Tables 4.1 and 5.2 again shows that for the beams without web reinforcement which failed statically in the flexure-shear mode the

companion beams loaded dynamically also failed in flexure-shear, except G44D-11 which failed in flexure. These beams exhibited generally an increase in both ultimate strength and deflection.

Beams With Web Reinforcement

The presence of a nominal amount of web reinforcement in a dynamically loaded beam had a greater influence on its behavior than was observed when web reinforcement was included in the deep beams under static loading. As in the static tests, the presence of web reinforcement tended to reduce the severity of the inclined cracks and force the beams more toward "beam-type" action rather than "arch" action, together with a tendency to change the mode of failure from shear to flexure. According to Table 5.2 all beams with web reinforcement failed in the same mode as their companion beams without web reinforcement except G23D-11, G24D-12 and G34D-12.

For the beams with web reinforcement which failed in flexure, the deflection at ultimate load was noticeably smaller than the deflection at ultimate load for the companion beams without web reinforcement; the ultimate strengths being about the same. This indicates that arch action is reduced by the presence of the web reinforcement (Figs. 5.1-5.11). Figure 5.11 should not be included in this comparison because there is some doubt about the measured deflection for Beam G44D-11.

Table 5.2 shows that Beam G23D-12 with web reinforcement failed in shear just beyond the peak load whereas its companion beam without web reinforcement, G23D-11, failed in flexure-shear. This phenomenon is not consistent with the general trend of the results and no explanation can be given for this change of behavior.

Table 5.2 and Fig. 5.5 show that the presence of web reinforcement in Beam G33D-12, which failed in shear, increased the deflection at ultimate

over that for its companion beam without web reinforcement, G33D-11. Table 5.2 and Fig. 5.7 show the opposite effect of the web reinforcement in Beam G33D-32 when compared to G33D-31 without web reinforcement.

The beams with web reinforcement which failed in shear showed more of a tendency to the "shear proper" type of failure than the beams without web reinforcement. This was probably caused by the web reinforcement restricting the development of the inclined cracks, causing them to become more vertical and giving the beams the appearance of this type of failure.

According to Table 5.2, Beams G24D-12 and G34D-12 failed in flexure whereas their companion beams without web reinforcement failed in flexure-shear. As in the flexure failures, there was a slight decrease in the deflection at ultimate, although not to the same degree. A change in the mode of failure from flexure-shear to flexure tends to increase the ultimate deflections, whereas adding web reinforcement tends to decrease the deflections; the net result could thus be a change in either direction.

Whether a beam fails in flexure or flexure-shear is really of no consequence from the point of view of strength. In this regard, then it may be said that all the dynamically loaded beams failed in the same mode as their static companions except one. Therefore, if the static behavior and mode of failure of a beam can be predicted, the dynamic behavior and mode of failure will generally be the same.

From the studies presented in this section, it seems that for deep beams subjected to dynamic loads the presence of a nominal amount of web reinforcement is detrimental from the point of view of deflection. Since the area under the load deflection curve is a measure of the amount of energy required to cause failure, the more a beam can deflect before failure the greater overall resistance it will have. From this point of view, it

seems that the beams without web reinforcement would be more suitable than those with web reinforcement for high-energy blast-resistant design.

5.5 Analysis of Test Results

Untrauer (3) found that the dynamic flexural resistance P'_{ud} could be expressed as a function of the static flexural resistance P'_u, and the time it takes the beam to fail dynamically, t_f, and could be expressed by the expression:

$$P'_{ud} = P'_u \left(1 + \frac{4.0}{t_f}\right) \tag{7}$$

This relationship assumes that the dynamic load capacity is directly proportional to the static load capacity; that the increase in resistance due to strain rate effects is a function of the reciprocal of the time to failure; and that the mode of failure does not change in the dynamic case from that of the static case.

To obtain this expression, the ratio P_{ud}/P_u was plotted against the time to failure and the best fit curve was drawn through the data. For the beams reported herein, the ratio P_{ud}/P_u was plotted against t_f and the results are shown in Fig. 5.17 and Table 5.4. For the beams which failed in flexure, the points scatter about the line given by Eq. 7. The points representing shear failures fall to the left of and below those representing flexure failures and seem to scatter about a line represented by the relationship:

$$\frac{P'_{ud}}{P'_s} = \left(1 + \frac{0.6}{t_f}\right) \tag{8}$$

The points representing the flexure-shear failures scatter about the line represented by Eq. 7. This would be expected since these beams had reached or almost reached their flexural capacities before failing in shear.

Although the data are too few to justify Eq. 8 or even another equation of the same form, it should be realized that it was intended only to show what was considered to be the trend of the data. Further tests are undoubtedly necessary to either refute or substantiate a relationship of this sort to represent the dynamic shear capacity of deep beams.

6. SUMMARY

Thirty-five beams were tested, 13 statically and 22 dynamically, in order to determine their strength and behavior in shear; to determine if failure under a dynamic load was different from that under a static load; and to evaluate the effectiveness of web reinforcement in moderately deep beams. Eleven of the static test beams had no web reinforcement and the remaining two had vertical stirrups. Half of the dynamic test beams had no web reinforcement and the other half were reinforced with either vertical or inclined stirrups. The major variables were the length-to-depth ratio, percentage of tension reinforcement, the strength of the concrete, and the presence or absence of web reinforcement. All beams had compression reinforcement equal to about one-half the amount of tension reinforcement.

Tests were conducted in series usually consisting of one static test of a beam without web reinforcement and two dynamic tests, one with and one without web reinforcement. The dynamic load was applied by a pneumatic loading device which produced an "infinite" duration pulse at a level of 110 to 200 percent of the static yield load.

All of the beams tested, both statically and dynamically, exhibited "arch action" prior to failure. Most of the beams had well developed vertical and inclined cracks at failure typical of this type of behavior. In those beams which did not have inclined cracks, the tension reinforcement became unbonded over the length of the beam resulting again in typical arch action.

Three types of failures are described for both the static and dynamic tests: flexure, shear, and flexure-shear. The beams were considered

to have failed in flexure if failure occurred by crushing of the concrete arch "rib" at the crown, or by rupture of the tension "tie", in both cases with a large amount of deformation taking place before failure. They were considered to have failed in shear if failure occurred by destruction of the inclined strut which formed between the load point and the support as a result of inclined cracking, with relatively little deformation taking place before failure. The term flexure-shear was used to describe the failure of beams which had almost reached their flexural capacity, as shown by the large amount of deformation, but which finally collapsed in the shear mode.

Web reinforcement in the beams tested both statically and dynamically contributed little toward an increase in strength or a change in behavior and mode of failure. Its presence, however, did have an effect on the deformation characteristics of the beams, generally reducing the ultimate deflections. This reduction in ultimate deflection was especially noticeable in the beams with web reinforcement tested dynamically. Where the mode of failure changed from flexure-shear to flexure, a slight increase in ultimate deflection was detected in both the static and dynamic tests.

Studies of the test results showed that the static strength at flexural yielding in these moderately deep beams could be predicted reasonably well by the conventional straight line theory, and that the ultimate static flexural strength could be predicted by the standard ultimate strength procedure provided an increased value of the limiting concrete strain equal to 0.008 is used at failure.

For the beams tested statically, the cracking load as given by Eq. 1 corresponded closely with the change in the distribution of the steel strains along the beam which marked the formation of the inclined cracks and the

development of arch action. For the beams which failed in shear, the ultimate static capacity beyond cracking increased rapidly as a/d increased below three. Consequently the cracking load cannot be considered as a measure of the useful capacity of deep beams failing in shear as it is for beams of ordinary span and depth.

Correlation of the test data for beams under concentrated loads with a "shear-moment" and a "shear-proper" criterion showed that the ultimate shear strength of the beams tested could be related better to the "shear proper" criterion as expressed by Eqs. 4 and 6 than it could to the "shear-moment" criterion as expressed by Eqs. 2 and 3. There appeared to be a transition from shallow beams, where the "shear moment" criterion governed and the web reinforcement was fully effective, to the deep beams, where "shear proper" governed and the web reinforcement in the form of vertical and inclined stirrups was no longer effective. This transition occurred at $x/D = 1$ or at approximately $a/d = 1.5$. When uniform loads were considered, it was also found that the "shear proper" criterion expressed the ultimate shear strength of these beams without web reinforcement better than the "shear moment" criterion for the range of L/d considered, and that Eq. 6 could be used to express their strength, although somewhat conservatively.

It was shown for the beams tested dynamically that the dynamic flexural strength is proportional to the static flexural strength as a function of the reciprocal of the time to failure and could be expressed by Eq. 7. The dynamic strengths of beams failing in shear also seemed to be a function of the static strengths and the time to failure, and the trend of the data was considered to be expressed roughly by Eq. 8.

The susceptibility of a deep beam to failure in shear does not seem to present the problem that was envisioned at the beginning of this

investigation. For the beams tested in this study, shear failures occurred only in those beams in which the concrete strength was low (f'_c = 3000 psi), the steel percentage was fairly high (p = 1.67 and 2.58 percent) and the L/d ratios were low (L/d = 2). The cracking load and "shear-moment" criteria used to determine the shear strengths of conventional beams underestimated the ultimate strength of the beams failing in shear. The fact that several beams failed in shear at or near their flexural capacity and with large deflections before failure serves only to illustrate further that shear is not the problem in deep beams that it is in ordinary beams.

It was shown that all of the beams tested, both statically and dynamically, formed the typical "arch" prior to failure. This, combined with the fact that web reinforcement did not completely prevent the formation of the arch, and was virtually ineffective in increasing the resistance of the beams to the type of shear failure described, leads to the conclusion that a deep beam should not be considered as a "beam" but rather as an "arch". Consideration should then be given to preventing a premature "shear" failure of the "arch rib" above the support, in order to produce the more ductile type of flexural failure by crushing of the concrete at the "crown" or by the rupture of the tension "tie".

7. BIBLIOGRAPHY

1. Austin, W. J., and Egger, W., Untrauer, R. E., and Winemiller, J. R., "An Investigation of the Behavior of Deep Members of Reinforced Concrete and Steel", Civil Engineering Studies, Structural Research Series No. 187, Department of Civil Engineering, University of Illinois, Urbana, Illinois, January 1960, Chapter II.

2. Untrauer, R. E., "Behavior and Design of Deep Structural Members, Part 4; Dynamic Tests of Reinforced Concrete Deep Beams", Civil Engineering Studies, Structural Research Series No. 195, Department of Civil Engineering, University of Illinois, Urbana, Illinois, May 1960.

3. Untrauer, R. E., "Strength and Behavior in Flexure of Deep Reinforced Concrete Beams Under Static and Dynamic Loading", Ph.D. Thesis, University of Illinois, Urbana, Illinois, 1961.

4. Egger, W., "60 Kip Capacity Slow or Rapid Loading Apparatus", Civil Engineering Studies, Structural Research Series No. 187, Department of Civil Engineering, University of Illinois, Urbana, Illinois, June 1957.

5. Winemiller, J. R., Austin, W. J., and Siess, C. P., "Behavior and Design of Deep Structural Members, Part 2; Tests of Reinforced Concrete Deep Beams with Web and Compression Reinforcement", Civil Engineering Studies, Structural Research Series No. 193, Department of Civil Engineering. University of Illinois, Urbana, Illinois, August 1960.

6. de Paiva, H. A. R., and Austin, W. J., "Behavior and Design of Deep Structural Members, Part 3; Tests of Reinforced Concrete Deep Beams", Civil Engineering Studies, Structural Research Series No. 194, Department of Civil Engineering, University of Illinois, Urbana, Illinois, March 1960.

7. de Cossio, R. D., and Siess, C. P., "Behavior and Strength in Shear of Beams and Frames Without Web Reinforcement", ACI Journal, Vol. 31, No. 8, February 1960 (Proceedings Vol. 56), pp. 695-735.

8. Viest, I. M., Discussion of "Shear Strength of Lightweight Reinforced Concrete Beams", by J. A. Hanson, ACI Journal, Vol. 30, No. 9, March 1959 (Proceedings Vol. 55), pp. 1062-1064.

9. Moody, K. G., and Viest, I. M., "Shear Strength of Reinforced Concrete Beams, Part 4; Analytical Studies", ACI Journal, Vol. 26, No. 7, March 1955 (Proceedings Vol. 51) pp. 697-729.

10. Morrow, J., and Viest, I. M., "Shear Strength of Reinforced Concrete Frame Members Without Web Reinforcement", ACI Journal, Vol. 28, No. 9, March 1957 (Proceedings Vol. 53) pp. 833-869.

11. Laupa, A., Siess, C. P., and Newmark, N. M., "Strength in Shear of Reinforced Concrete Beams", Bulletin No. 428, University of Illinois, Engineering Experiment Station, March 1955.

12. Graf, O., "Versuche über die Widerstandsfähigkeit von Eisenbetonbalken gegen Abscheren", Deutscher Ausschuss für Eisenbeton, Heft 80, Berlin, 1935.

13. Bernaert, S., and Siess, C. P., "Strength in Shear of Reinforced Concrete Beams Under Uniform Load", Civil Engineering Studies, Structural Research Series No. 120, Department of Civil Engineering, University of Illinois, Urbana, Illinois, June 1956.

14. de Cossio, R. D., and Siess, C. P., "Development of Design Criteria for Reinforced Concrete Box Culverts, Part 1; Strength and Behavior of Reinforced Concrete Beams and Frames", Civil Engineering Studies, Structural Research Series No. 163, Department of Civil Engineering, University of Illinois, Urbana, Illinois, September 1958.

15. McHenry, Douglas and Shideler, J. J., "Review of Data on Effect of Speed in Mechanical Testing of Concrete", Bulletin D9, Portland Cement Association, Development Department, Chicago, Illinois, 1956.

16. Keenan, W. A., and Feldman, A., "Behavior and Design of Deep Structural Members, Part 6; The Yield Strength of Intermediate Grade Reinforcing Bars Under Rapid Loading", Civil Engineering Studies, Structural Research Series No. 197, Department of Civil Engineering, University of Illinois, Urbana, Illinois, March 1960.

17. Sozen, M. A., "Strength in Shear of Prestressed Concrete Beams Without Web Reinforcement", Ph.D. Thesis University of Illinois, Urbana, Illinois, 1957.

18. "Building Code Requirements for Reinforced Concrete (ACI 318-56)", ACI Journal, Vol. 27, No. 9, May 1956 (Proceedings Vol. 52).

TABLE 2.1 PROPERTIES OF TEST SPECIMENS

All beams: span = 24 in. c. to c. of supports, overall length = 28 in.

Beam Mark	L/d	Width b in.	Effective Depth d in.	Type of Test	f'_c psi	Tension Reinforcement: No. and Size	Tension Reinforcement: p	Tension Reinforcement: f_y ksi	Compression Reinforcement: No. and Size	Compression Reinforcement: p'	Compression Reinforcement: f'_y ksi	Ratio of web Rein. r*
G23S-11	2	2	12	Static	3560	1-#4	0.0083	45.7	1-#3	0.0046	48.9	0
D-11	"	"	"	Dynamic	"	"	"	"	"	"	"	0
D-12	"	"	"	"	"	"	"	"	"	"	"	0.0035
G23S-21	2	2	12	Static	3420	1-#3	0.0046	51.4	1-#2	0.0021	44.2	0
D-21	"	"	"	Dynamic	"	"	" "	"	"	"	"	0
D-22	"	"	"	"	"	"	"	"	"	"	"	0.0071
G24S-11	2	2	12	Static	5600	1-#4	0.0083	45.7	1-#3	0.0046	48.9	0
D-11	"	"	"	Dynamic	"	"	"	"	"	"	"	0
D-12	"	"	"	"	"	"	"	"	"	"	"	0.0071
G24S-21	2	2	12	Static	5240	1-#3	0.0046	51.4	1-#2	0.0021	44.2	0
D-21	"	"	"	Dynamic	"	"	" "	"	"	"	"	0
D-22	"	"	"	"	"	"	"	"	"	"	"	0.0071
G33S-11	3	3	8	Static	3380	2-#4	0.0167	47.3	2-#3	0.0092	51.5	0
D-11	"	"	"	Dynamic	"	"	"	"	"	"	"	0
S-12	"	"	"	Static	2890	"	"	"	"	"	"	0.0109
D-12	"	"	"	Dynamic	3380	"	"	"	"	"	"	"
G33S-21	3	3	8	Static	3050	1-#4	0.0083	45.2	1-#3	0.0046	50.5	0
D-21	"	"	"	Dynamic	"	"	"	"	"	"	"	0
D-22	"	"	"	"	"	"	"	"	"	"	"	0.0055
G33S-31	3	3	8	Static	2890	2-#5	0.0258	45.2	2-#3	0.0083	50.3	0
D-31	"	"	"	Dynamic	"	"	"	"	"	"	"	0
S-32	"	"	"	Static	2910	"	"	44.2	"	"	"	0.0109
D-32	"	"	"	Dynamic	"	"	"	"	"	"	"	"

TABLE 2.1 PROPERTIES OF TEST SPECIMENS (Cont'd)

Beam Mark	L/d	Width b in.	Effective Depth d in.	Type of Test	f'_c psi	Tension Reinforcement			Compression Reinforcement			Ratio of web Rein. r
						No. and Size	p	f_y ksi	No. and Size	p'	f'_y ksi	
G34S-11	3	3	8	Static	5100	2-#4	0.0167	47.2	2-#3	0.0083	51.2	0
D-11	"	"	"	Dynamic	"	"	"	"	"	"	"	0
D-12	"	"	"	"	"	"	"	"	"	"	"	0.0109
G34S-21	3	3	8	Static	4960	1-#4	0.0083	47.0	1-#3	0.0046	49.4	0
D-21	"	"	"	Dynamic	"	"	"	"	"	"	"	0
D-22	"	"	"	"	"	"	"	"	"	"	"	0.0055
G43S-11	4	4	6	Static	3510	2-#4	0.0167	44.1	2-#3	0.0092	50.8	0
D-11	"	"	"	Dynamic	"	"	"	"	"	"	"	0
D-12	"	"	"	"	"	"	"	"	"	"	"	0.0062
G44S-11	4	4	6	Static	5360	2-#4	0.0167	47.9	2-#3	0.0092	48.1	0
D-11	"	"	"	Dynamic	"	"	"	"	"	"	"	0
D-12	"	"	"	"	"	"	"	"	"	"	"	0.0082

* $r = \frac{A_w}{sb}$

TABLE 2.2 PROPERTIES OF THE CONCRETE MIXES

Beam Mark	Cement:Sand:Gravel by weight	Water/Cement Ratio by weight	Slump in.	Compressive Strength f'_c psi	Modulus of Rupture psi	Age at Test days
G23S-11	1:4.51:4.49	1.03	5 1/2	3560	500	15
D-11	"	"	"	"	"	"
D-12	"	"	"	"	"	"
G23S-21	1:4.47:4.49	1.05	5 1/2	3420	560	12
D-21	"	"	"	"	"	"
D-22	"	"	"	"	"	"
G24S-11	1:3.87:3.81	0.86	2	5600	580	35
D-11	"	"	"	"	"	"
D-12	"	"	"	"	"	"
G24S-21	1:3.95:3.81	0.77	1 1/4	5240	590	16
D-21	"	"	"	"	"	"
D-22	"	"	"	"	"	"
G33S-11	1:4.49:4.49	1.03	5 1/2	3380	510	13
D-11	"	"	"	"	"	"
S-12	1:4.51:4.58	1.00	4 1/2	2890	470	16
D-12	1:4.49:4.49	1.03	5 1/2	3380	510	13
G33S-21	1:4.49:4.49	1.05	7	3050	510	19
D-21	"	"	"	"	"	"
D-22	"	"	"	"	"	"
G33S-31	1:4.51:4.58	1.00	4 1/2	2890	470	16
D-31	"	"	"	"	"	"
S-32	1:4.48;4.50	1.05	5	2910	490	15
D-32	"	"	"	"	"	"
G34S-11	1:3.86:3.84	0.85	2 1/4	5100	760	76
D-11	"	"	"	"	"	"
D-12	"	"	"	"	"	"
G34S-21	1:4.04:3.80	0.71	1	4960	570	13
D-21	"	"	"	"	"	"
D-22	"	"	"	"	"	"
G43S-11	1:4.40:4.49	1.14	5 1/4	3510	500	14
D-11	"	"	"	"	"	"
D-12	"	"	"	"	"	"
G44S-11	1:3.89:3.81	0.83	1 3/4	3560	810	79
D-11	"	"	"	"	"	"
D-12	"	"	"	"	"	"

TABLE 2.3 PROPERTIES OF REINFORCING STEEL

Beam Mark	Tension Reinforcement*				Compression Reinforcement*			
	f_y	ϵ_y	ϵ_o	f_u	f'_y	ϵ'_y	ϵ'_o	f'_u
	ksi	%	%	ksi	ksi	%	%	ksi
G23S-11	45.7	0.170	1.49	77.0	48.9	0.178	1.63	77.0
D-11	"	"	"	"	"	"	"	"
D-12	"	"	"	"	"	"	"	"
G23S-21	51.4	0.180	1.63	80.0	44.2	0.157	--	67.9
D-21	"	"	"	"	"	"	--	"
D-22	"	"	"	"	"	"	--	"
G24S-11	45.7	0.170	1.49	77.0	48.9	0.178	1.63	77.0
D-11	"	"	"	"	"	"	"	"
D-12	"	"	"	"	"	"	"	"
G24S-21	51.4	0.180	1.63	80.0	44.2	0.157	--	67.9
D-21	"	"	"	"	"	"	--	"
D-22	"	"	"	"	"	"	--	"
G33S-11	47.3	0.152	1.52	78.5	51.5	0.178	1.54	79.7
D-11	"	"	"	"	"	"	"	"
S-12	"	"	"	"	"	"	"	"
D-12	"	"	"	"	"	"	"	"
G33S-21	45.2	0.155	1.78	73.0	50.5	0.170	1.38	76.7
D-21	"	"	"	"	"	"	"	"
D-22	"	"	"	"	"	"	"	"
G33S-31	45.2	0.170	1.56	72.8	50.3	0.178	1.45	80.0
D-31	"	"	"	"	"	"	"	"
S-32	44.2	0.162	1.46	70.0	"	"	"	"
D-32	"	"	"	"	"	"	"	"
G34S-11	47.2	0.162	1.63	76.7	51.2	0.173	1.64	80.7
D-11	"	"	"	"	"	"	"	"
D-12	"	"	"	"	"	"	"	"
G34S-21	47.0	0.162	1.51	76.8	49.4	0.165	1.38	76.0
D-21	"	"	"	"	"	"	"	"
D-22	"	"	"	"	"	"	"	"
G43S-11	44.1	0.148	1.46	74.6	50.8	0.170	0.45	79.1
D-11	"	"	"	"	"	"	"	"
D-12	"	"	"	"	"	"	"	"

TABLE 2.3 PROPERTIES OF REINFORCING STEEL (Cont'd)

Beam Mark	Tension Reinforcement*				Compression Reinforcement*			
	f_y	ϵ_y	ϵ_o	f_u	f'_y	ϵ'_y	ϵ'_o	f'_u
	ksi	%	%	ksi	ksi	%	%	ksi
G44S-11	47.9	0.150	1.40	78.8	48.1	0.160	1.67	75.5
D-11	"	"	"	"	"	"	"	"
D-12	"	"	"	"	"	"	"	"

*
f_y and f'_y = yield point stress
ϵ_y and ϵ'_y = yield point strain
ϵ_o and ϵ'_o = strain at beginning of strain hardening
f_u and f'_u = ultimate stress

TABLE 4.1 SUMMARY OF STATIC TEST RESULTS

Beam Mark	L/d	Duration of Test Minutes	Yield Load P_y kip	Ultimate Load P_u kip	Yield Deflection Δ_y in.	Ultimate Deflection Δ_u in.	$\frac{\Delta_u}{\Delta_y}$	Mode of Failure
Beams without Web Reinforcement								
G23S-11	2	1.6	27.7	40.4	0.035	0.98	28.0	Flexure-Shear
G23S-21	2	1.1	16.9	24.0	0.028	0.96	34.0	Flexure
G24S-11	2	1.4	27.8	40.8	0.042	1.37	33.0	Flexure
G24S-21	2	0.9	16.8	22.6	0.035	1.21	35.0	Flexure
G33S-11	3	1.2	36.0	38.4	0.070	0.31	4.4	Shear
G33S-21	3	1.9	17.5	24.5	0.045	1.92	43.0	Flexure
G33S-31	3	1.8	46.5	48.1	0.068	0.94	1.4	Shear
G34S-11	3	1.0	37.5	49.4	0.056	1.16	21.0	Flexure-Shear
G34S-21	3	1.2	19.4	25.2	0.044	1.21	28.0	Flexure
G43S-11	4	1.3	26.6	34.6	0.062	0.91	15.0	Flexure-Shear
G44S-11	4	1.1	29.7	37.6	0.068	1.47	22.0	Flexure-Shear
Beams with Web Reinforcement								
G33S-12	3	1.9	36.0	38.0	0.068	0.21	3.1	Shear
G33S-32	3	2.3	43.8	45.6	0.064	0.09	1.5	Shear

TABLE 4.2 MAXIMUM MEASURED CONCRETE STRAINS

STATIC TESTS

Beam Mark	Compressive Strength of Concrete f'_c psi	Maximum Measured Concrete Strain ϵ_c	Mode of Failure
	Beams without Web Reinforcement		
G23S-11	3560	0.0053	Flexure-Shear
G23S-21	3420	0.0070	Flexure
G24S-11	5600	0.0072	Flexure
G24S-21	5240	0.0092	Flexure
G33S-11	3380	0.0047	Shear
G33S-21	3050	0.0060	Flexure
G33S-31	2890	0.0017	Shear
G34S-11	5100	0.0032	Flexure-Shear
G34S-21	4960	0.0060	Flexure
G43S-11	3510	0.0044	Flexure-Shear
G44S-11	5360	0.0046	Flexure-Shear
	Beams with Web Reinforcement		
G33S-12	2890	0.0040	Shear
G33S-32	2910	0.0010	Shear

TABLE 4.3 TEST RESULTS, UNTRAUER'S BEAMS

Beam Mark	L/d	Concrete Strength f'_c psi	Tension Steel p %	Compression Steel p' %	Web Steel r %	Yield Load P_y kips	Ultimate Load P_u kips	Yield Deflection Δ_y in.	Ultimate Deflection Δ_u in.	Mode of Failure
F2S1	2	4920	0.83	0.46	1.42	29.3	43.3	0.036	0.95	F
F2S2	2	4600	1.29	0.46	1.42	42.5	55.1	0.048	0.52	S
F3S2	3	3530	0.83	0.46	0.94	20.5	27.6	0.061	1.58	F
F3S3	3	4980	1.67	0.92	1.31	40.6	54.6	0.058	1.38	F-S
F4S1	4	4970	0.83	0.46	0.70	14.7	21.2	0.043	1.67	F
F4S22	4	5030	1.67	0.92	0.98	29.5	41.0	0.059	1.88	F

TABLE 4.4 COMPARISON OF MEASURED AND COMPUTED LOADS FOR THE STATIC TESTS

Beam Mark	L/d	Test P_y kip	Theoretical P'_y kip	$\frac{P_y}{P'_y}$	Test P_u kip	Theoretical P'_u kip	$\frac{P_u}{P'_u}$	Mode of Failure
			Beams without Web Reinforcement					
G23S-11	2	27.7	24.9	1.07	40.4	40.7	0.99	Flexure-Shear
G23S-21	2	16.9	15.6	1.08	24.0	24.7	0.97	Flexure
G24S-11	2	27.8	25.0	1.11	40.8	42.1	0.97	Flexure
G24S-21	2	16.8	15.7	1.07	22.6	24.9	0.91	Flexure
G33S-11	3	36.0	33.6	1.07	38.4	46.6	0.82	Shear
G33S-21	3	17.5	16.3	1.07	24.5	25.2	0.97	Flexure
G33S-31	3	46.5	48.2	0.96	48.1	59.9	0.83	Shear
G34S-11	3	37.5	33.3	1.12	49.4	48.7	1.01	Flexure-Shear
G34S-21	3	19.4	17.0	1.14	25.2	26.8	0.94	Flexure
G43S-11	4	26.6	23.1	1.15	34.6	33.0	1.05	Flexure-Shear
G44S-11	4	29.7	25.3	1.17	37.6	35.2	1.07	Flexure-Shear
			Beams with Web Reinforcement*					
G33S-12	3	36.0	33.3	1.08	38.0	45.8	0.83	Shear
G33S-32	3	43.8	47.4	0.96	45.6	55.6	0.82	Shear

* r = 1.09 percent

TABLE 4.5 SUMMARY OF CRACKING LOAD CALCULATIONS

Beam Mark	a/d	Cylinder Strength f'_c psi	Cracking Load P_c comp. kip	Ultimate Load P_u meas. kip	$\frac{P_u}{P_c}$	Mode of Failure
(1)	(2)	(3)	(4)	(5)	(6)	(7)
		Beams without Web Reinforcement				
G23S-11	0.67	3560	11.70	40.4	3.46	F-S
G23S-21	0.67	3420	9.04	24.0	2.66	F
G24S-11	0.67	5600	13.16	40.8	3.10	F
G24S-21	0.67	5240	10.50	22.6	1.35	F
G33S-11	1.00	3380	13.32	38.4	2.88	S
G33S-21	1.00	3050	9.70	24.5	2.52	F
G33S-31	1.00	2890	16.96	48.1	2.84	S
G34S-11	1.00	5100	14.70	49.4	3.36	F-S
G34S-21	1.00	4960	10.84	25.2	2.32	F
G43S-11	1.67	3510	11.62	34.6	2.98	F-S
G44S-11	1.67	5360	13.00	37.6	2.89	F-S
		Beams with Web Reinforcement *				
G33S-12	1.00	2890	12.90	38.0	2.94	S
G33S-32	1.00	2910	16.96	45.6	2.69	S

* r = 1.09 percent

TABLE 4.6 CRACKING LOAD COMPUTATIONS - UNTRAUER'S BEAMS

$bd = 24$ in.^{2} $a = 8$ in. $L = 24$ in.

Beam Mark	a/d	p	r	f'_c	P_c comp.	P_u meas.	$\frac{P_u}{P_c}$	Mode of Failure
		%	%	psi	kip	kip		
			Beams with Web Reinforcement					
F2S1	0.67	0.83	1.42	4920	12.70	43.3	3.41	F
F2S2	0.67	1.29	1.42	4600	15.50	55.1	3.56*	S
F3S2	1.00	0.83	0.94	3530	9.74	27.6	2.84	F
F3S3	1.00	1.67	1.31	4980	14.64	54.6	3.73*	F-S
F4S1	1.33	0.83	0.70	4970	9.98	21.2	2.12	F
F4S22	1.33	1.67	0.98	5030	12.90	41.0	3.18*	F

* The points plotted on Figure 4.12

TABLE 4.7 COMPARISON OF MEASURED AND COMPUTED ULTIMATE LOADS BY EQUATION 2

Beam Mark	L/d	f'_c psi	k	np'	Theor. p_s kip	Test P_u kip	$\frac{P_u}{P_s}$	Mode of Failure
			Beams without Web Reinforcement					
G23S-21	2	3420	0.238	0.0187	26.3	24.0	0.91	F
G24S-11	2	5600	0.281	0.0358	40.6	40.8	1.01	F
G24S-21	2	5240	0.227	0.0166	24.8	22.6	0.91	F
G33S-21	3	3050	0.303	0.0427	21.9	24.5	1.12	F
G34S-21	3	4960	0.287	0.0369	26.8	25.2	0.94	F
G23S-11	2	3560	0.294	0.0405	24.6	40.4	1.64	F-S
G34S-11	3	5100	0.366	0.0732	36.5	49.4	1.35	F-S
G43S-11	4	3510	0.382	0.0814	24.1	34.6	1.44	F-S
G44S-11	4	3560	0.368	0.0724	23.2	37.6	1.62	F-S
G33S-11	3	3380	0.346	0.0824	29.0	38.4	1.32	S
G33S-31	3	2890	0.455	0.0871	33.1	48.1	1.46	S
			Beams with Web Reinforcement					
G33S-12	3	2890	0.385	0.0871	30.0	38.0	1.27	S
G33S-32	3	2910	0.456	0.0868	33.6	45.6	1.36	S

TABLE 4.8 COMPARISON OF MEASURED AND COMPUTED ULTIMATE LOADS BY EQUATION 2, UNTRAUER'S BEAMS

Beam Mark	L/d	f'_c	k	np'	Theor. P_s	Test P_u	$\frac{P_u}{P_s}$	Mode of Failure
		psi			kip	kip		
F2S1	2	4920	0.286	0.0391	40.2	43.3	1.08	F
F2S2	2	4600	0.346	0.0375	46.1	55.1	1.20	S
F3S2	3	3530	0.298	0.0391	27.8	27.6	0.99	F
F3S3	3	4980	0.366	0.0736	36.3	54.6	1.50	F-S
F4S1	4	4970	0.291	0.0369	20.3	21.2	1.04	F
F4S22	4	5030	0.344	0.0781	26.3	41.0	1.56	F

TABLE 4.9 COMPARISON OF MEASURED AND COMPUTED ULTIMATE LOADS BY EQUATIONS 4 AND 5

Beam Mark	f'_c psi	b in.	D in.	x in.	P'_s kip	P_u kip	$\frac{P_u}{P'_s}$	Mode of Failure
				Beams without Web Reinforcement				
G23S-11	3560	2	13	4	58.2	40.4	0.70	F-S
G23S-21	3420	2	13	4	50.5	24.0	0.48	F
G24S-11	5600	2	13	4	78.0	40.8	0.52	F
G24S-21	5240	2	13	4	68.6	22.6	0.33	F
G33S-11	3380	3	9	4	71.3	38.4	0.54	S
G33S-21	3050	3	9	4	55.1	24.5	0.44	F
G33S-31	2890	3	9	4	75.5	48.1	0.64	S
G34S-11	5100	3	9	4	89.1	49.4	0.55	F-S
G34S-21	4960	3	9	4	74.5	25.2	0.34	F
G43S-11	3510	4	7	4	74.5	34.6	0.46	F-S
G44S-11	3560	4	7	4	75.0	37.6	0.50	F-S
				Beams with Web Reinforcement				
G33S-12	2890	3	9	4	66.5	38.0	0.57	S
G33S-32	2910	3	9	4	75.5	45.6	0.60	S

TABLE 4.10 COMPARISON OF MEASURED AND COMPUTED ULTIMATE LOADS BY EQUATIONS 4 AND 5, UNTRAUER'S BEAMS

Beam Mark	f'_c psi	b in.	D in.	x in.	P'_s kip	P_u kip	$\frac{P_u}{P'_s}$	Mode of Failure
F2S1	4920	2	13	4	71.8	43.3	0.60	F
F2S2	4600	2	13	4	73.3	55.1	0.75	S
F3S2	3530	3	9	4	59.9	27.6	0.46	F
F3S3	4980	3	9	4	88.0	54.6	0.62	F-S
F4S1	4970	4	7	4	76.7	21.2	0.28	F
F4S22	5030	4	7	4	90.8	41.0	0.45	F

TABLE 4.11 COMPARISON OF MEASURED AND COMPUTED ULTIMATE LOADS FOR UNIFORMLY LOADED BEAMS BY EQUATION 2

b = 4.5 in. L = 36 in.

Beam Mark	L/d	f'_c psi	P_s* kip	P_u kip	$\frac{P_u}{P_s}$	Mode of Failure
D10	1.0	4090	340	253	0.74	F
D12	1.2	4300	318	264	0.83	F-S
D15	1.5	3550	207	215	1.04	F-S
D20	2.0	3910	138	153	0.90	F
D20-1	2.0	4340	204	251	1.23	F-S
D20-2	2.0	5030	161	187	1.16	F
D30	3.0	2700	60.2	63	1.05	S-C
D30-1	3.0	3980	83.7	90	1.08	F
D40	4.0	2730	33.2	36	1.08	F
D60	6.0	3410	16.4	16	0.98	F

* P_s for M_s at M/Vd = 4.5

TABLE 4.12 COMPARISON OF MEASURED AND COMPUTED ULTIMATE LOADS UNIFORMLY LOADED BEAMS BY MODIFIED EQUATION 2

b = 4.5 in. L = 36 in.

Beam Mark	L/d	f'_c psi	P_s** kip	P_u kip	$\frac{P_u}{P_s}$	Mode of Failure
D10	1.0	4090	515	253	0.49	F
D12	1.2	4300	480	264	0.55	F-S
D15	1.5	3550	313	215	0.69	F-S
D20	2.0	3910	207	153	0.74	F
D20-1	2.0	4340	306	251	0.82	F-S
D20-2	2.0	5030	242	187	0.77	F
D30	3.0	2700	89	63	0.71	S-C
D30-1	3.0	3980	124	90	0.73	F
D40	4.0	2730	48	36	0.74	F
D60	6.0	3410	22	16	0.71	F

** P_s for M_s at L/3

TABLE 4.13 COMPARISON OF MEASURED AND COMPUTED ULTIMATE LOADS FOR UNIFORMLY LOADED BEAMS BY EQUATIONS 4 AND 5

b = 4.5 in. L = 36 in.

Beam Mark	f'_c psi	L' in.	D in.	x in.	P'_s kip	P_u kip	$\frac{P_u}{P'_s}$	Mode of Failure
D10	4090	24	37.75	6.00	347	253	0.73	F
D12	4300	24	31.81	6.00	315	264	0.84	F-S
D15	3550	27	25.81	6.75	228	215	0.94	F-S
D20	3910	27	19.81	6.75	192	153	0.80	F
D20-1	4340	24	20.56	6.00	252	251	1.00	F-S
D20-2	5030	27	19.81	6.75	248	187	0.75	F
D30	2700	30	13.81	7.50	114	63	0.55	S
D30-1	3980	30	13.81	7.50	161	90	0.56	F
D40	2730	30	10.75	7.50	86	36	0.42	F
D60	3410	30	7.69	7.50	68	16	0.24	F

TABLE 4.14 COMPARISON OF MEASURED AND COMPUTED MIDSPAN MOMENTS FOR UNIFORMLY LOADED BEAMS OF REFERENCE 13 BY EQUATION 2

Beam Mark	L/d	Comp. M_s in. kip	Meas. M_u in. kip	$\frac{M_u}{M_s}$
D-1	11.07	485	626	1.30
D-2	11.07	513	744	1.45
D-3	13.28	489	761	1.55
D-5	6.07	384	498	1.30
D-6	11.07	426	702	1.65
D-7	11.07	381	652	1.71
D-8	11.07	505	829	1.64
D-9	8.85	382	566	1.48
D-10	8.85	441	625	1.42
D-11	8.85	516	795	1.54
D13	11.07	247	367	1.49
D14	8.85	309	487	1.57
D15	3.85	295	466	1.58
D16	8.85	324	574	1.77
D17	11.07	322	447	1.37
D-18	15.59	475	691	1.46

TABLE 5.1 SUMMARY OF DYNAMIC TEST LOADING INFORMATION

Beam Mark	Applied Load Level P_{dyn} kips	Peak Load Test P_{yd} kip	Yield Load of Static Companion P_y kip	$\frac{P_{dyn}}{P_y}$	Rise Time to Max. Load ms.
(1)	(2)	(3)	(4)	(5)	(6)
G23D-11	51.0	59.8	27.7	1.84	2.6
G23D-12	50.0	58.4		1.81	2.3
G23D-21	41.3	50.4	16.9	2.45	2.2
G23D-22	41.3	51.2		2.45	1.8
G24D-11	50.5	62.4	27.8	1.82	2.1
G24D-12	49.5	67.1		1.78	2.3
G24D-21	38.0	50.3	16.8	2.26	2.2
G24D-22	41.6	59.0		2.48	1.8
G33D-11	51.5	53.3	36.0	1.43	2.9
G33D-12	51.3	59.3		1.42	3.4
G33D-21	28.6	35.9	17.5	1.63	2.6
G33D-22	28.4	33.7		1.62	3.7
G33D-31	50.3	71.8	46.5	1.08	4.1
G33D-32	50.9	64.8		1.10	2.8
G34D-11	50.8	63.2	37.5	1.36	2.9
G34D-12	49.2	63.2		1.31	4.0
G34D-21	29.6	37.0	19.4	1.53	2.1
G34D-22	27.0	39.1		1.39	2.4
G43D-11	50.4	51.0	26.6	1.89	3.2
G43D-12	50.5	50.6		1.90	3.9
G44D-11	42.0	49.6	29.7	1.42	3.3
G44D-12	41.4	49.6		1.39	4.0

TABLE 5.2 SUMMARY OF TEST RESULTS

Beam Mark	L/d	r*	P_{yd} kip	P_{ud} kip	Δ_{yd} in.	Δ_{ud} in.	Mode of Failure	Mode of Failure of Static Companion
G23D-11	2	0	59.8	46.9	0.085	1.56	F-S (b)**	F-S
G23D-12		0.0035	58.4	44.7	0.090	0.16	S	
G23D-21	2	0	50.4	31.7	0.070	1.29	F (b)	F
G23D-22		0.0071	51.2	33.3	0.101	0.74	F (b)	
G24D-11	2	0	62.4	46.6	0.096	1.42	F-S	F
G24D-12		0.0071	67.1	44.7	0.071	1.06	F (b)	
G24D-21	2	0	50.3	30.9	0.065	1.58	F (b)	F
G24D-22		0.0071	59.0	34.4	0.074	0.58	F (b)	
G33D-11	3	0	53.3	43.0	0.123	0.170	S	S
G33D-12		0.0109	59.3	47.5	0.117	0.236	S	
G33D-21	3	0	35.9	28.8	0.063	2.19	F (b)	F
G33D-22		0.0055	33.7	28.2	0.102	1.67	F (b)	
G33D-31	3	0	71.8	49.3	0.116	0.167	S	S
G33D-32		0.0109	64.8	58.2	0.107	0.134	S	
G34D-11	3	0	63.2	54.4	0.108	1.17	F-S	F-S
G34D-12		0.0109	63.2	54.4	0.108	1.09	F	
G34D-21	3	0	37.0	28.5	0.058	2.02	F (b)	F
G34D-22		0.0055	39.1	28.5	0.075	1.81	F (b)	
G43D-11	4	0	51.0	45.4	0.151	1.93	F-S	F-S
G43D-12		0.0062	50.6	45.6	0.117	1.40	F-S	
G44D-11	4	0	49.6	42.8	0.114	1.21	F	F-S
G44D-12		0.0082	49.6	42.5	0.103	1.83	F	

* r = ratio of web reinforcement

** (b) = rupture of tension reinforcement

TABLE 5.3 MAXIMUM MEASURED CONCRETE STRAINS

DYNAMIC TESTS

Beam Mark	Compressive Strength of Concrete f'_c psi	Maximum Concrete Strain ϵ_c	Mode of Failure
G23D-11	3560	0.0042	F-S
G23D-12	"	0.0071	S
G23D-21	3420	0.0089	F
G23D-22	"	0.0074	F
G24D-11	5600	0.0082	F-S
G24D-12	"	0.0050	F
G24D-21	5240	0.0064	F
G24D-22	"	0.0042	F
G33D-11	3380	0.0050	S
G33D-12	"	0.0050	S
G33D-21	3050	0.0058	F
G33D-22	"	0.0090	F
G33D-31	2890	0.0074	S
G33D-32	2910	0.0016	S
G34D-11	5100	0.0046	F-S
G34D-12	"	0.0055	F
G34D-21	4960	0.0062	F
G34D-22	"	0.0045	F
G43D-11	3510	0.0052	F-S
G43D-12	"	0.0044	F-S
G44D-11	3560	0.0056	F
G44D-12	"	0.0062	F

TABLE 5.4 SUMMARY OF DYNAMIC LOAD ANALYSIS

Beam Mark	Meas. P_u kip	Meas. P_{ud} kip	$\frac{P_{ud}}{P_u}$	t_f ms.	Mode of Failure
G23D-11	40.4	46.9	1.16	16.4	F-S
G23D-12		44.7	1.11	4.8	S
G23D-21	24.0	31.7	1.32	13.0	F
G23D-22		33.3	1.39	9.5	F
G24D-11	40.8	46.6	1.14	18.1	F-S
G24D-12		44.7	1.09	15.2	F
G24D-21	22.6	30.9	1.34	15.4	F
G24D-22		34.4	1.52	8.6	F
G33D-11	38.4	43.0	1.12	4.2	S
G33D-12		47.5	1.26	10.6	S
G33D-21	24.5	28.8	1.18	30.1	F
G33D-22		28.2	1.15	28.9	F
G33D-31	48.1	49.3	1.02	10.7	S
G33D-32		58.2	1.21	4.8	S
G34D-11	49.4	54.4	1.10	17.5	F-S
G34D-12		54.4	1.10	29.5	F
G34D-21	25.2	28.5	1.13	28.5	F
G34D-22		28.5	1.13	27.7	F
G43D-11	34.6	45.4	1.31	15.7	F-S
G43D-12		45.6	1.32	14.5	F-S
G44D-11	37.6	42.8	1.14	18.2	F
G44D-12		42.5	1.13	27.9	F

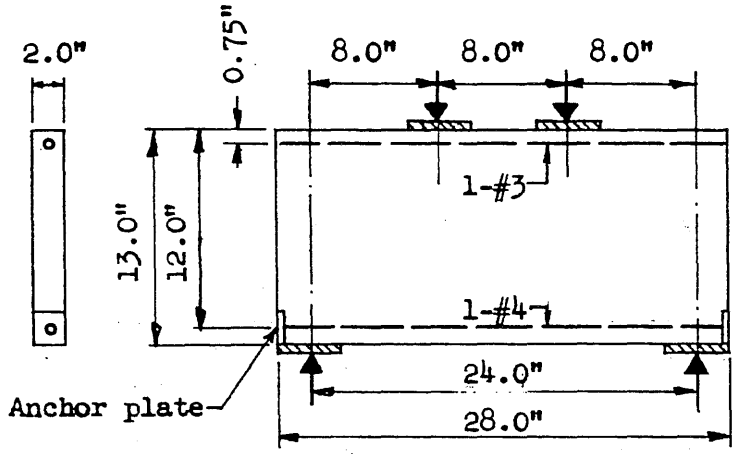

BEAMS

G23S-11
G23D-11
G24S-11
G24D-11

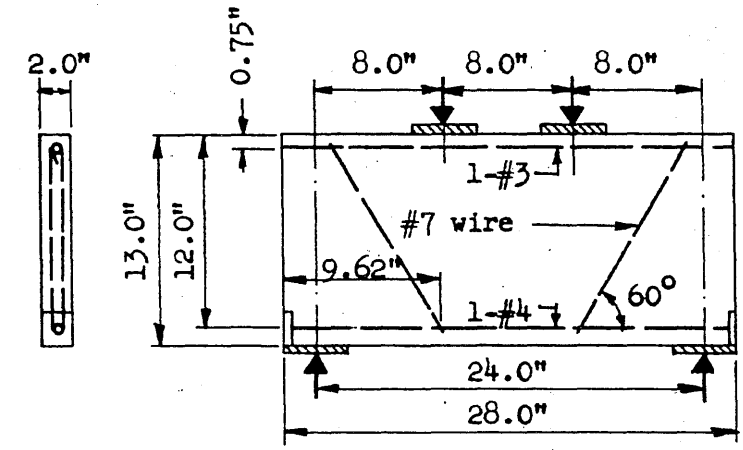

BEAM

G23D-12

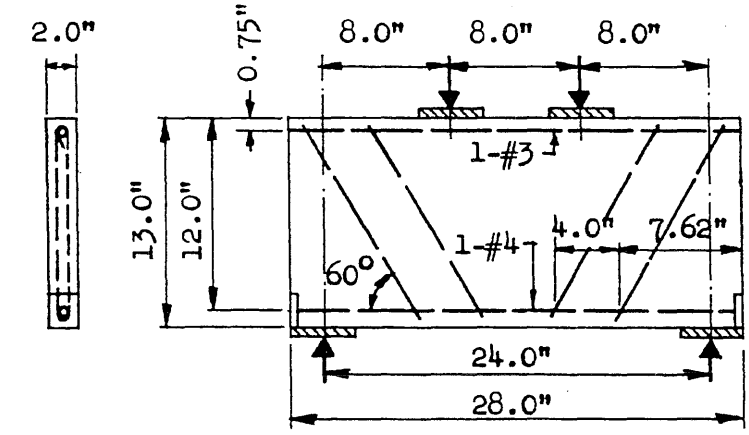

BEAM

G24D-12

FIG. 2.1a DETAILS AND DIMENSIONS OF TEST SPECIMENS

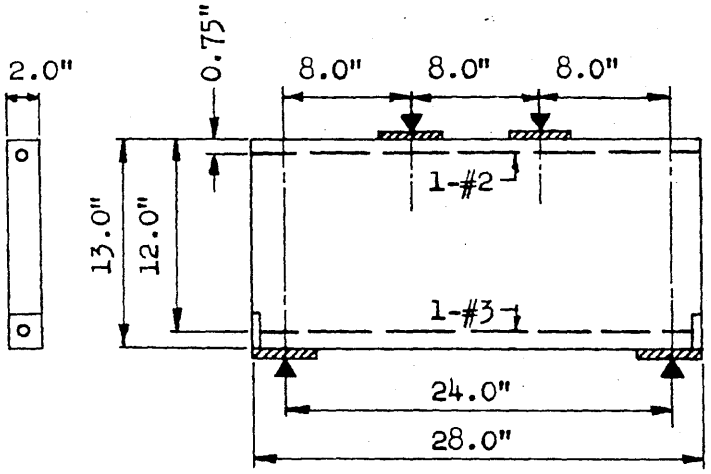

BEAMS

G23S-21
G23D-21
G24S-21
G24D-21

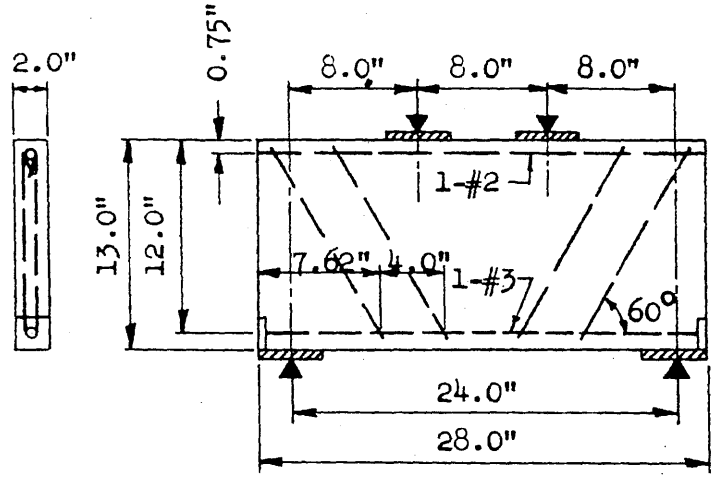

BEAMS

G23D-22
G24D-22

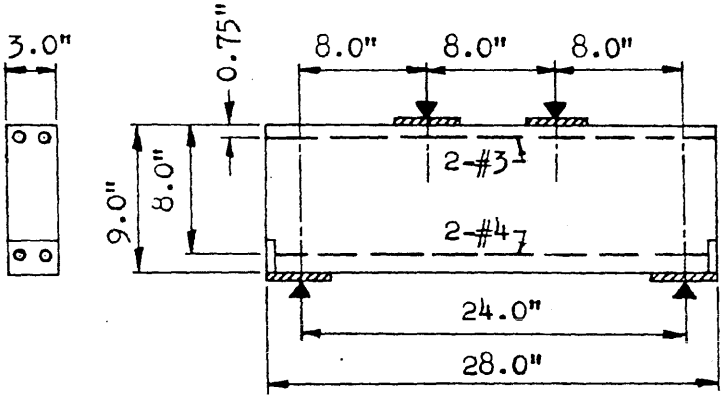

BEAMS

G33S-11
G33D-11
G34S-11
G34D-11

FIG. 2.1b DETAILS AND DIMENSIONS OF TEST SPECIMENS

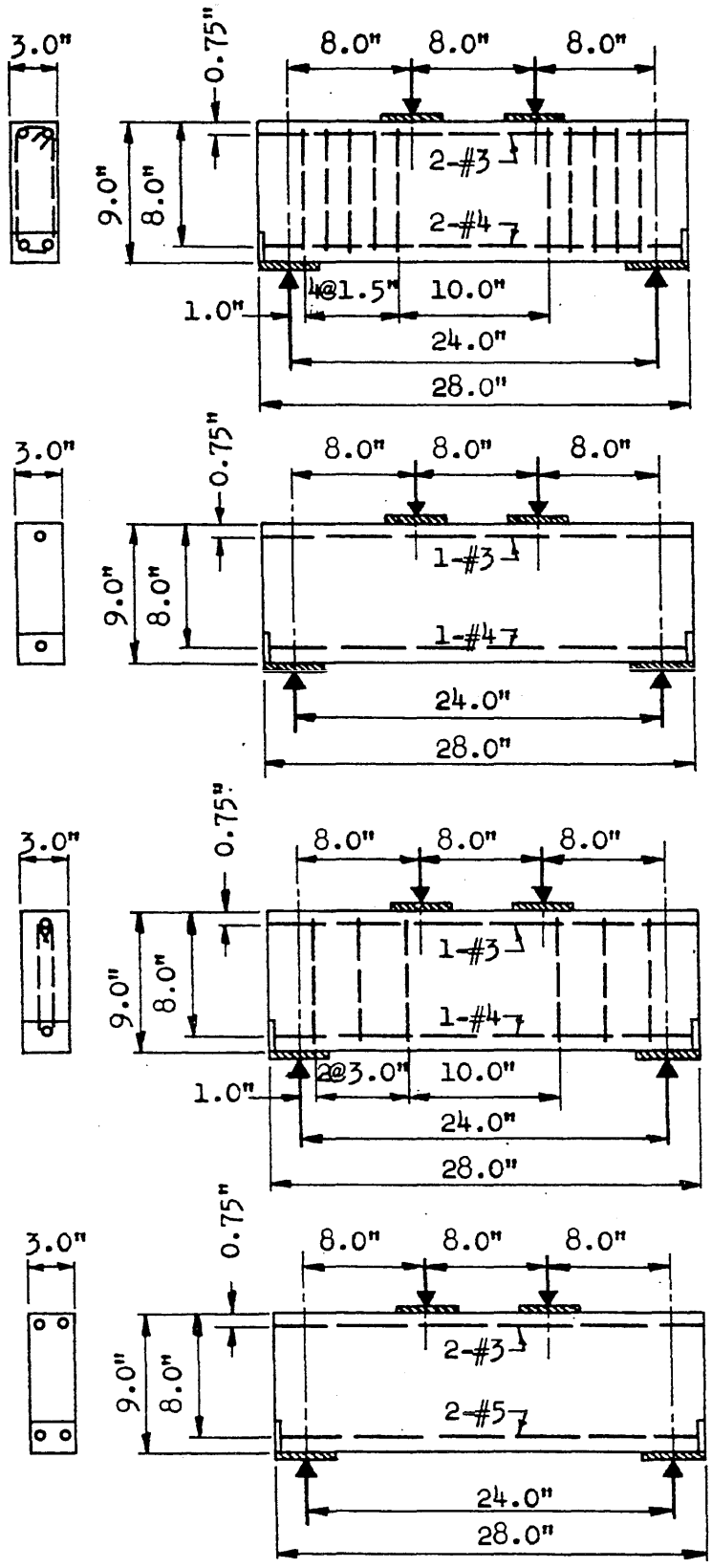

FIG. 2.1c DETAILS AND DIMENSIONS OF TEST SPECIMENS

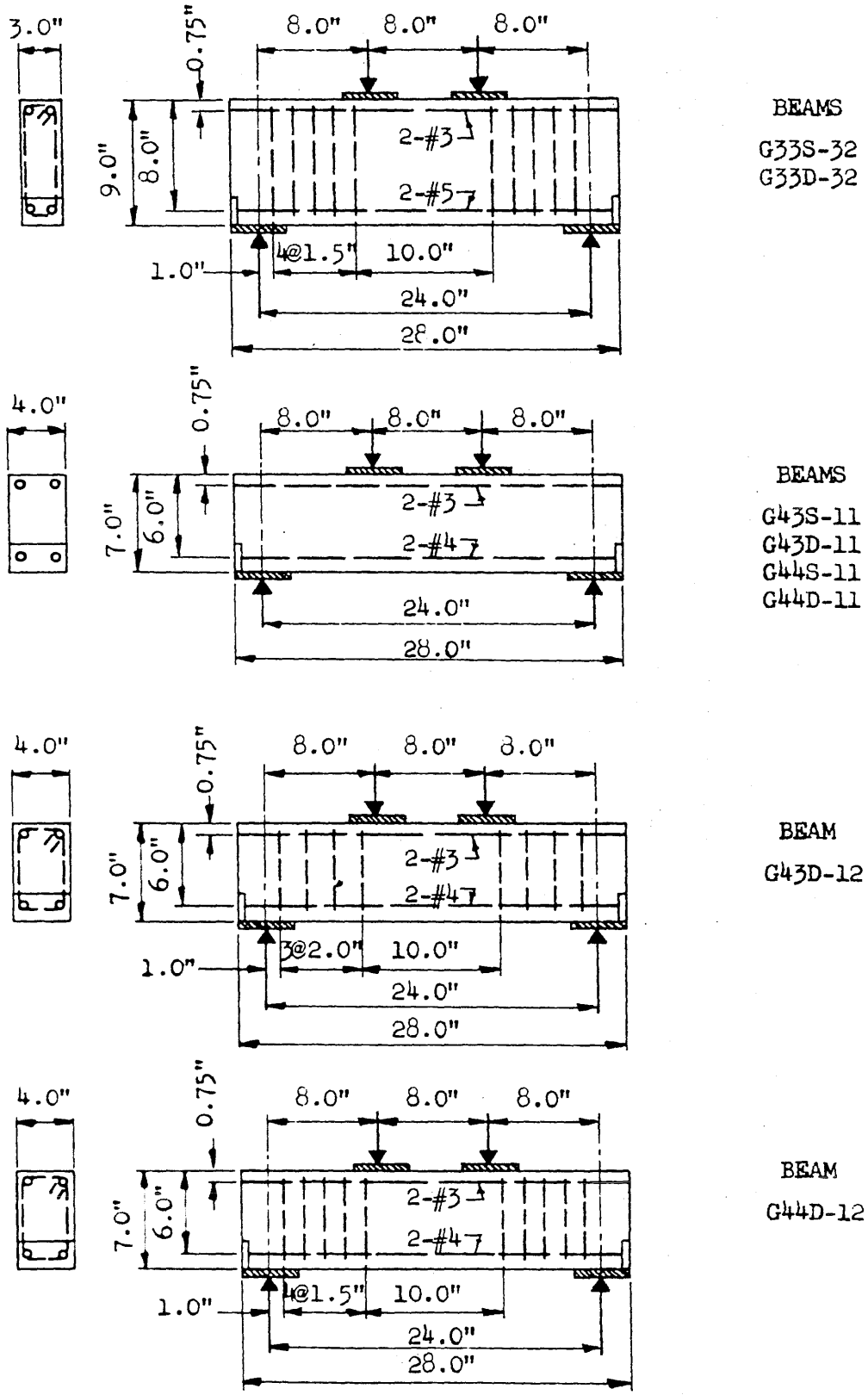

FIG. 2.1d DETAILS AND DIMENSIONS OF TEST SPECIMENS

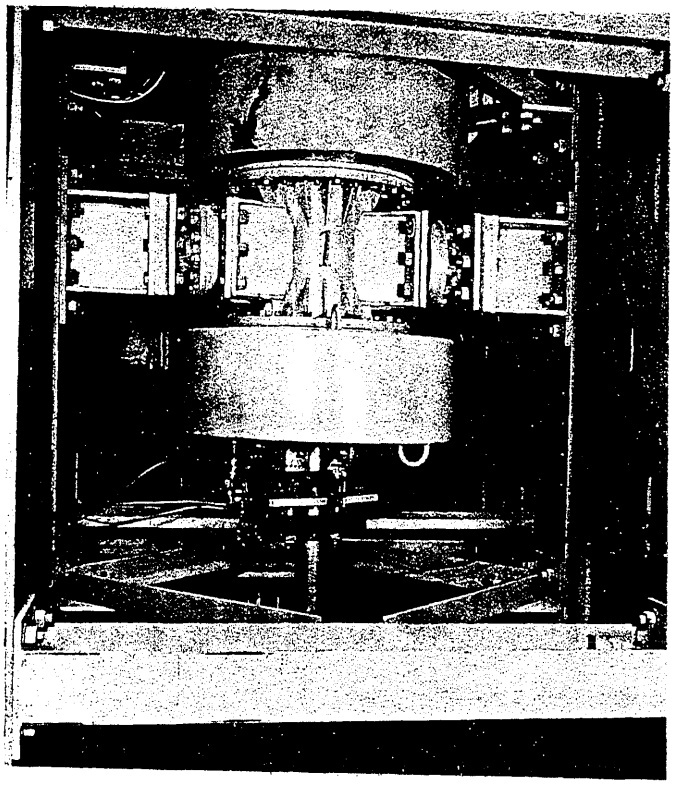

(a) 60 Kip Pneumatic Loading Device

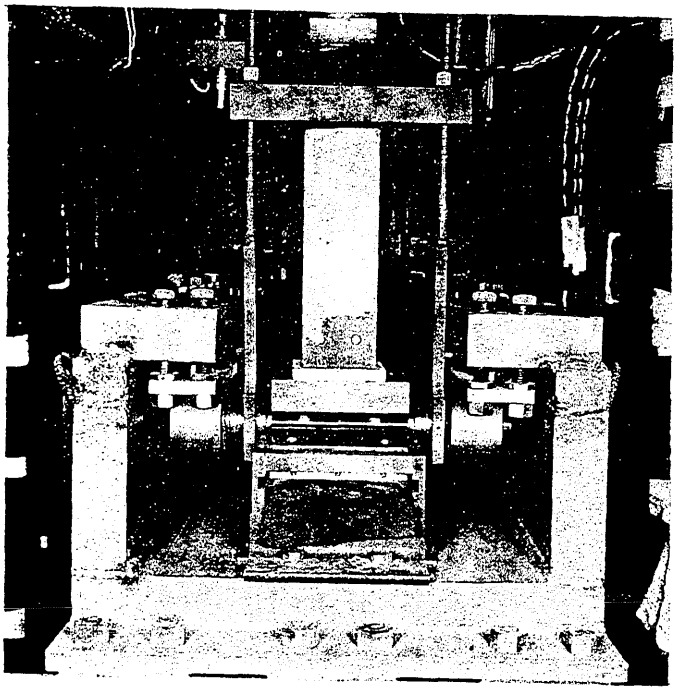

(b) End View of Reaction System

FIG. 3.1 PHOTOGRAPHS OF TEST EQUIPMENT

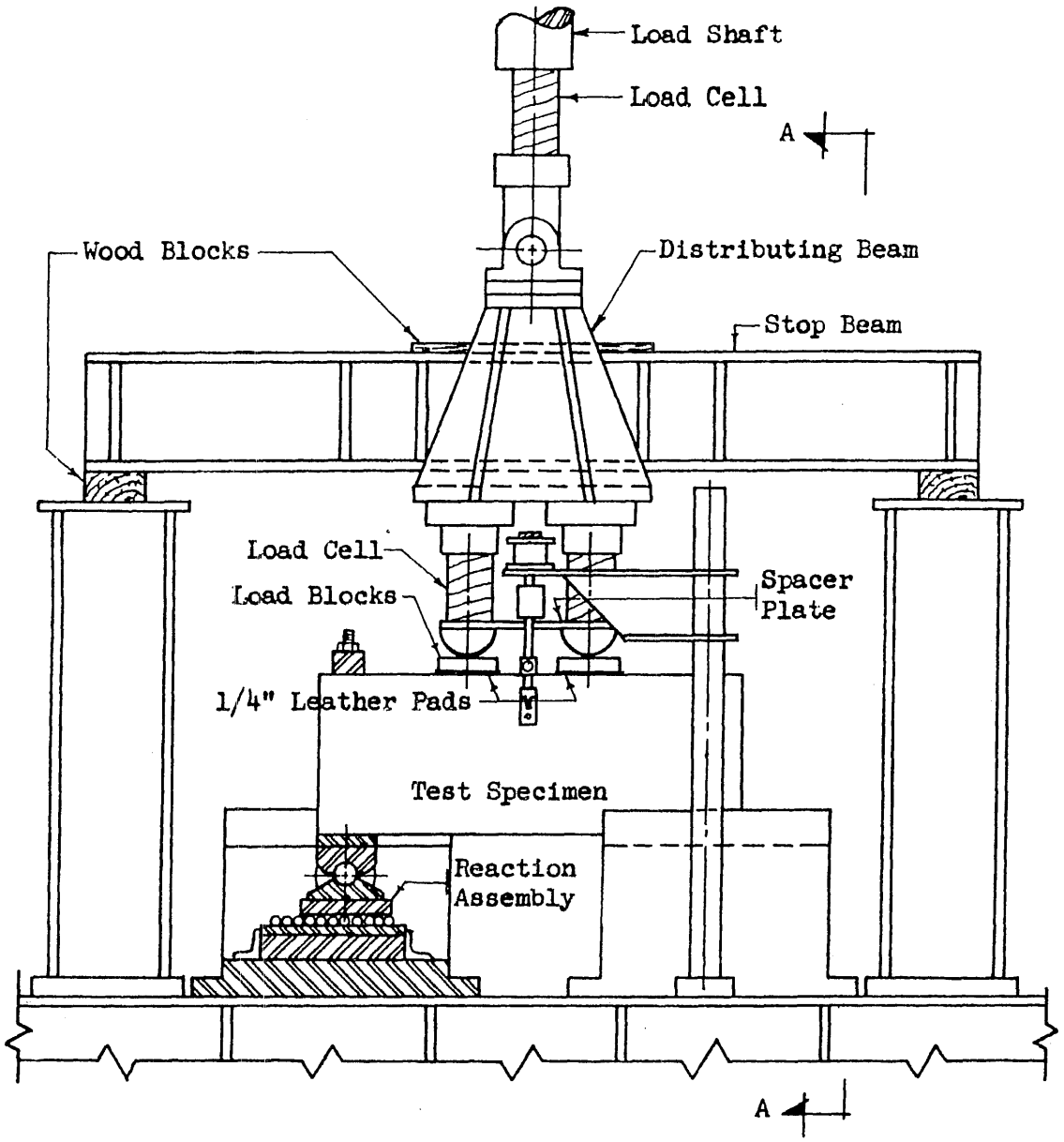

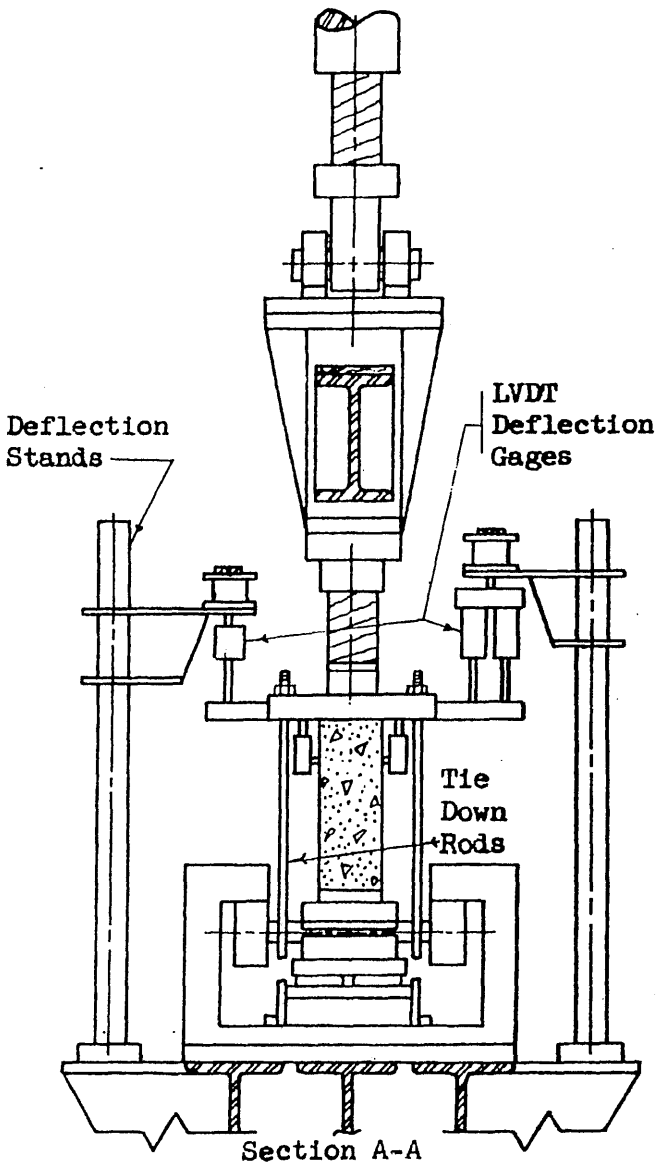

FIG. 3.2 TEST SETUP

(a) Test Frame

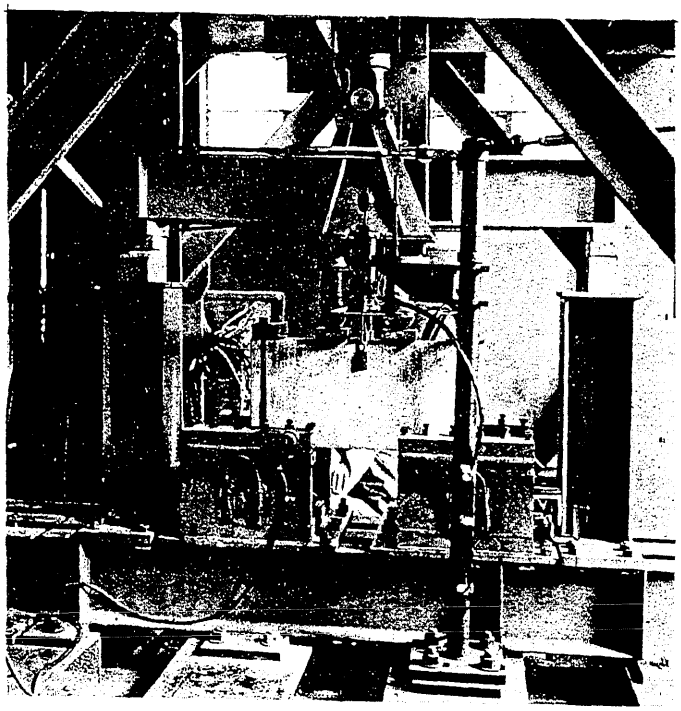

(b) Test Setup

FIG. 3.3 PHOTOGRAPHS OF TEST FRAME AND TEST SETUP

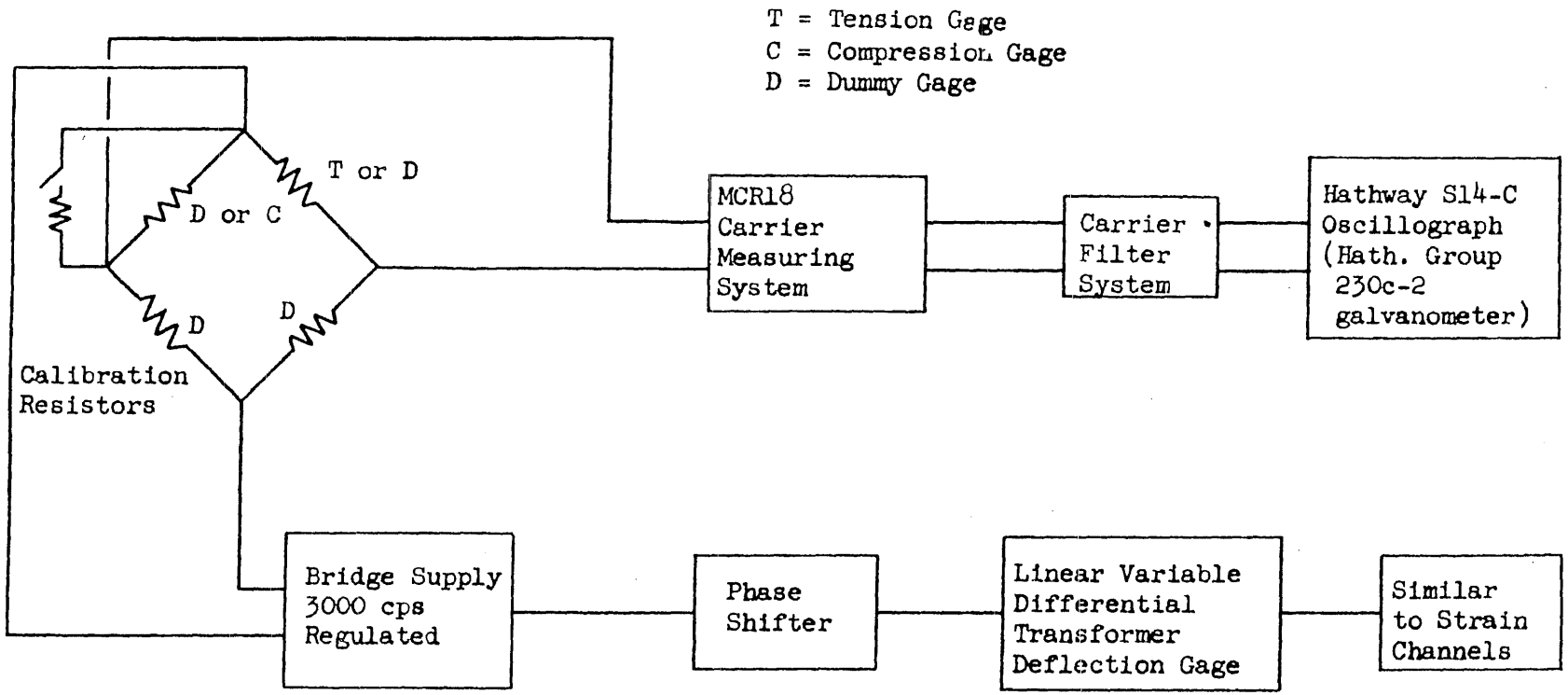

FIG. 3.4 BLOCK DIAGRAM FOR MEASUREMENTS OF STRAINS, DEFLECTIONS, AND LOADS

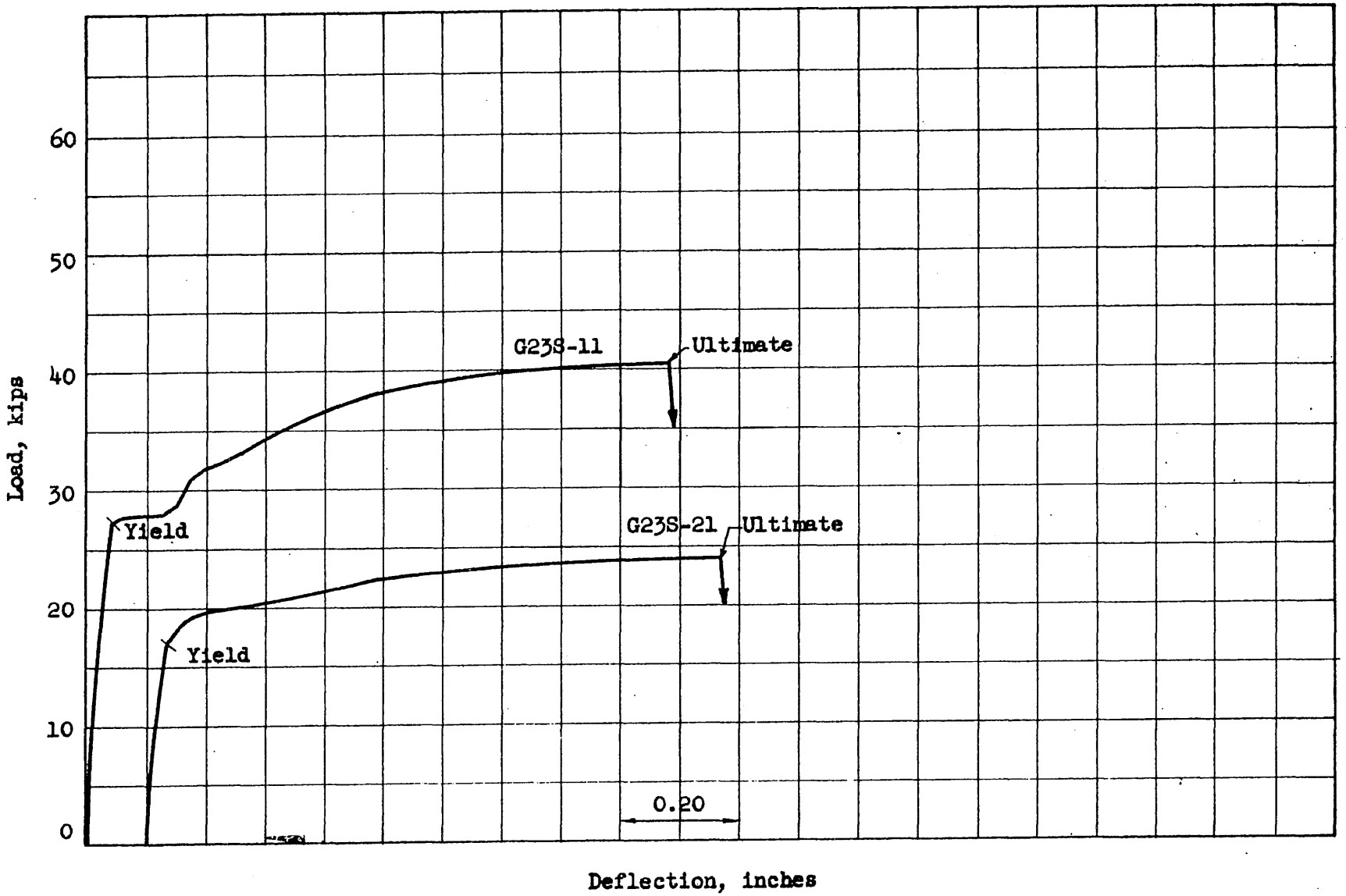

FIG. 4.1 LOAD VERSUS MIDSPAN DEFLECTION FOR BEAMS G23S-11 AND G23S-21

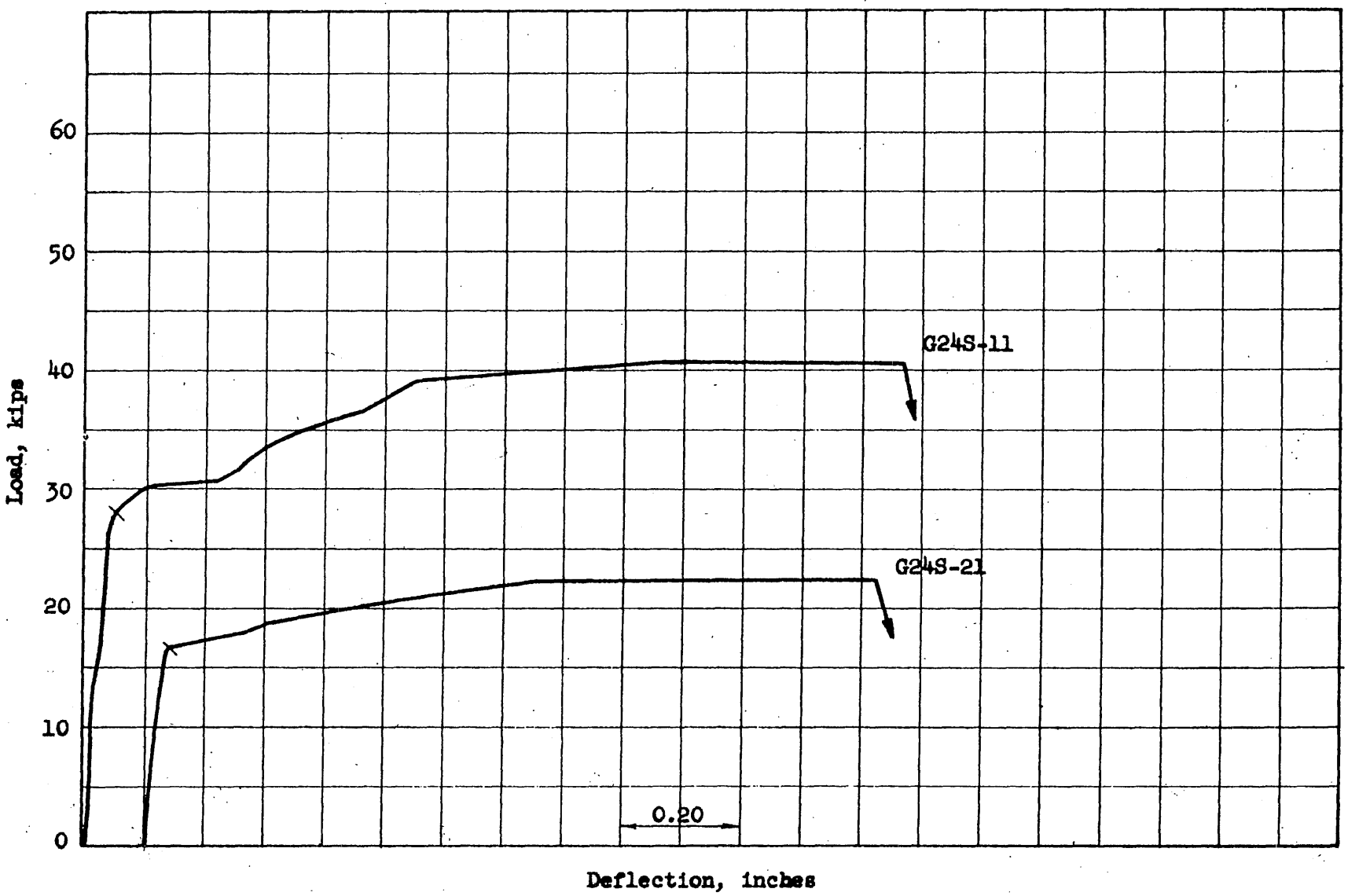

FIG. 4.2 LOAD VERSUS MIDSPAN DEFLECTION FOR BEAMS G24S-11 AND G24S-21

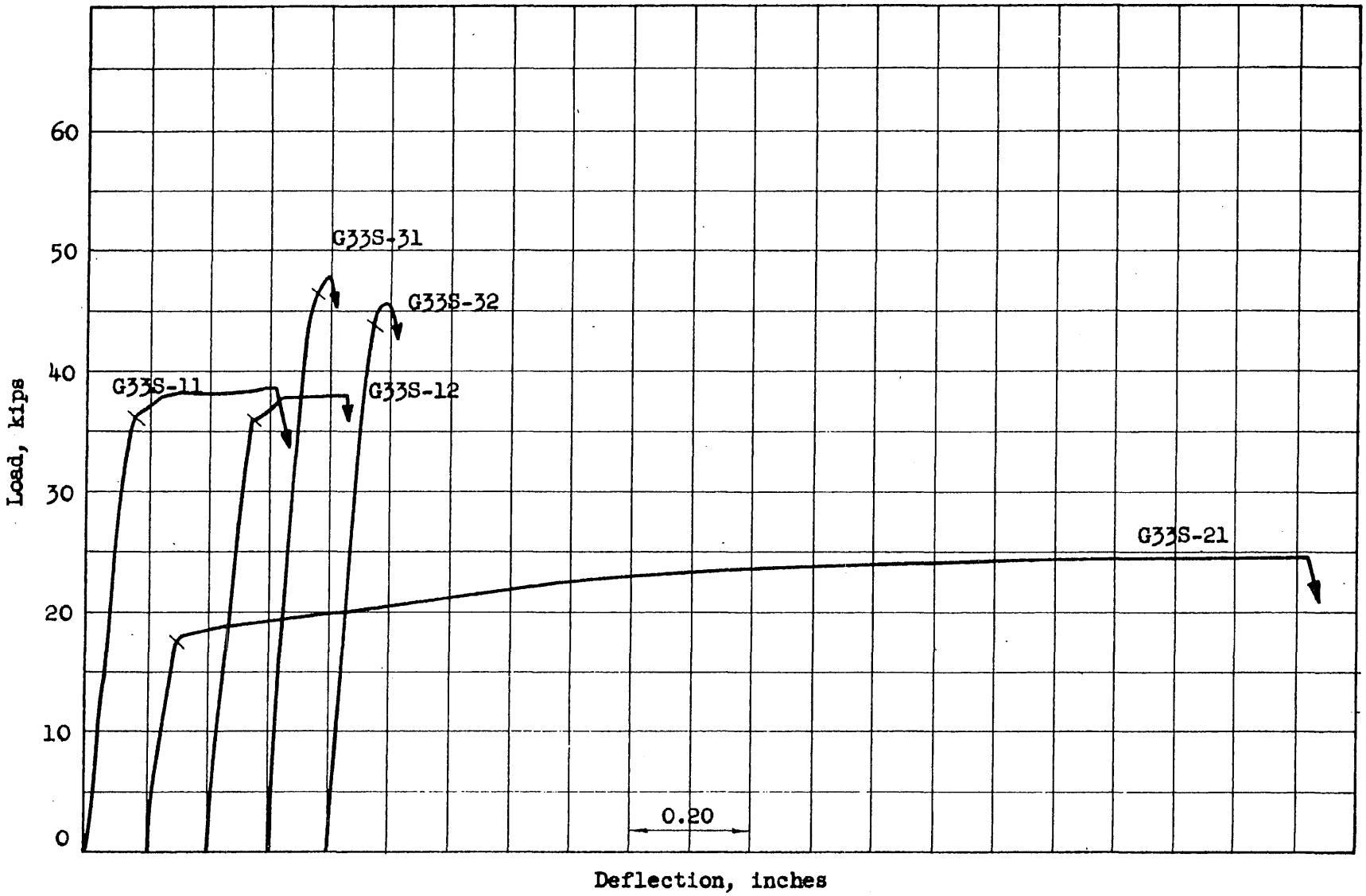

FIG. 4.3 LOAD VERSUS MIDSPAN DEFLECTION FOR BEAMS G33S-11, G33S-12, G33S-21, G33S-31 AND G33S-32

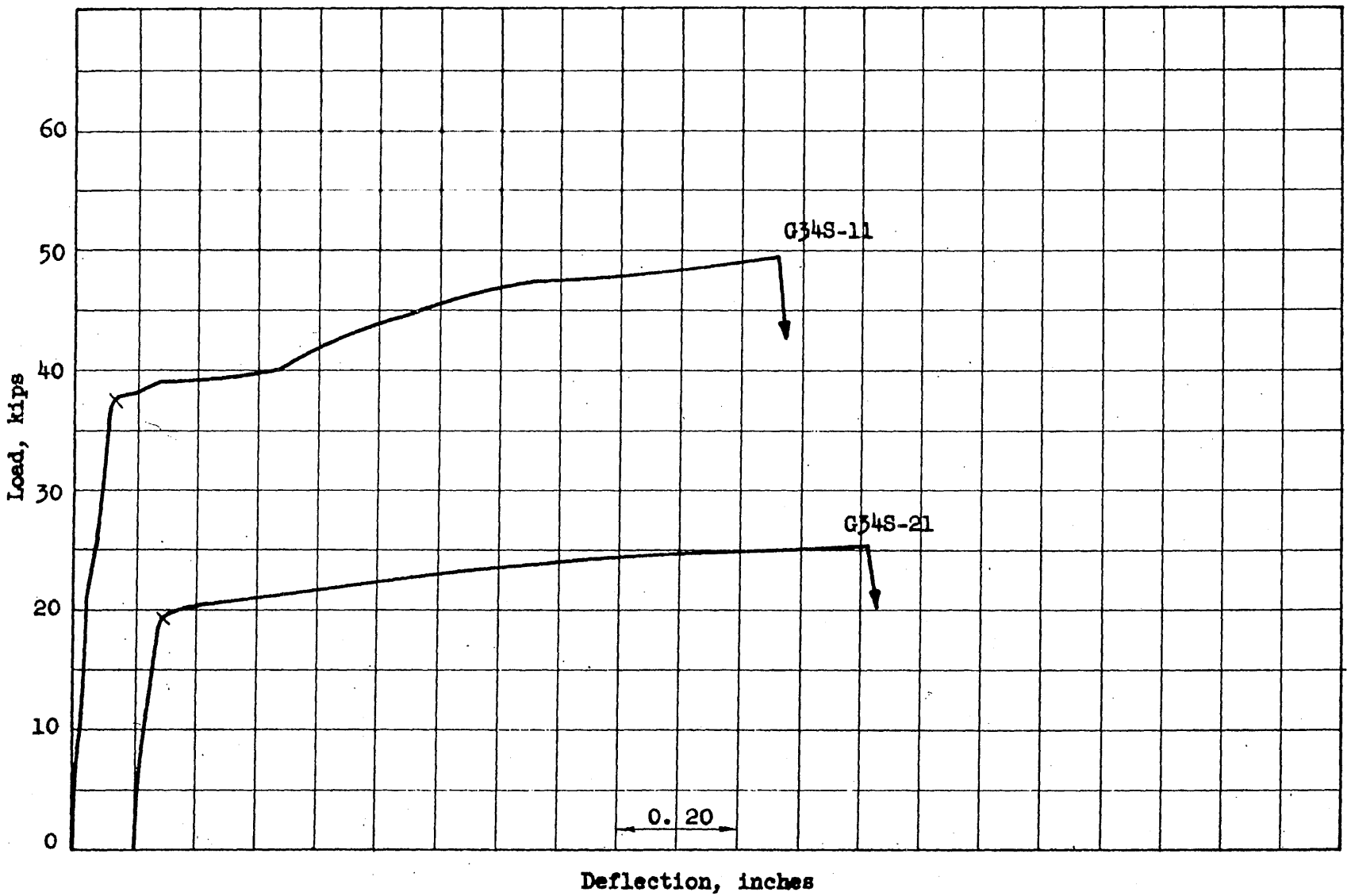

FIG. 4.4 LOAD VERSUS MIDSPAN DEFLECTION FOR BEAMS G34S-11 AND G34S-21

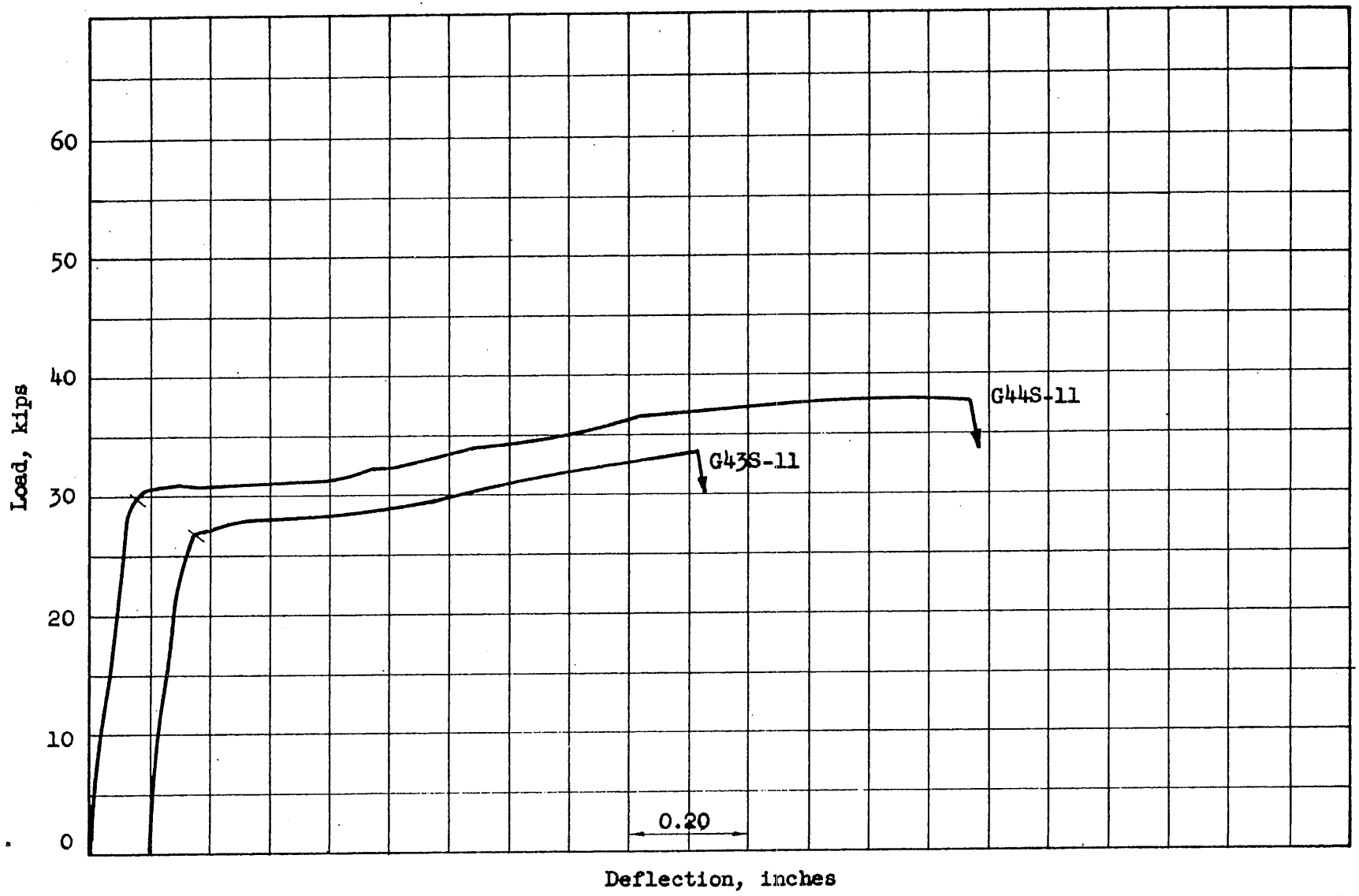

FIG. 4.5 LOAD VERSUS MIDSPAN DEFLECTION FOR BEAMS G43S-11 AND G44S-11

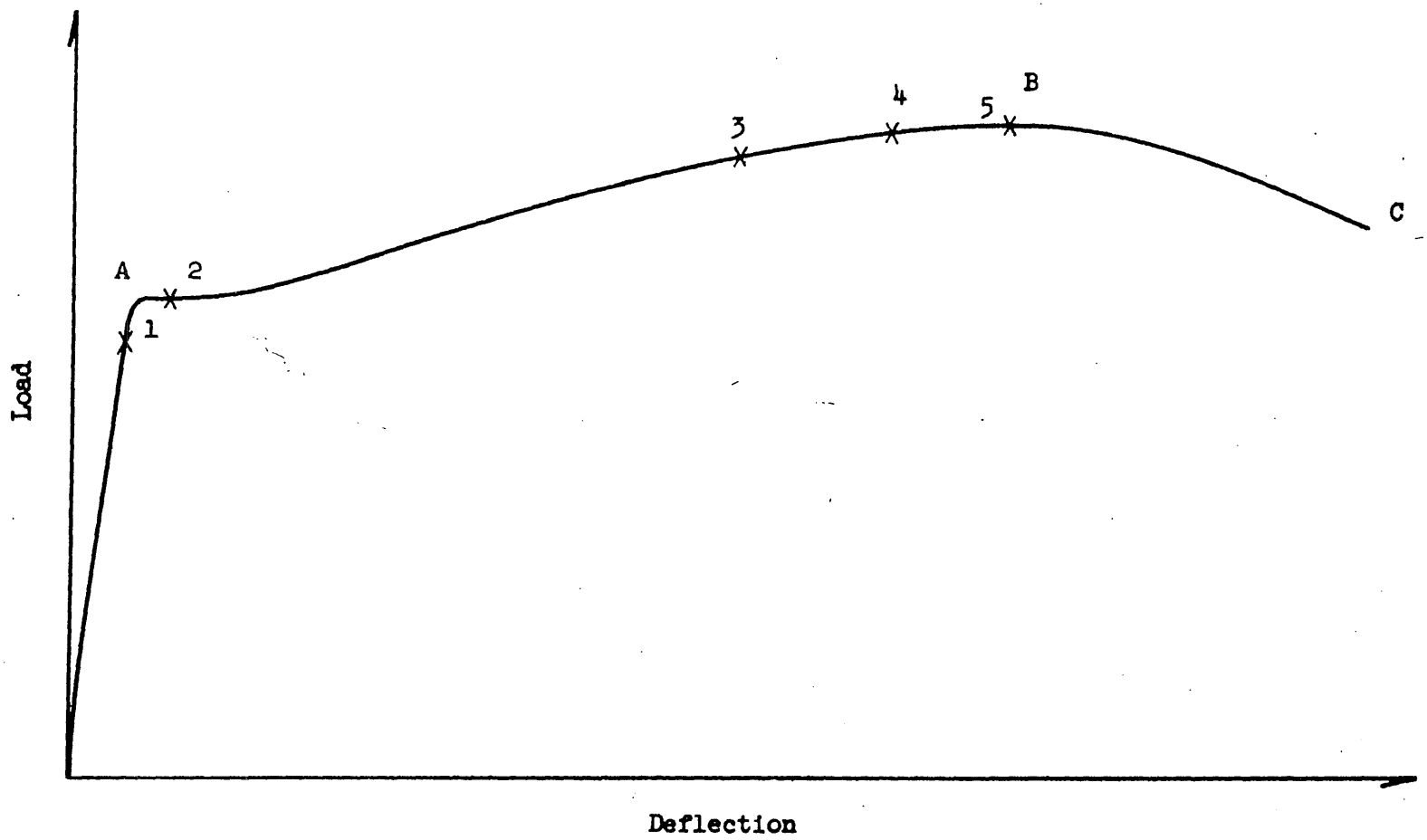

FIG. 4.6 TYPICAL LOAD-DEFLECTION CURVE FOR A FLEXURE FAILURE

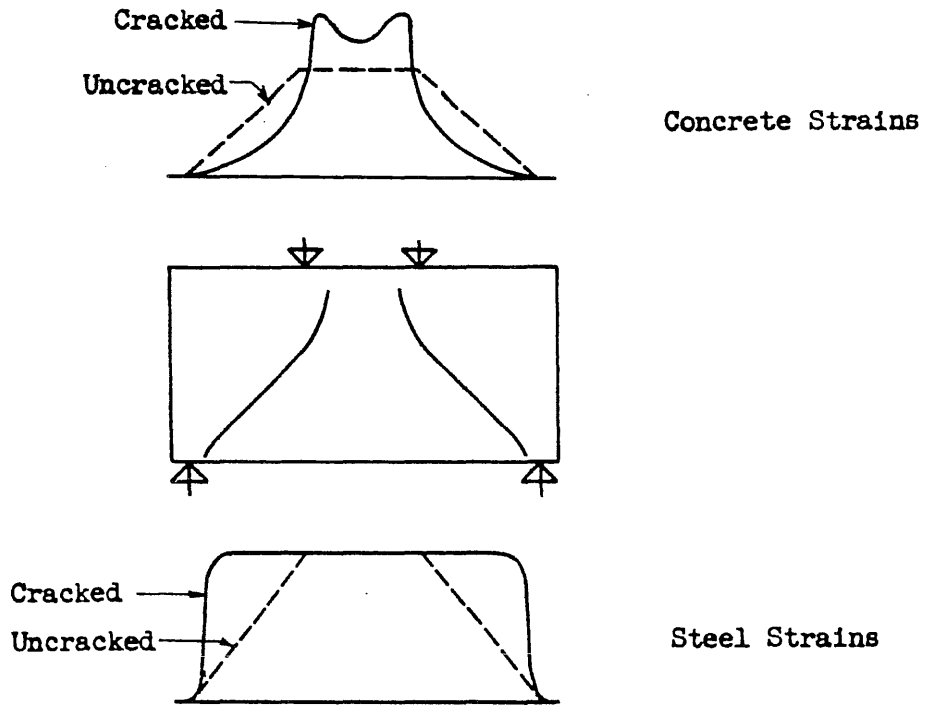

(a) Deep Beams

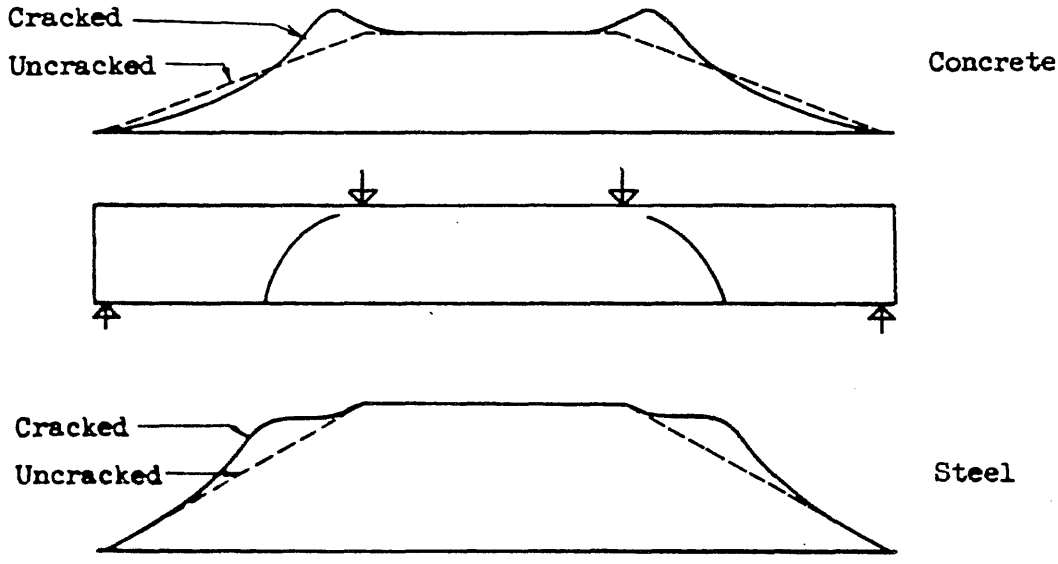

(b) Ordinary Beams

FIG. 4.7 EFFECT OF INCLINED CRACKING ON THE DISTRIBUTION OF STEEL AND CONCRETE STRAINS

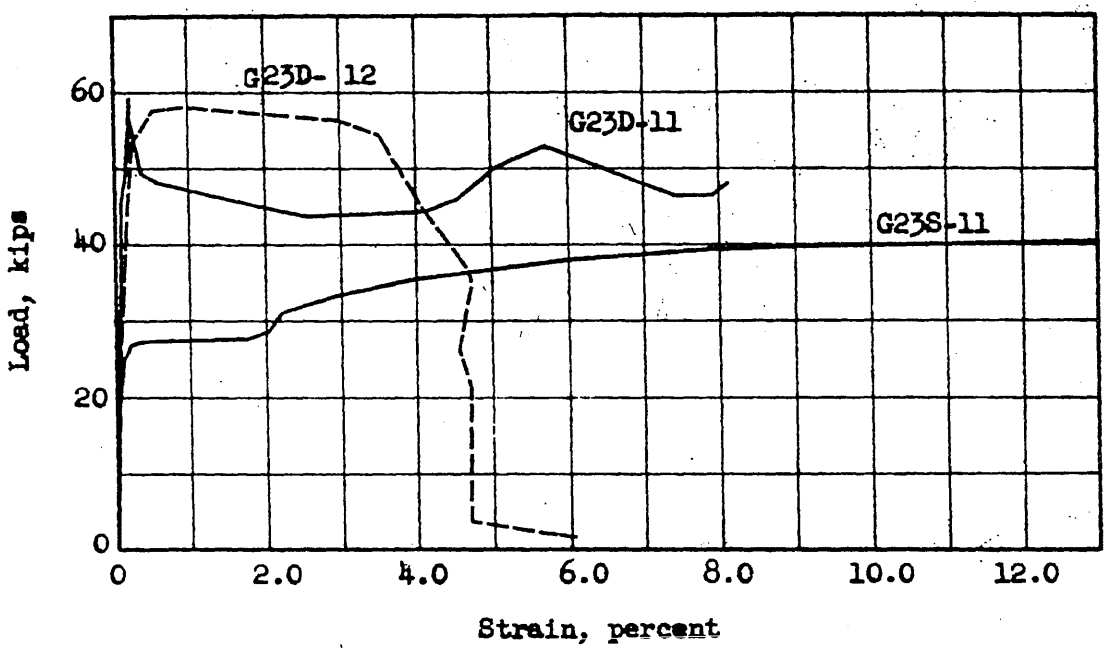

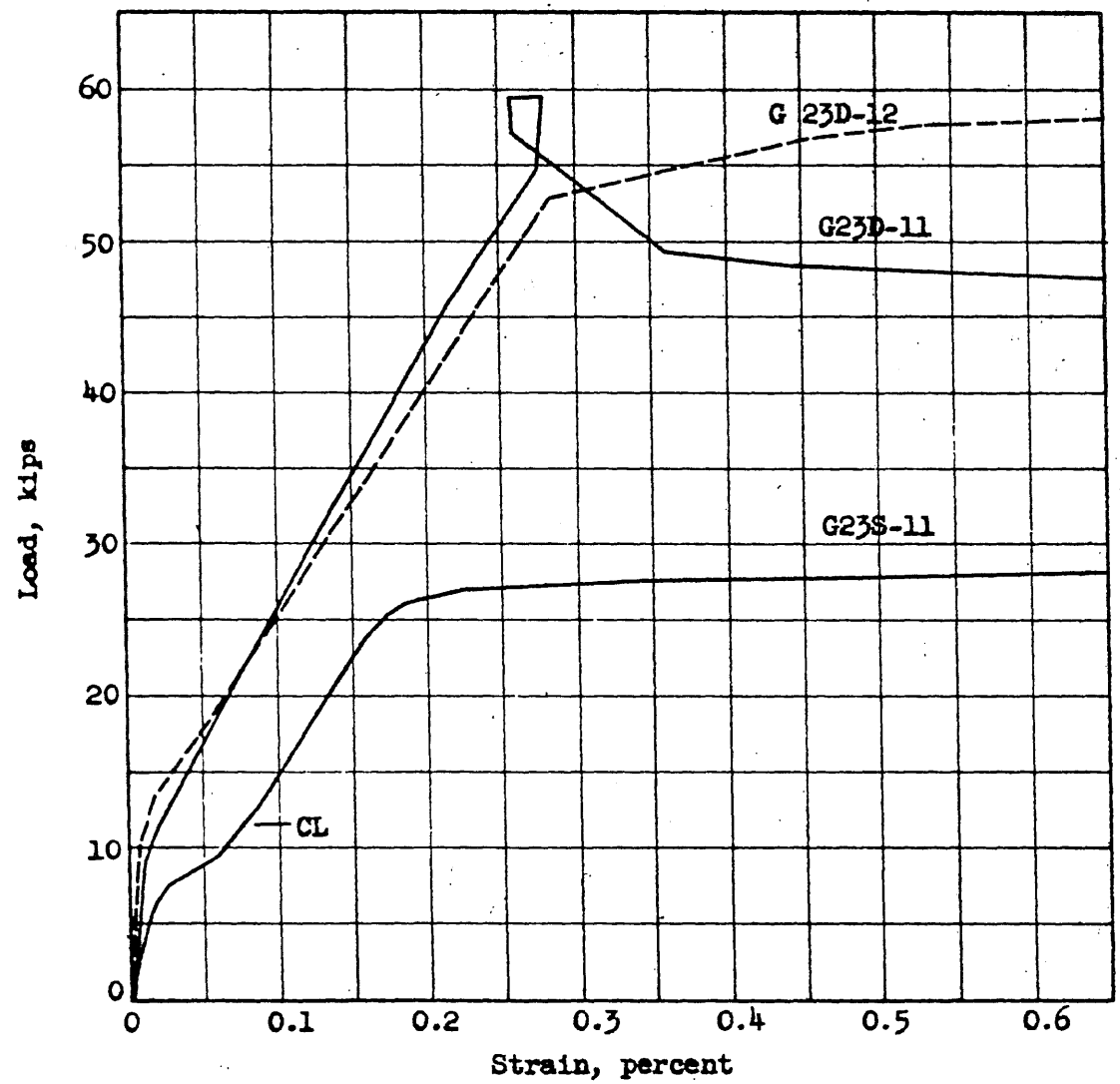

FIG. 4.8 LOAD VERSUS STEEL STRAIN FOR BEAMS G23S-11, G23D-11 AND G23D-12

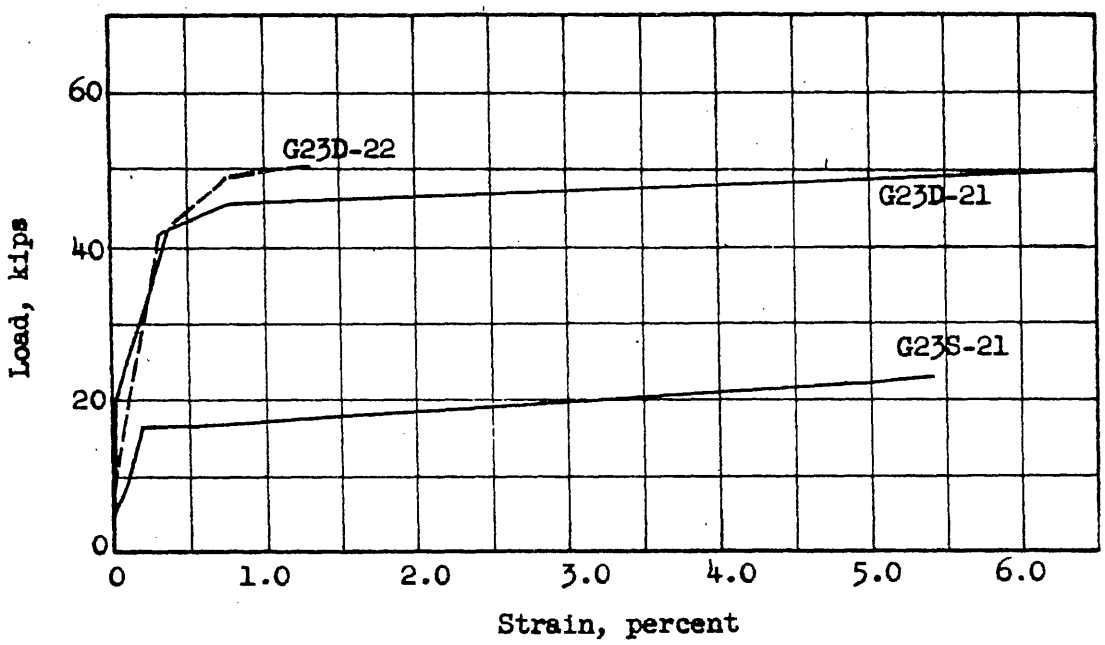

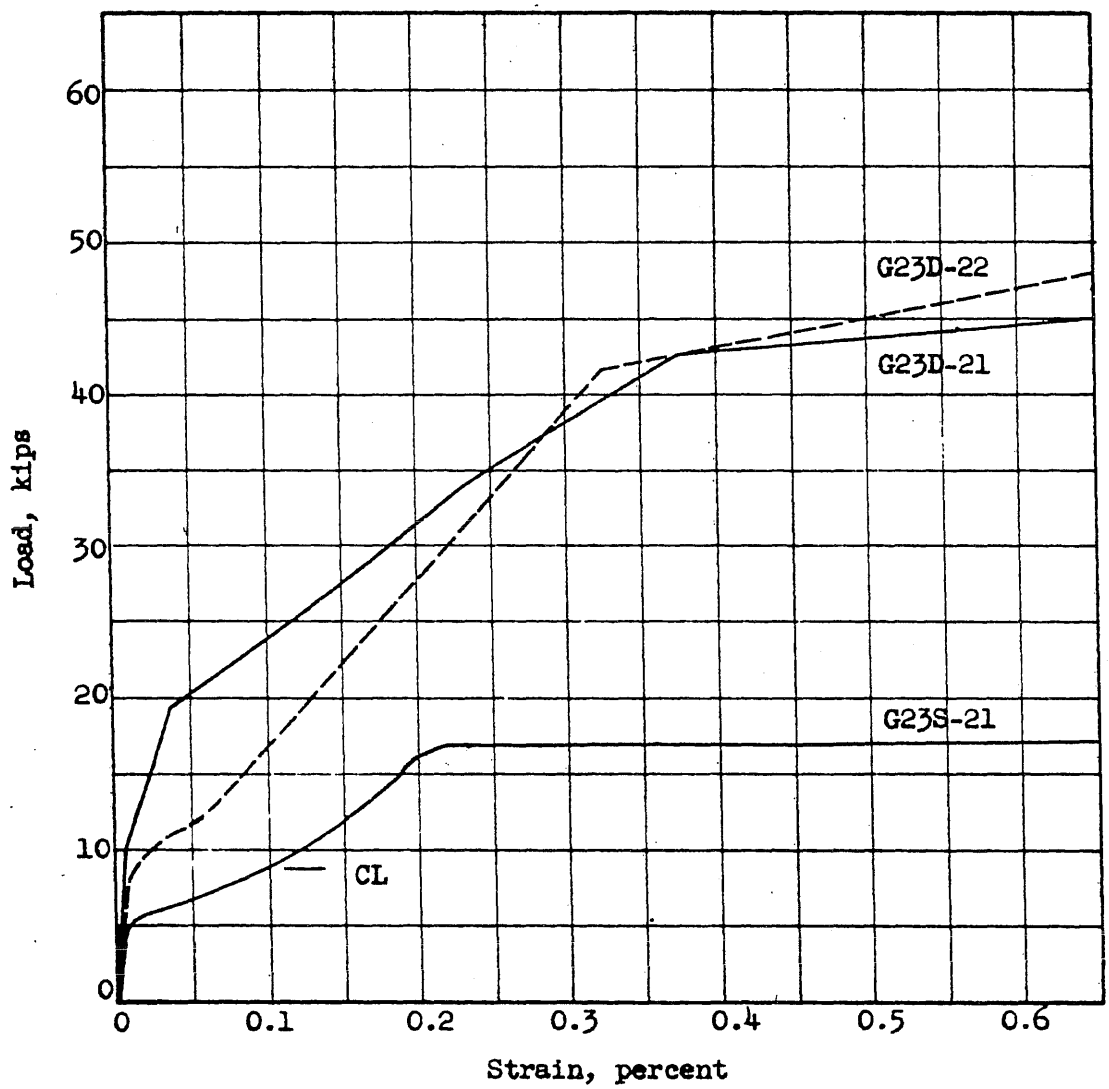

FIG. 4.9 LOAD VERSUS STEEL STRAIN FOR BEAMS G23S-21, G23D-21 AND G23D-22

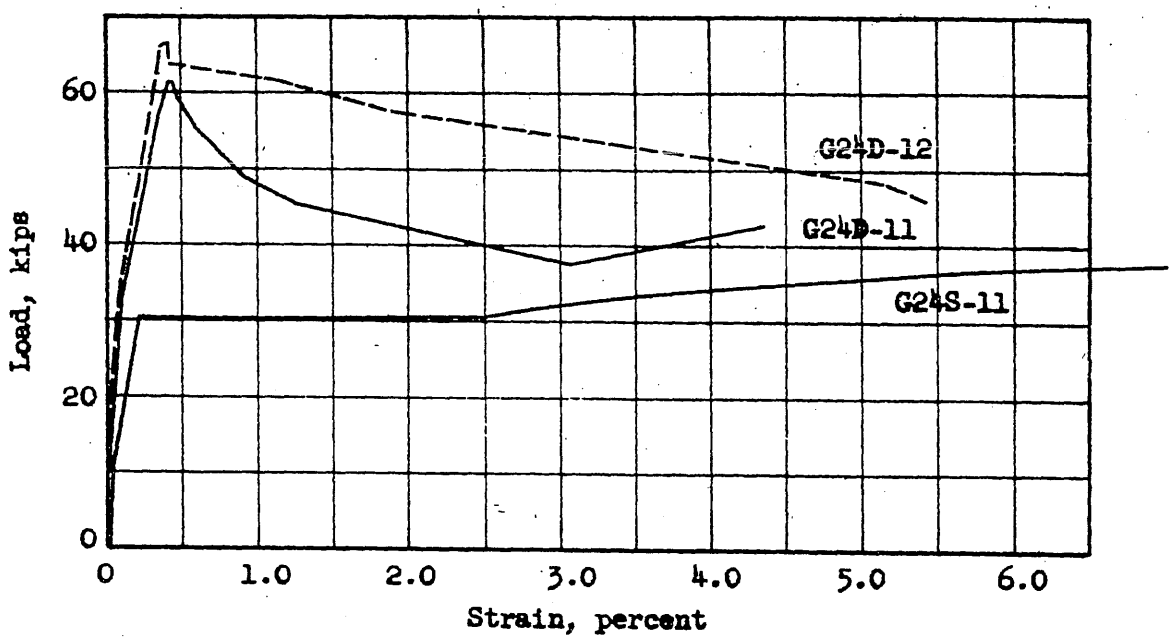

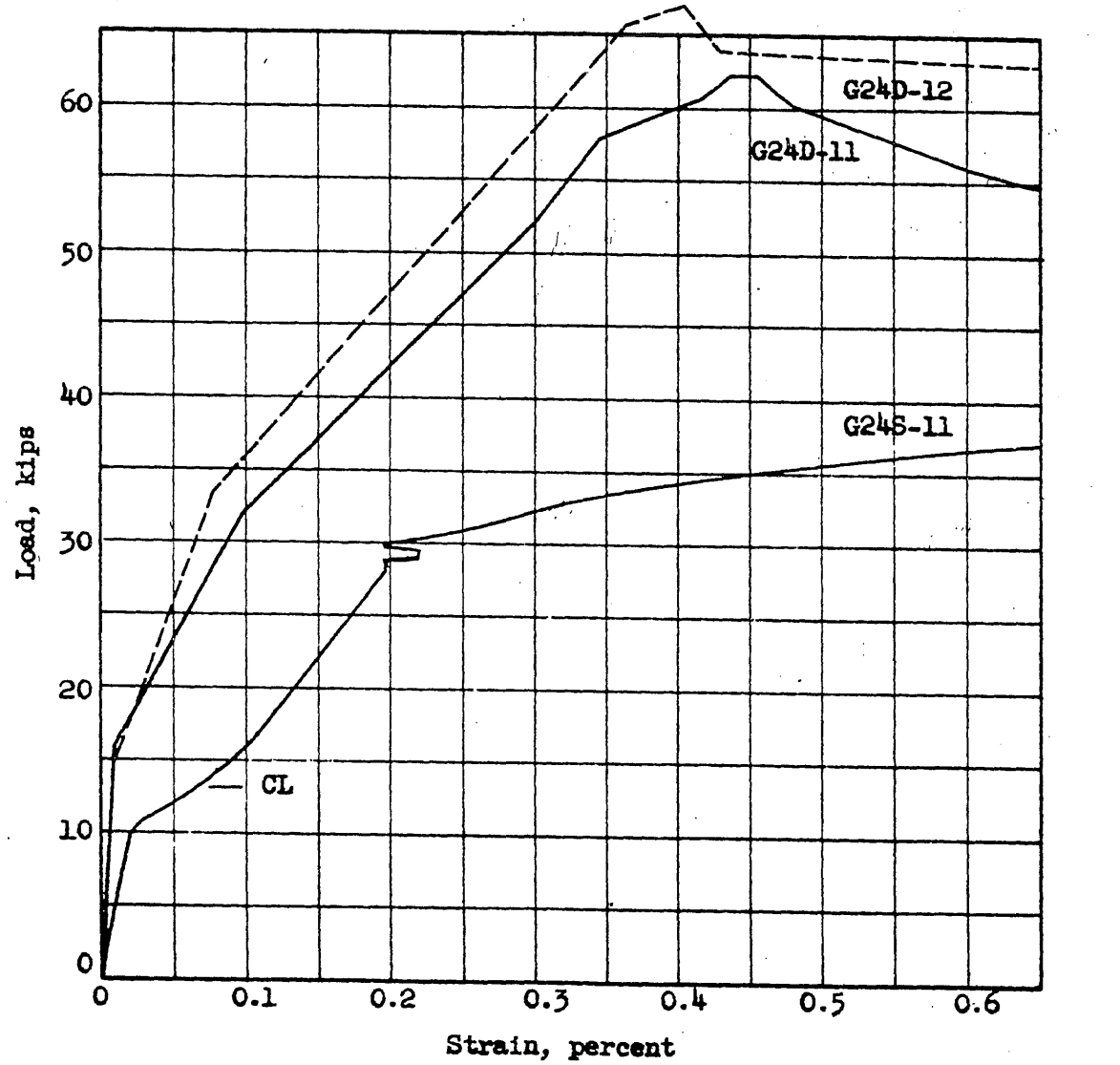

FIG. 4.10 LOAD VERSUS STEEL STRAIN FOR BEAMS G24S-11, G24D-11 AND G24D-12

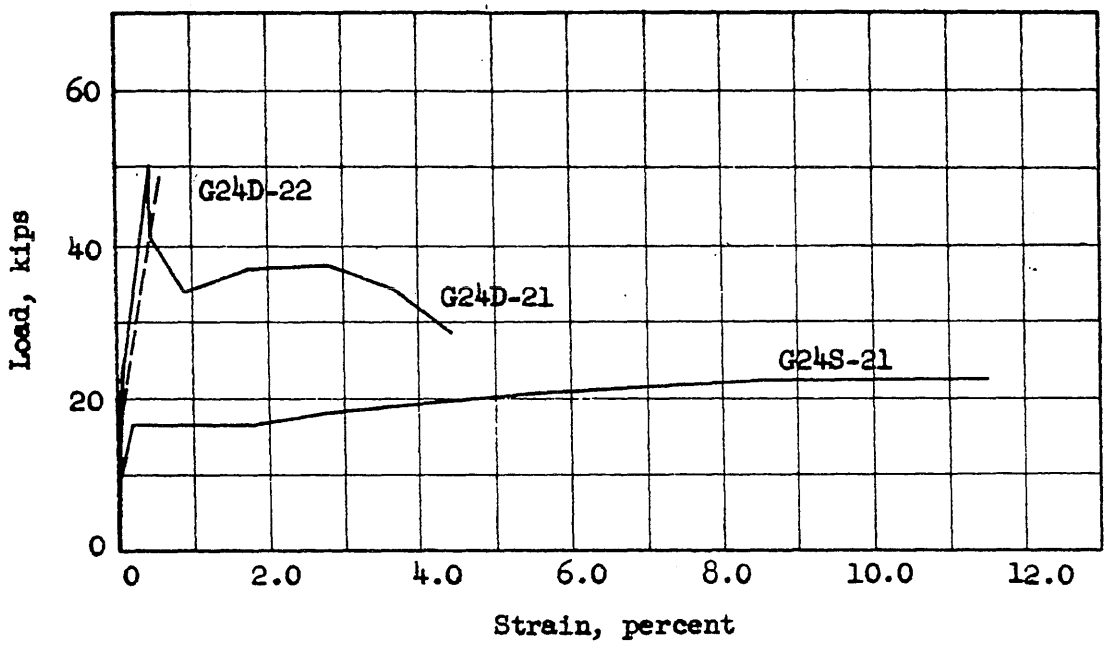

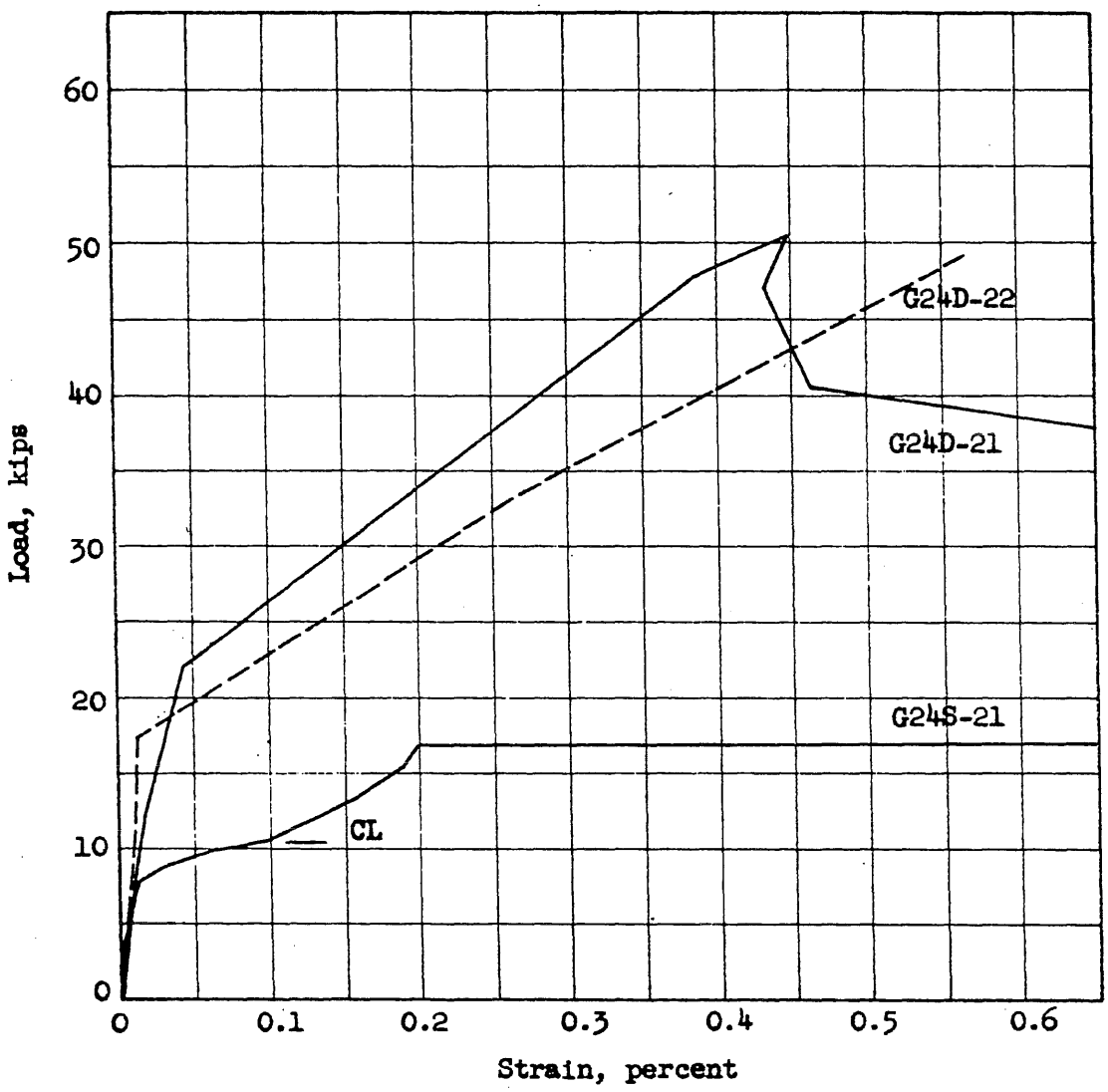

FIG. 4.11 LOAD VERSUS STEEL STRAIN FOR BEAMS G24S-21, G24D-21 AND G24D-22

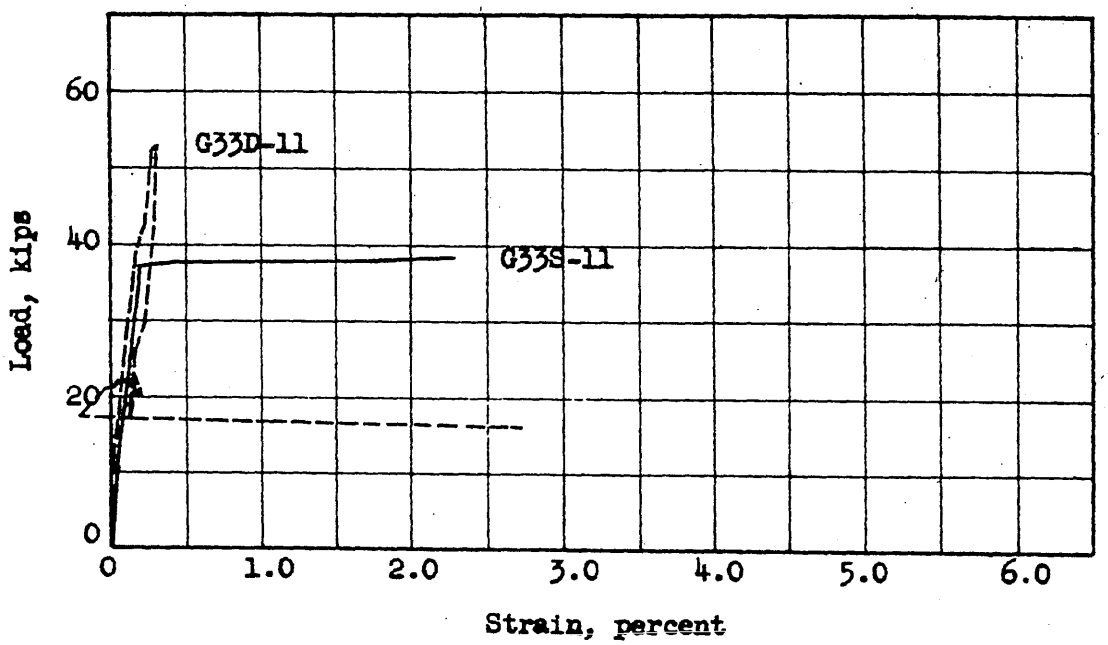

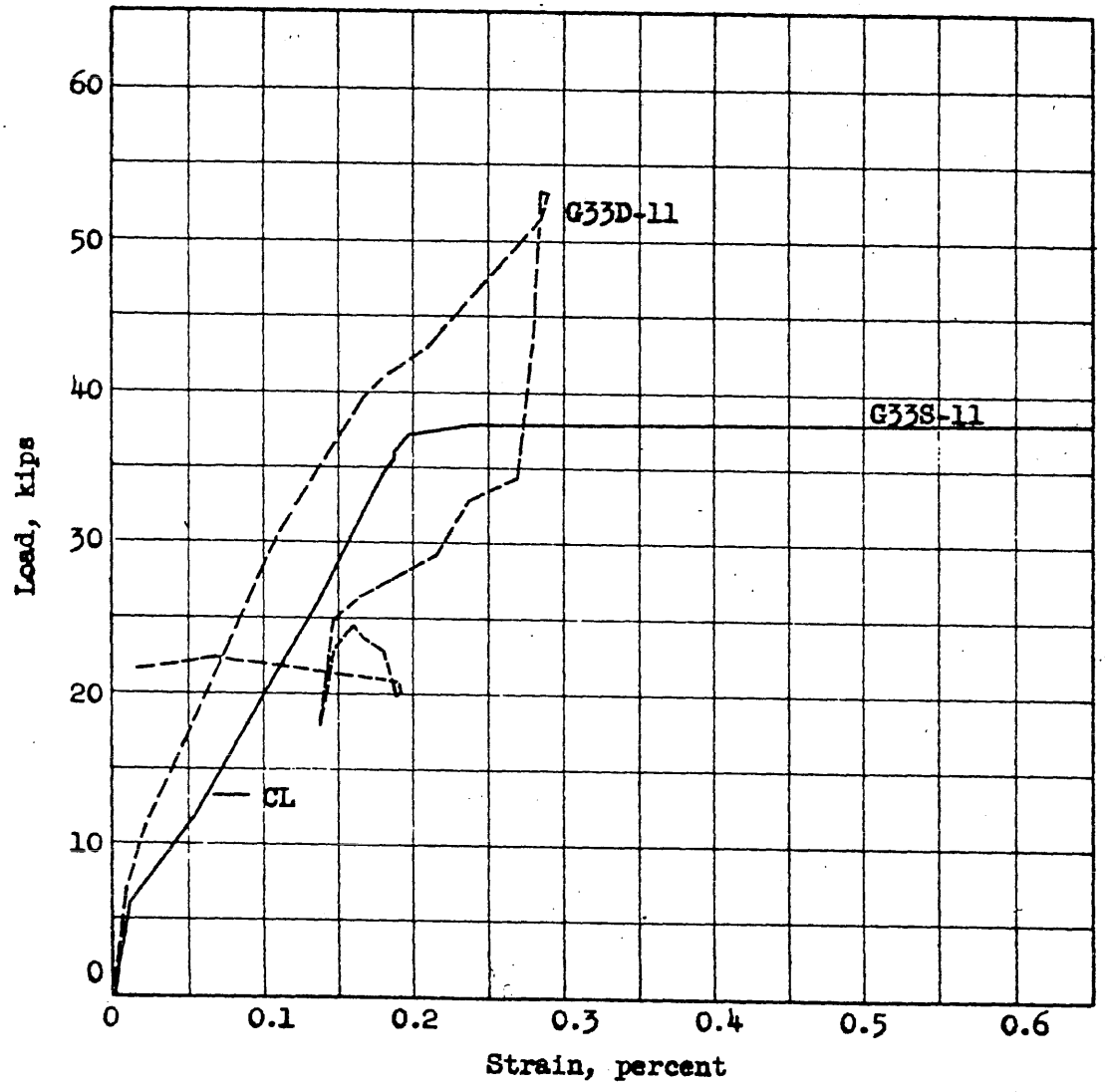

FIG. 4.12 LOAD VERSUS STEEL STRAIN FOR BEAMS G33S-11 AND G33D-11

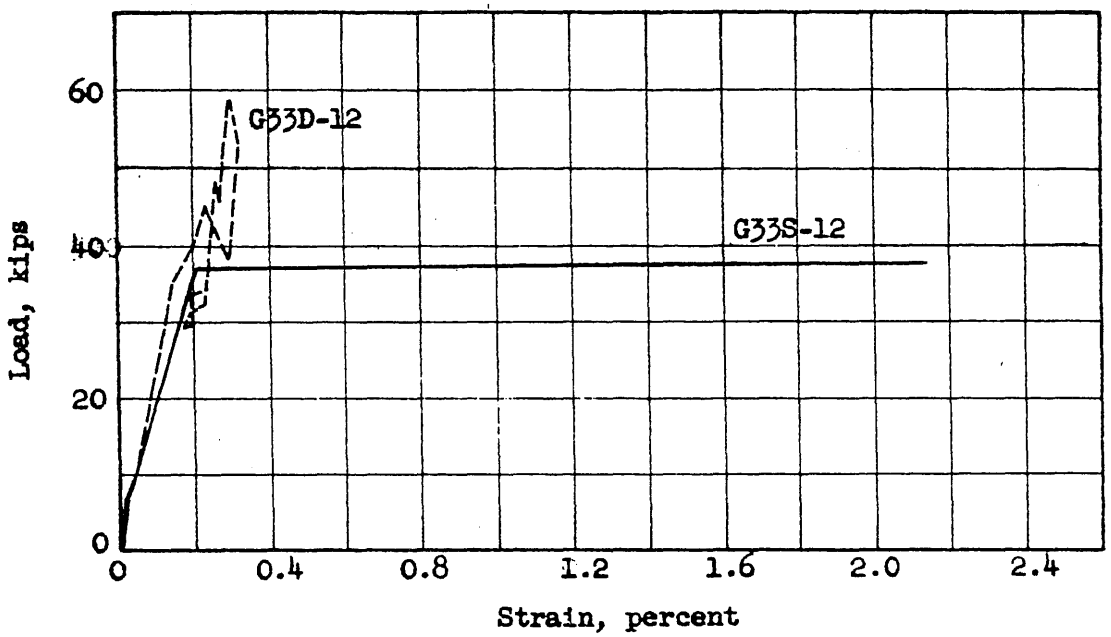

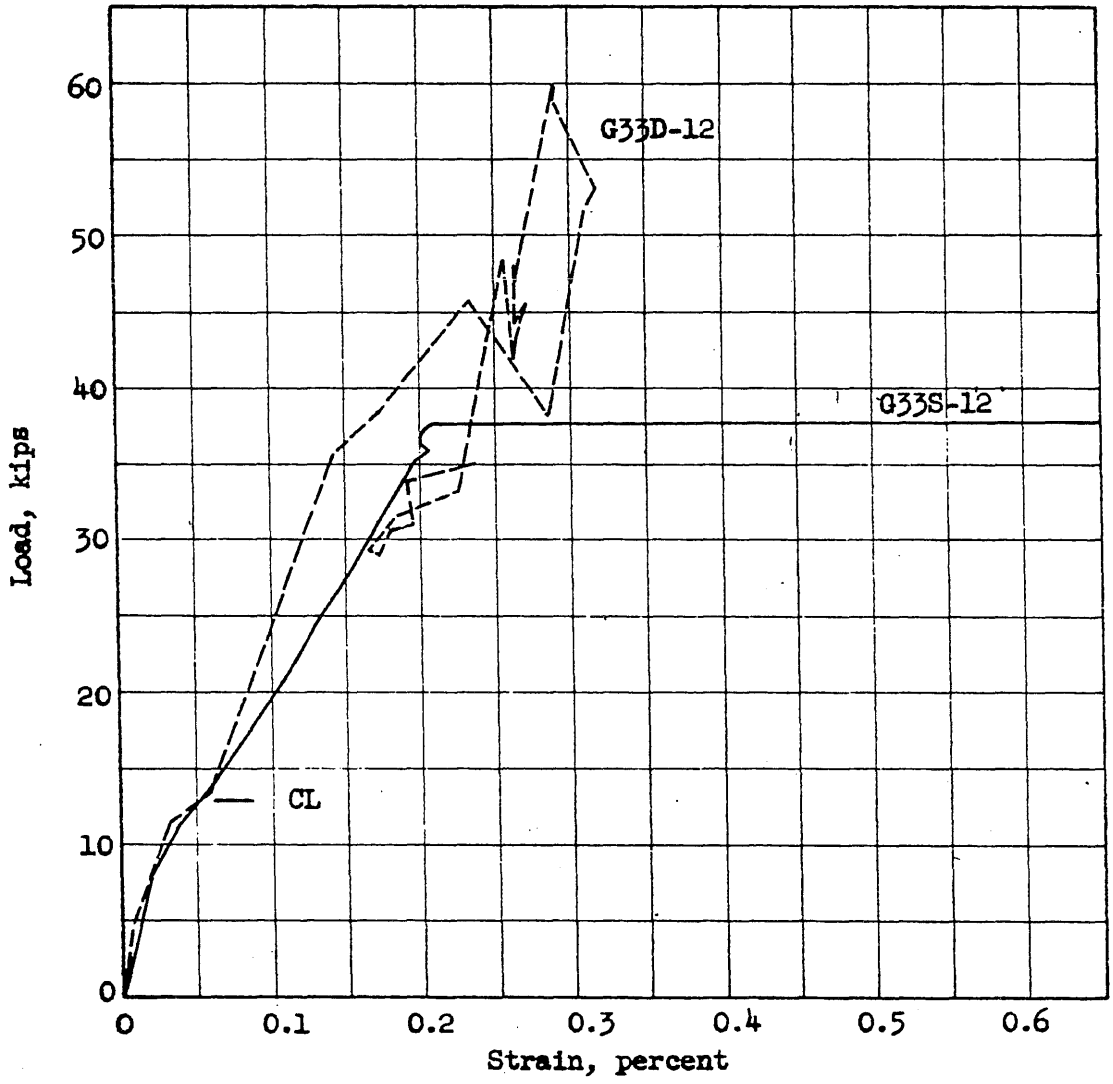

FIG. 4.13 LOAD VERSUS STEEL STRAIN FOR BEAMS G33S-12 AND G33D-12

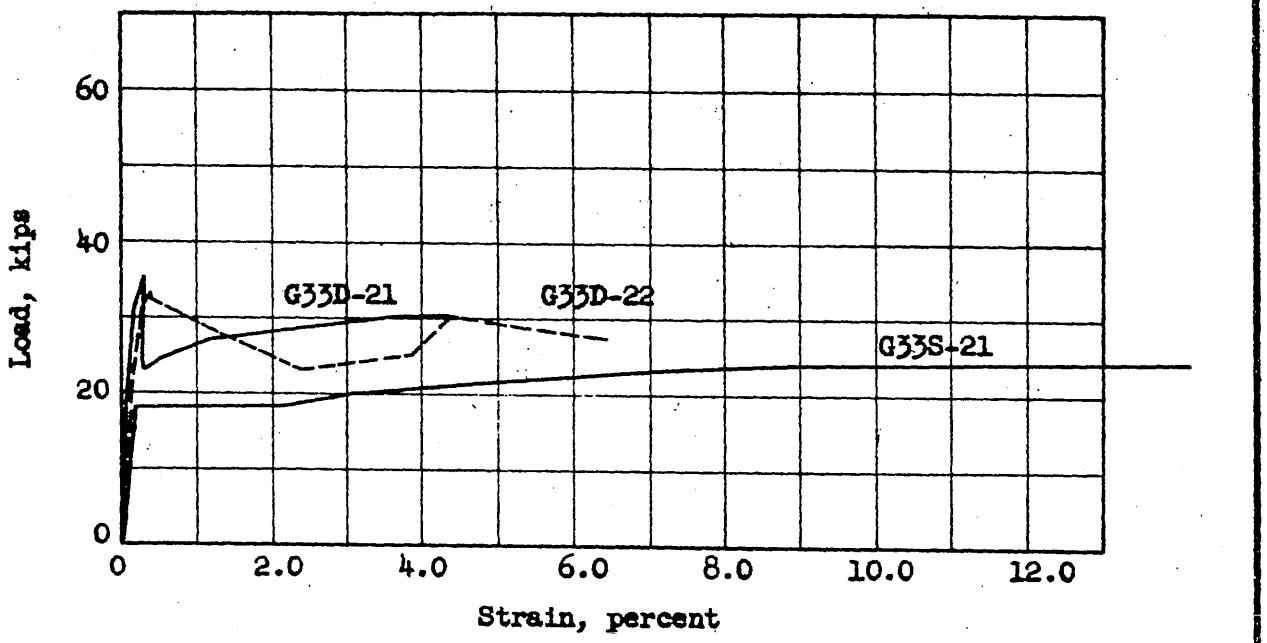

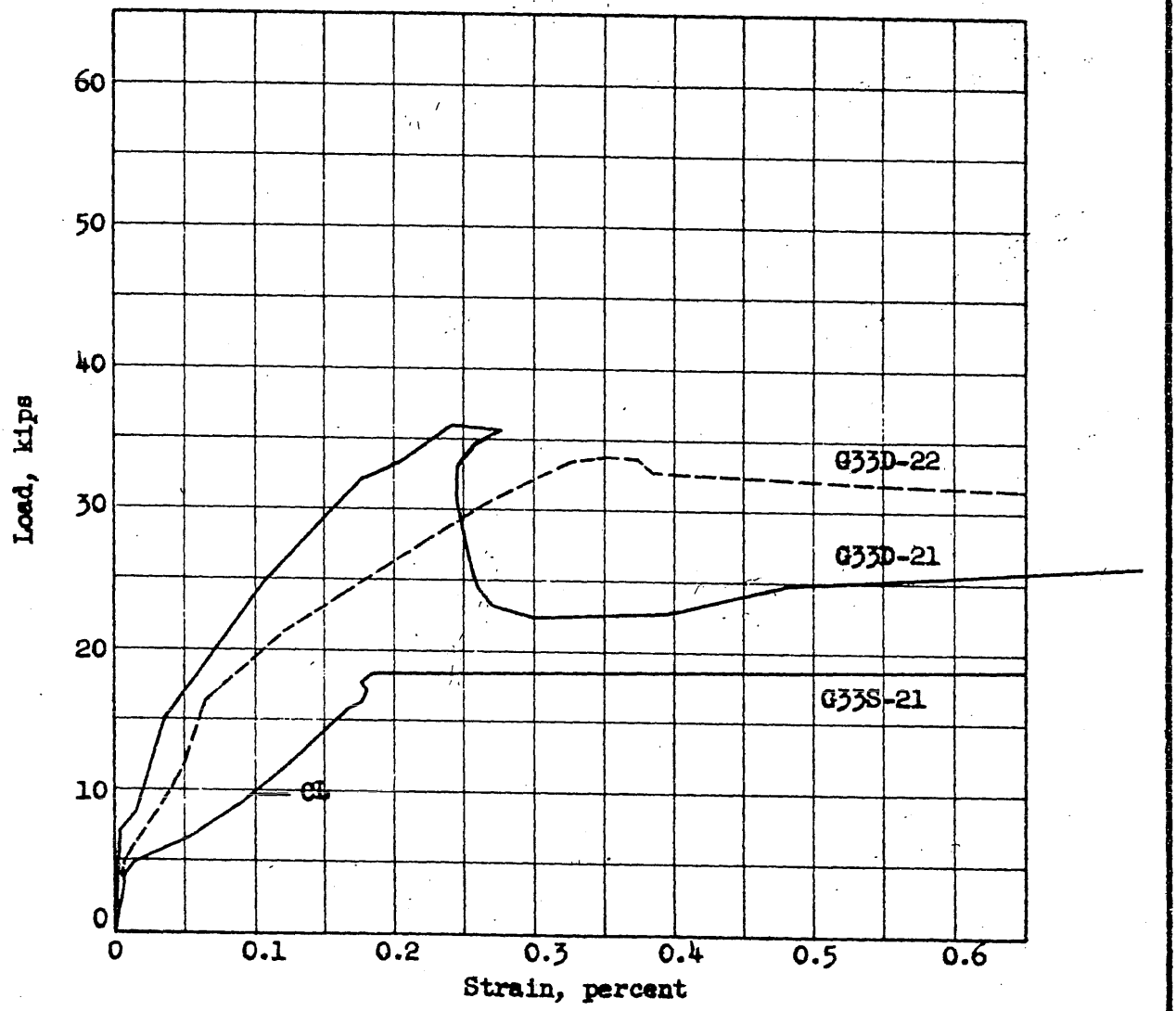

FIG. 4.14 LOAD VERSUS STEEL STRAIN FOR BEAMS G33S-21, G33D-21 AND G33D-22

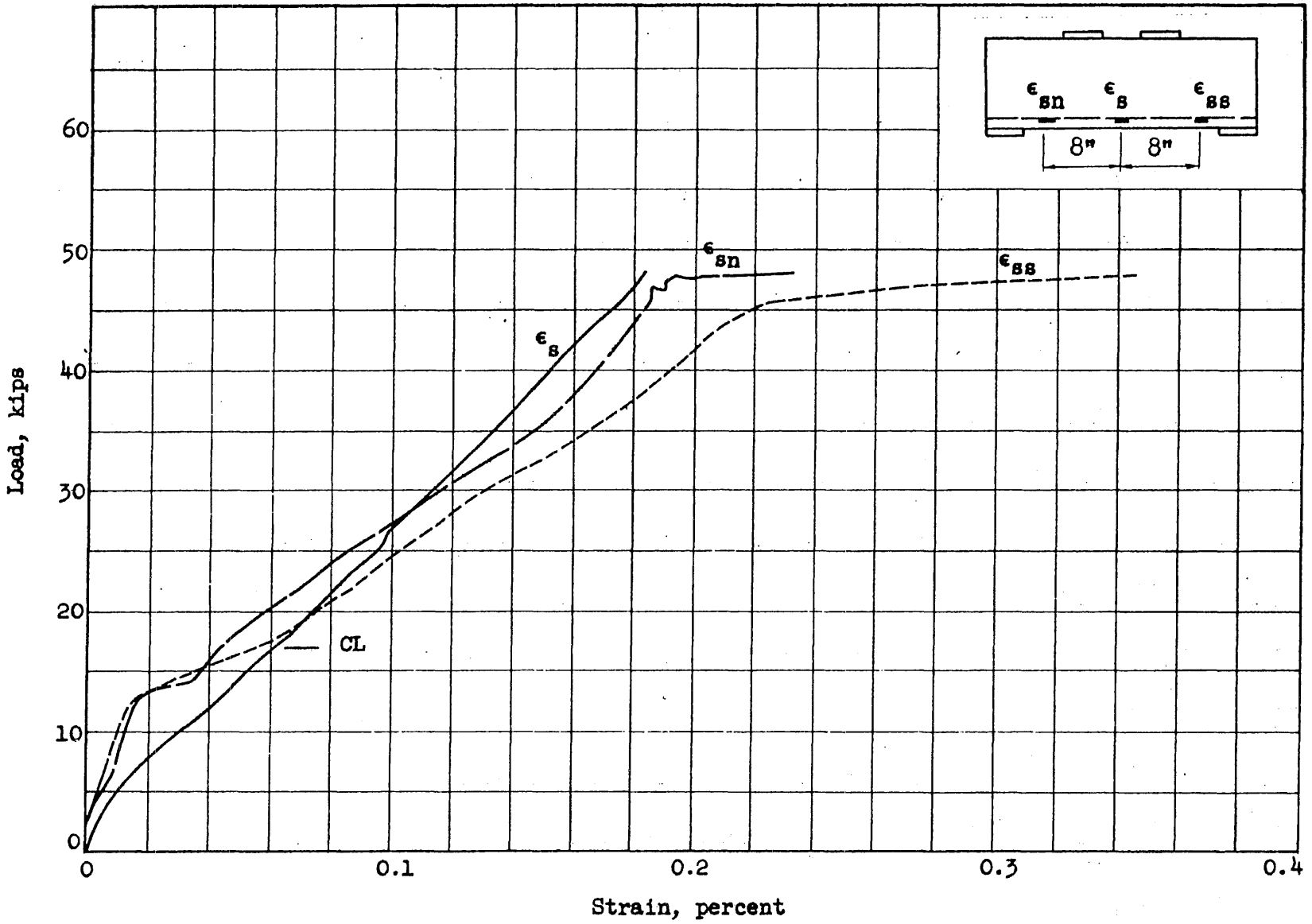

FIG. 4.15 LOAD VERSUS STEEL STRAIN FOR BEAM G33S-31

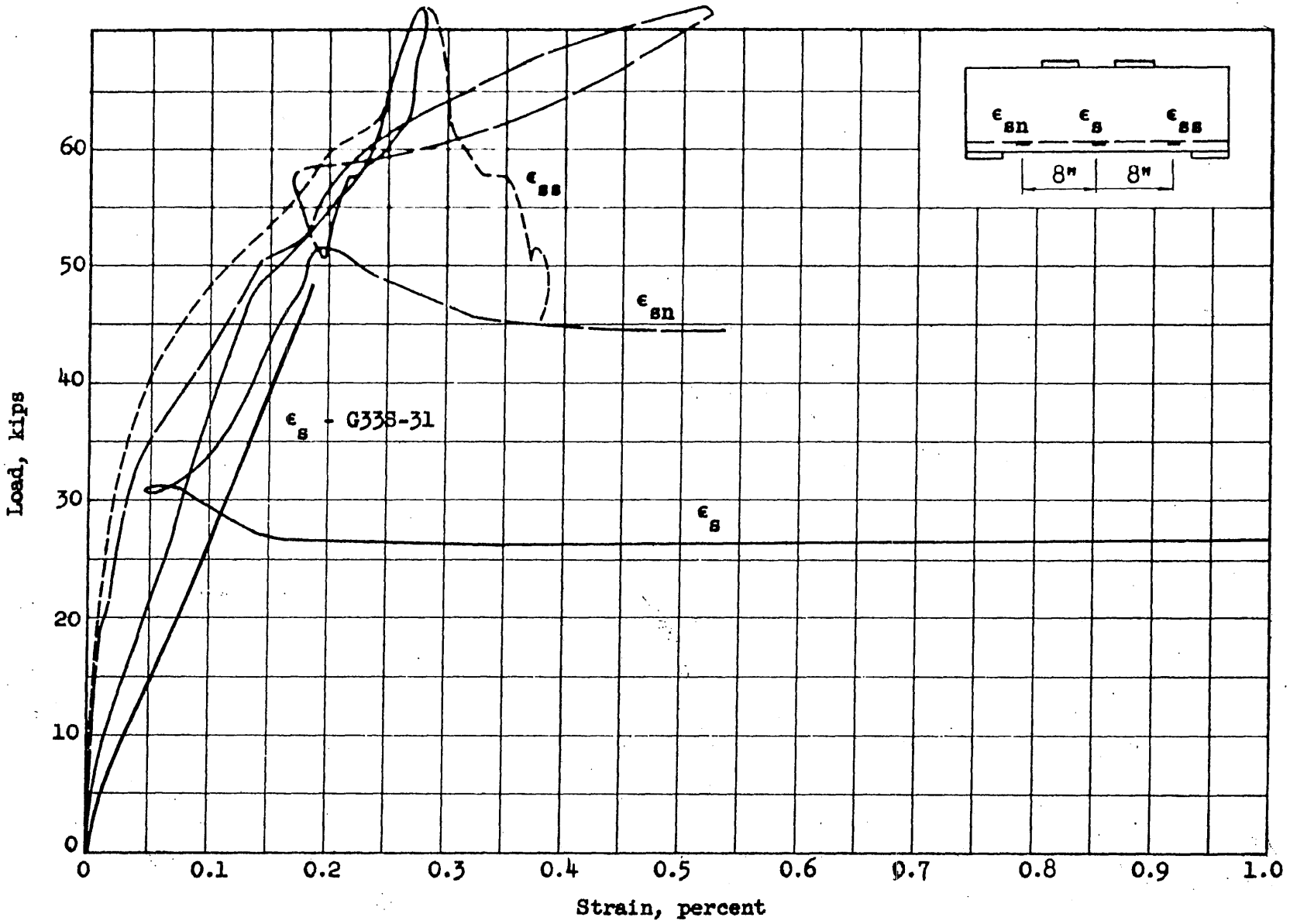

FIG. 4.16 LOAD VERSUS STEEL STRAIN FOR BEAM G33D-31

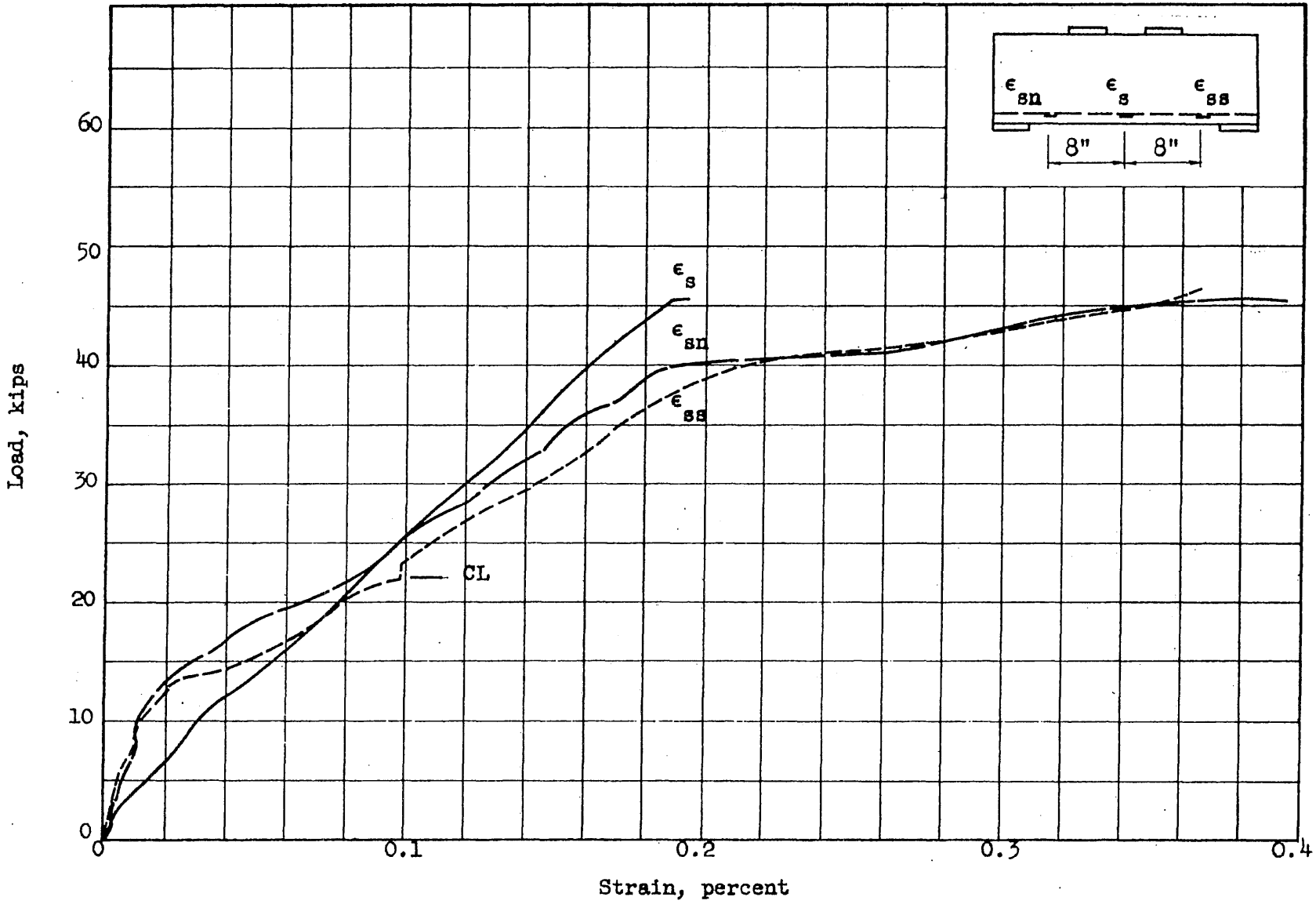

FIG. 4.17 LOAD VERSUS STEEL STRAIN FOR BEAM G33S-32

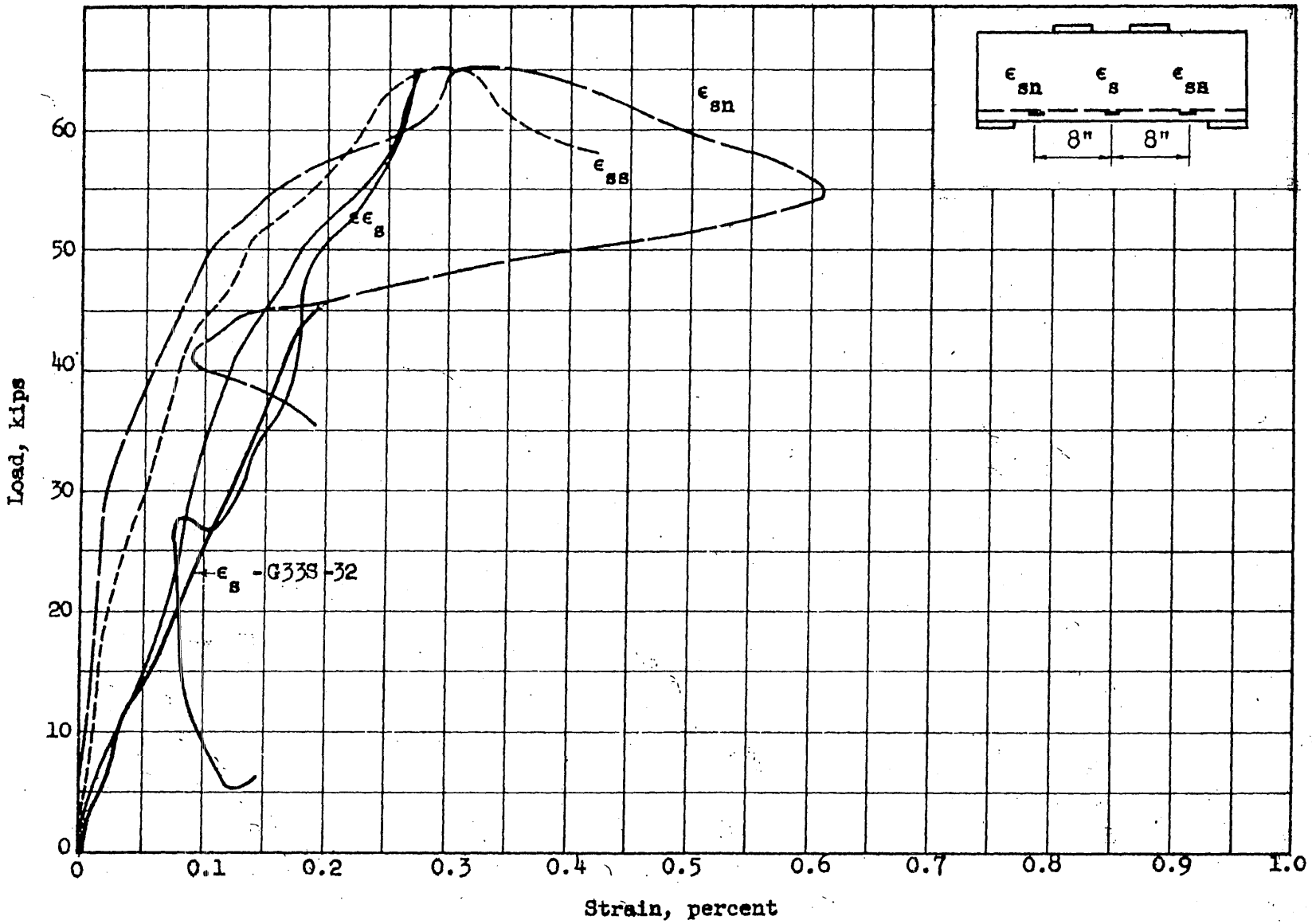

FIG. 4.18 LOAD VERSUS STEEL STRAIN FOR BEAM G33D-32

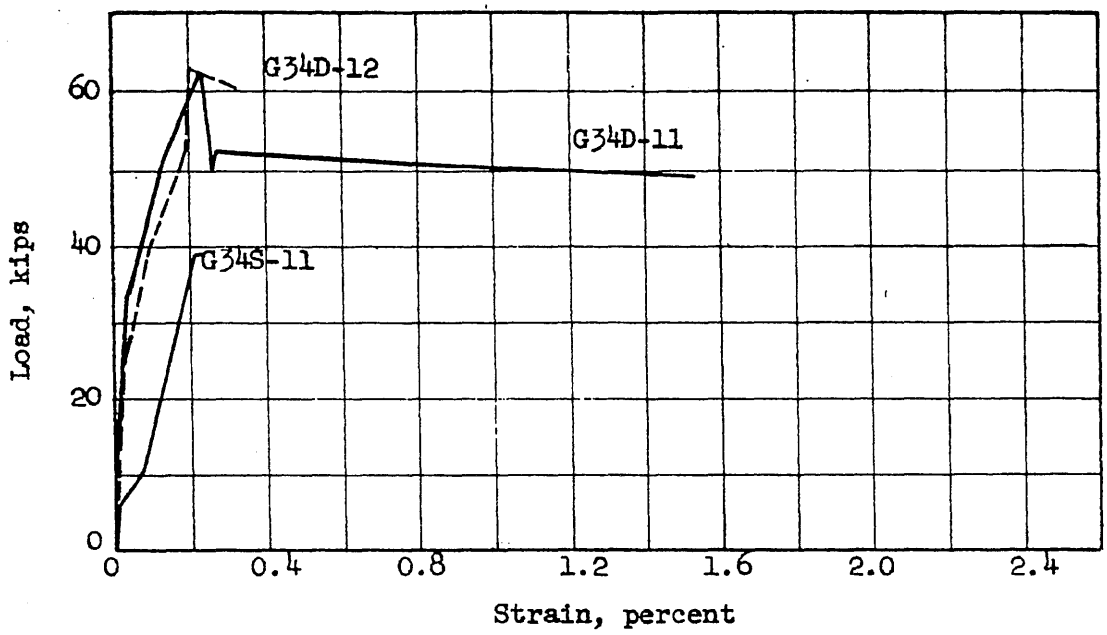

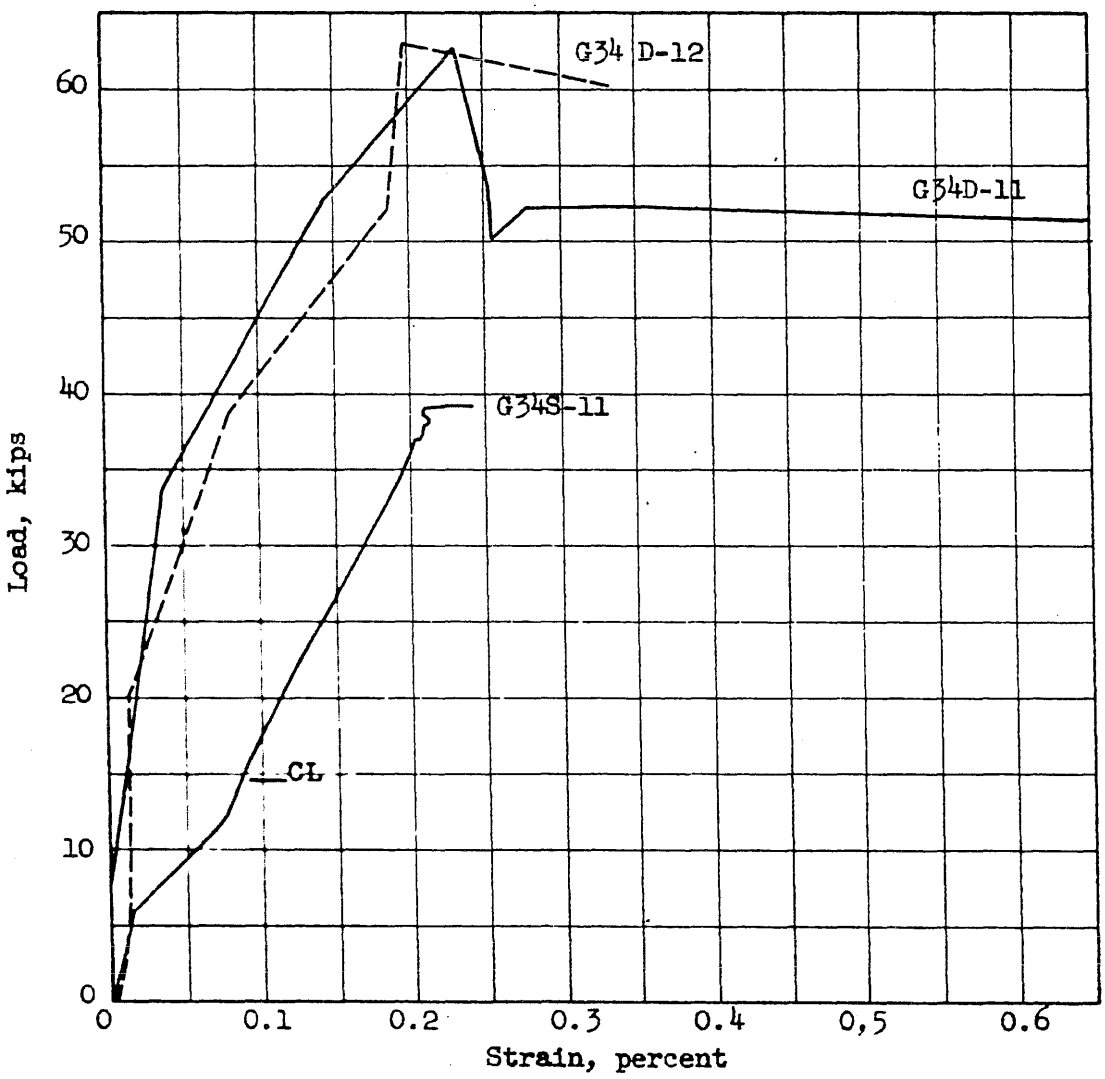

FIG. 4.19 LOAD VERSUS STEEL STRAIN FOR BEAMS G34S-11, G34D-11 AND G34D-12

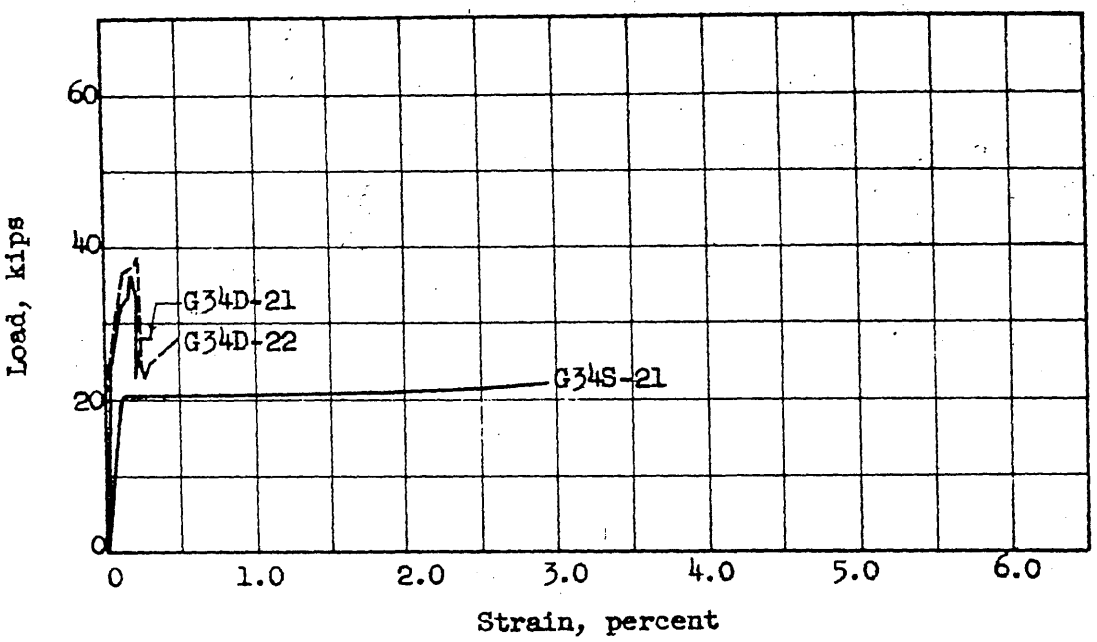

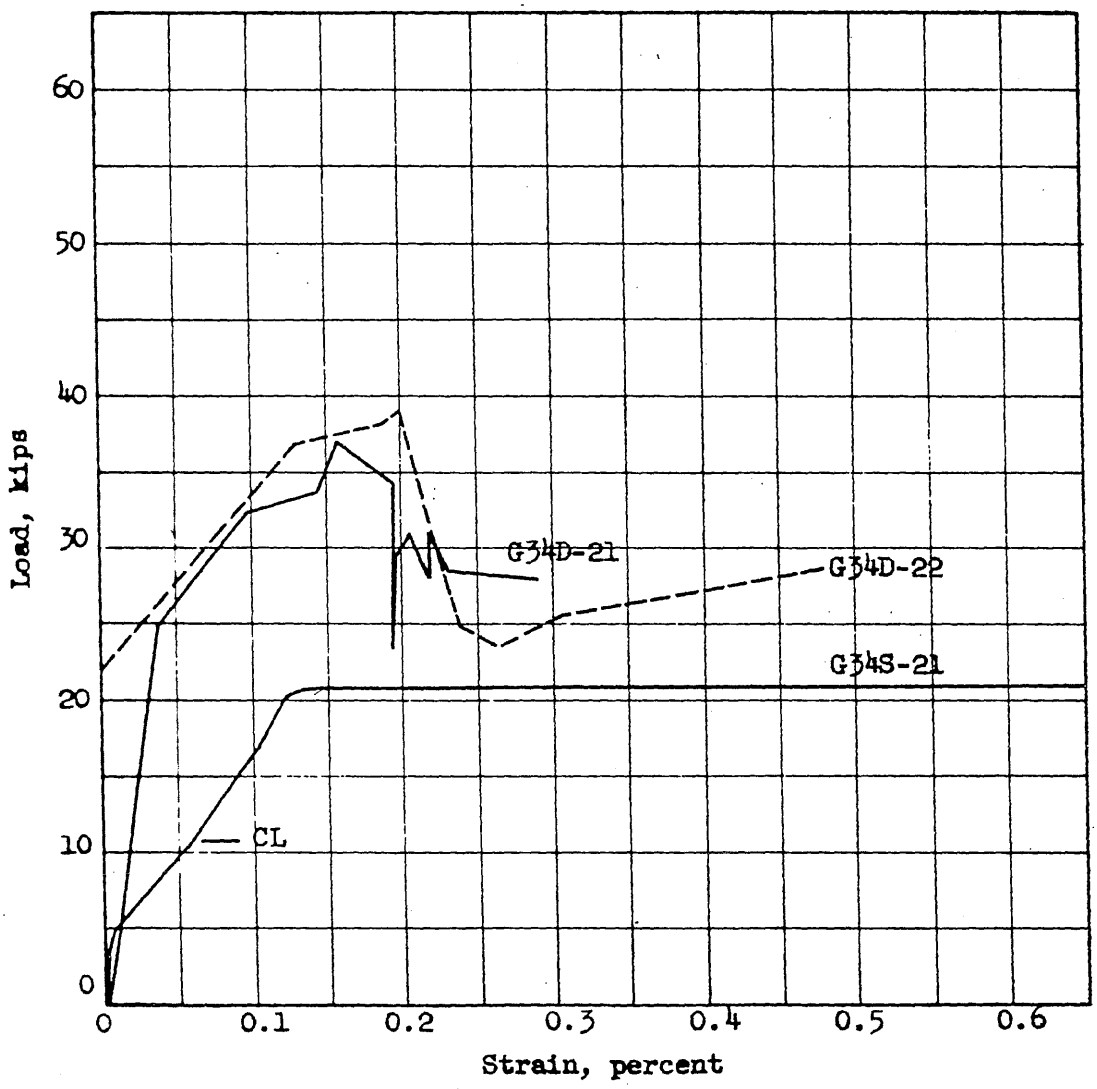

FIG. 4.20 LOAD VERSUS STEEL STRAIN FOR BEAMS G34S-21, G34D-21 AND G34D-22

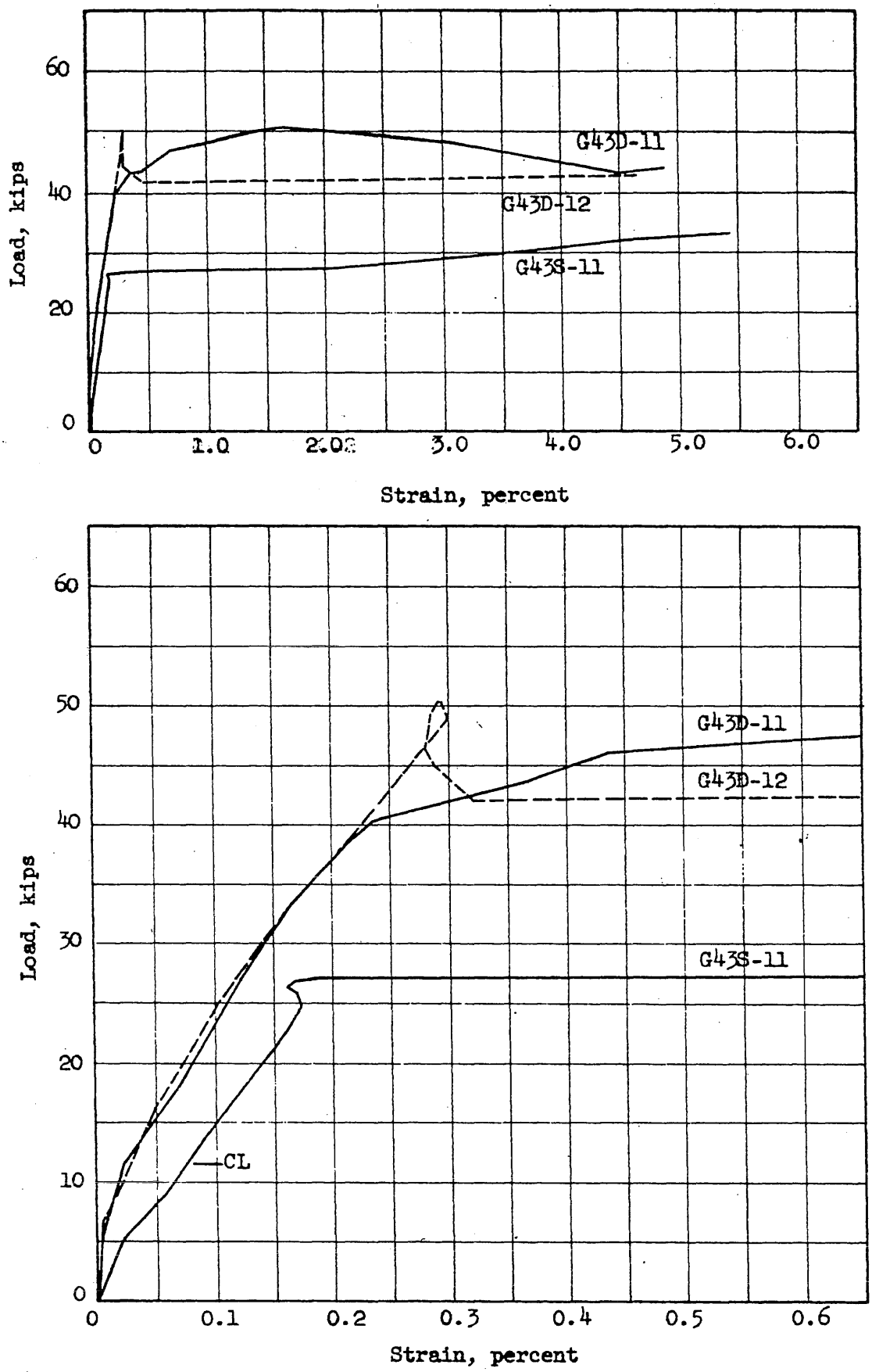

FIG. 4.21 LOAD VERSUS STEEL STRAIN FOR BEAMS G43S-11, G43D-11, AND G43D-12

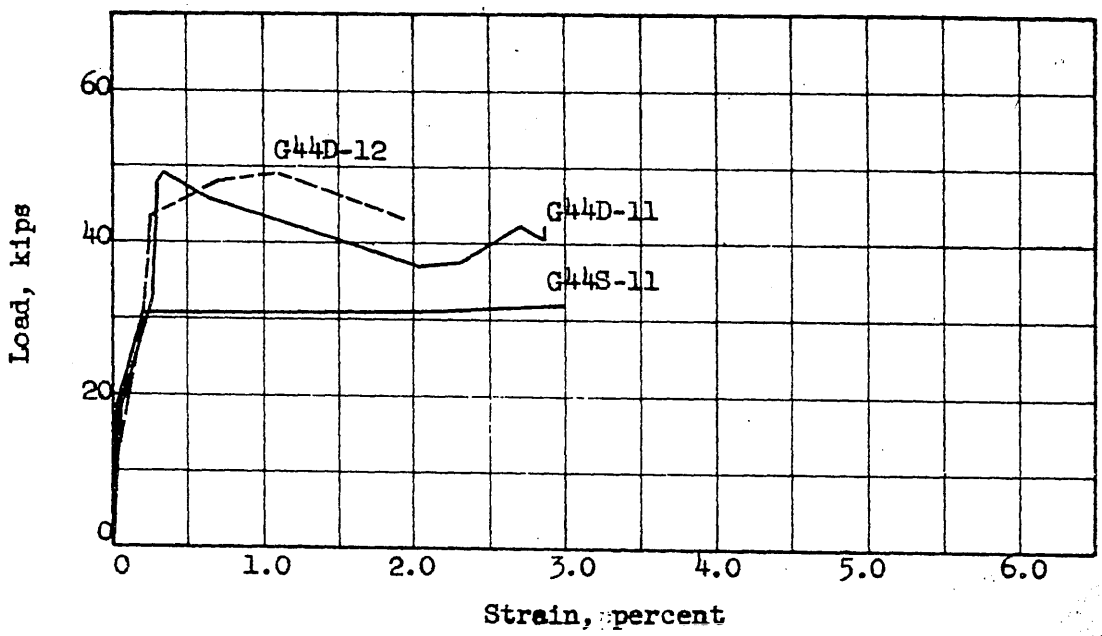

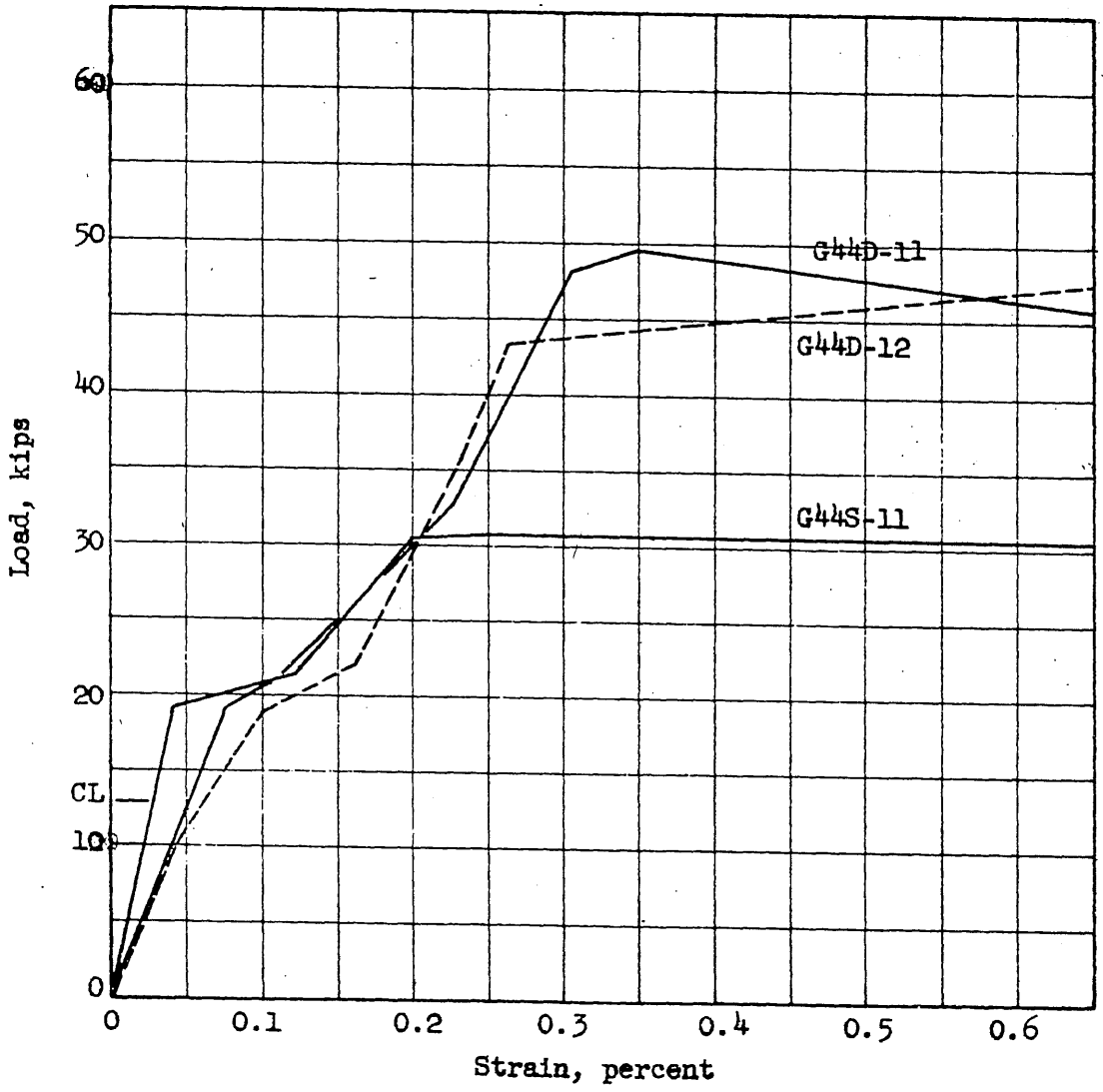

FIG. 4.22 LOAD VERSUS STEEL STRAIN FOR BEAMS G44S-11, G44D-11 AND G44D-12

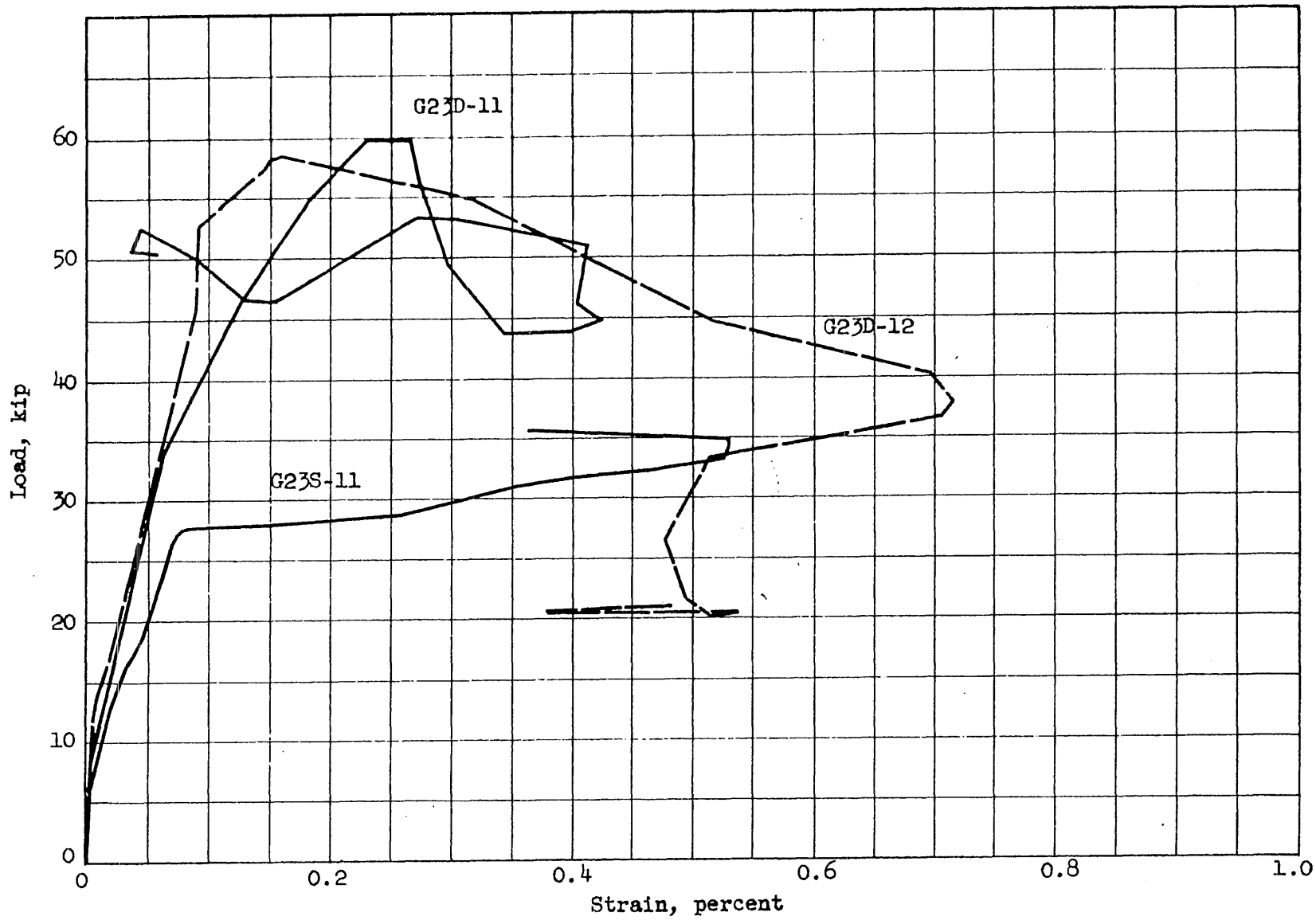

FIG. 4.23 LOAD VERSUS CONCRETE STRAIN FOR BEAMS G23S-11, G23D-11 AND G23D-12

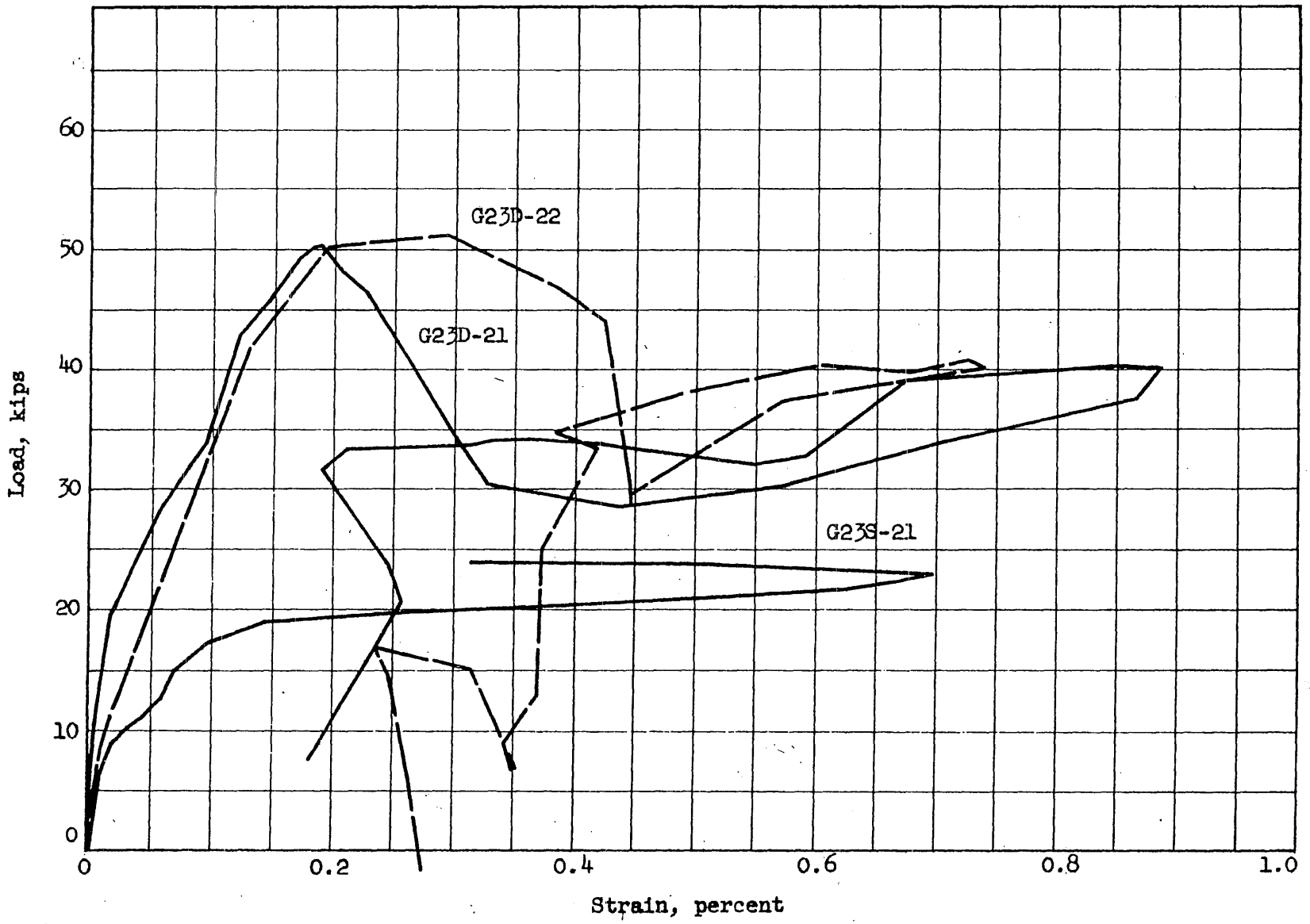

FIG. 4.24 LOAD VERSUS CONCRETE STRAIN FOR BEAMS G23S-21, G23D-21 AND G23D-22

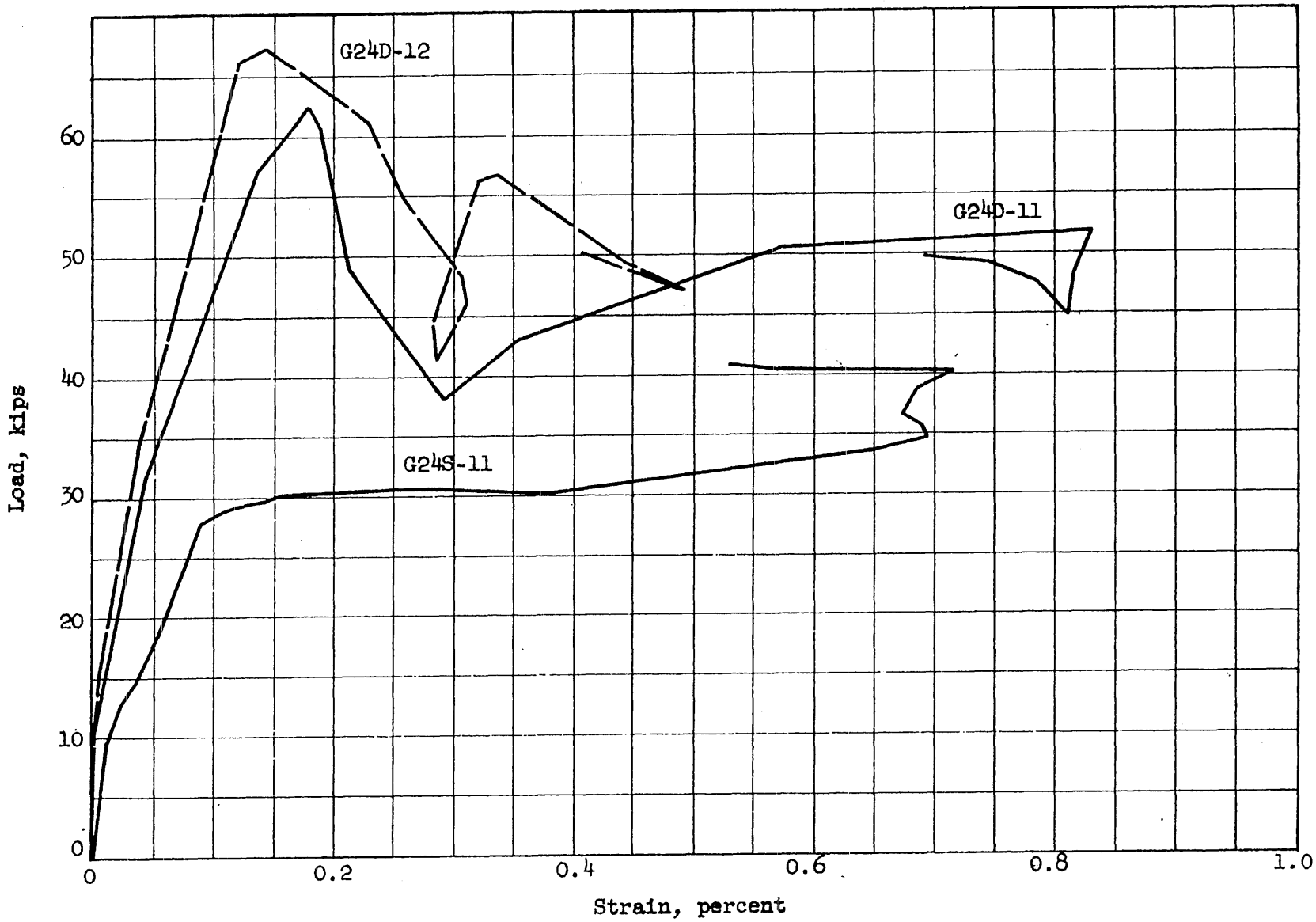

FIG. 4.25 LOAD VERSUS CONCRETE STRAIN FOR BEAMS G24S-11, G24D-11 AND G24D-12

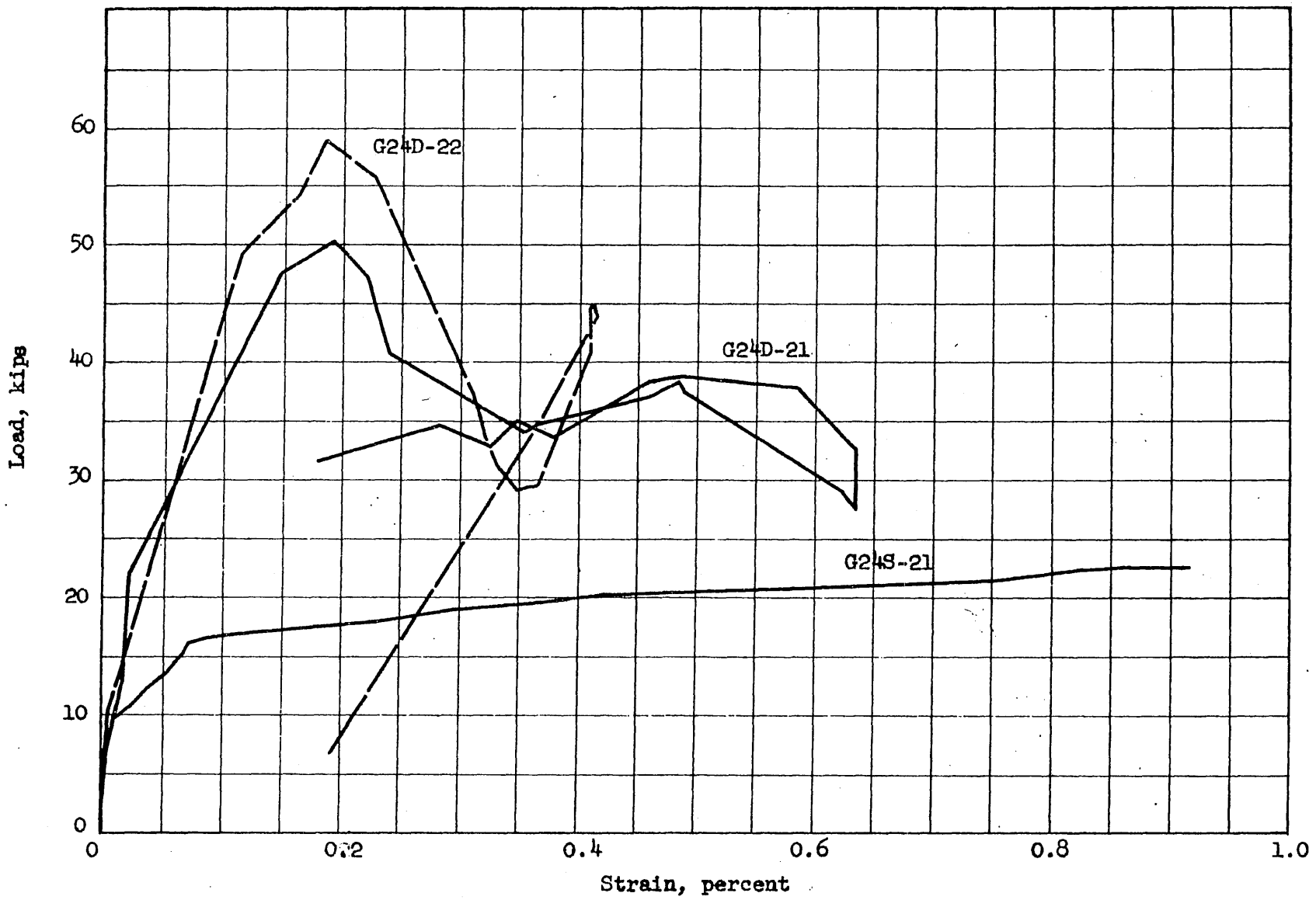

FIG. 4.26 LOAD VERSUS CONCRETE STRAIN FOR BEAMS G24S-21, G24D-21 AND G24D-22

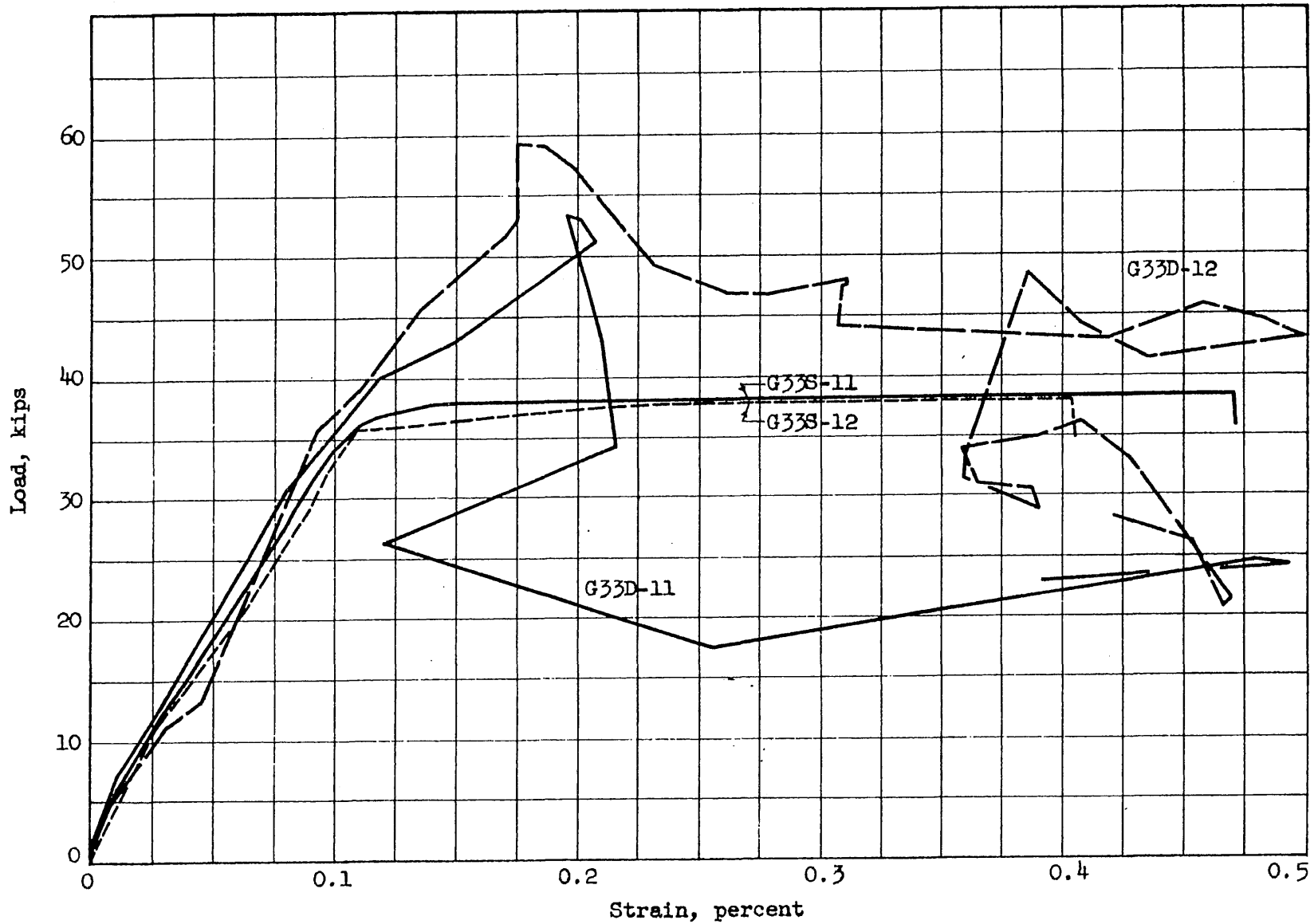

FIG. 4.27 LOAD VERSUS CONCRETE STRAIN FOR BEAMS G33S-11, G33S-12, G33D-11 AND G33D-12

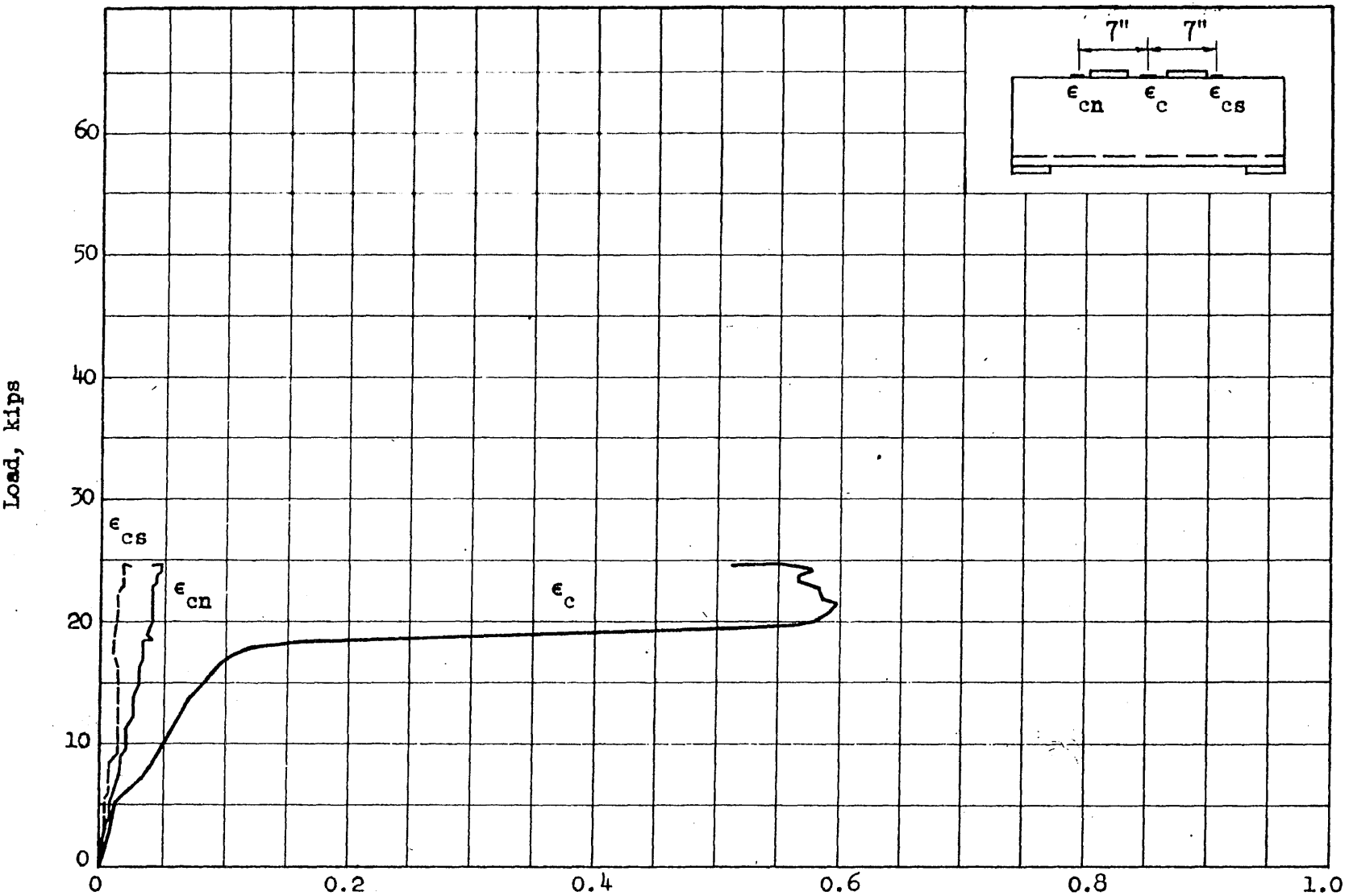

FIG. 4.28 LOAD VERSUS CONCRETE STRAIN FOR BEAM G33S-21

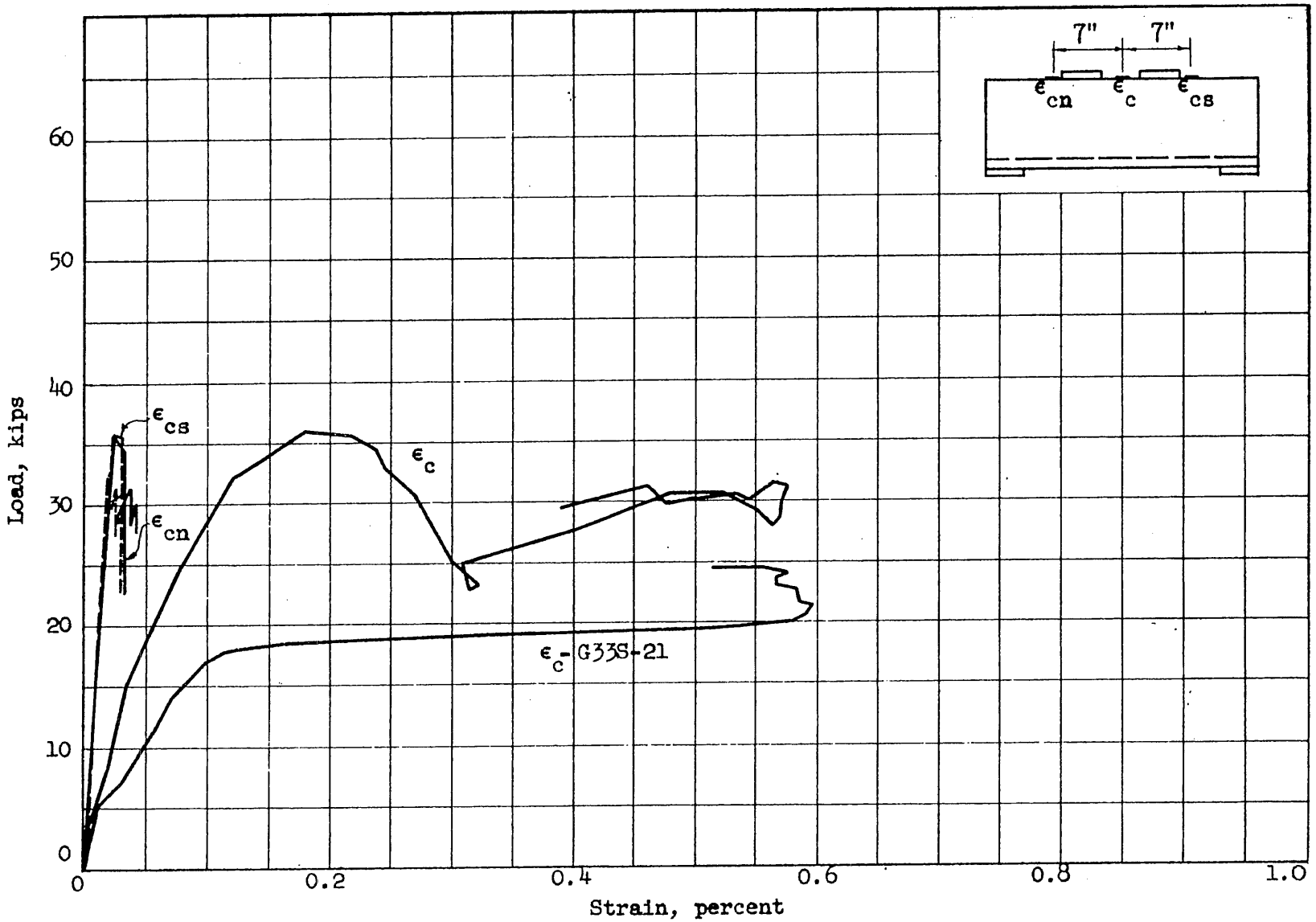

FIG. 4.29 LOAD VERSUS CONCRETE STRAIN FOR BEAM G33D-21

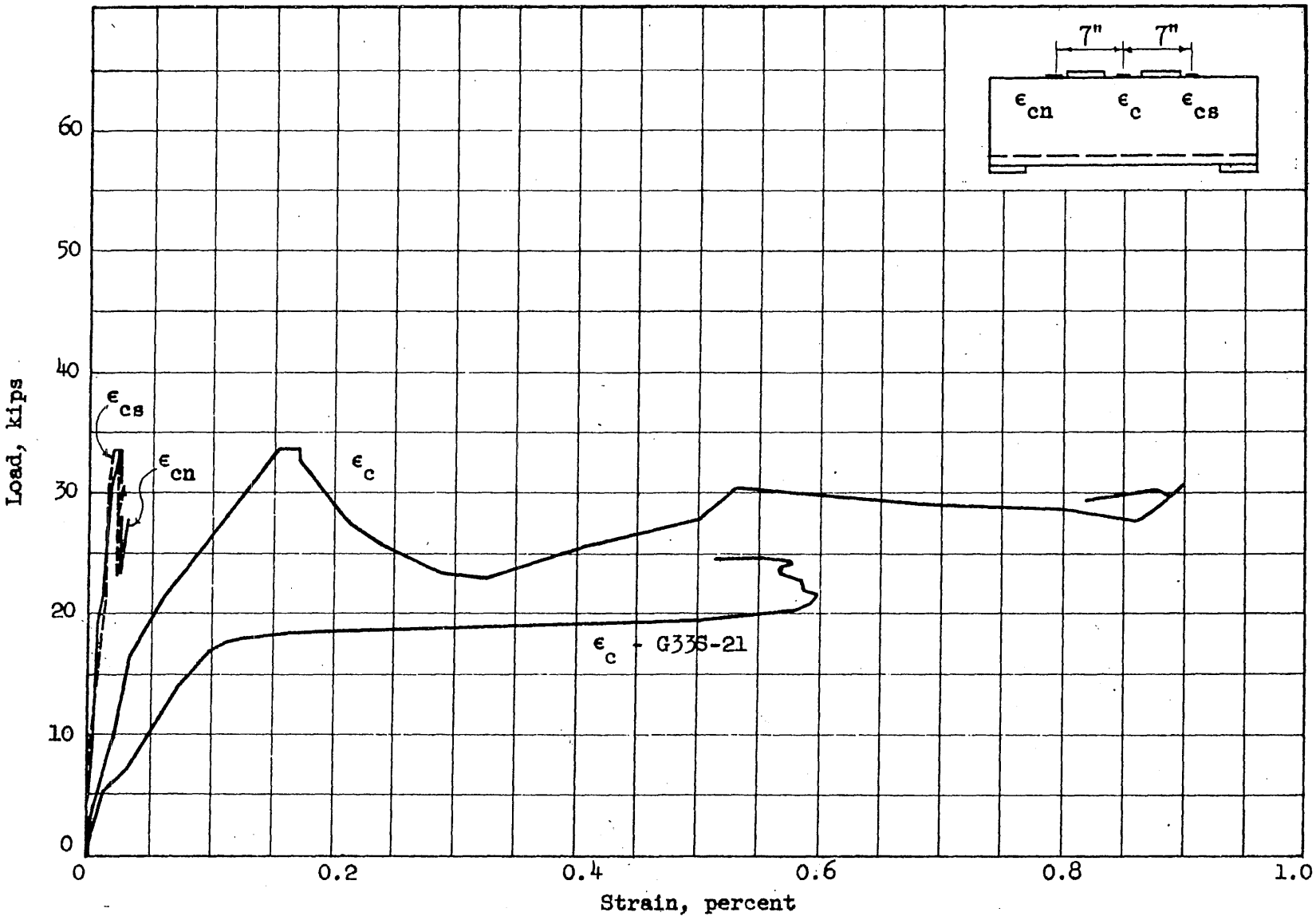

FIG. 4.30 LOAD VERSUS CONCRETE STRAIN FOR BEAM G33D-22

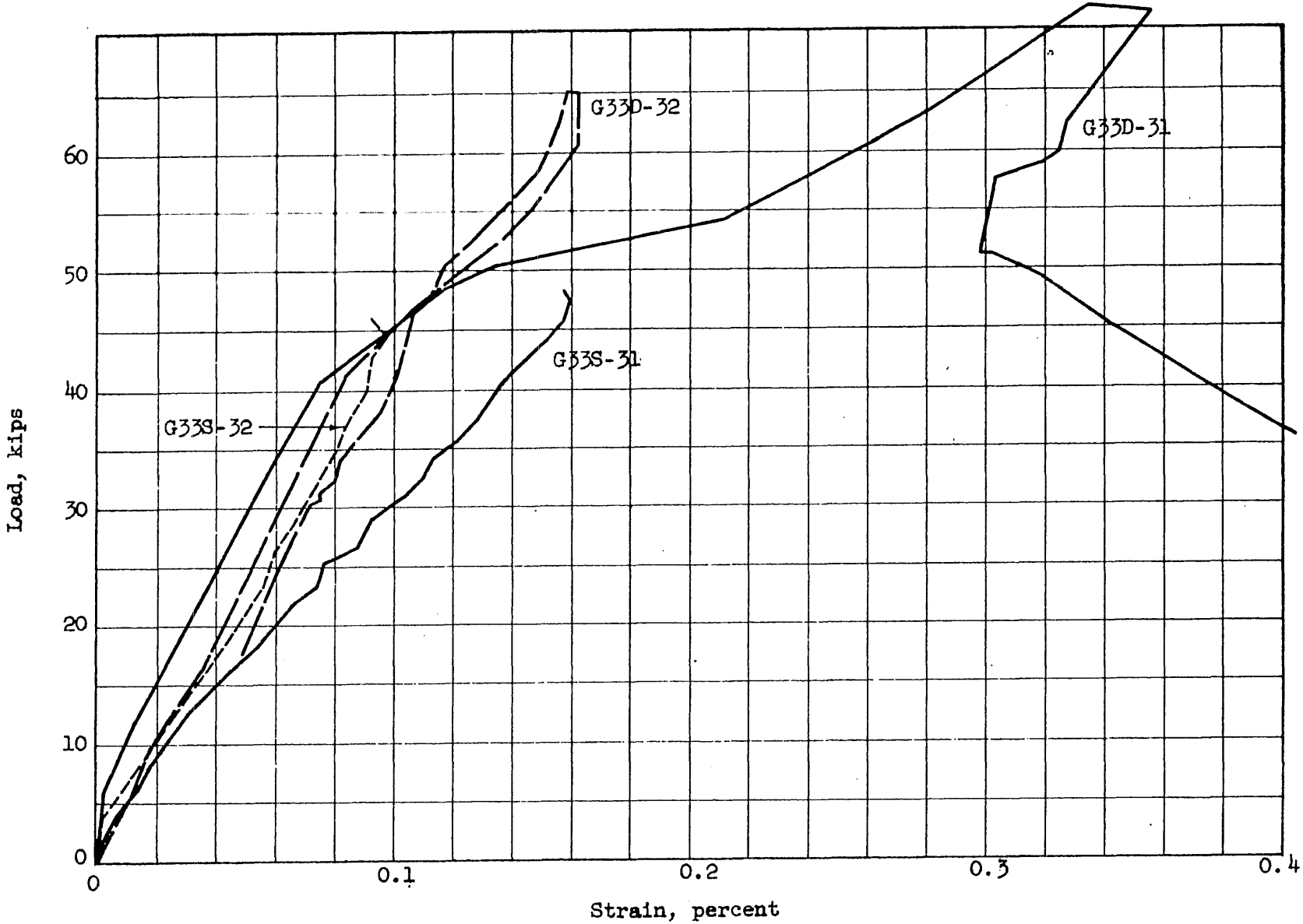

FIG. 4.31 LOAD VERSUS CONCRETE STRAIN FOR BEAMS G33S-31, G33S-32, G33D-31 AND G33D-32

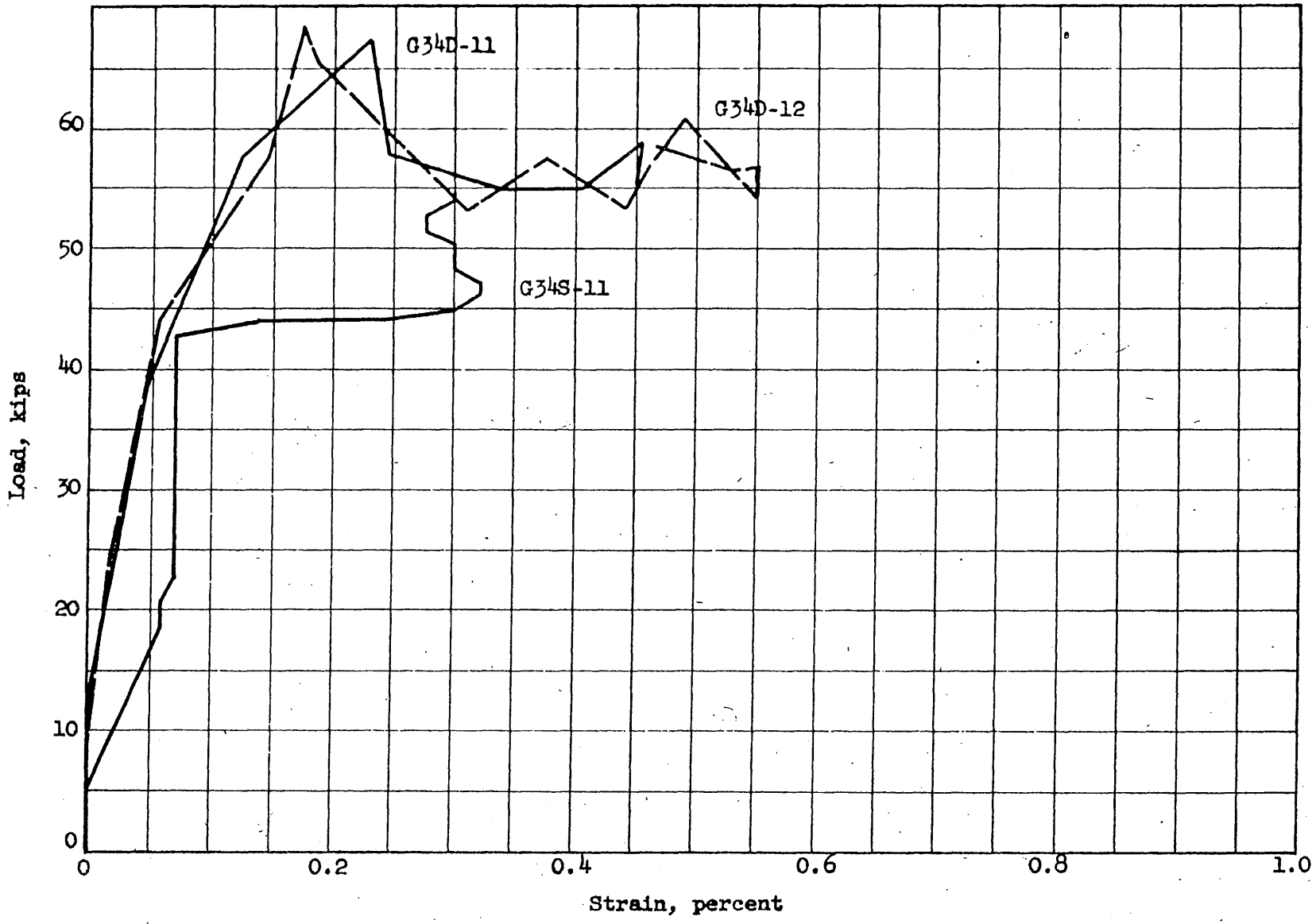

FIG. 4.32 LOAD VERSUS CONCRETE STRAIN FOR BEAMS G34S-11, G34D-11 AND G34D-12

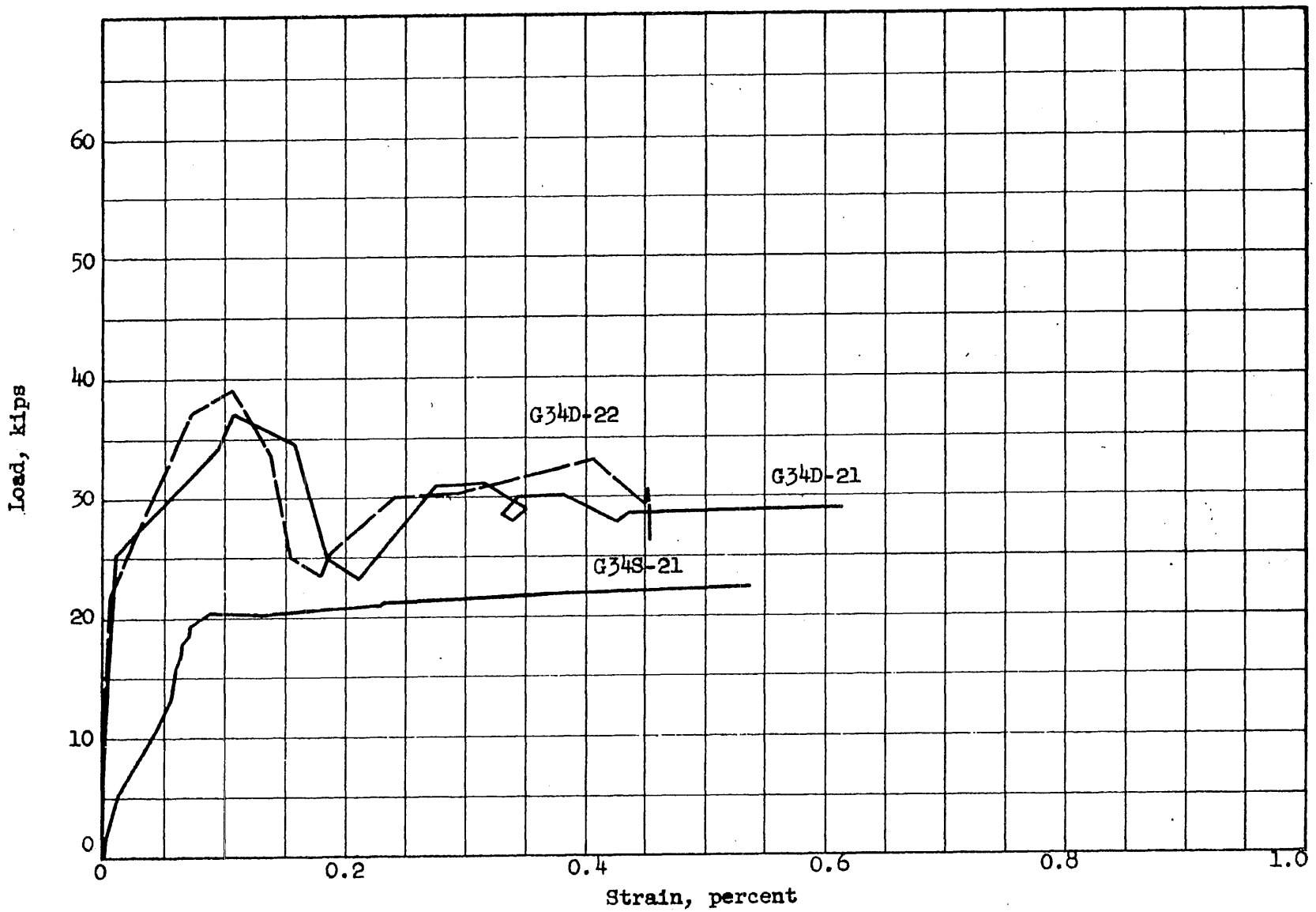

FIG. 4.33 LOAD VERSUS CONCRETE STRAIN FOR BEAMS G34S-21, G34D-21 AND G34D-22

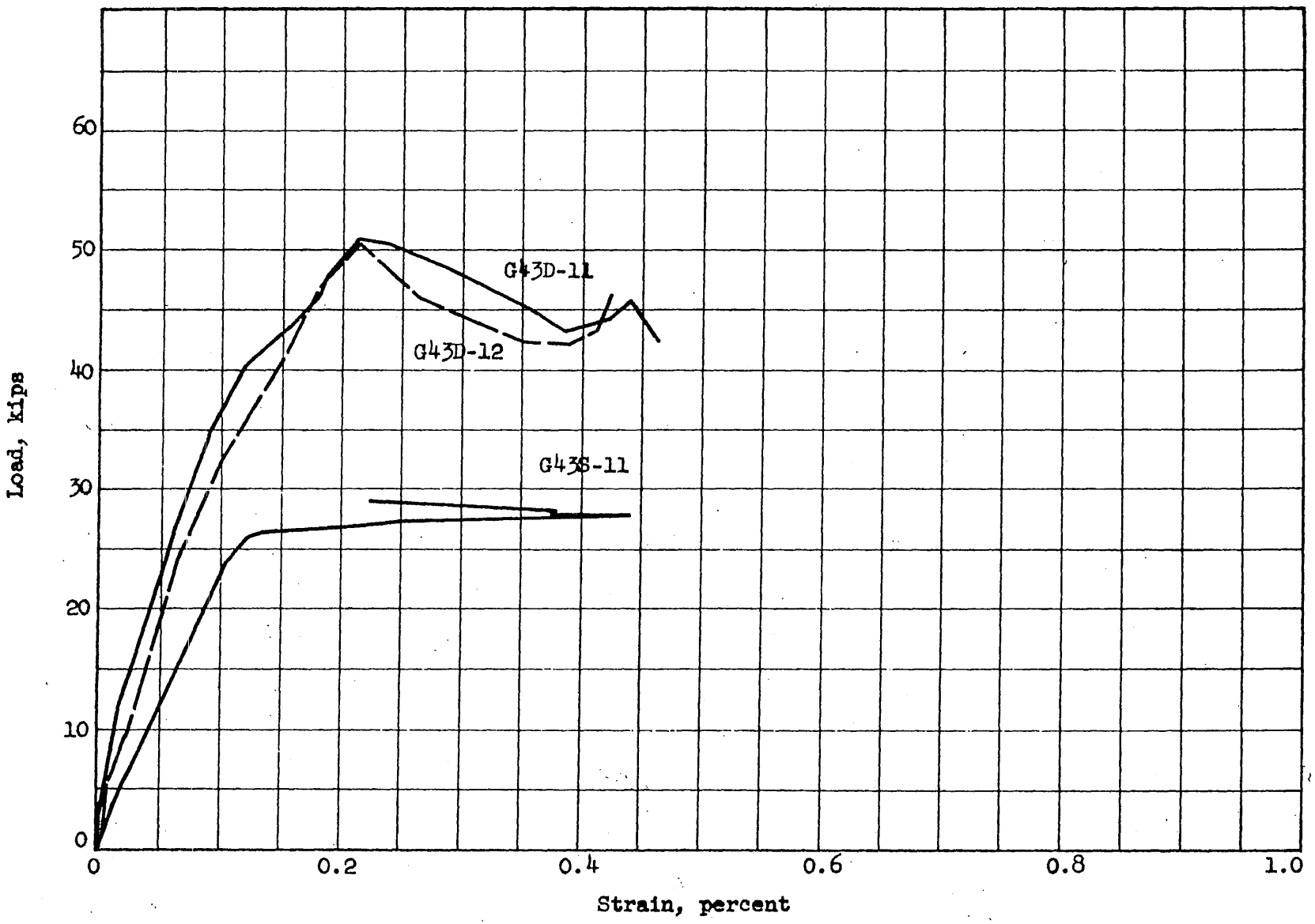

FIG. 4.34 LOAD VERSUS CONCRETE STRAIN FOR BEAMS G43S-11, G43D-11 AND G43D-12

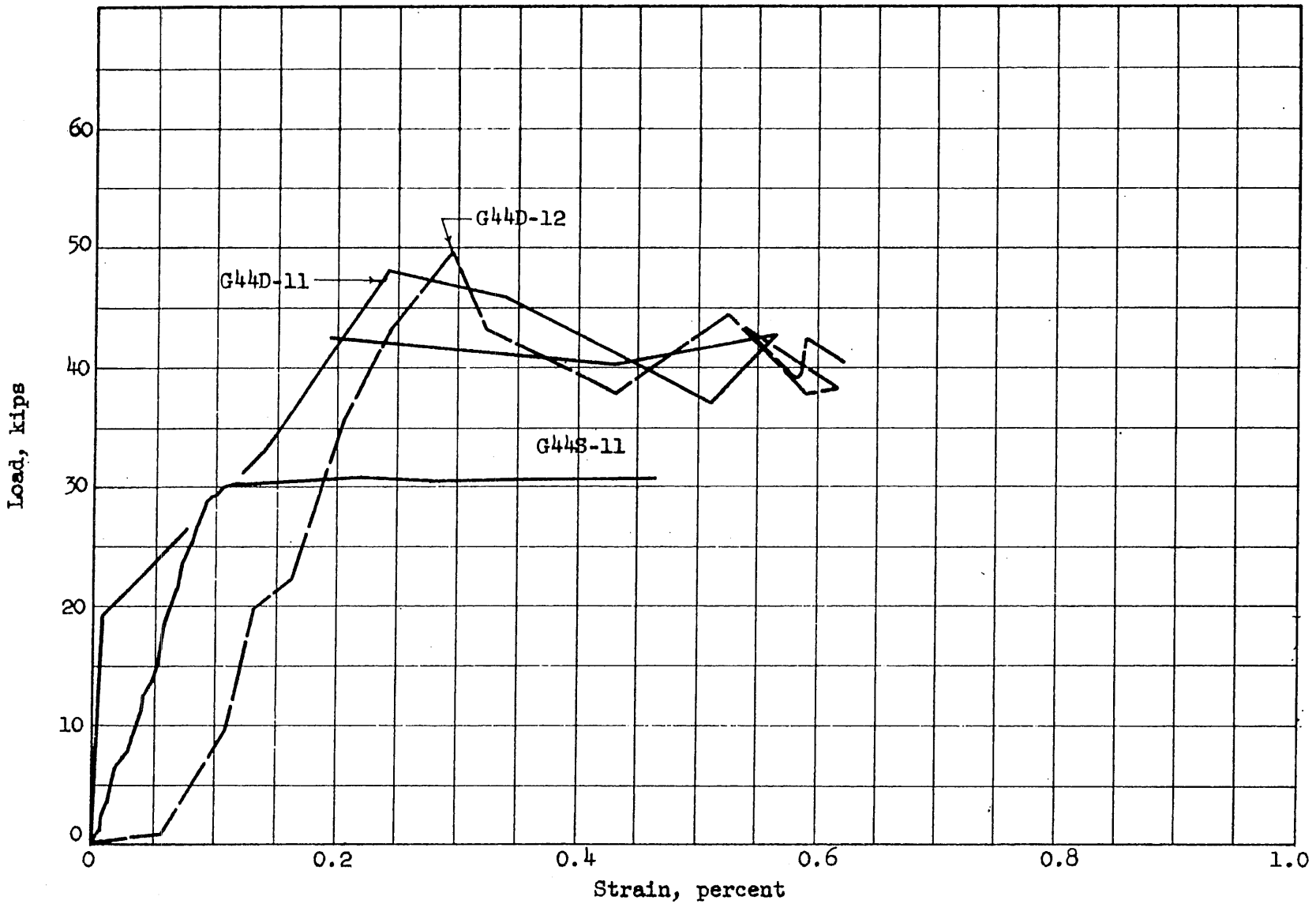

FIG. 4.35 LOAD VERSUS CONCRETE STRAIN FOR BEAMS G44S-11, G44D-11 AND G44D-12

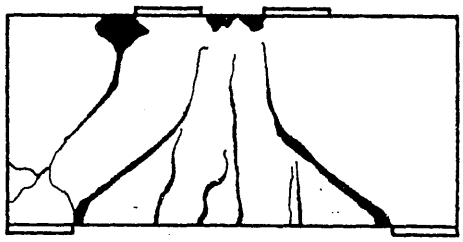

G23S-11

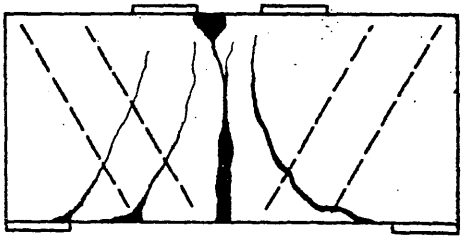

G23D-22

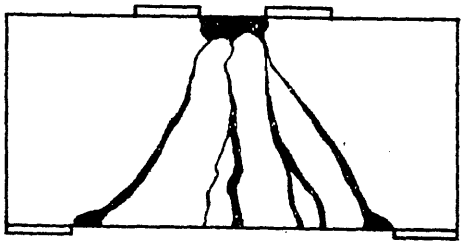

G23D-11

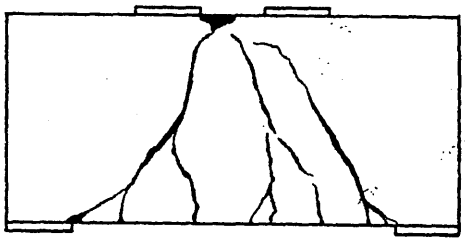

G24S-11

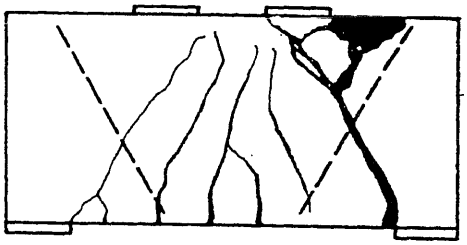

G23D-12

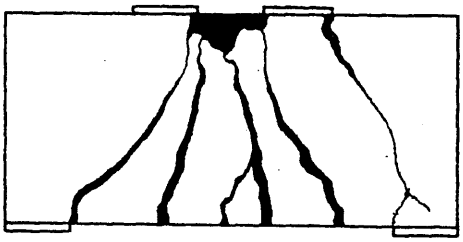

G24D-11

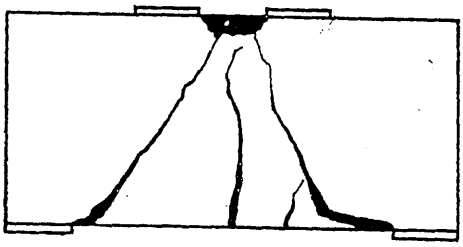

G23S-21

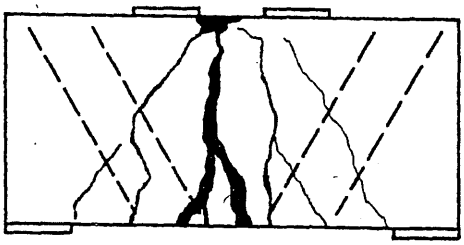

G24D-12

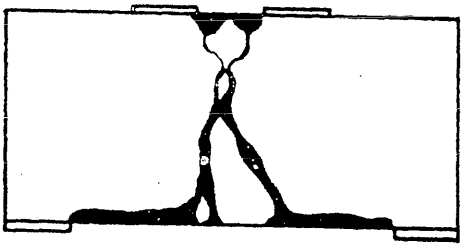

G23D-21

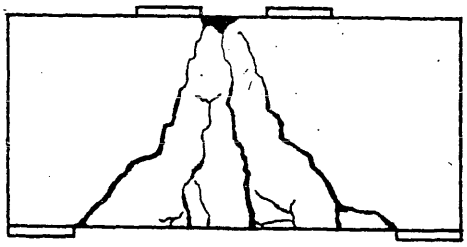

G24S-21

FIG. 4.36a CRACK PATTERNS AT FAILURE

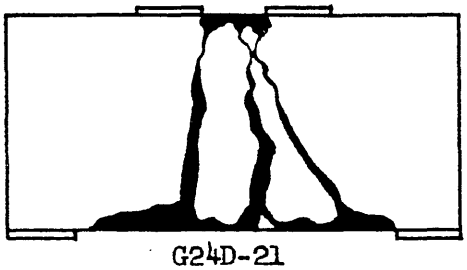

G24D-21

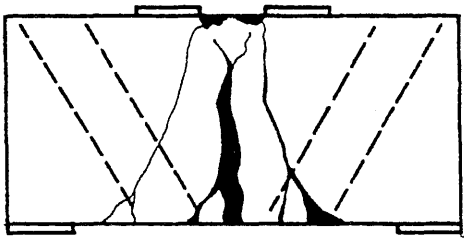

G24D-22

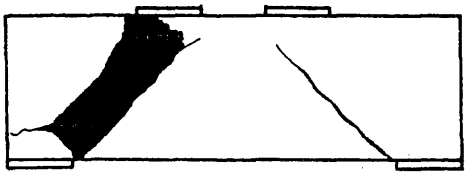

G33S-11

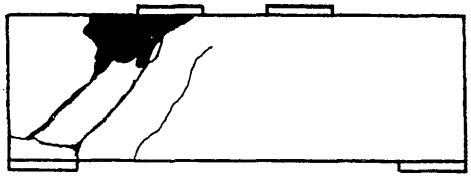

G33D-11

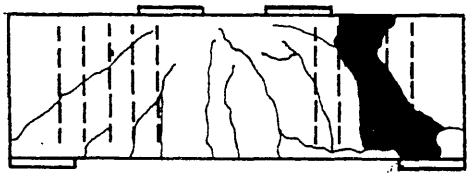

G33S-12

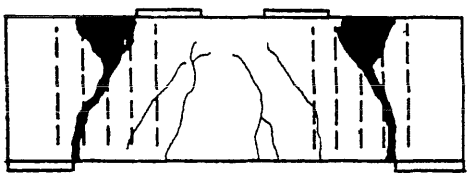

G33D-12

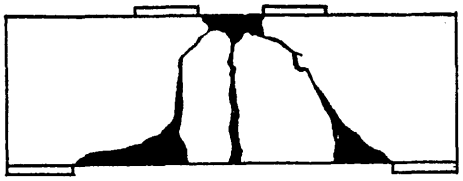

G33S-21

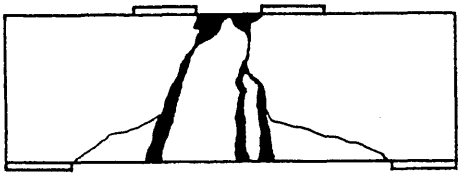

G33D-21

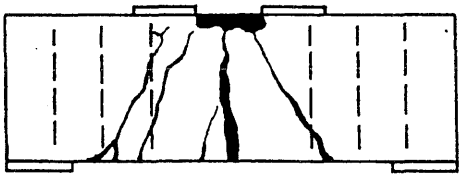

G33D-22

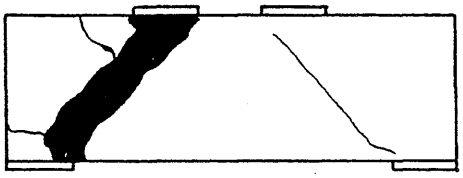

G33S-31

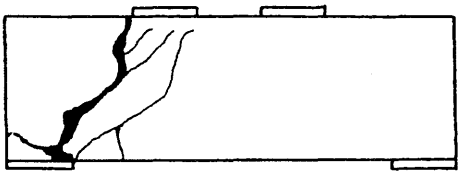

G33D-31

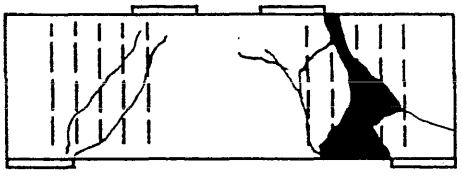

G33S-32

FIG. 4.36b CRACK PATTERNS AT FAILURE

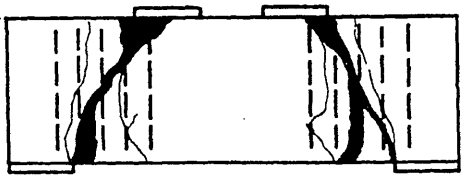

G33D-32

G34D-22

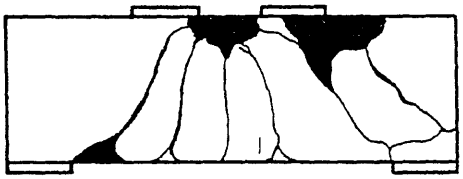

G34S-11

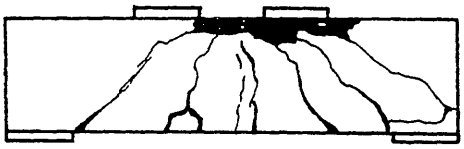

G43S-11

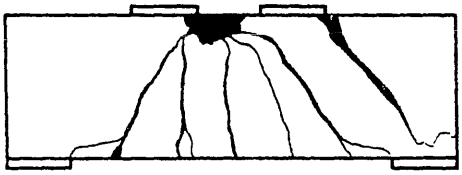

G34D-11

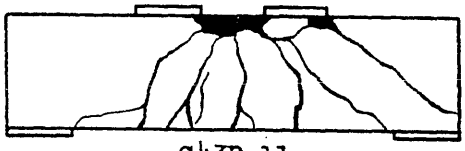

G43D-11

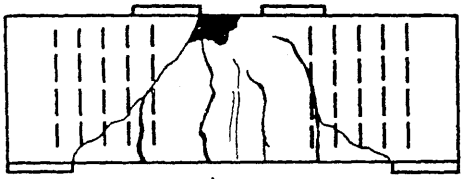

G34D-12

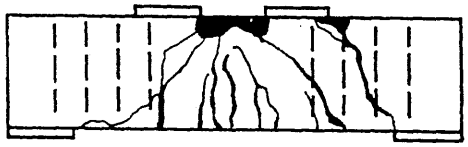

G43D-12

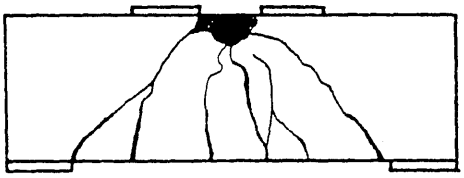

G34S-21

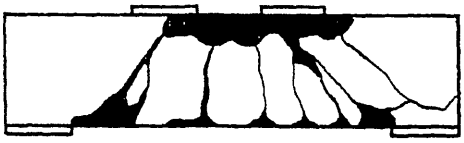

G44S-11

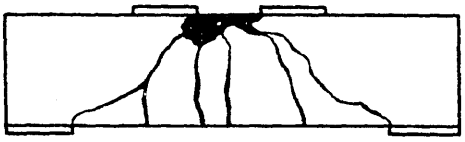

G44D-11

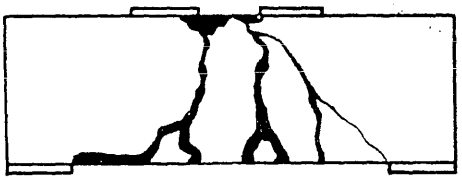

G34D-21

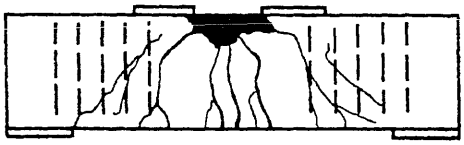

G44D-12

FIG. 4.36c CRACK PATTERNS AT FAILURE

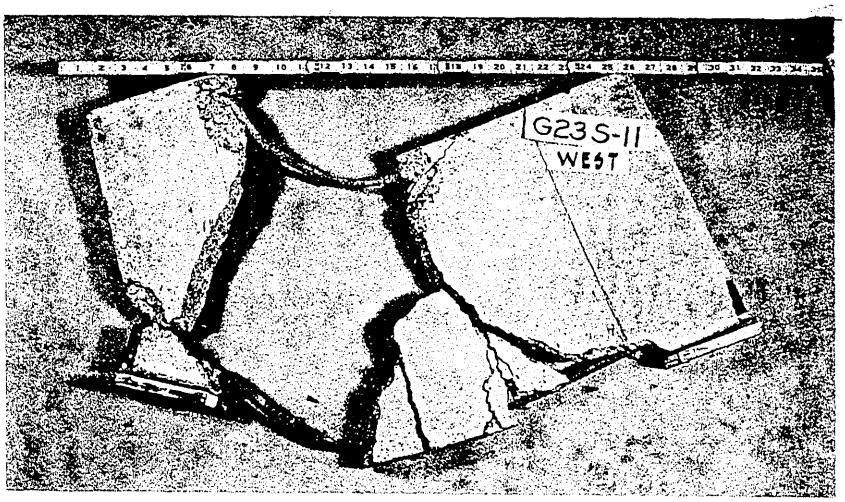

G23S-11

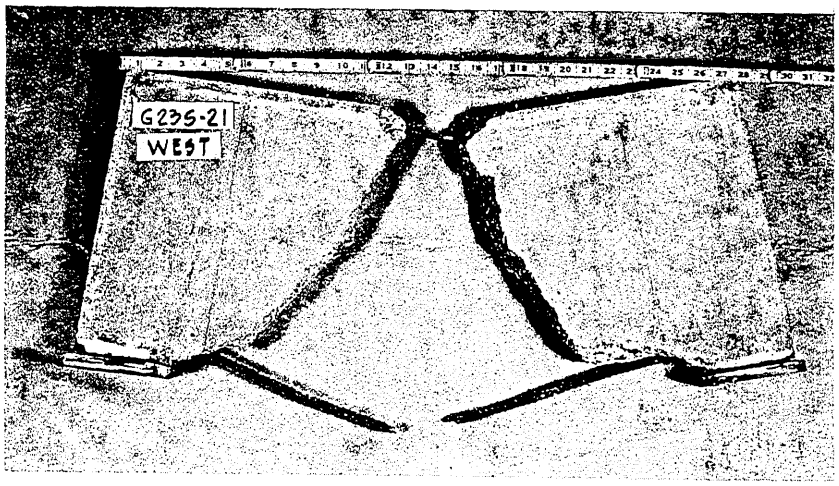

G23S-21

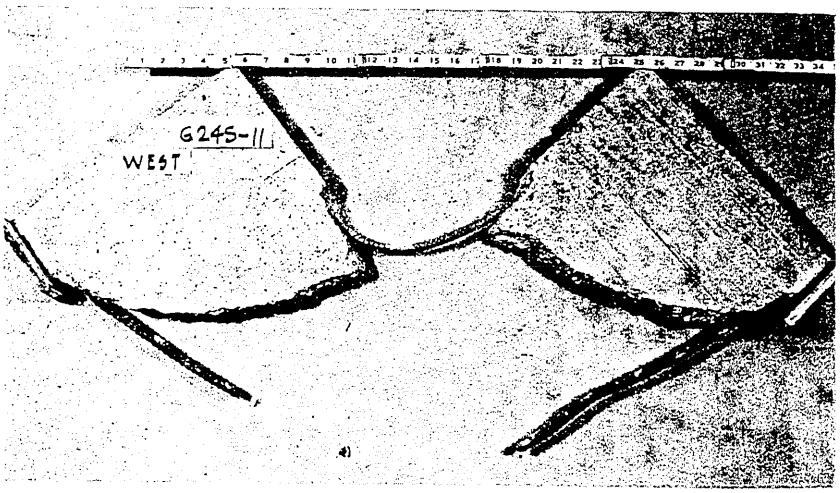

G24S-11

FIG. 4.37a PHOTOGRAPHS OF STATIC TEST FAILURES

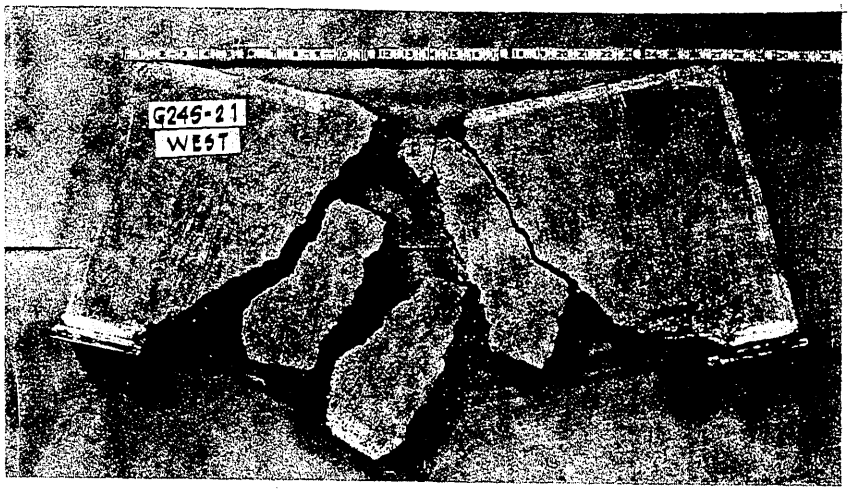

G24S-21

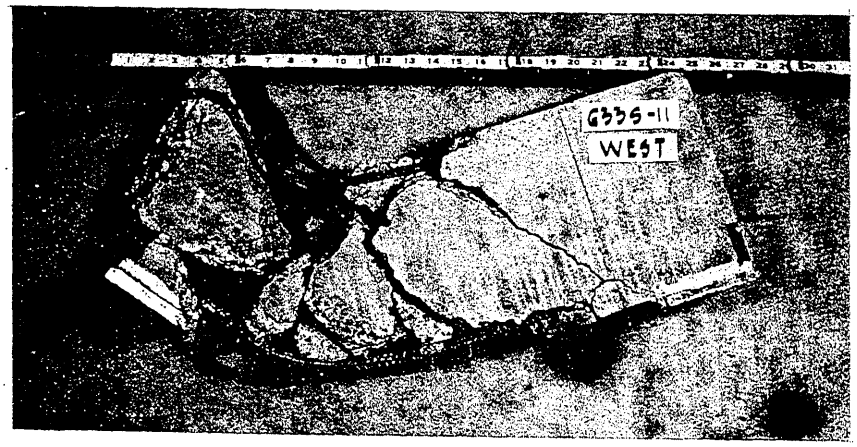

G33S-11

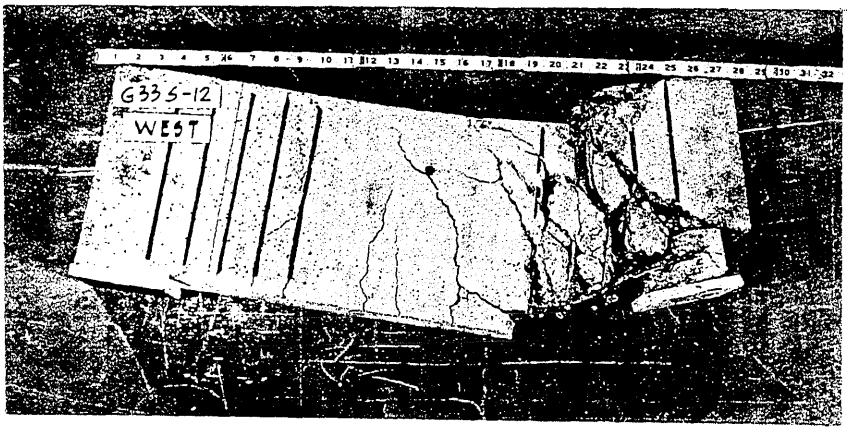

G33S-12

FIG. 4.37b PHOTOGRAPHS OF STATIC TEST FAILURES

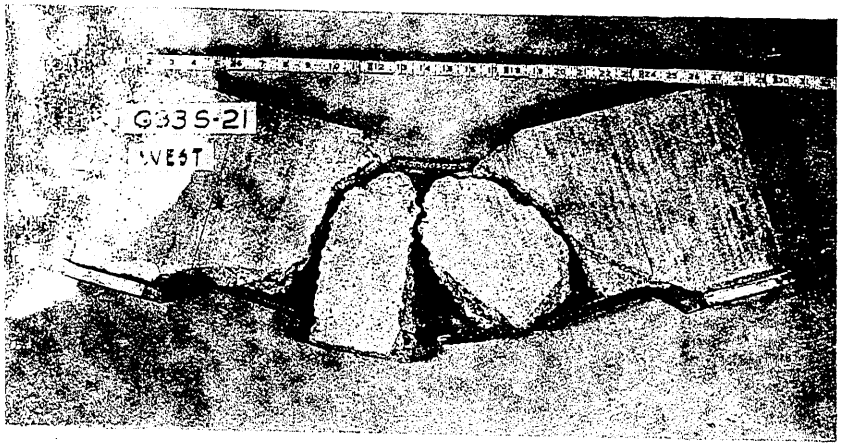

G33S-21

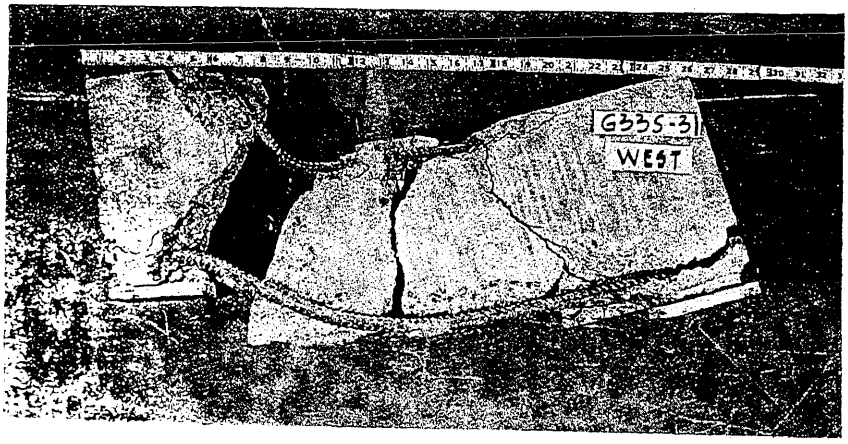

G33S-31

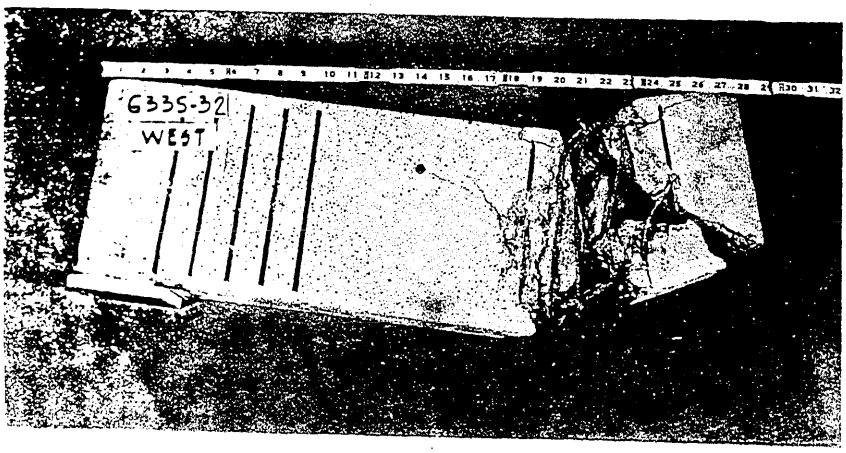

G33S-32

FIG. 4.37c PHOTOGRAPHS OF STATIC TEST FAILURES

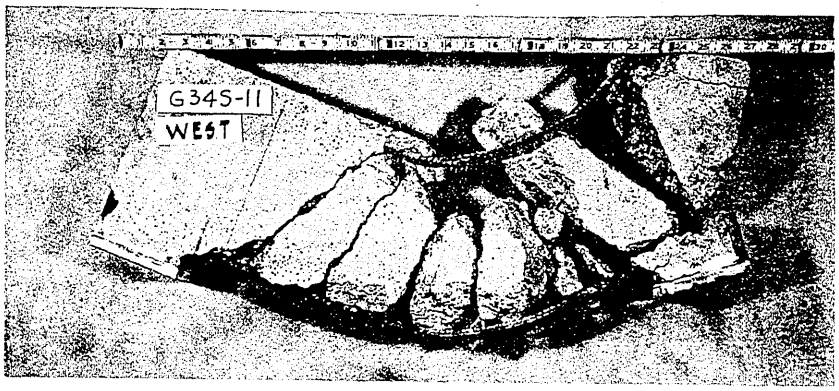

G34S-11

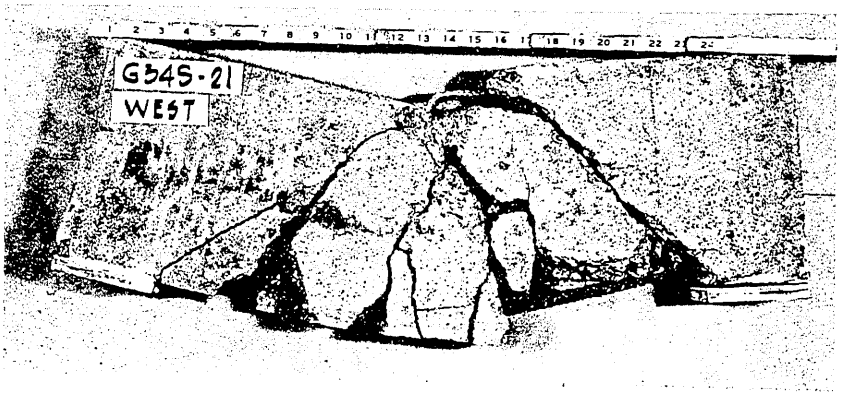

G34S-21

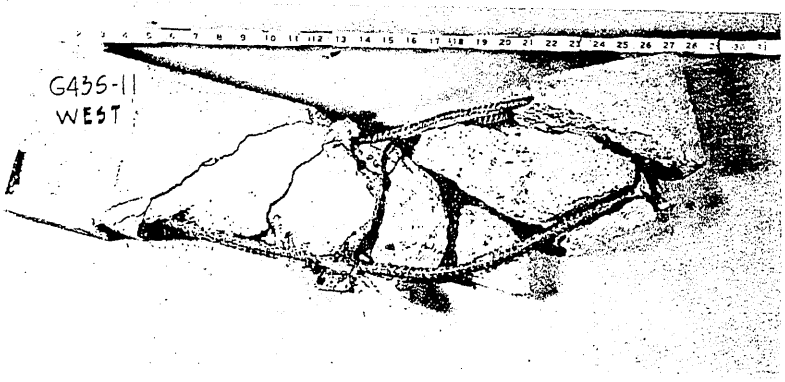

G43S-11

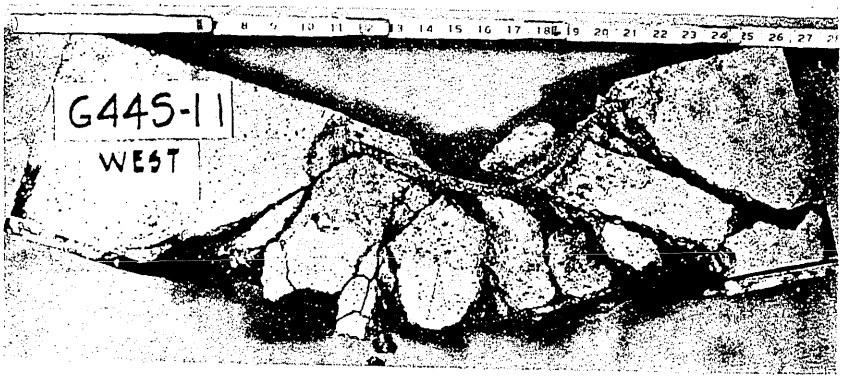

G44S-11

FIG. 4.37d PHOTOGRAPHS OF STATIC TEST FAILURES

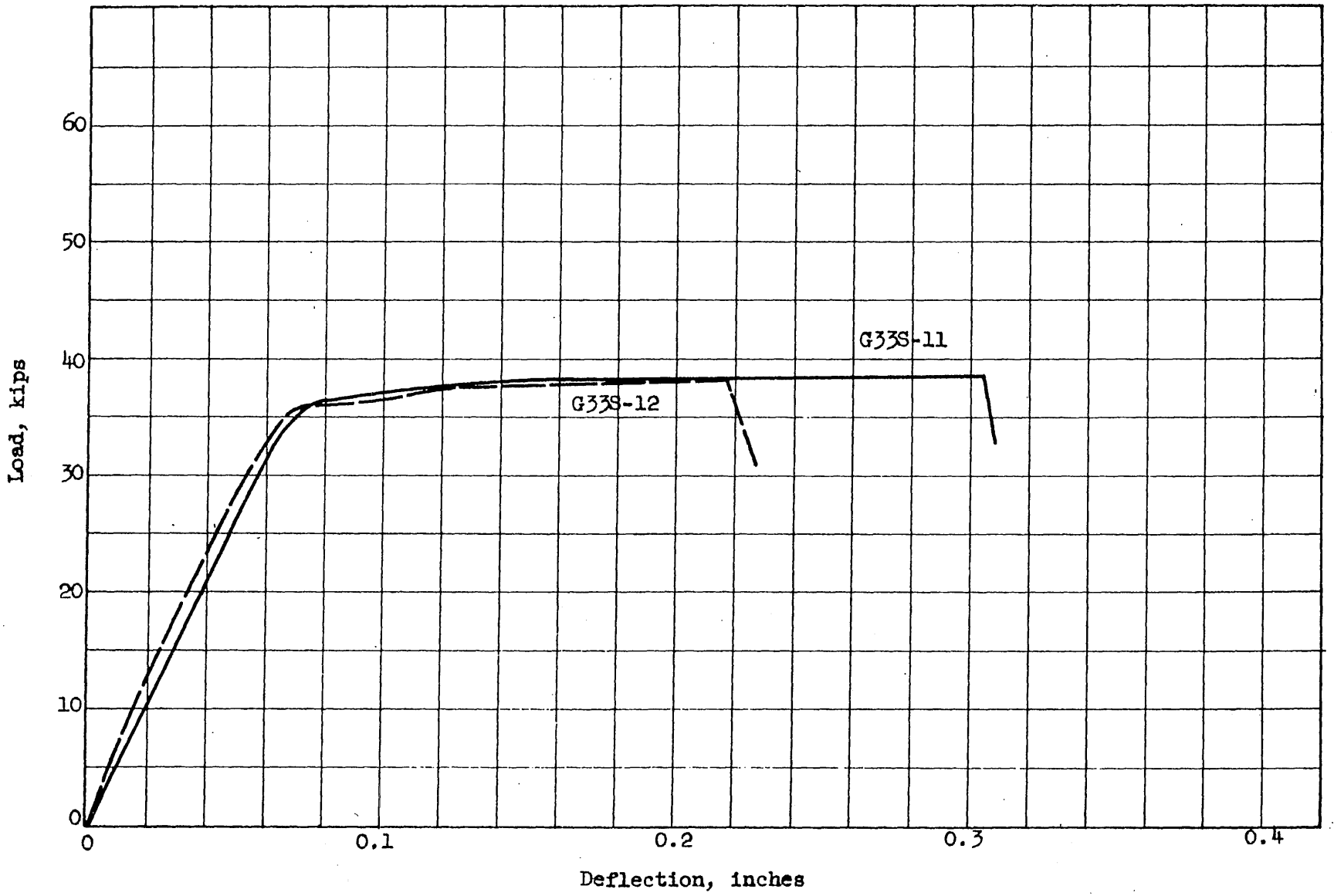

FIG. 4.38 LOAD VERSUS MIDSPAN DEFLECTION CURVES FOR BEAMS G33S-11 AND G33S-12

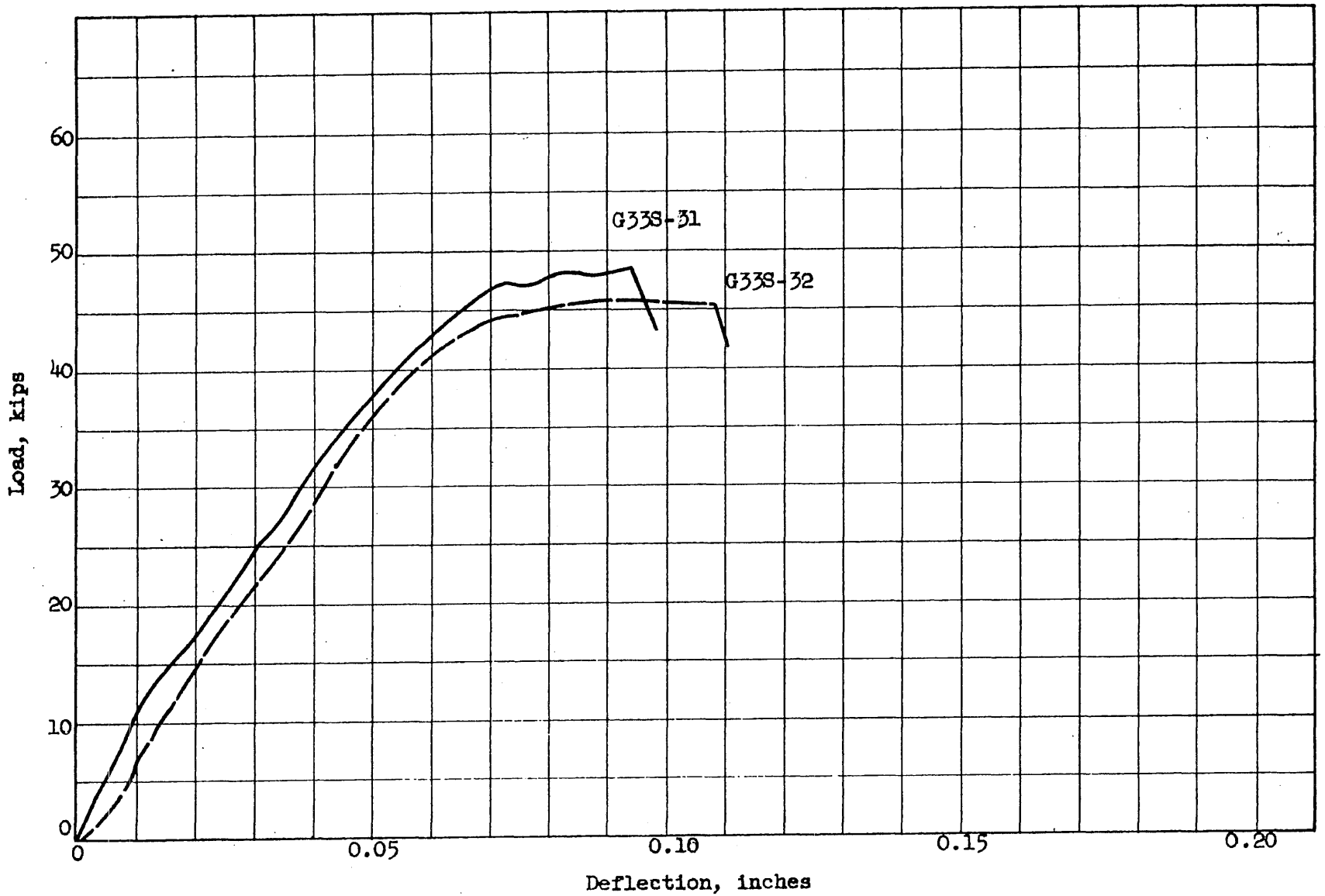

FIG. 4.39 LOAD VERSUS MIDSPAN DEFLECTION CURVES FOR BEAMS G33S-31 AND G33S-32

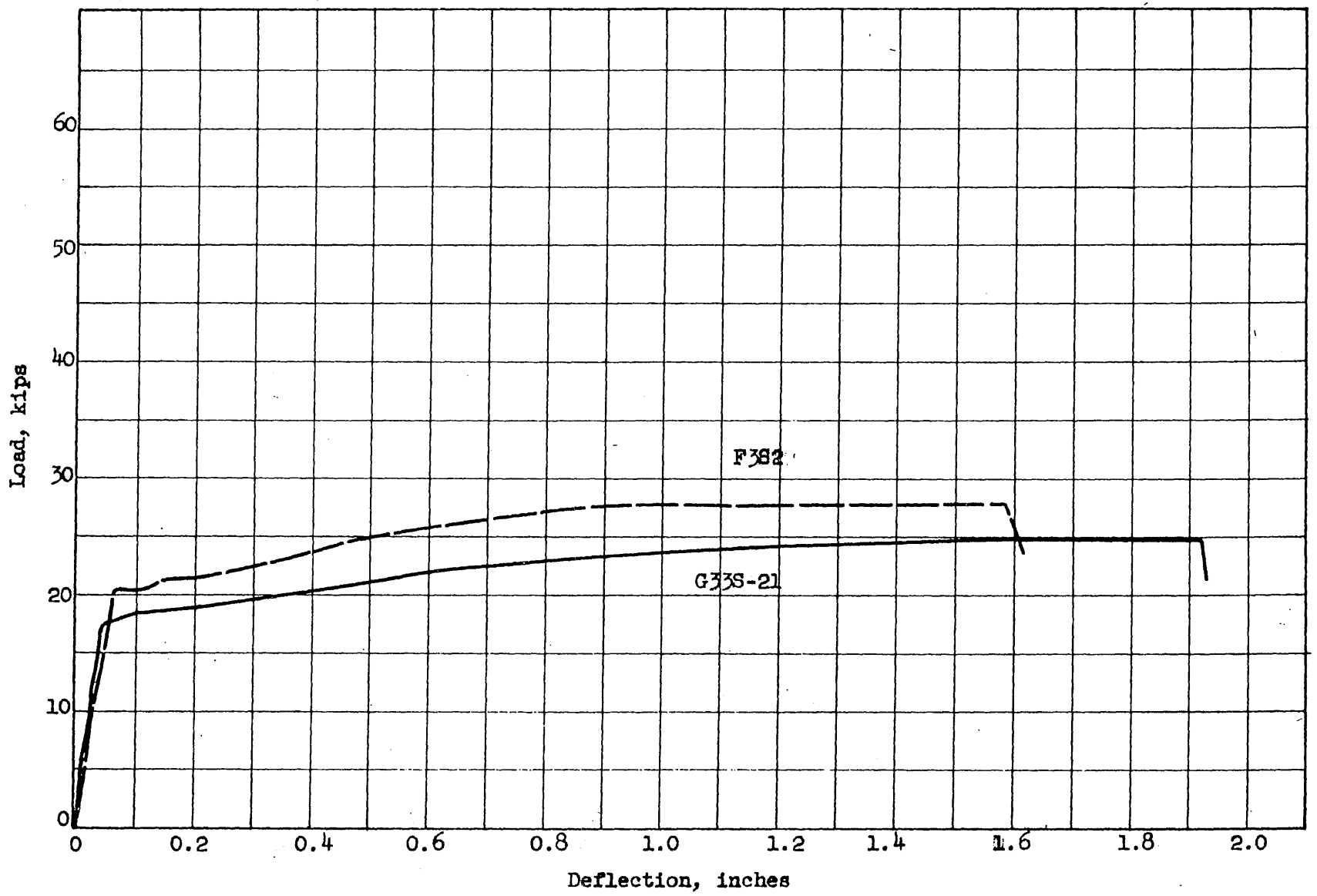

FIG. 4.40 LOAD VERSUS MIDSPAN DEFLECTION CURVES FOR BEAMS G33S-21 AND F3S2

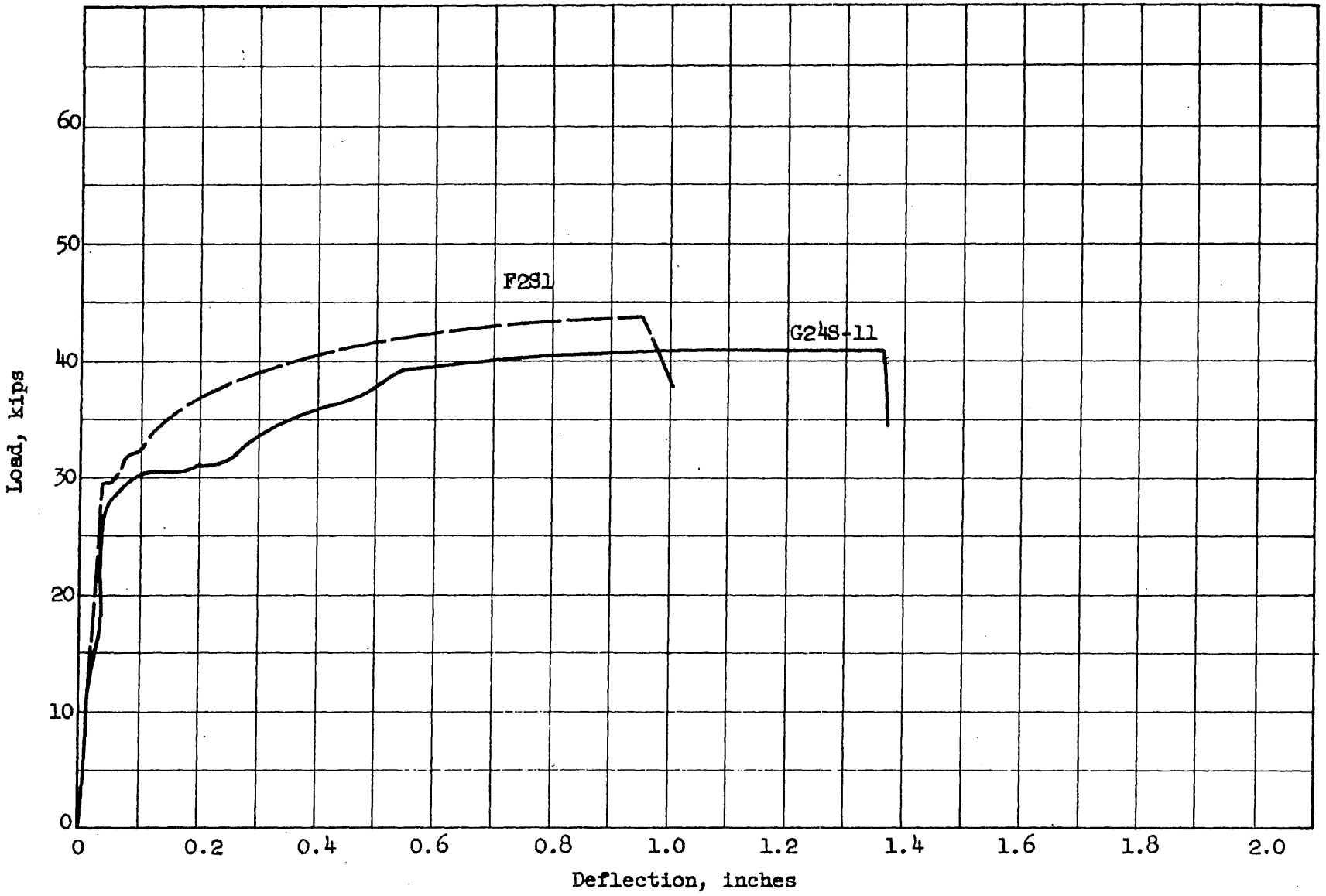

FIG. 4.41 LOAD VERSUS MIDSPAN DEFLECTION CURVES FOR BEAMS G24S-11 AND F2S1

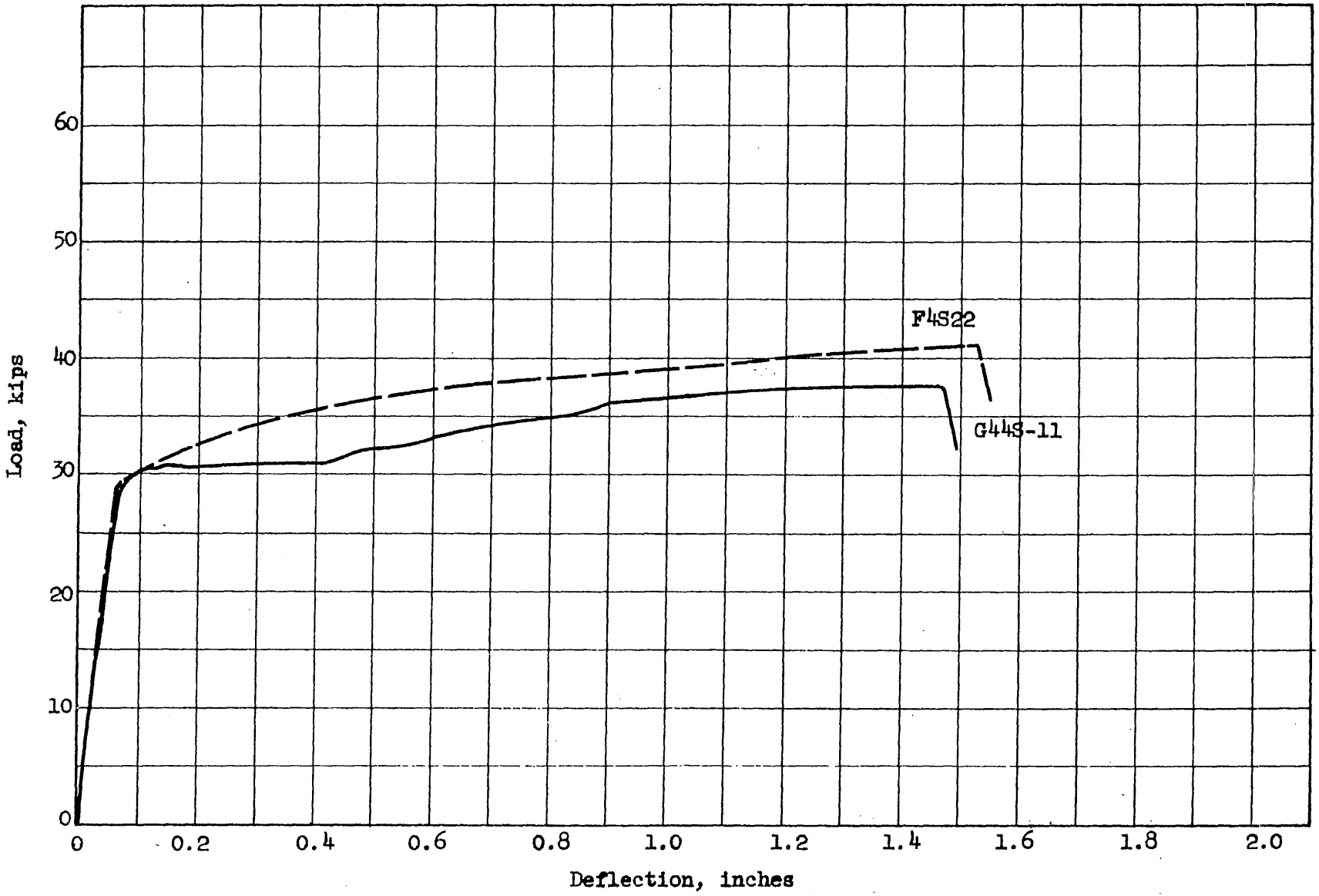

FIG. 4.42 LOAD VERSUS MIDSPAN DEFLECTION CURVES FOR BEAMS G4S-11 AND F4S22

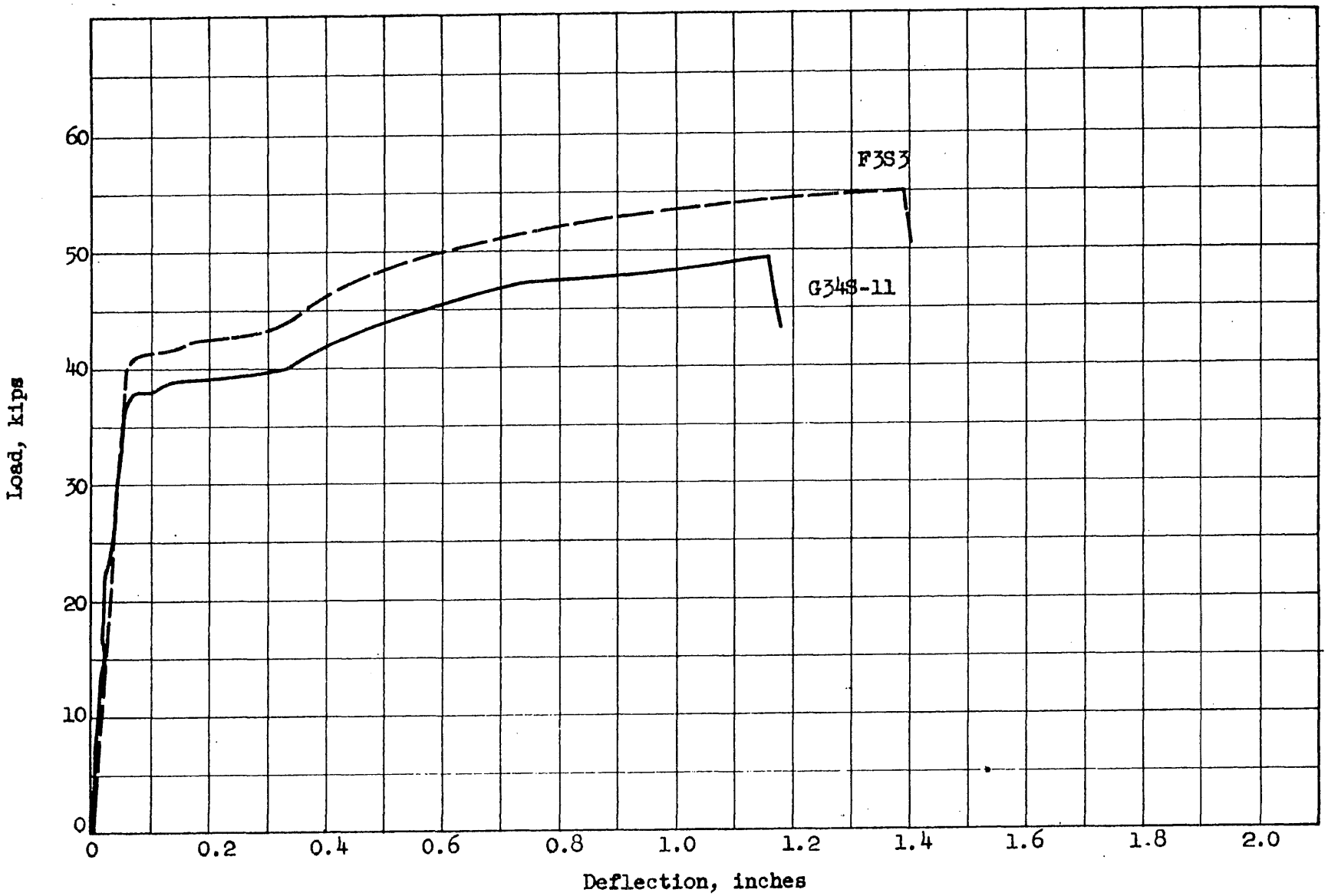

FIG. 4.43 LOAD VERSUS MIDSPAN DEFLECTION CURVES FOR BEAMS G34S-11 AND F3S3

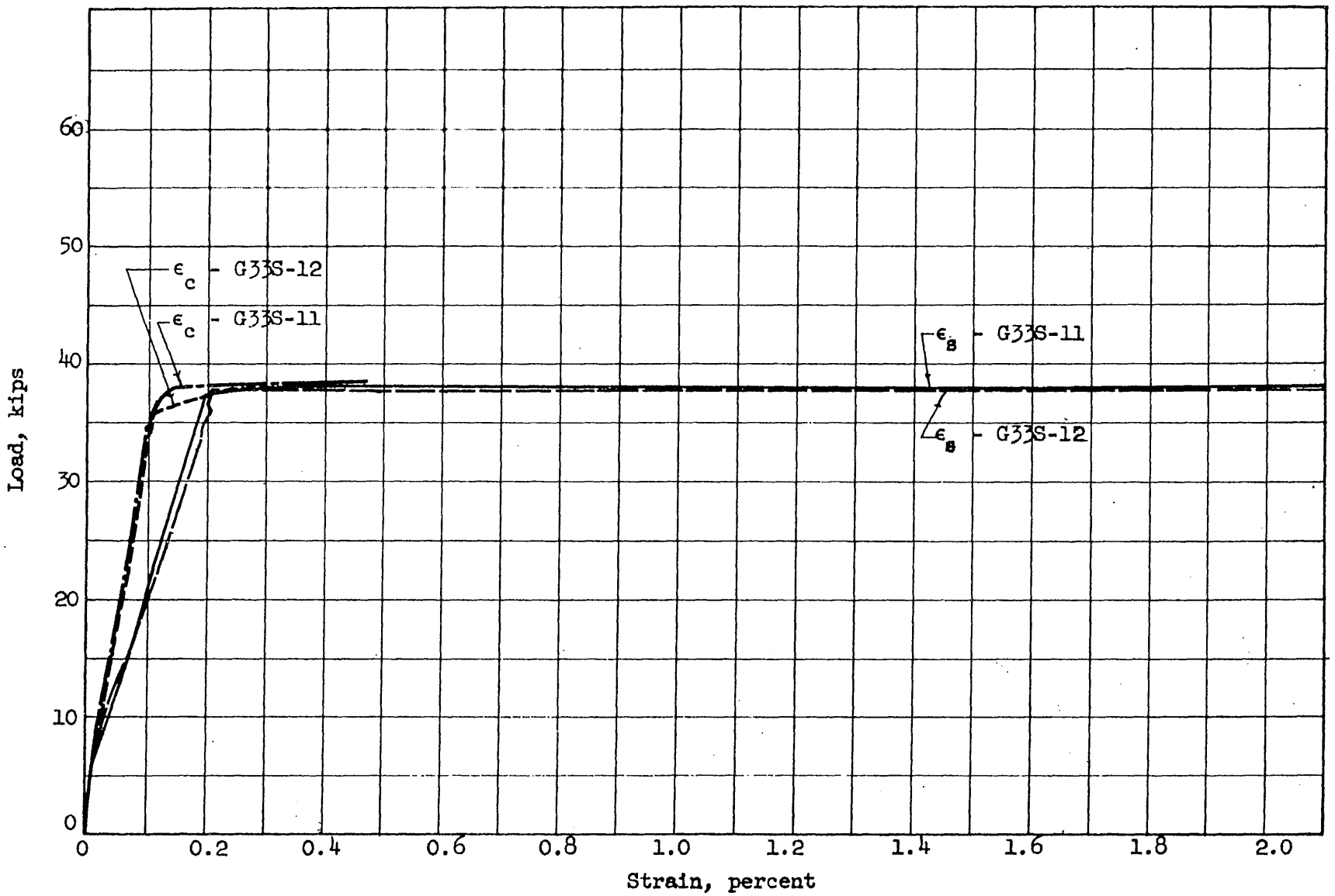

FIG. 4.44 LOAD-STRAIN CURVES FOR BEAMS G33S-11 AND G33S-12

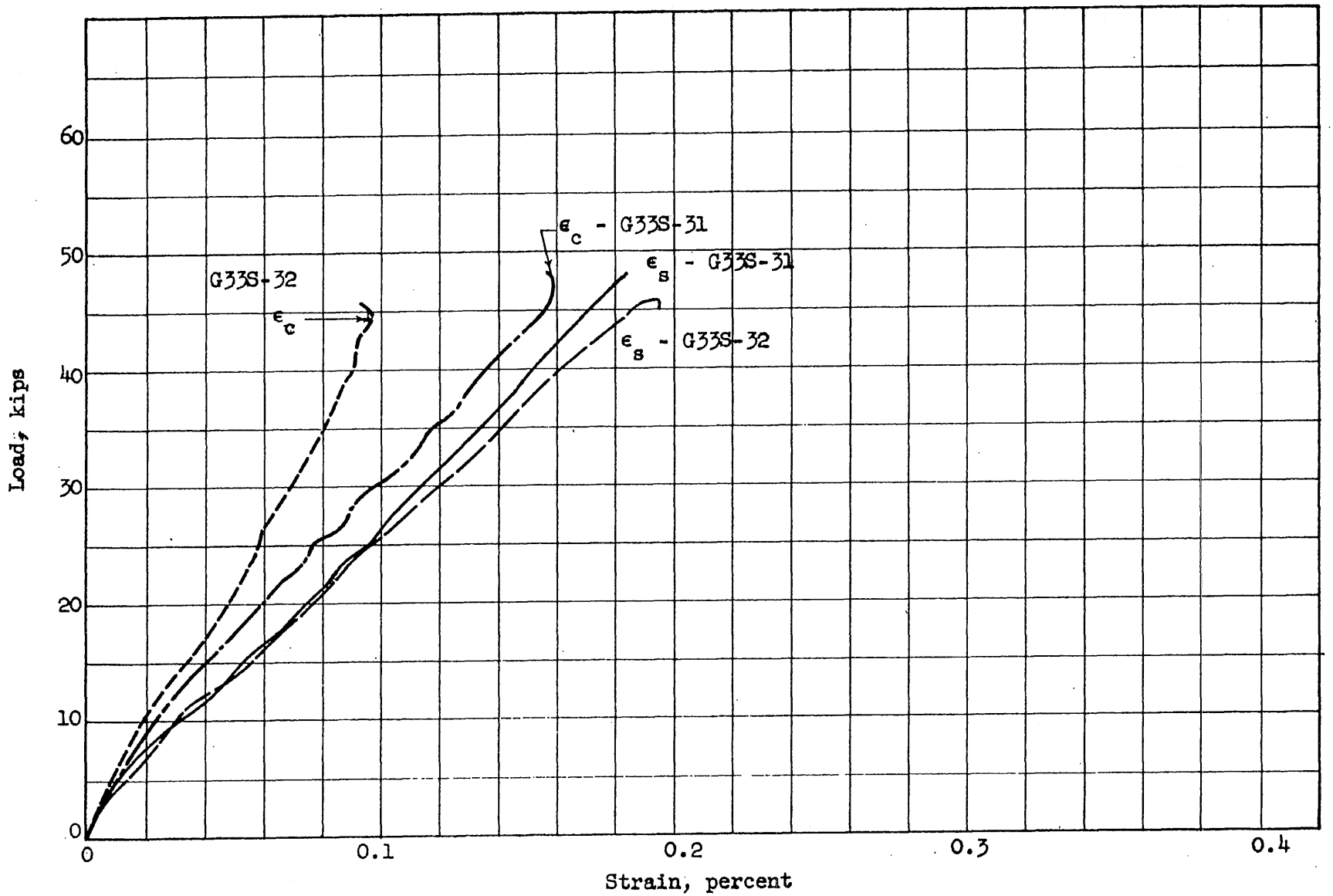

FIG. 4.45 LOAD-STRAIN CURVES FOR BEAMS G33S-31 AND G33S-32

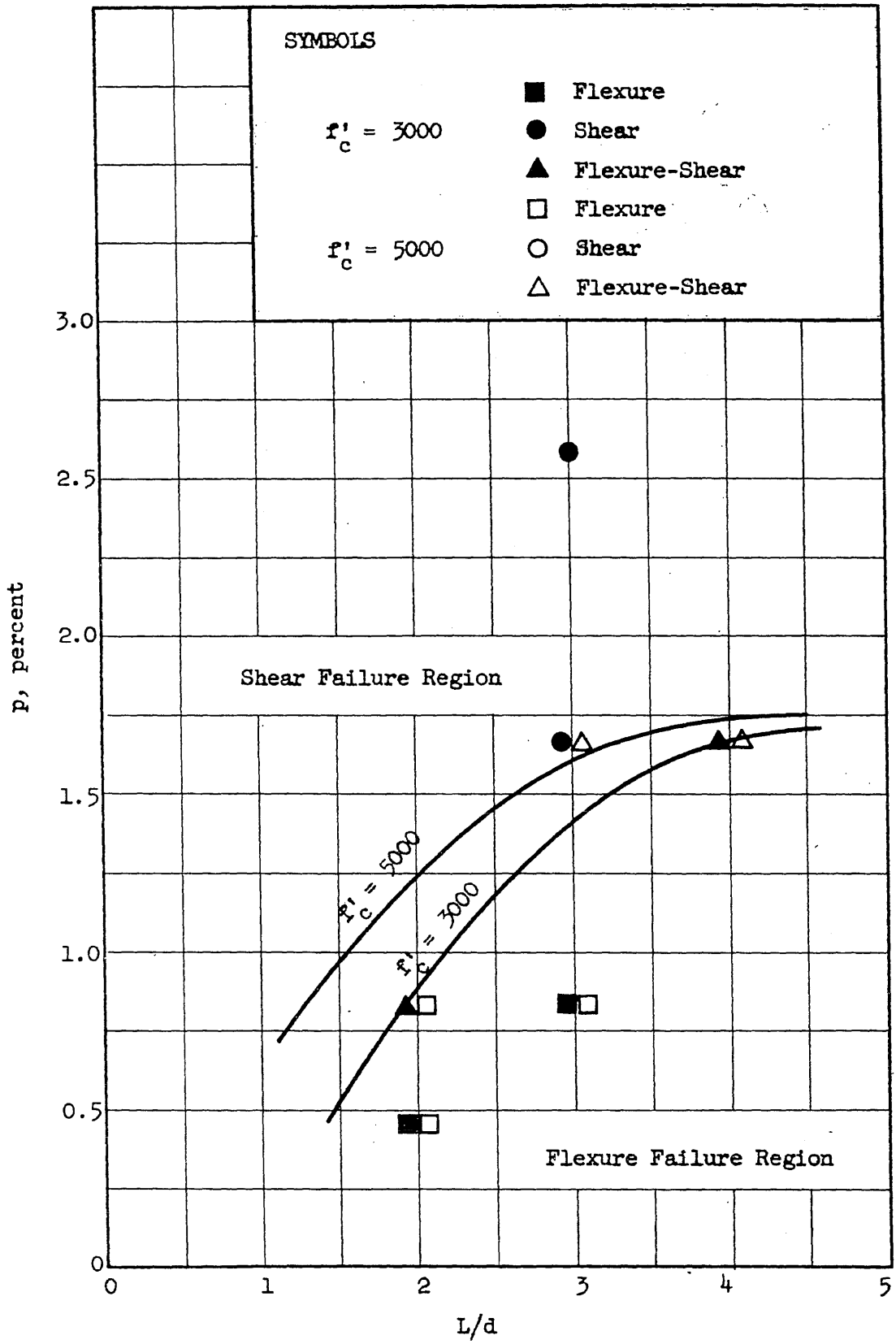

FIG. 4.46 EFFECT OF VARIABLES ON THE MODE OF FAILURE OF DEEP BEAMS WITHOUT WEB REINFORCEMENT

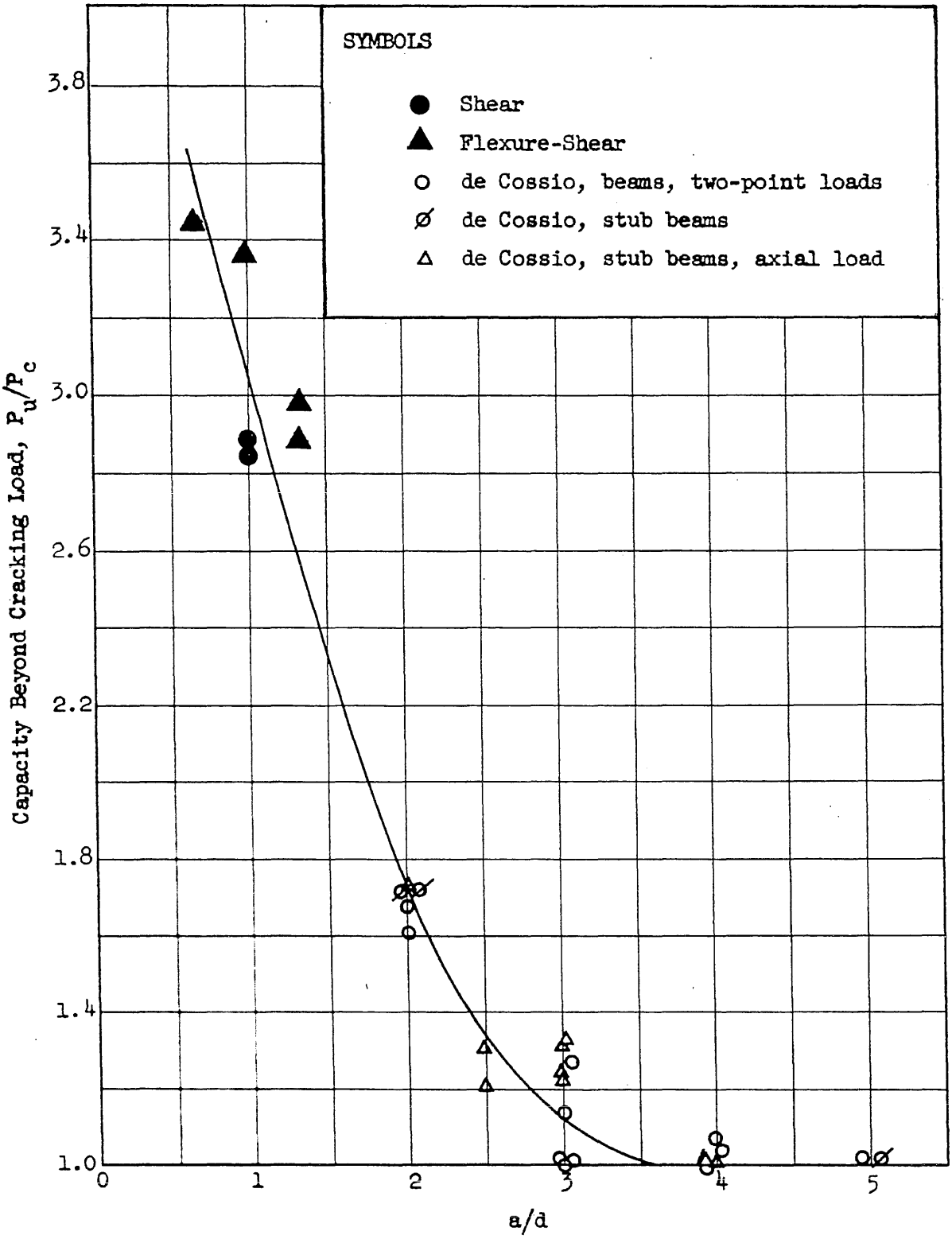

FIG. 4.47 CAPACITY BEYOND CRACKING LOAD FOR BEAMS WITHOUT WEB REINFORCEMENT - SHEAR FAILURES

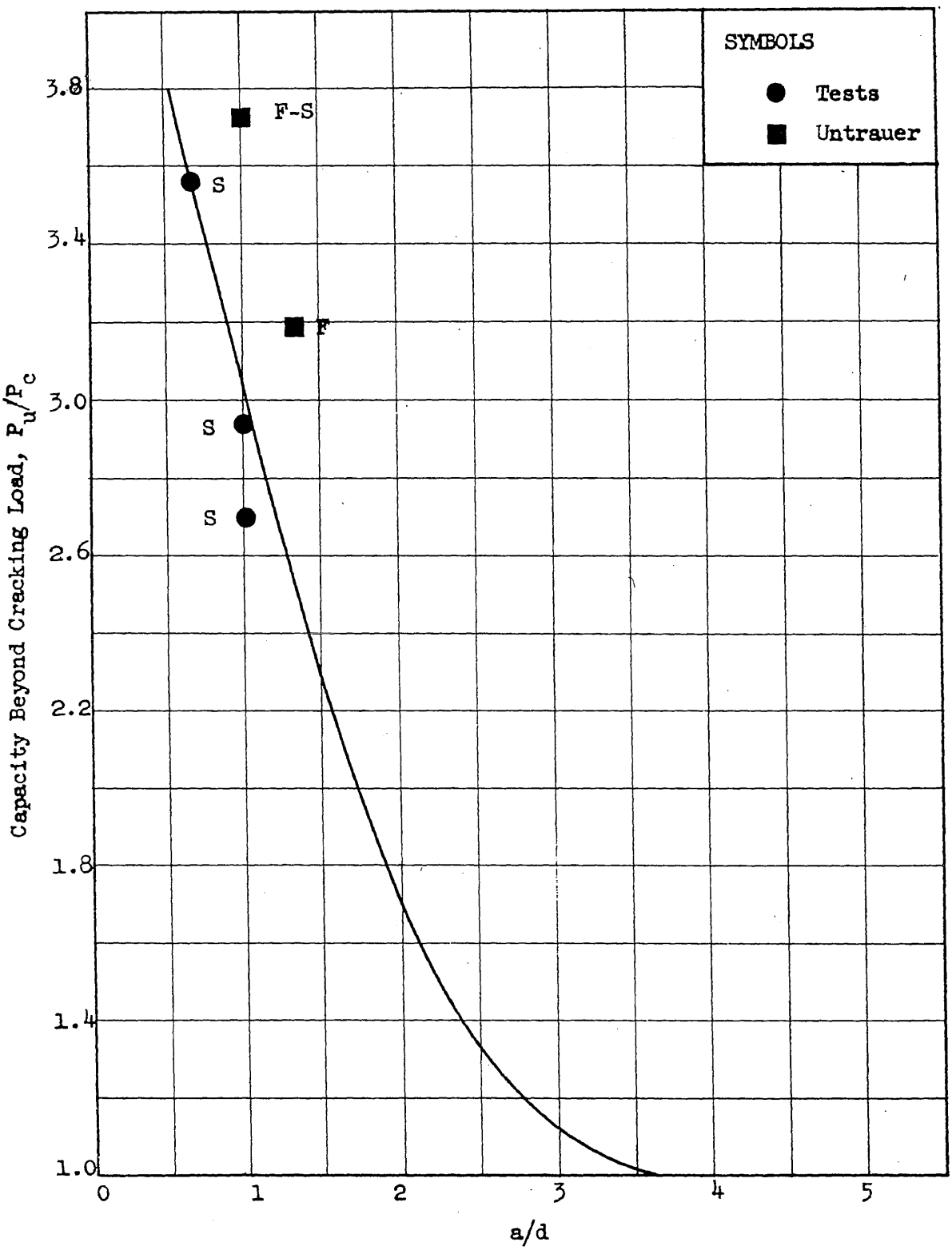

FIG. 4.48 CAPACITY BEYOND CRACKING LOAD FOR BEAMS WITH WEB REINFORCEMENT

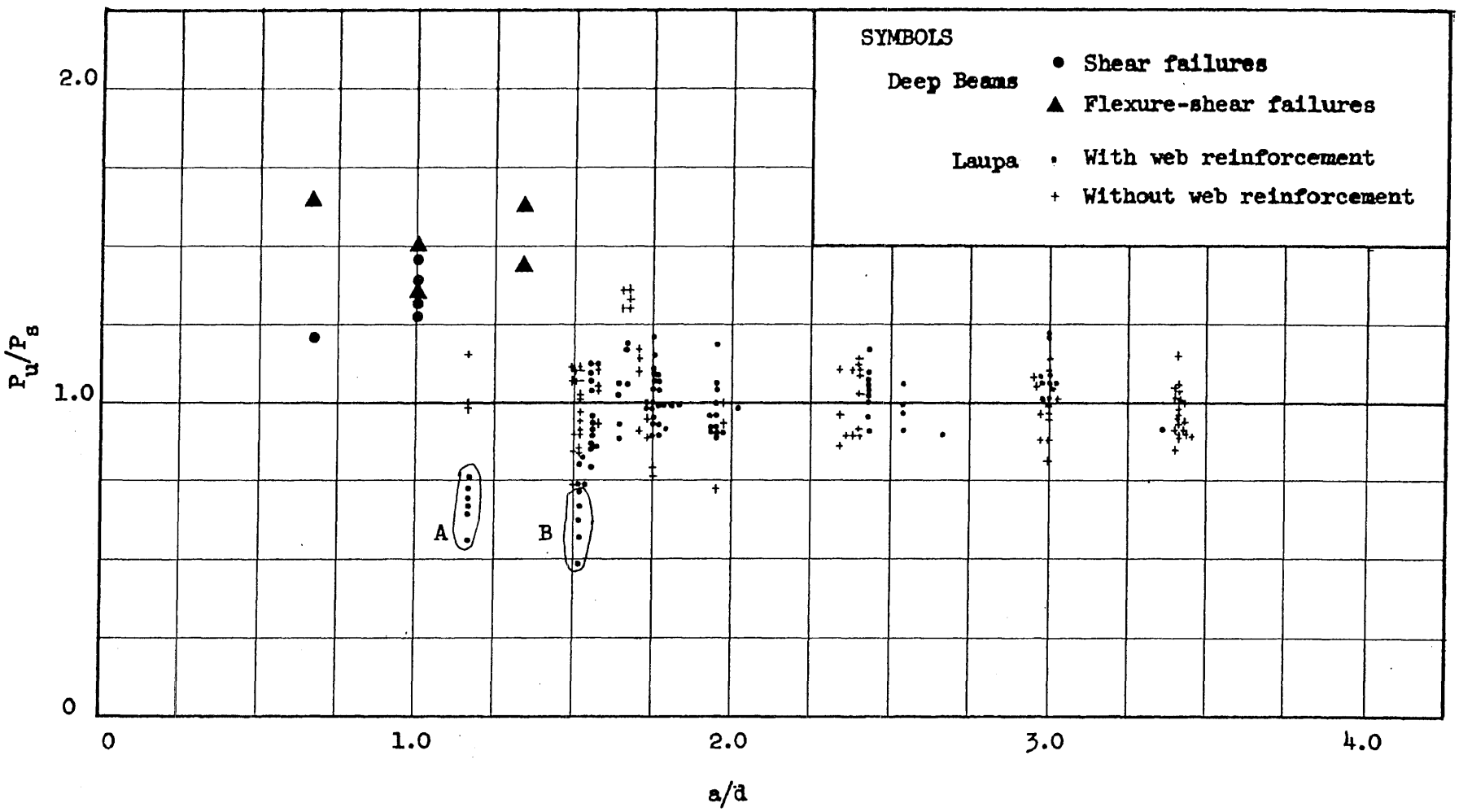

FIG. 4.49 COMPARISON OF MEASURED AND COMPUTED ULTIMATE SHEAR STRENGTHS BY EQUATION 2

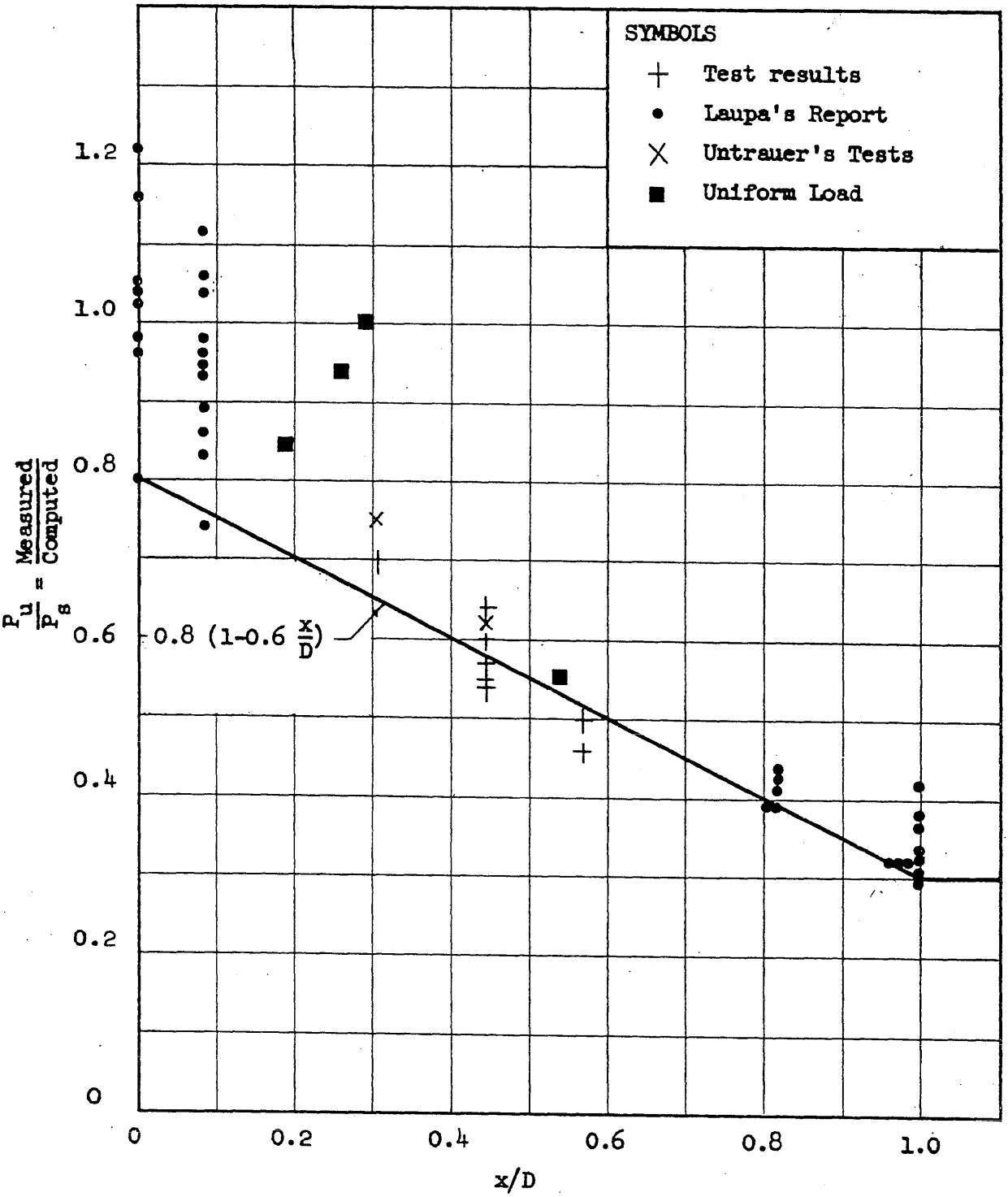

FIG. 4.50 COMPARISON OF MEASURED AND COMPUTED ULTIMATE SHEAR STRENGTH BY EQUATION 5

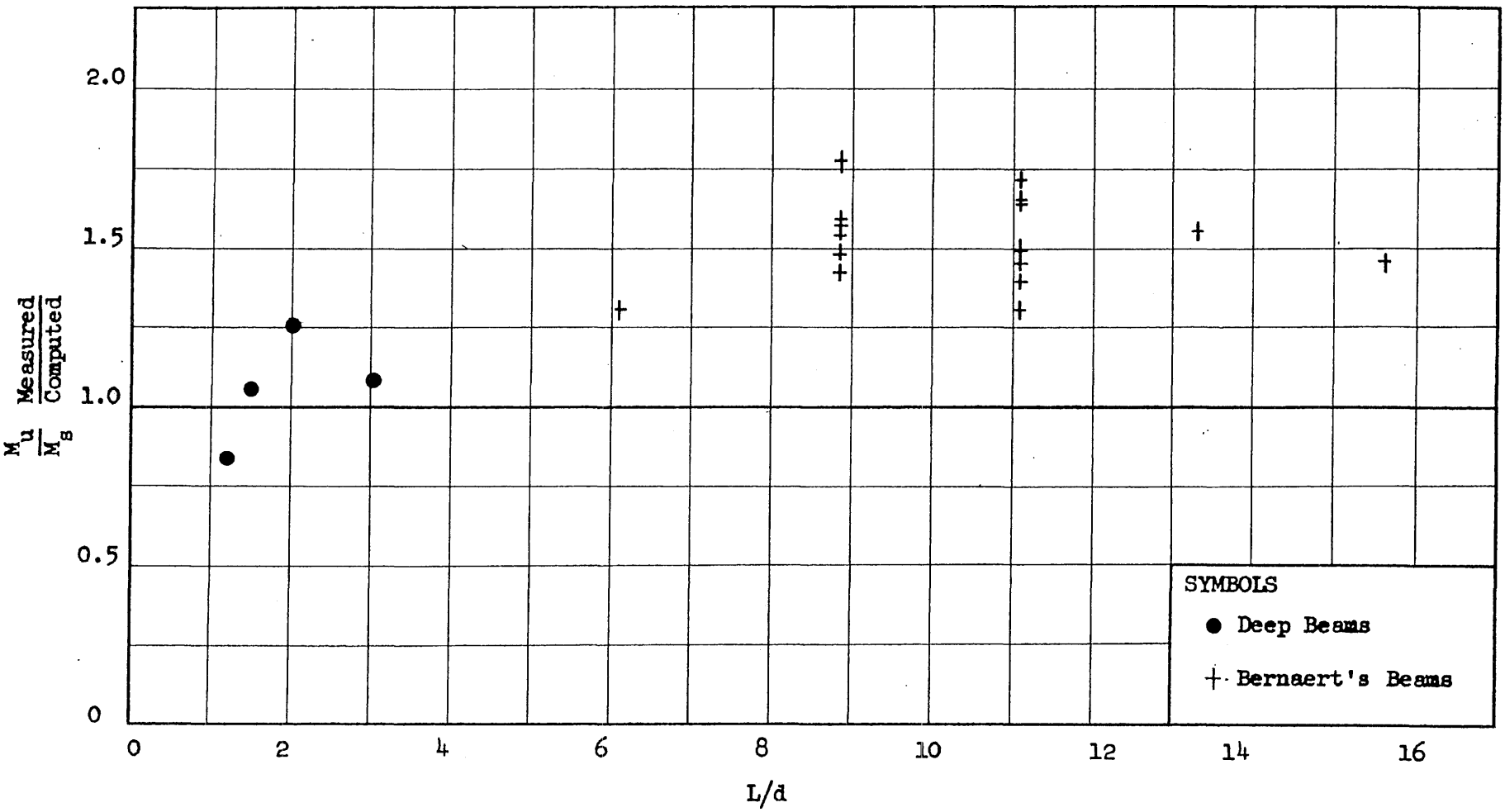

FIG. 4.51 COMPARISON OF MEASURED AND COMPUTED MIDSPAN MOMENTS FOR UNIFORMLY LOADED BEAMS BY EQUATION 2

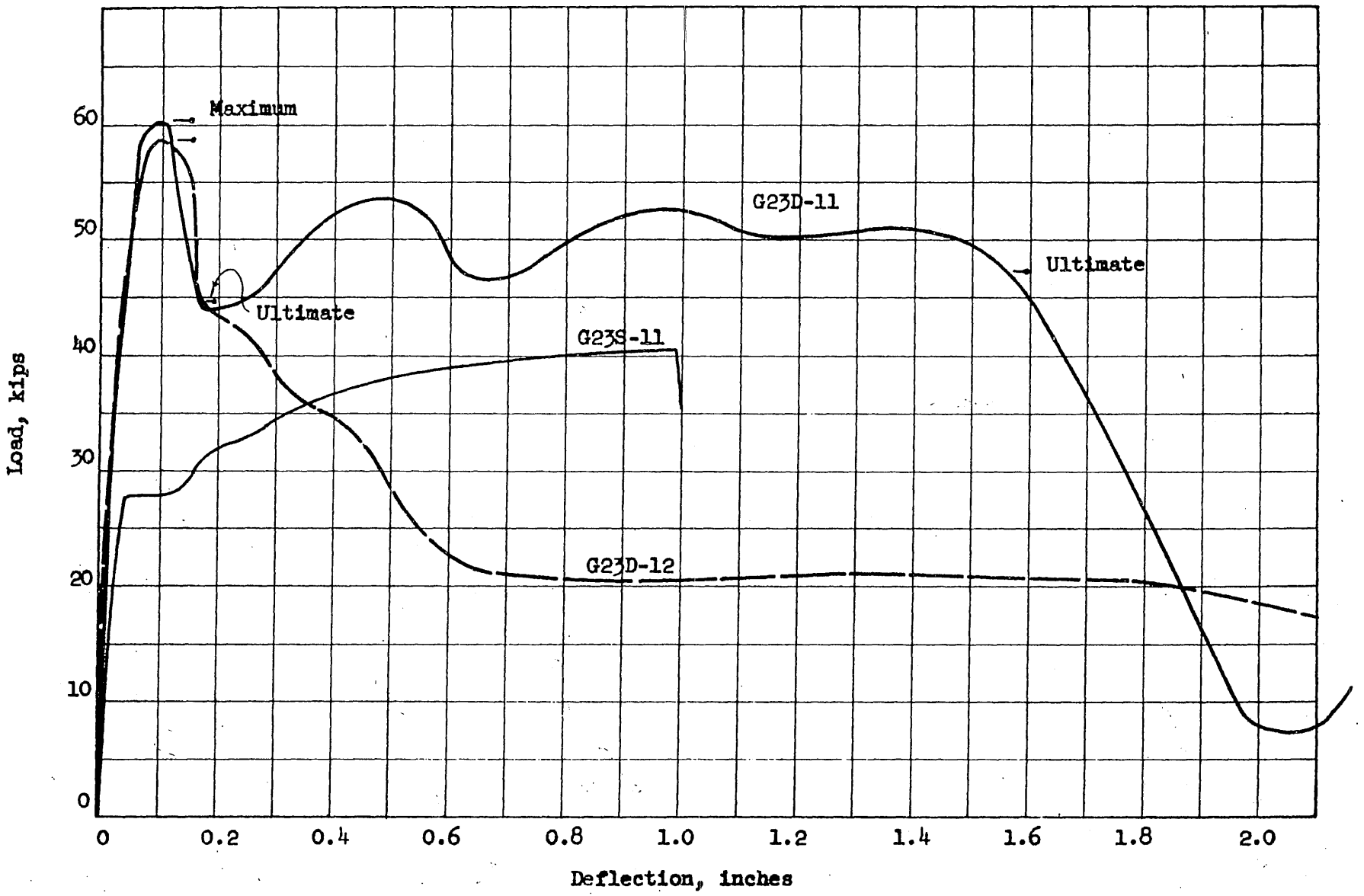

FIG. 5.1 LOAD-DEFLECTION CURVES FOR BEAMS G23S-11, G23D-11 AND G23D-12

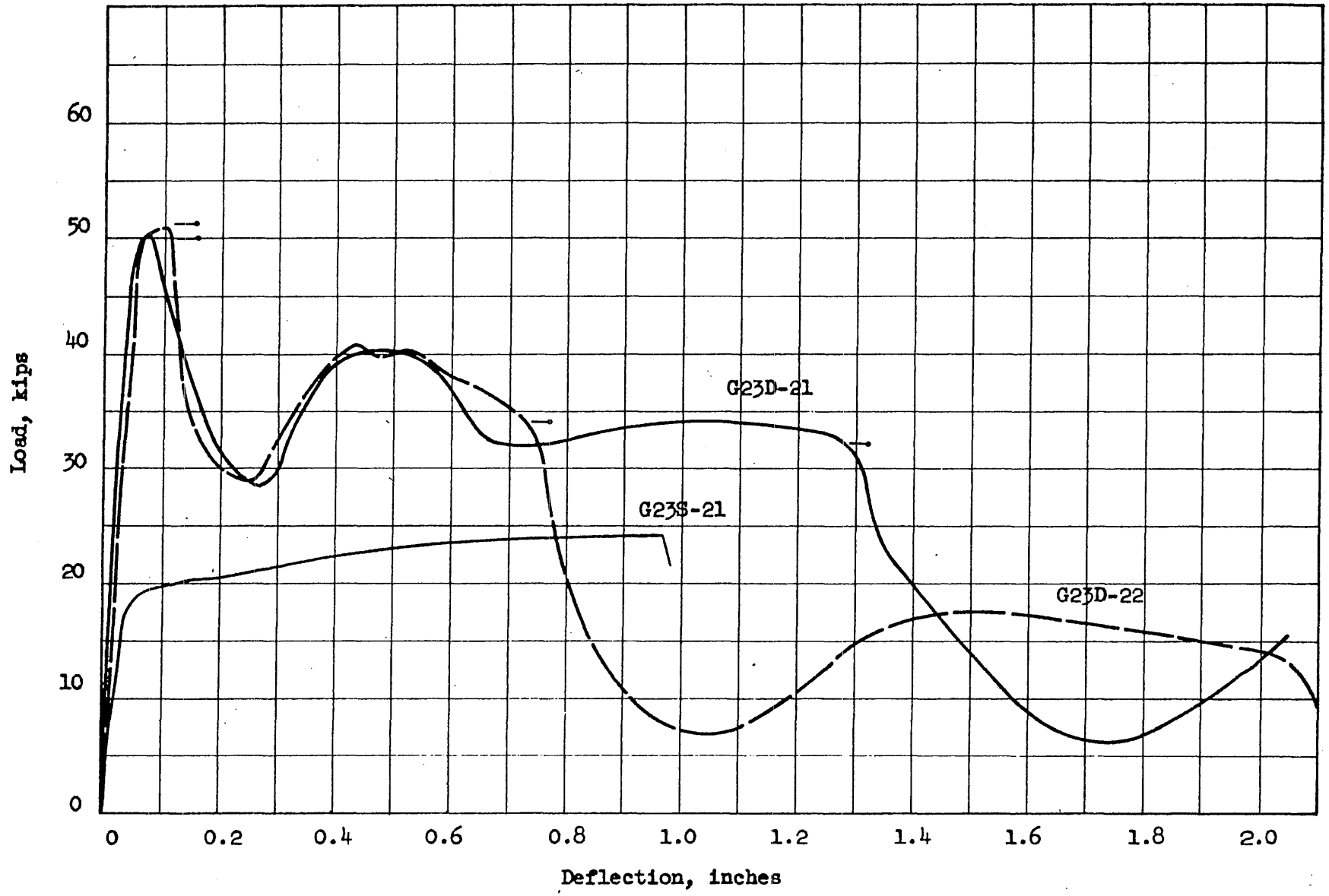

FIG. 5.2 LOAD-DEFLECTION CURVES FOR BEAMS G23S-21, G23D-21 AND G23D-22

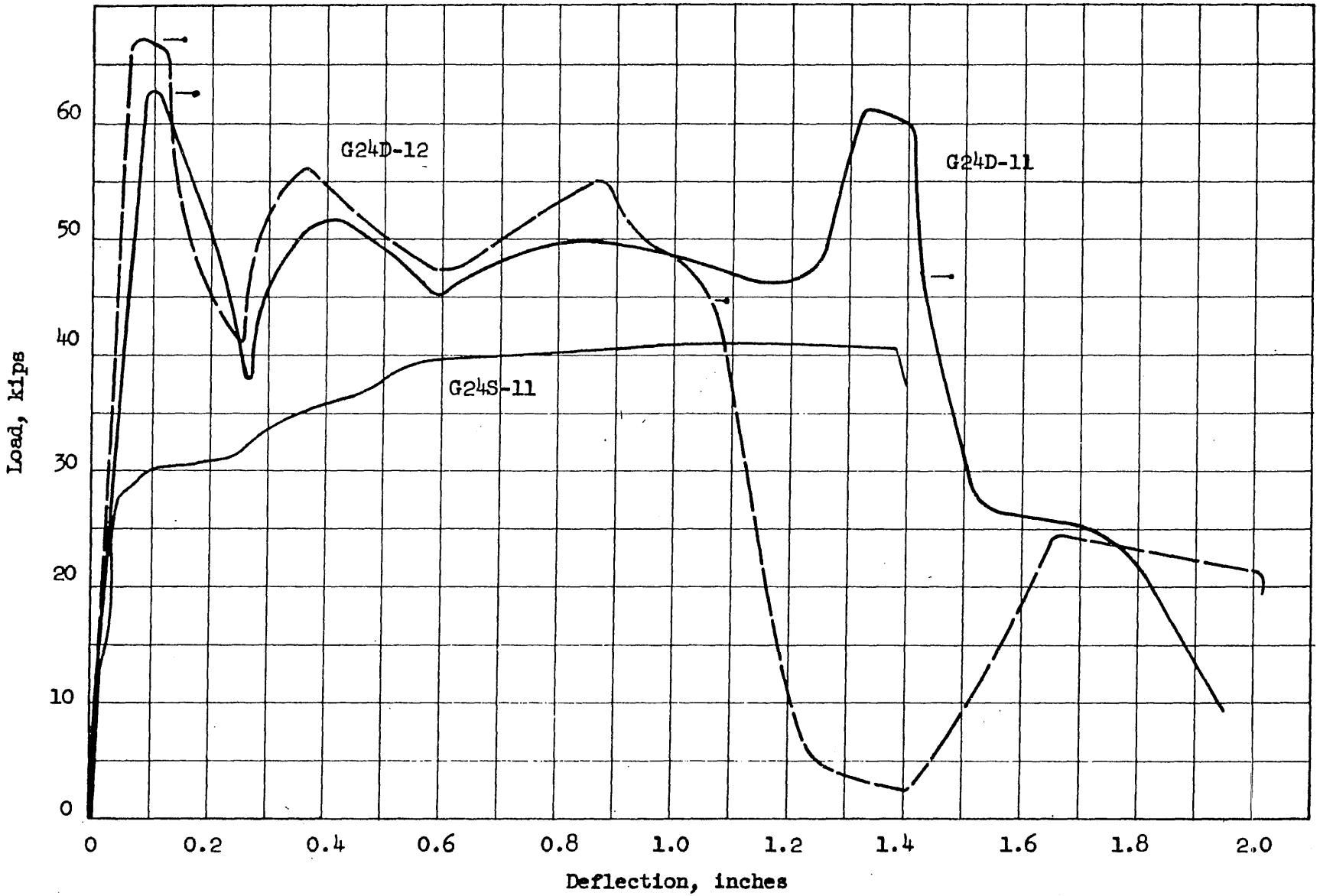

FIG. 5.3 LOAD-DEFLECTION CURVES FOR BEAMS G24S-11, G24D-11 AND G24D-12

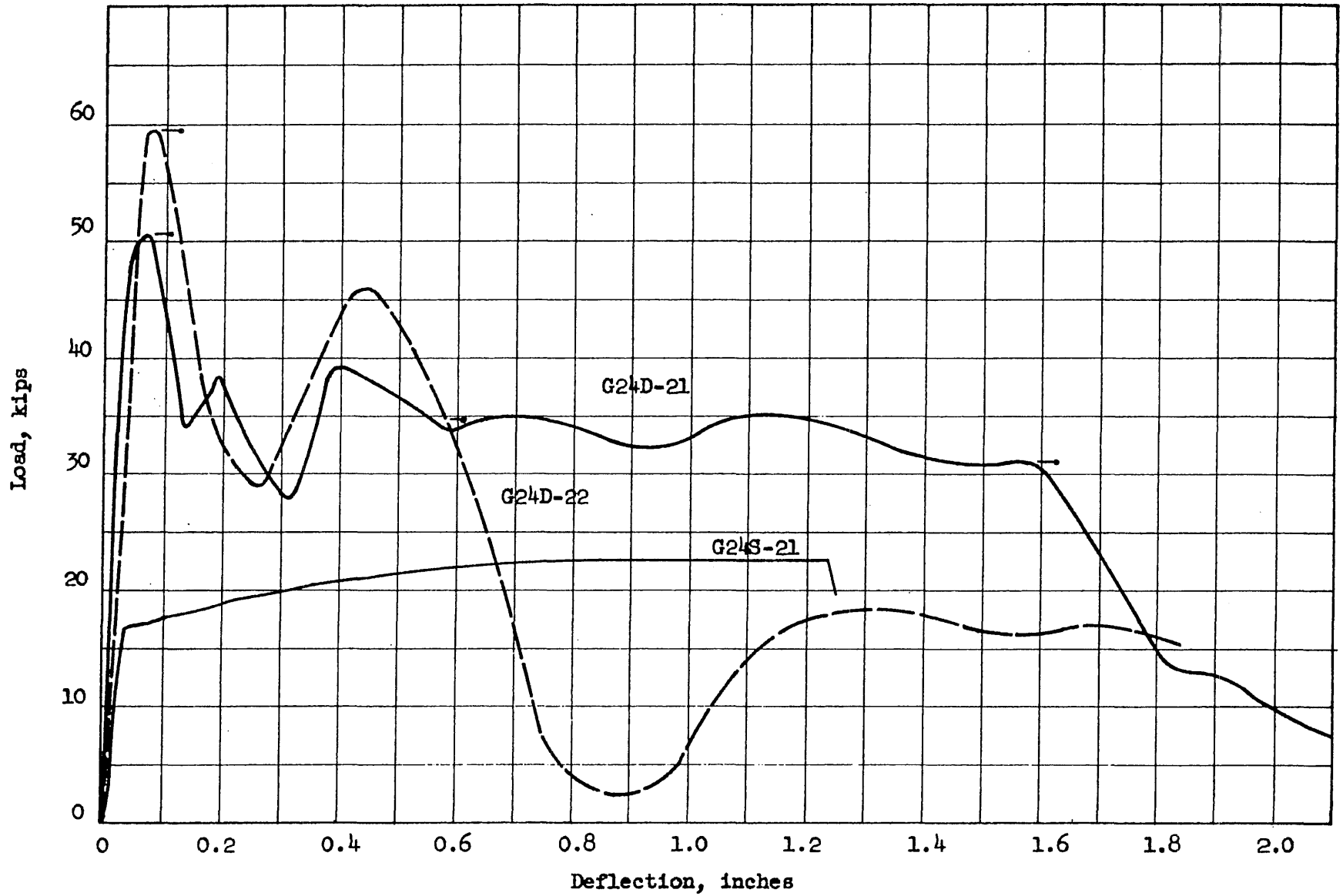

FIG. 5.4 LOAD-DEFLECTION CURVES FOR BEAMS G24S-21, G24D-21 AND G24D-22

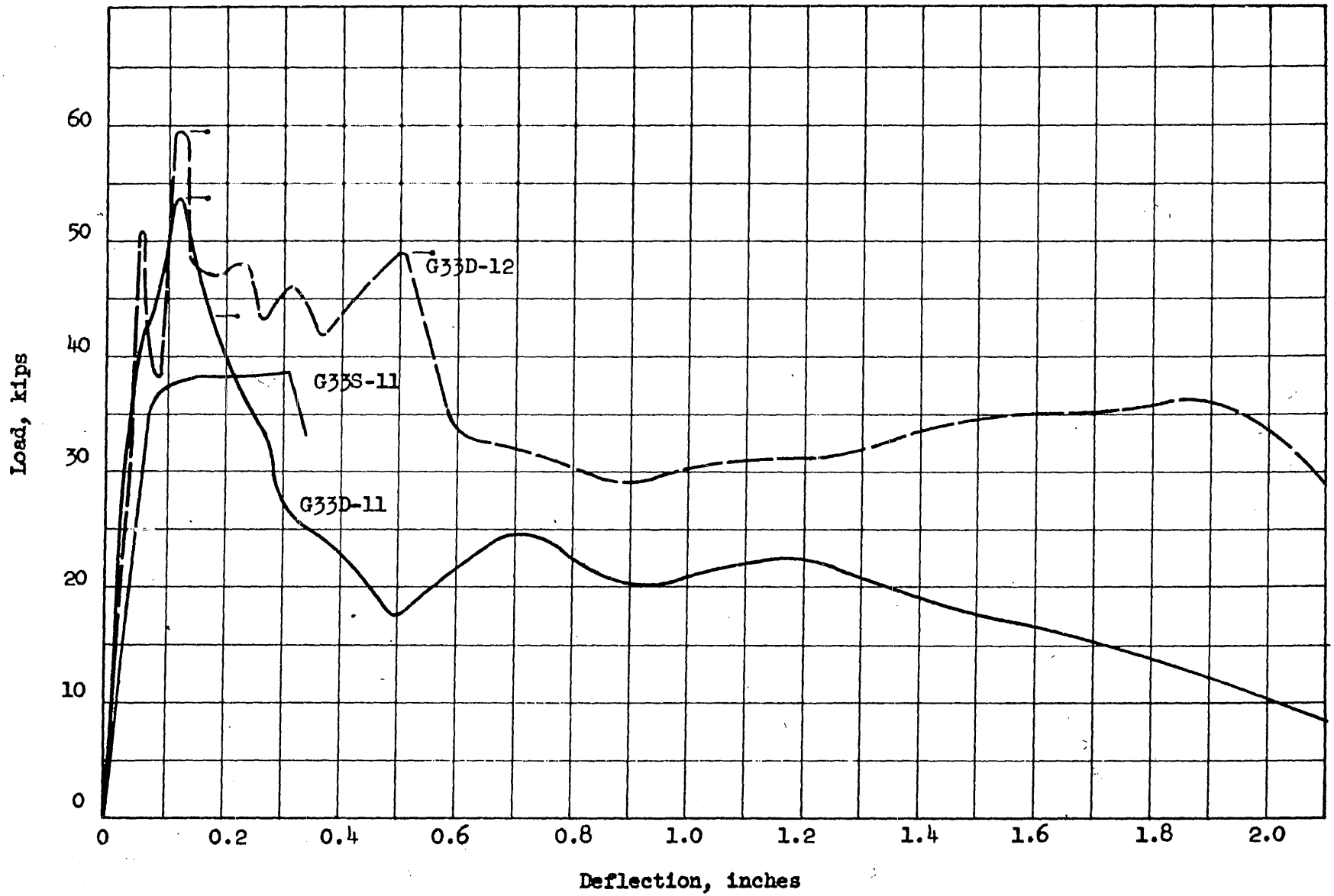

FIG. 5.5 LOAD-DEFLECTION CURVES FOR BEAMS G33S-11, G33D-11 AND G33D-12

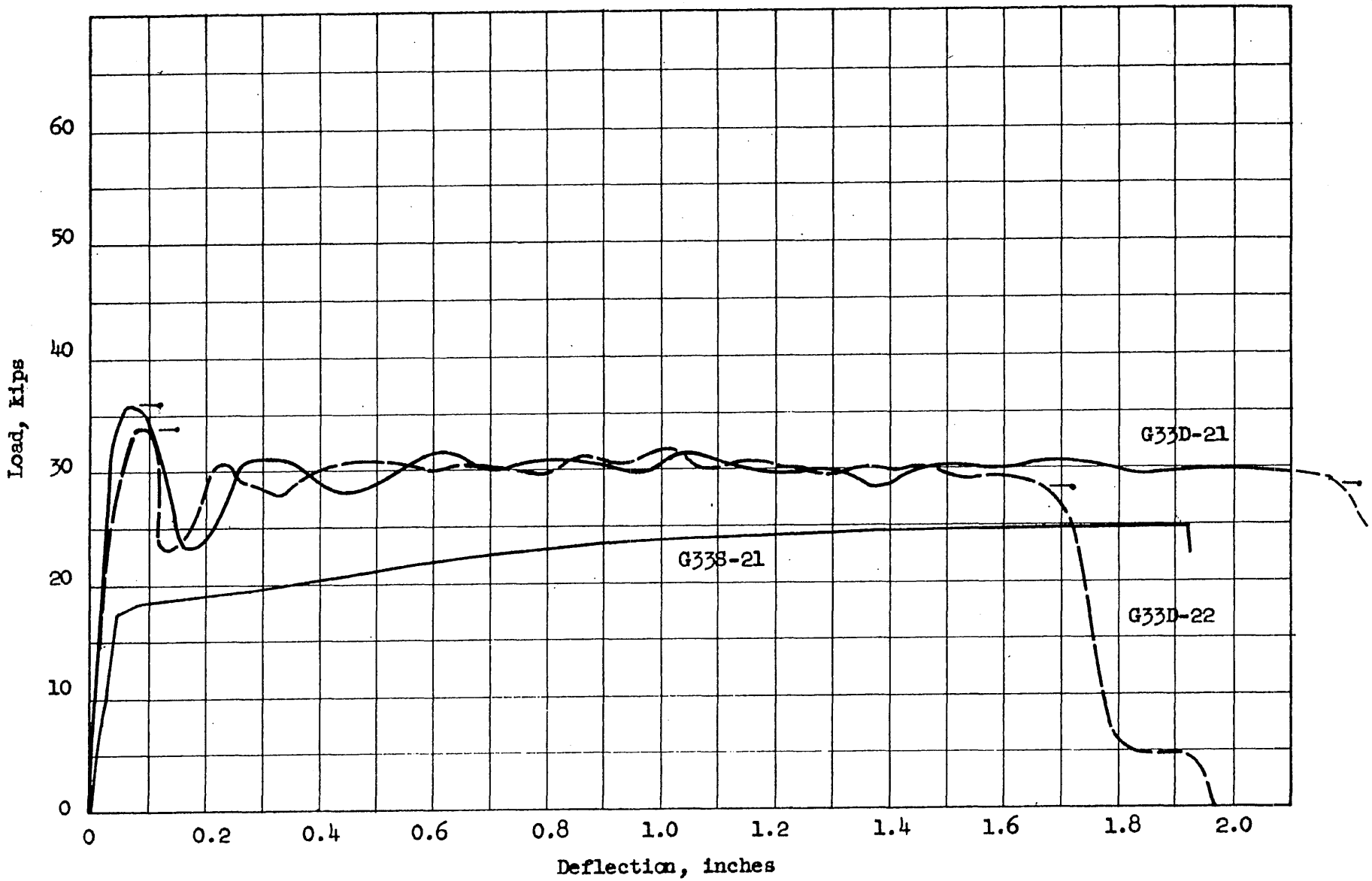

FIG. 5.6 LOAD-DEFLECTION CURVES FOR BEAMS G33S-21, G33D-21 AND G33D-22

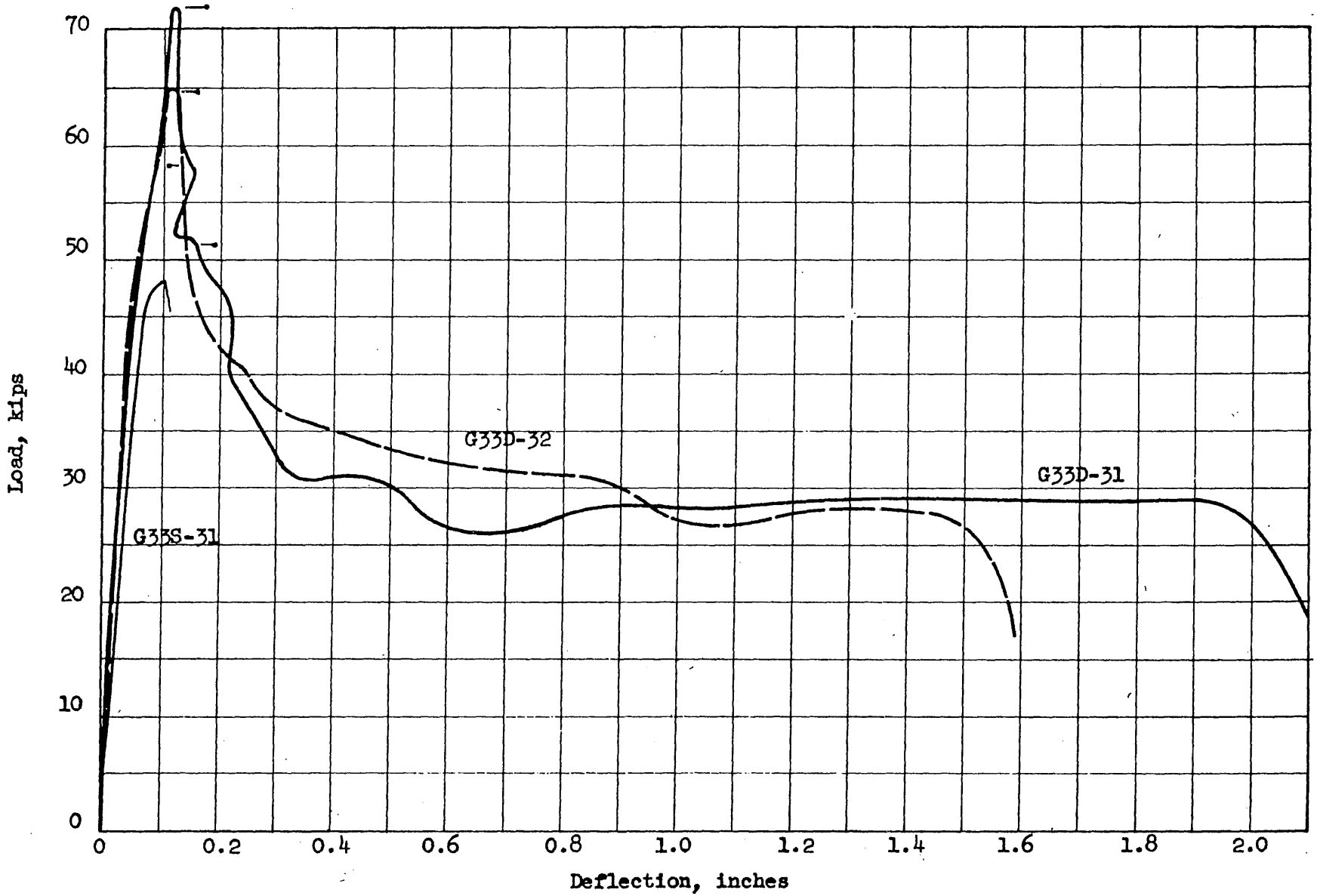

FIG. 5.7 LOAD-DEFLECTION CURVES FOR BEAMS G33S-31, G33D-31 AND G33D-32

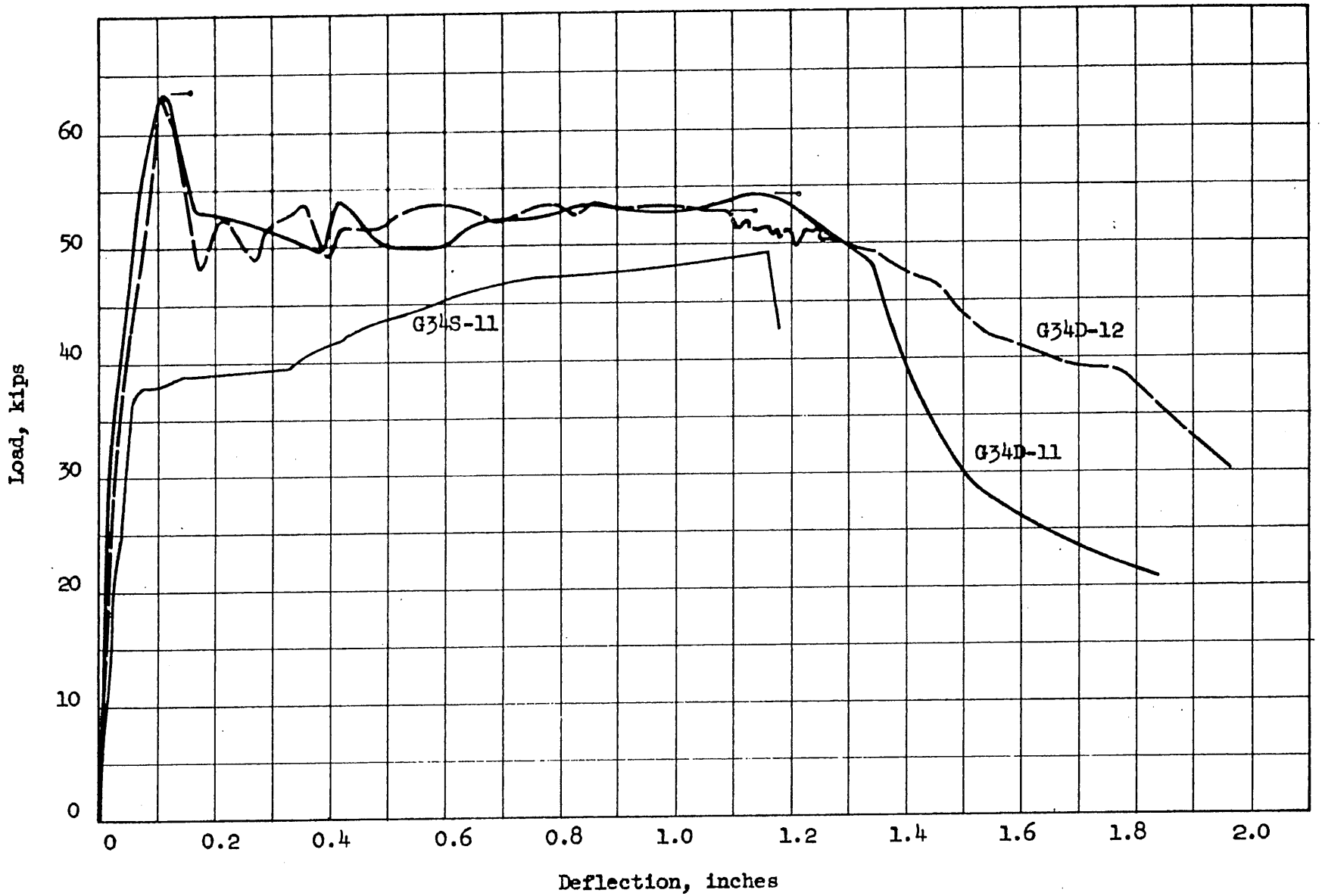

FIG. 5.8 LOAD-DEFLECTION CURVES FOR BEAMS G34S-11, G34D-11 AND G34D-12

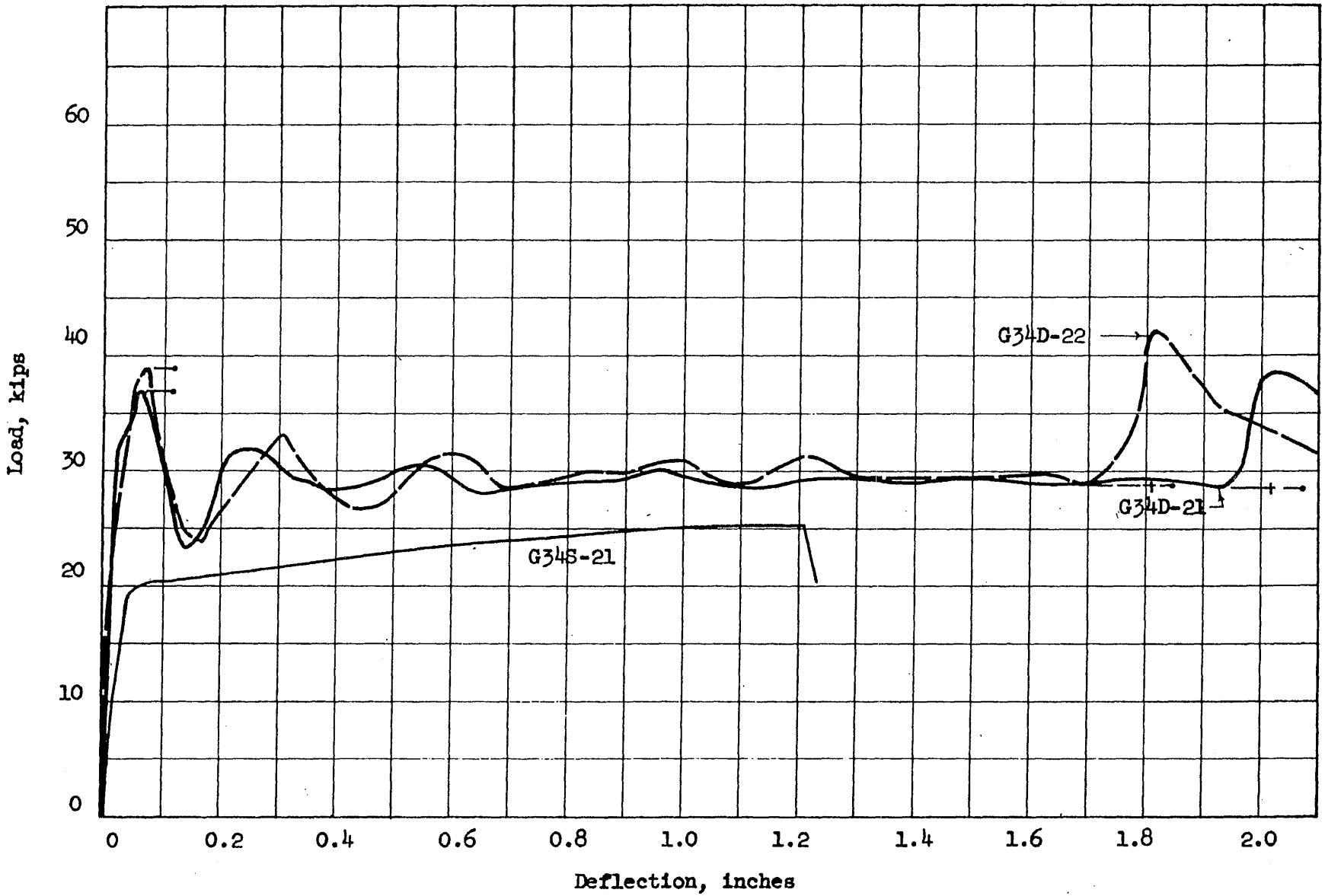

FIG. 5.9 LOAD-DEFLECTION CURVES FOR BEAMS G34S-21, G34D-21 AND G34D-22

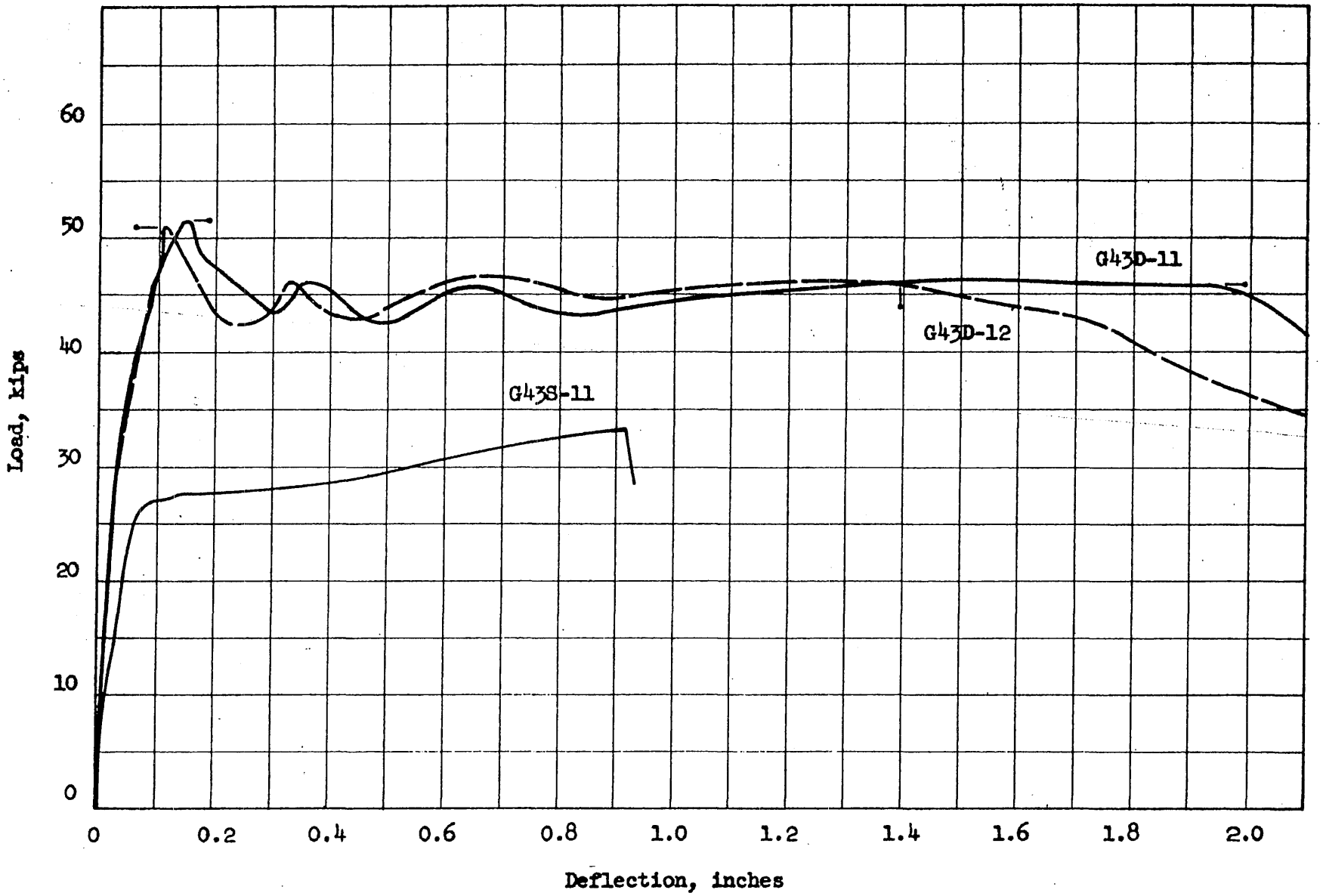

FIG. 5.10 LOAD-DEFLECTION CURVES FOR BEAMS G43S-11, G43D-11 AND G43D-12

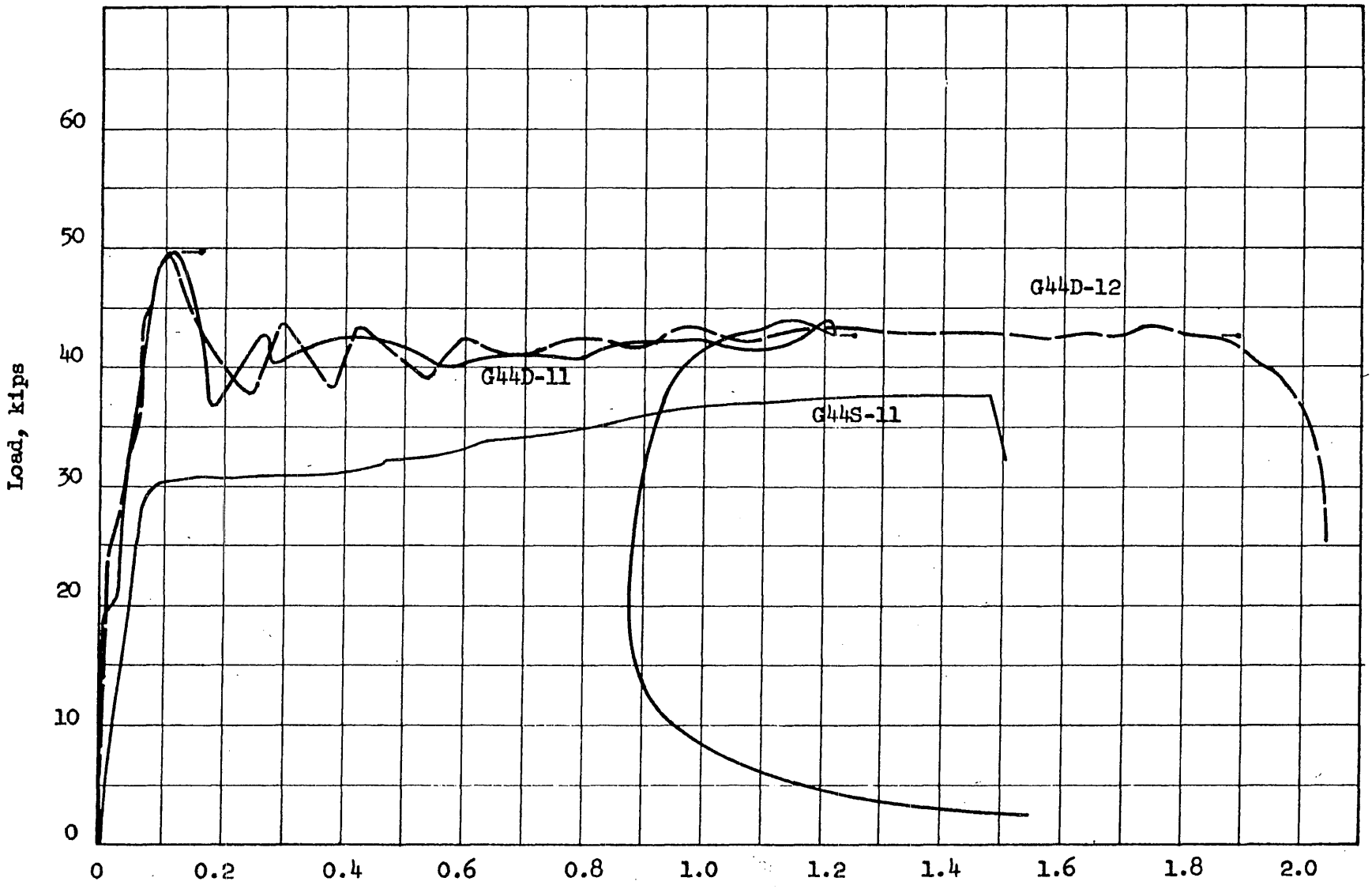

FIG. 5.11 LOAD-DEFLECTION CURVES FOR BEAMS G44S-11, G44D-11 AND G44D-12

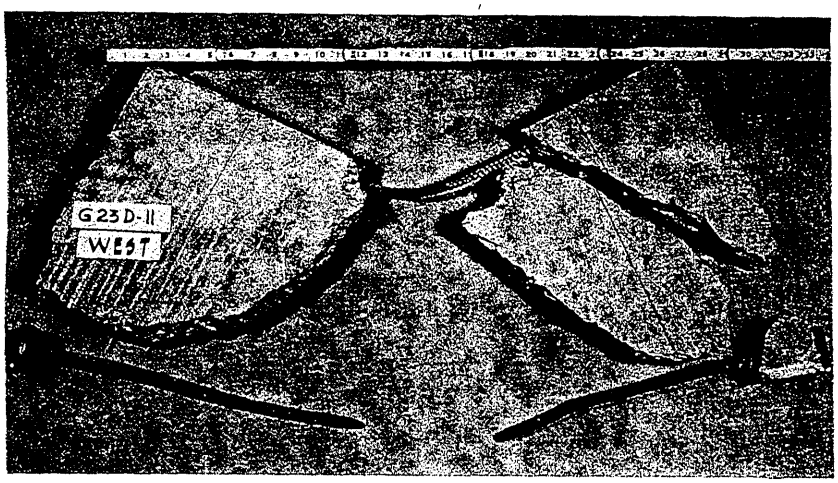

G23D-11

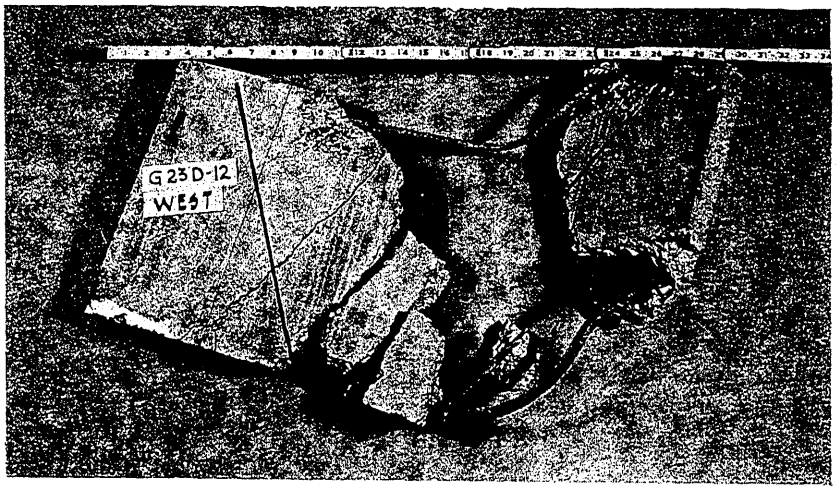

G23D-12

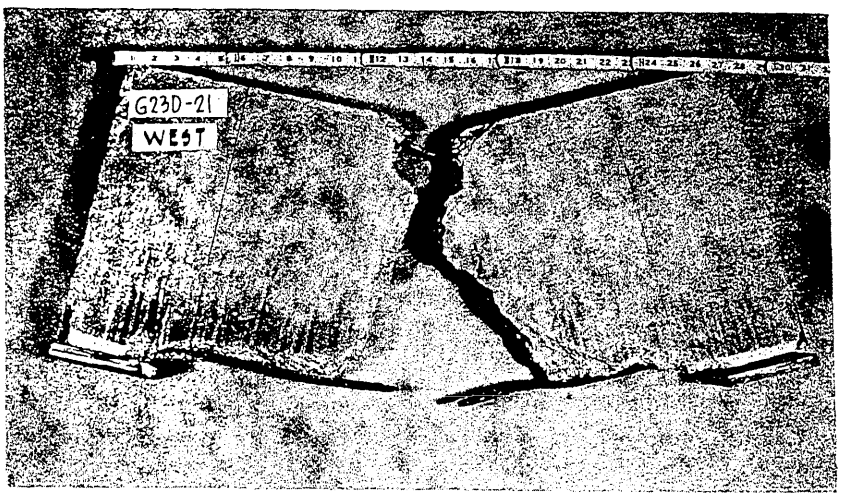

G23D-21

FIG. 5.12a PHOTOGRAPHS OF DYNAMIC TEST FAILURES

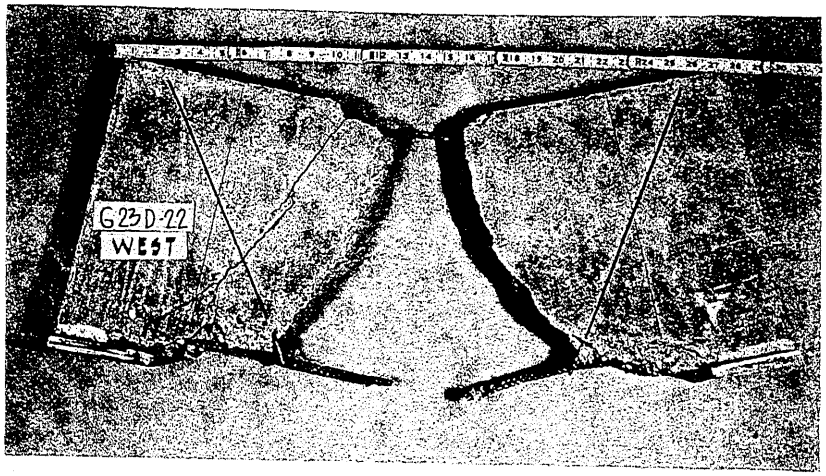

G23D-22

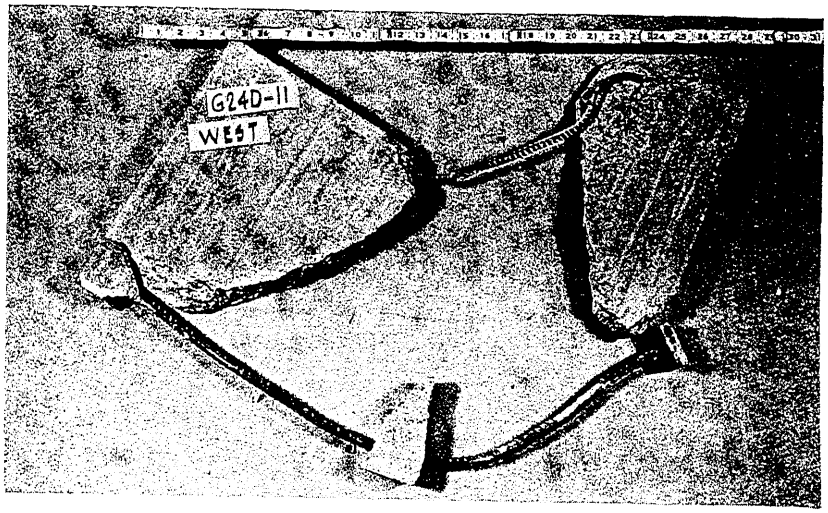

G24D-11

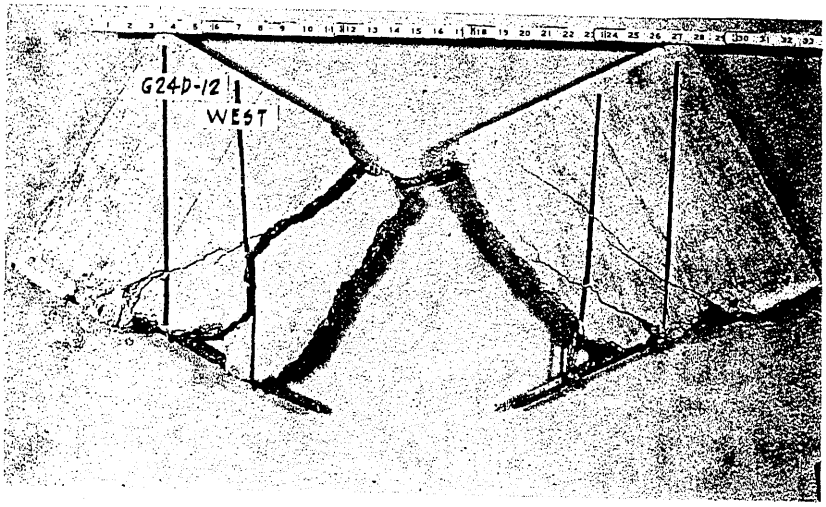

G24D-12

FIG. 5.12b PHOTOGRAPHS OF DYNAMIC TEST FAILURES

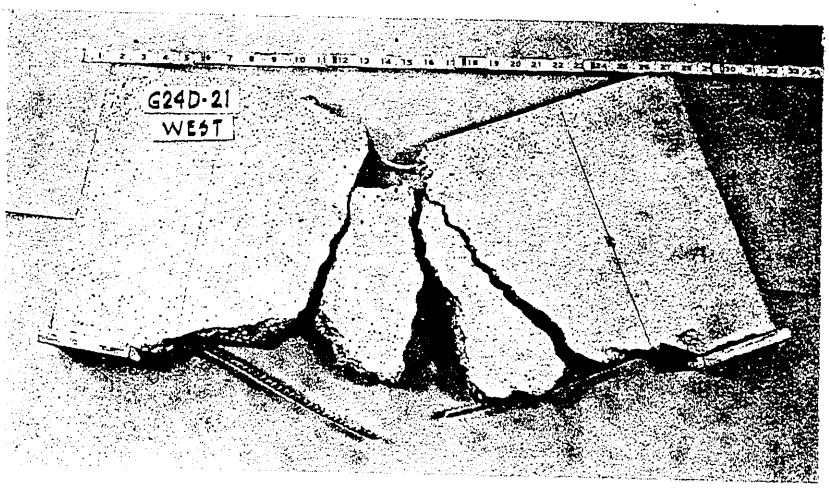

G24D-21

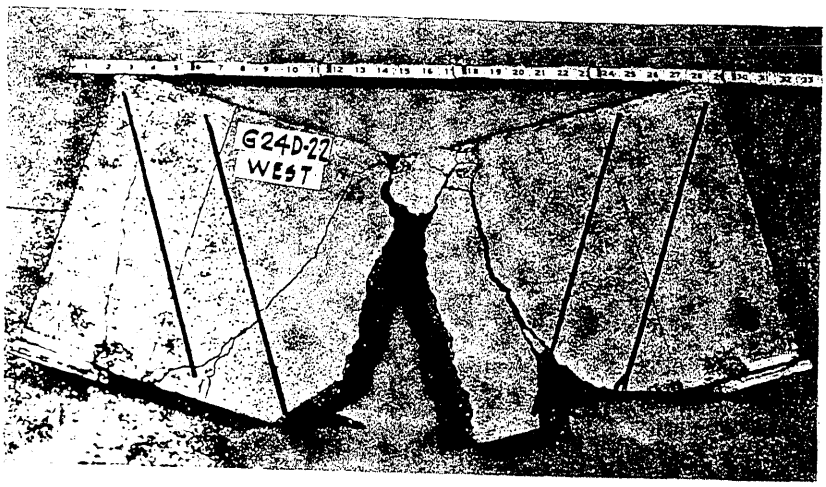

G24D-22

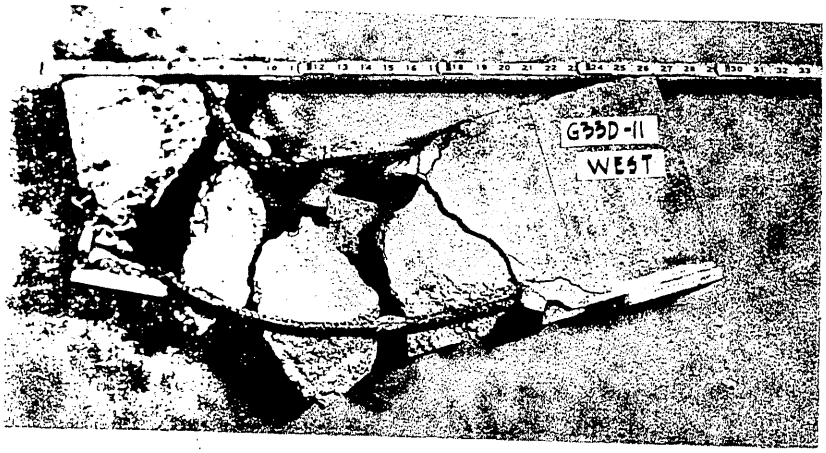

G33D-11

FIG. 5.12c PHOTOGRAPHS OF DYNAMIC TEST FAILURES

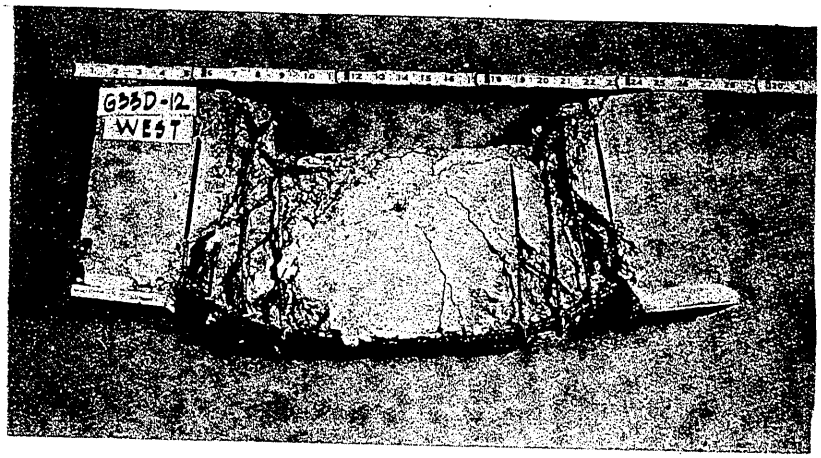

G33D-12

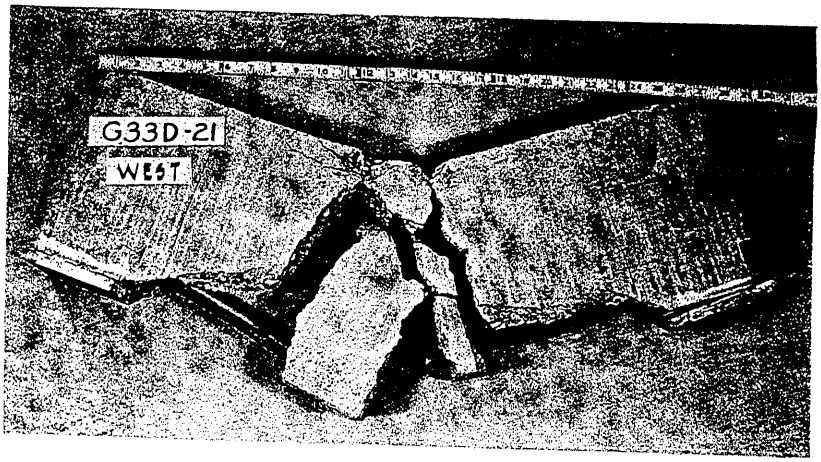

G33D-21

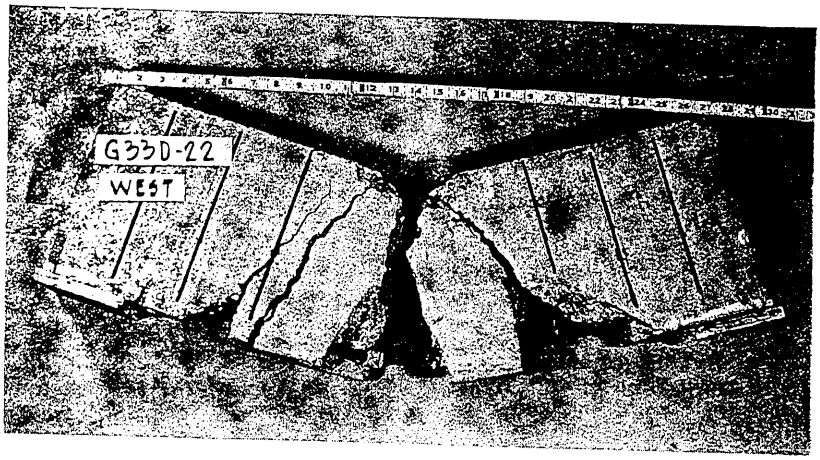

G33D-22

FIG. 5.12d PHOTOGRAPHS OF DYNAMIC TEST FAILURES

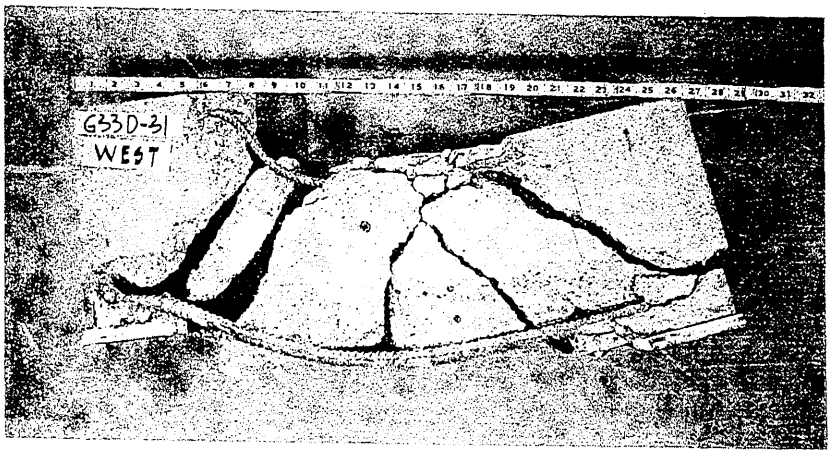

G33D-31

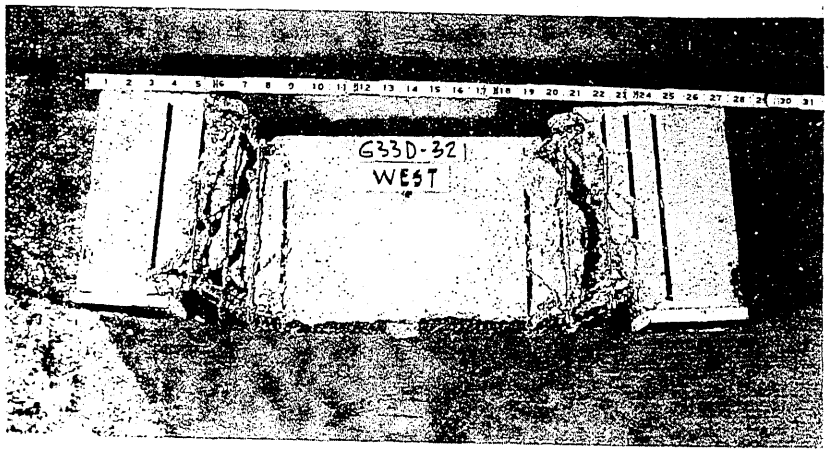

G33D-32

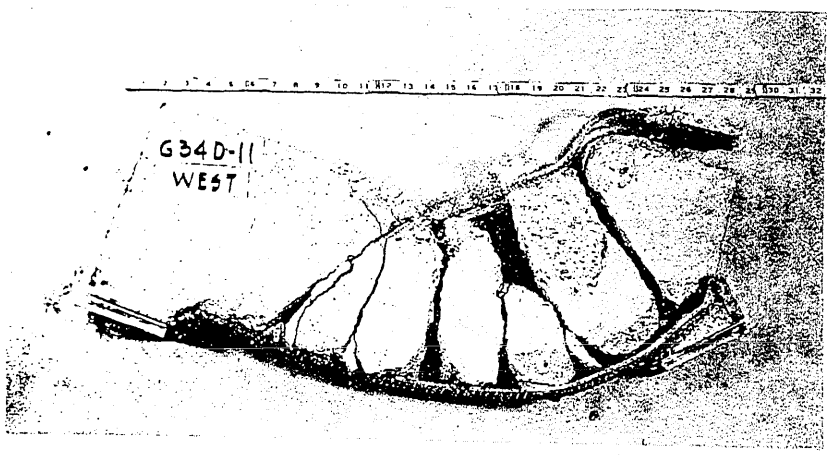

G34D-11

FIG. 5.12e PHOTOGRAPHS OF DYNAMIC TEST FAILURES

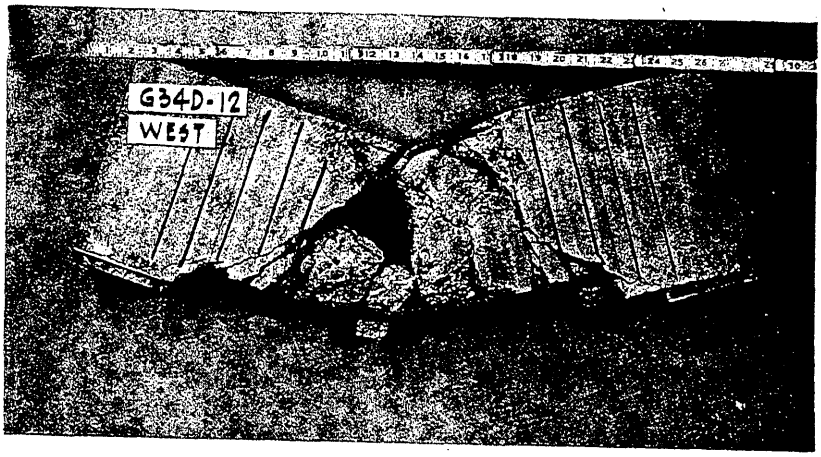

G34D-12

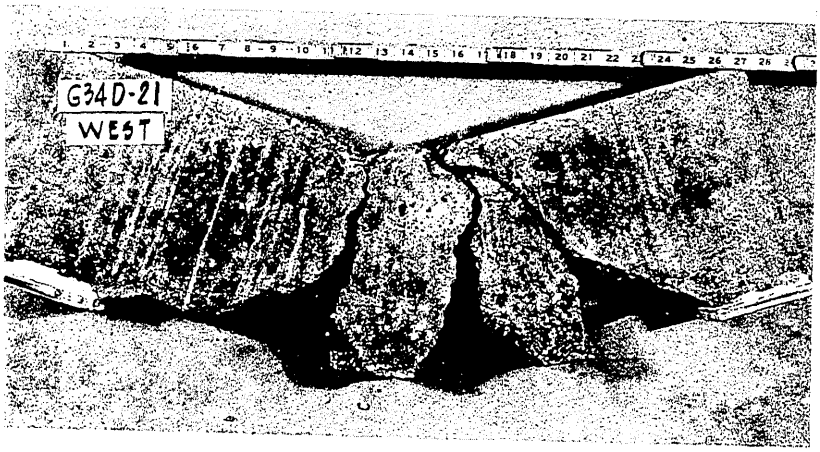

G34D-21

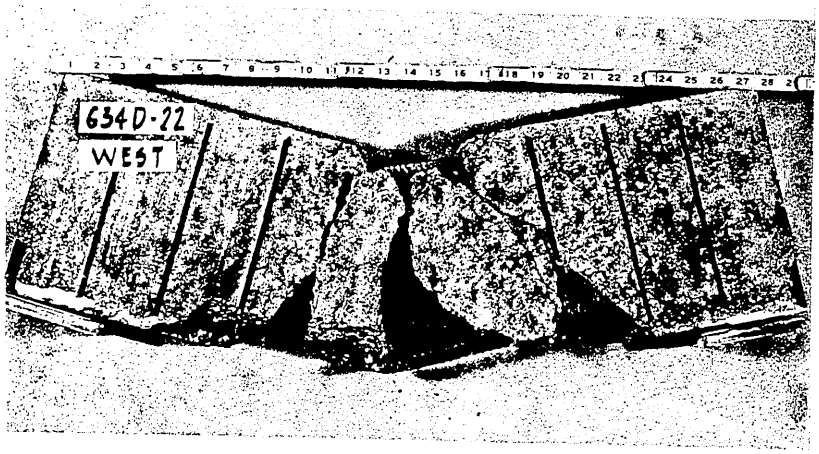

G34D-22

FIG. 5.12f PHOTOGRAPHS OF DYNAMIC TEST FAILURES

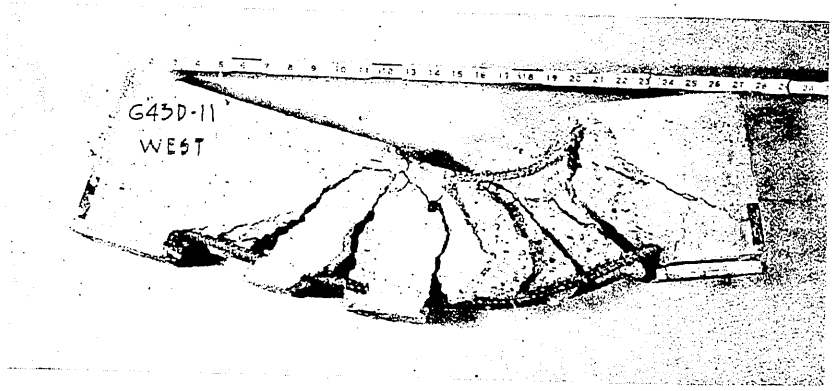

G43D-11

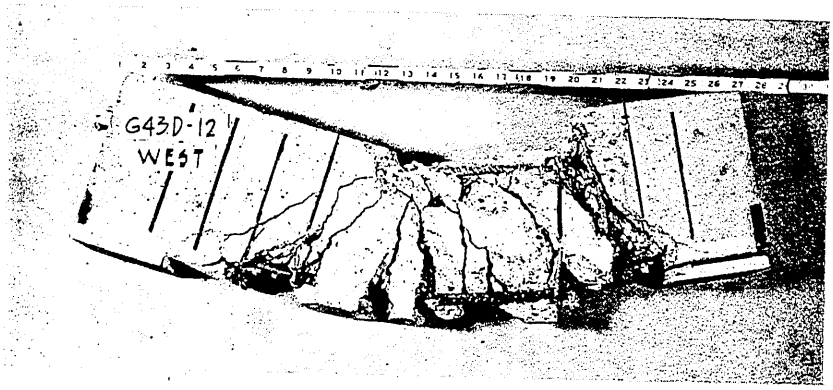

G43D-12

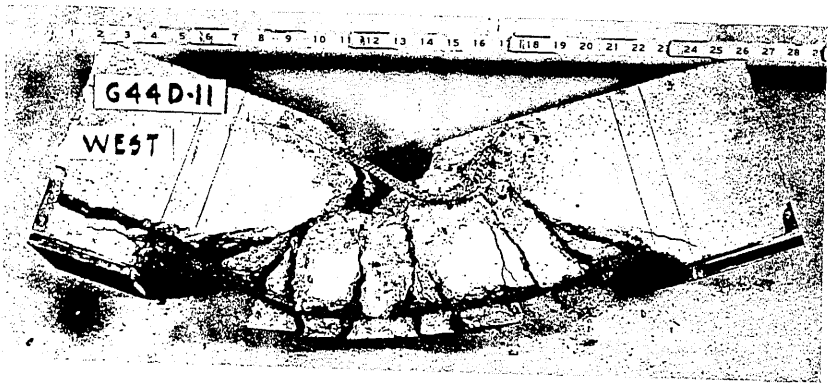

G44D-11

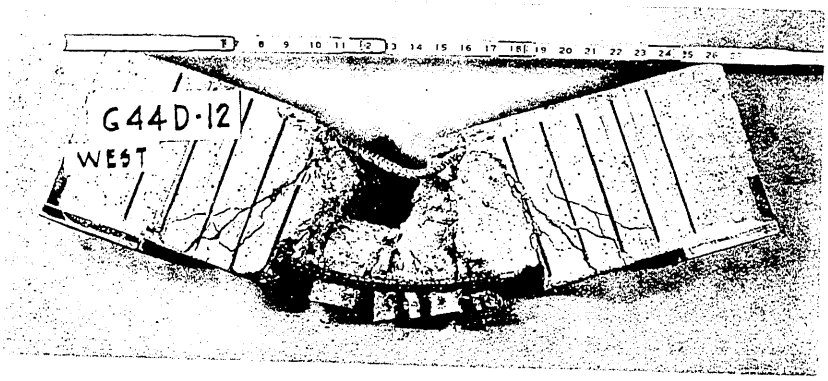

G44D-12

FIG. 5.12g PHOTOGRAPHS OF DYNAMIC TEST FAILURES

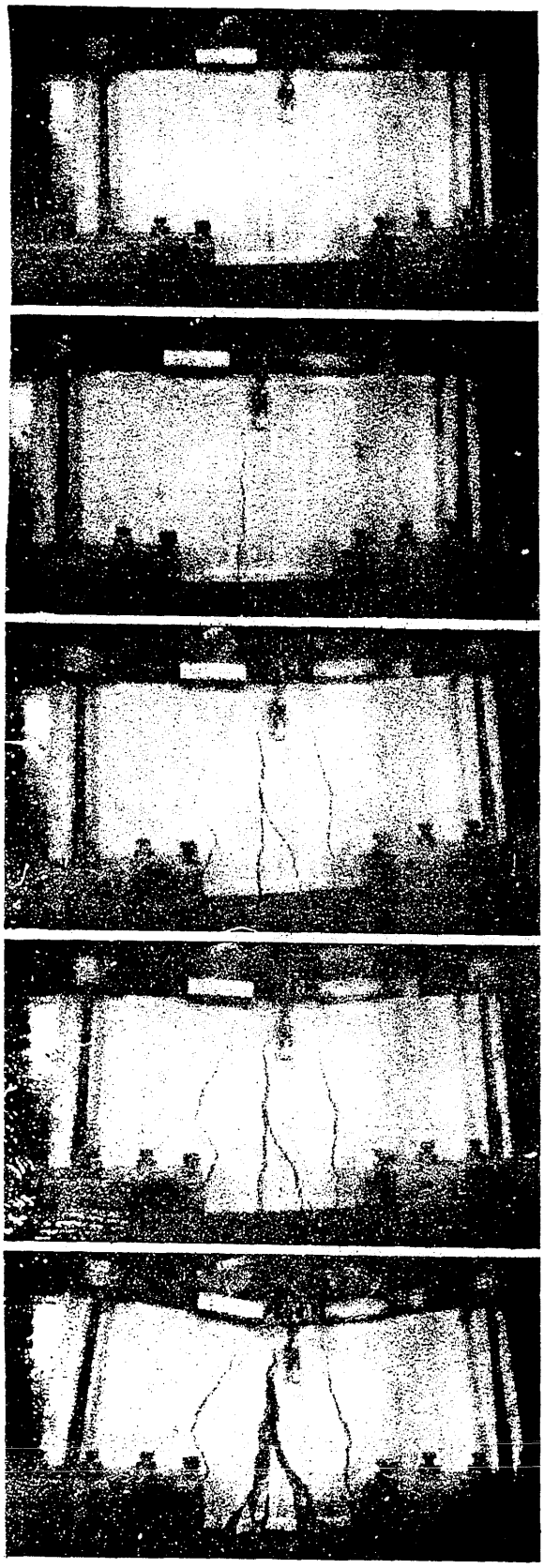

P = 65.9 kips

Δ = 0.054 in.

P = 55.0 kips

Δ = 0.137 in.

P = 54.8 kips

Δ = 0.396 in.

P = 52.4 kips

Δ = 0.771 in.

P = 2.5 kips

Δ = 1.40 in.

FIG 5.13 SEQUENCE PHOTOGRAPHS FOR BEAM G24D-12

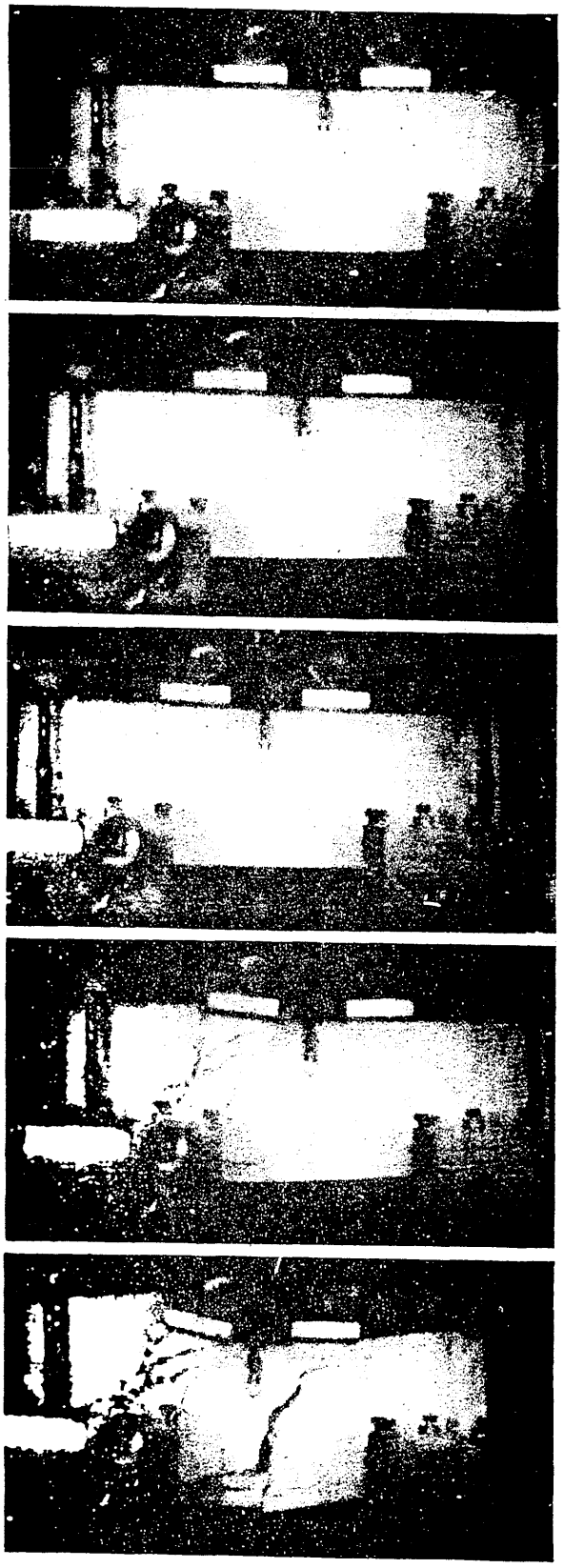

P = 71.8 kips

Δ = 0.116 in.

P = 52.3 kips

Δ = 0.158 in.

P = 45.6 kips

Δ = 0.216 in.

P = 26.8 kips

Δ = 0.587 in.

P = 23.5 kips

Δ = 0.195 in.

FIG. 5.14 SEQUENCE PHOTOGRAPHS FOR BEAM G33D-31

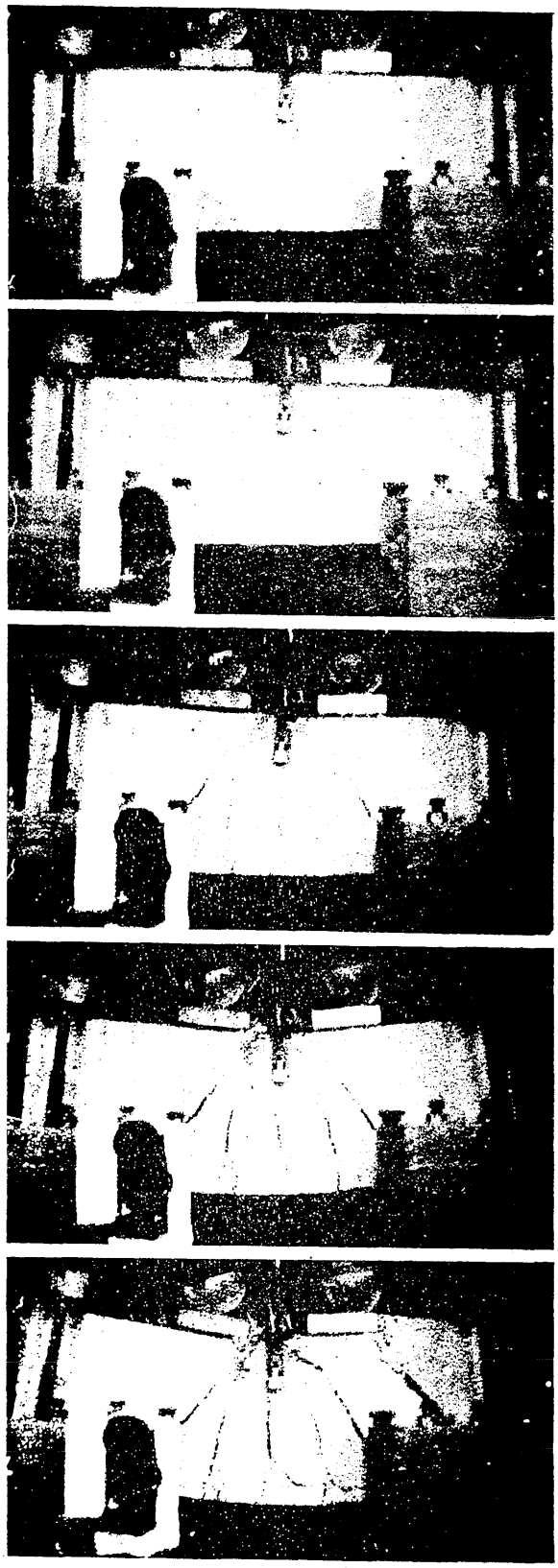

P = 63.2 kips

Δ = 0.108 in.

P = 53.2 kips

Δ = 0.161 in.

P = 50.1 kips

Δ = 0.600 in.

P = 54.4 kips

Δ = 1.170 in.

P = 21.0 kips

Δ = 1.84 in.

FIG. 5.15 SEQUENCE PHOTOGRAPHS FOR BEAM G34D-11

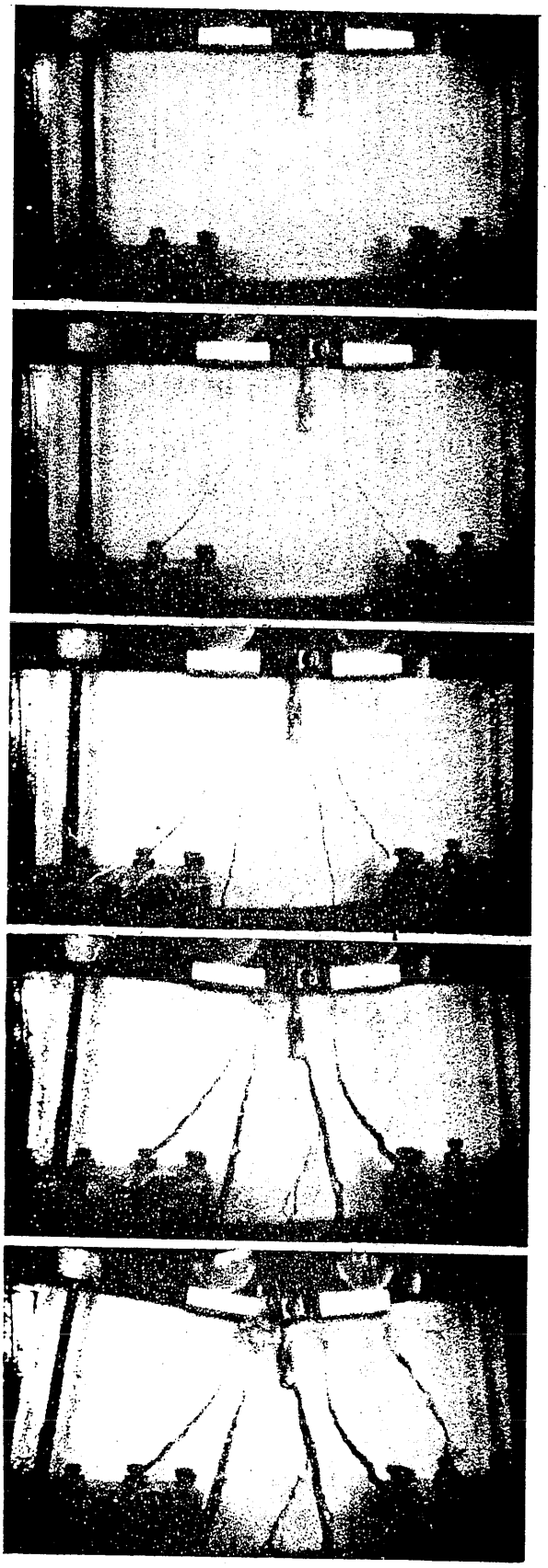

P = 62.4 kips

Δ = 0.096 in.

P = 55.9 kips

Δ = 0.188 in.

P = 45.0 kips

Δ = 0.587 in.

P = 46.9 kips

Δ = 1.38 in.

P = 29.2 kips

Δ = 1.55 in.

FIG. 5.16 SEQUENCE PHOTOGRAPHS FOR BEAM G24D-11

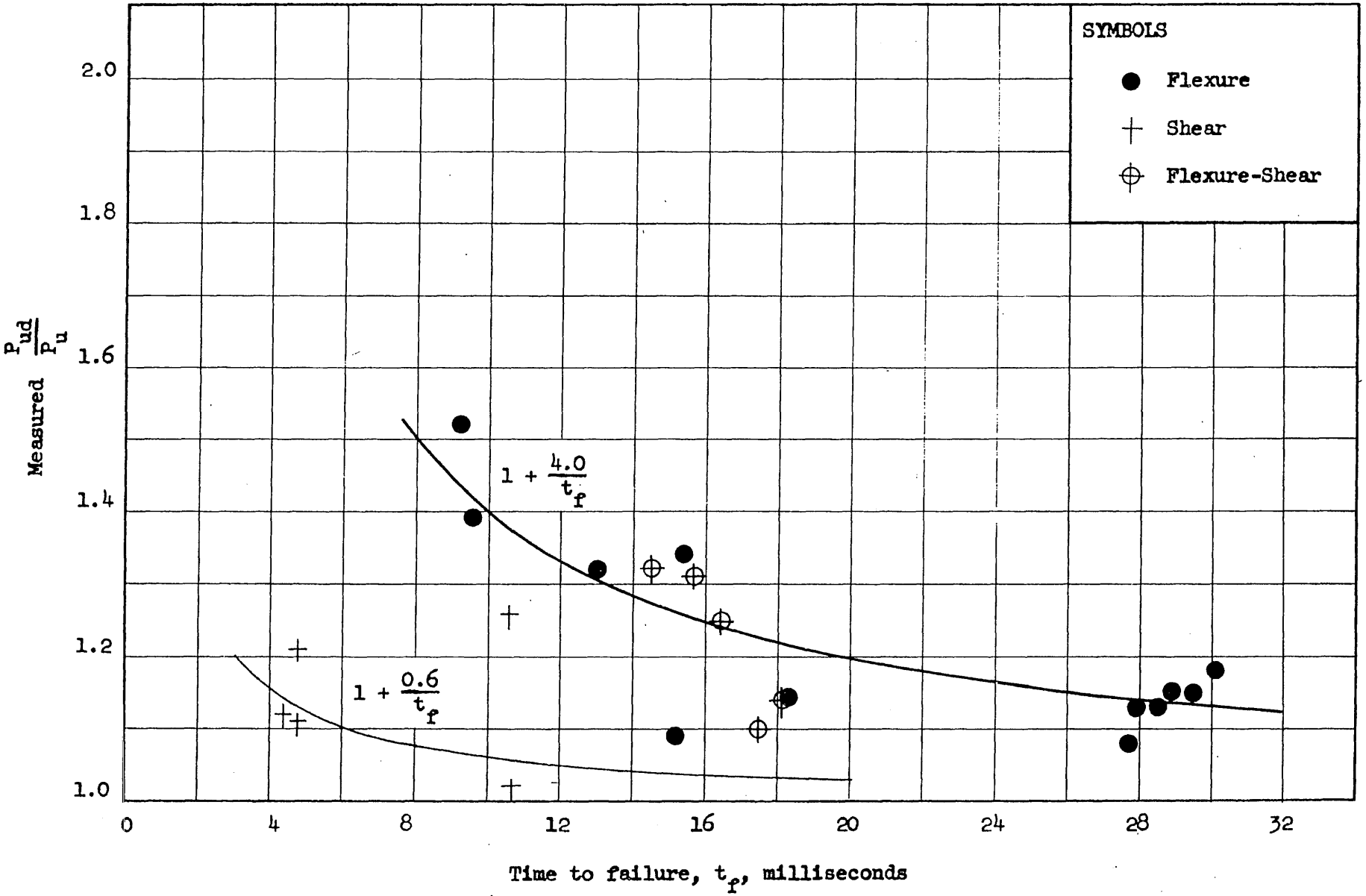

FIG. 5.17 COMPARISON OF MEASURED AND COMPUTED DYNAMIC ULTIMATE STRENGTHS

APPENDIX A

APPENDIX A: SUMMARY OF FORMULAS FOR DETERMINING THE FLEXURAL STRENGTH OF REINFORCED CONCRETE BEAMS

Yield Moment: For beams reinforced in tension only the moment at yield for the stress-strain relationships shown in Fig. A.1 is given by

$$M_y = A_s f_y jd \tag{A1}$$

where

$$j = 1 - \frac{k}{3} \tag{A2}$$

$$k = \sqrt{2pn + (pn)^2} - pn \tag{A3}$$

where n in this report is taken as

$$n = 6 + \frac{10{,}000}{f'_c} \tag{A4}$$

which was found by Sozen (17) to be satisfactory for the materials used in the beams.

For beams reinforced in both tension and compression the moment at yield for the stress-strain relationships shown in Fig. A.1 is given by

$$M_y = 0.5\, f_c k d^2 b \left(1 - \frac{k}{3}\right) + d'A'_s \left(f'_s - E_c \epsilon'_s\right) \tag{A5}$$

where

$$k = \sqrt{2\left[np + (n-1)p'\,(1-k')\right] + \left[(n-1)p' + np\right]^2} - \left[(n-1)p' + np\right] \tag{A6}$$

$$f_c = \frac{f_y\, k}{n(1-k)} \tag{A7}$$

$$f'_s = f_y \left[\frac{k'}{(1-k)} - 1\right] \tag{A8}$$

$$k' = \frac{d'}{d} \tag{A9}$$

$$n = 6 + \frac{10{,}000}{f'_c} \tag{A4}$$

Ultimate Moment: The ultimate moment of beams failing by the crushing of the concrete in the compression zone can be found by consideration of the distributions of stresses and strains shown in Fig. A-1. For beams reinforced in tension only:

$$M_f = A_s f_s d \left(1 - \frac{k_2}{k_1 k_3} \frac{p f_s}{f'_c}\right) \tag{A10}$$

where $$k_1 k_3 = 1.37 - 0.000108\, f'_c \tag{A11}$$

which is an empirical relation derived from tests (17).

$$k_2 = 0.42$$

If the beam fails in the yield range

$$f_s = f_y$$

If the beam fails above the yield range

$$f_s = \frac{k_1 k_3 f'_c \epsilon_u}{p (\epsilon_u + \epsilon_s)} \tag{A12}$$

where ϵ_u is the limiting strain in the concrete at crushing and is assumed to be equal to 0.008 for the beams tested. This expression can be solved graphically utilizing the stress-strain curve for the reinforcing bar.

For beams reinforced in tension and compression, the following relationship was developed considering the stress and strain distributions of Fig. A-1, provided the area of the compression steel is less than the area

of the tension steel.

$$M_f = [A_s f_s - A'_s f'_s]d \left[1 - \frac{k_2}{k_1 k_3}\left(\frac{pf_s - p'f'_s}{f'_c}\right)\right] + A'_s f'_s d' \qquad (A13)$$

In this expression no correction has been made for the concrete area displaced by the compression reinforcement. If it is desired to make this correction then the stress in the compression steel at failure, f_s should be modified to f where

$$f = f'_s - 0.85\, f'_c \qquad (A14)$$

which is recommended by ACI 318-56 (18).

When the compression steel is in the yield range at failure;

$$f'_s = f'_y$$

When the compression steel is not in the yield range at failure

$$f'_s = E'\, \epsilon'_s$$

$$\epsilon'_s = \epsilon_u - (\epsilon_u + \epsilon_s)\left(1 - \frac{d'}{d}\right) \qquad (A15)$$

When the tension steel is in the yield range at failure:

$$f_s = f_y$$

When the tension steel is in the strain hardening range at failure:

$$f_s = \frac{k_1 k_3 f'_c\, \epsilon_u}{p(\epsilon_s + \epsilon_u)} + \frac{p'f'_s}{p} \qquad (A16)$$

If conditions are such that the compression steel ratio does not satisfy the assumptions, these equations are no longer valid. However, moments may

be computed by considering the equilibrium of the transverse forces on the section and summing the moments of the forces about a convenient point on the section.

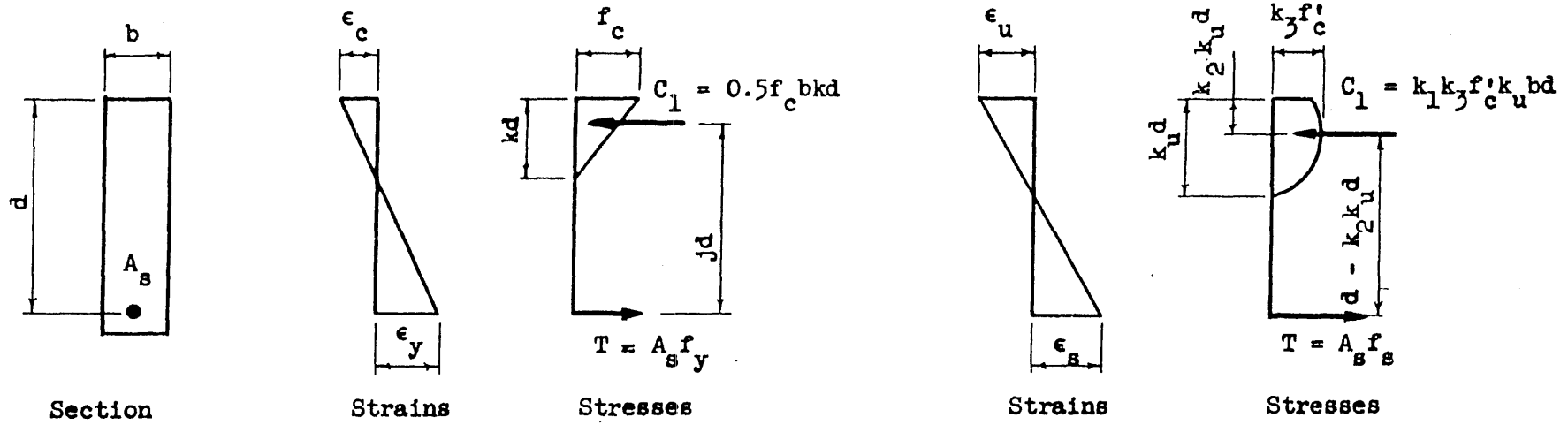

Beams Reinforced in Tension Only

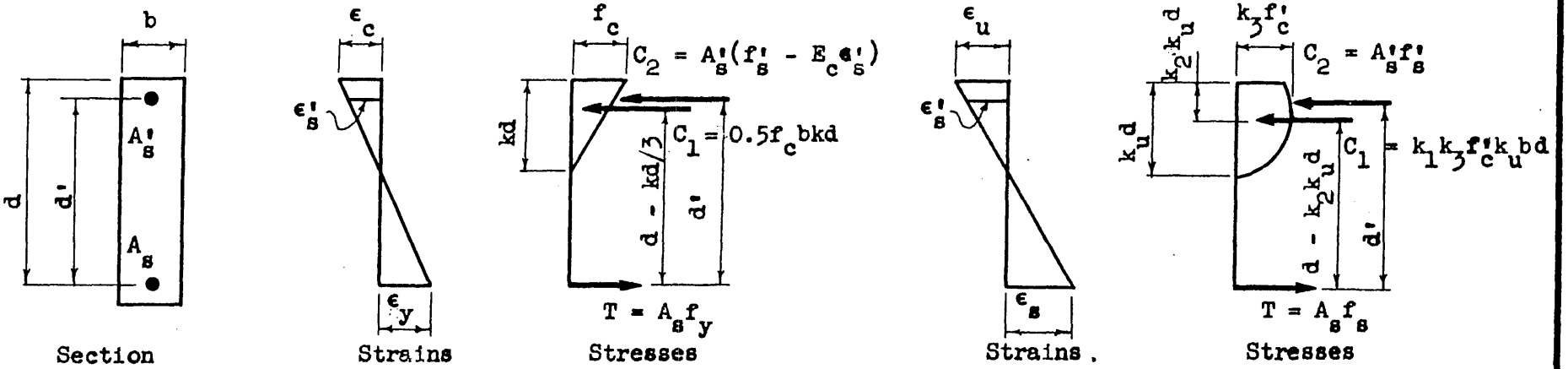

Beams Reinforced in Tension and Compression

FIG. A.1 STRESS AND STRAIN RELATIONSHIPS AT FLEXURAL YIELD AND ULTIMATE

APPENDIX B

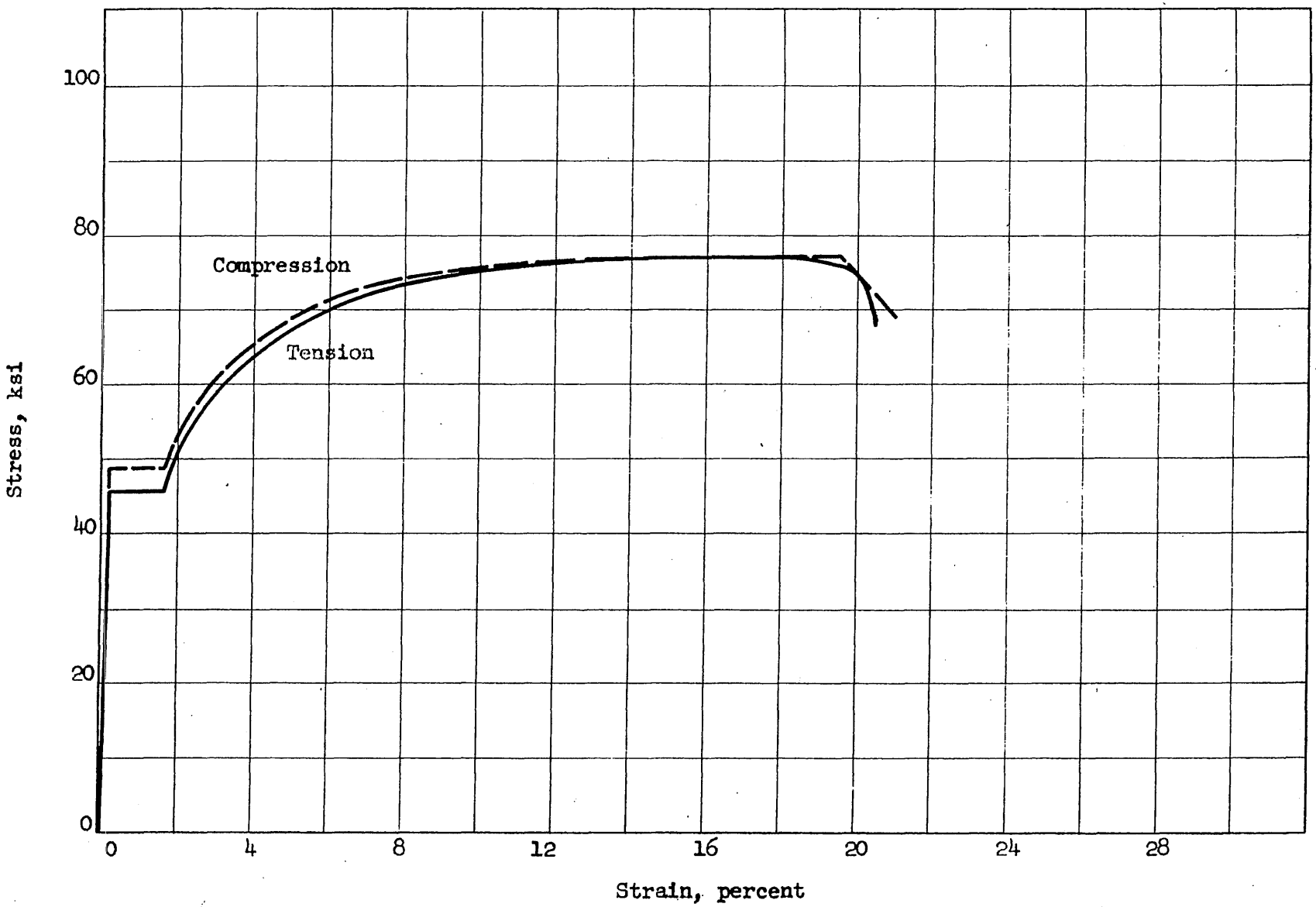

FIG. B.1 STRESS-STRAIN CURVES FOR REINFORCEMENT USED IN BEAMS OF SERIES G23S-11 AND G24S-11

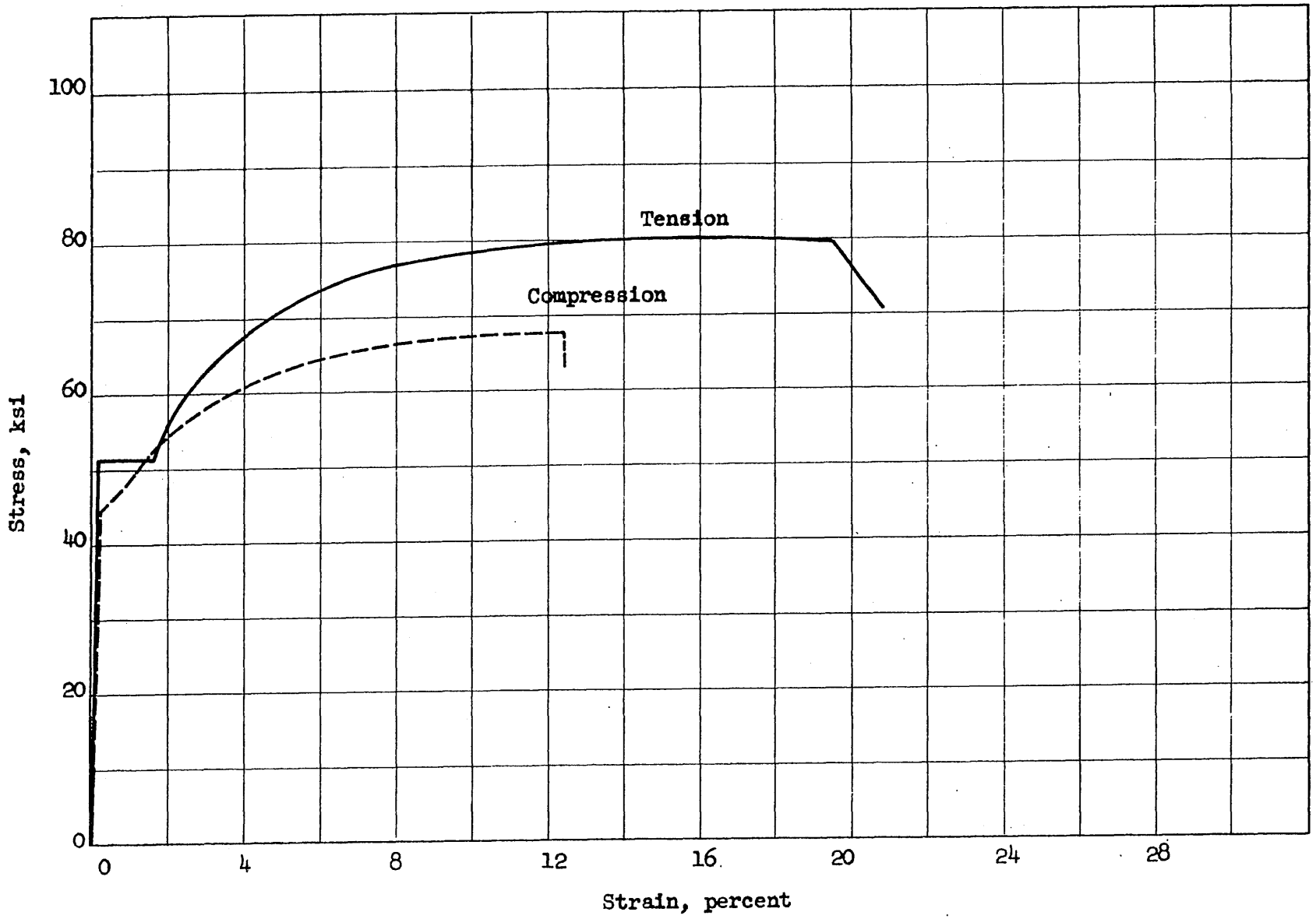

FIG. B.2 STRESS-STRAIN CURVES FOR REINFORCEMENT USED IN BEAMS OF SERIES G23S-21 AND G24S-21

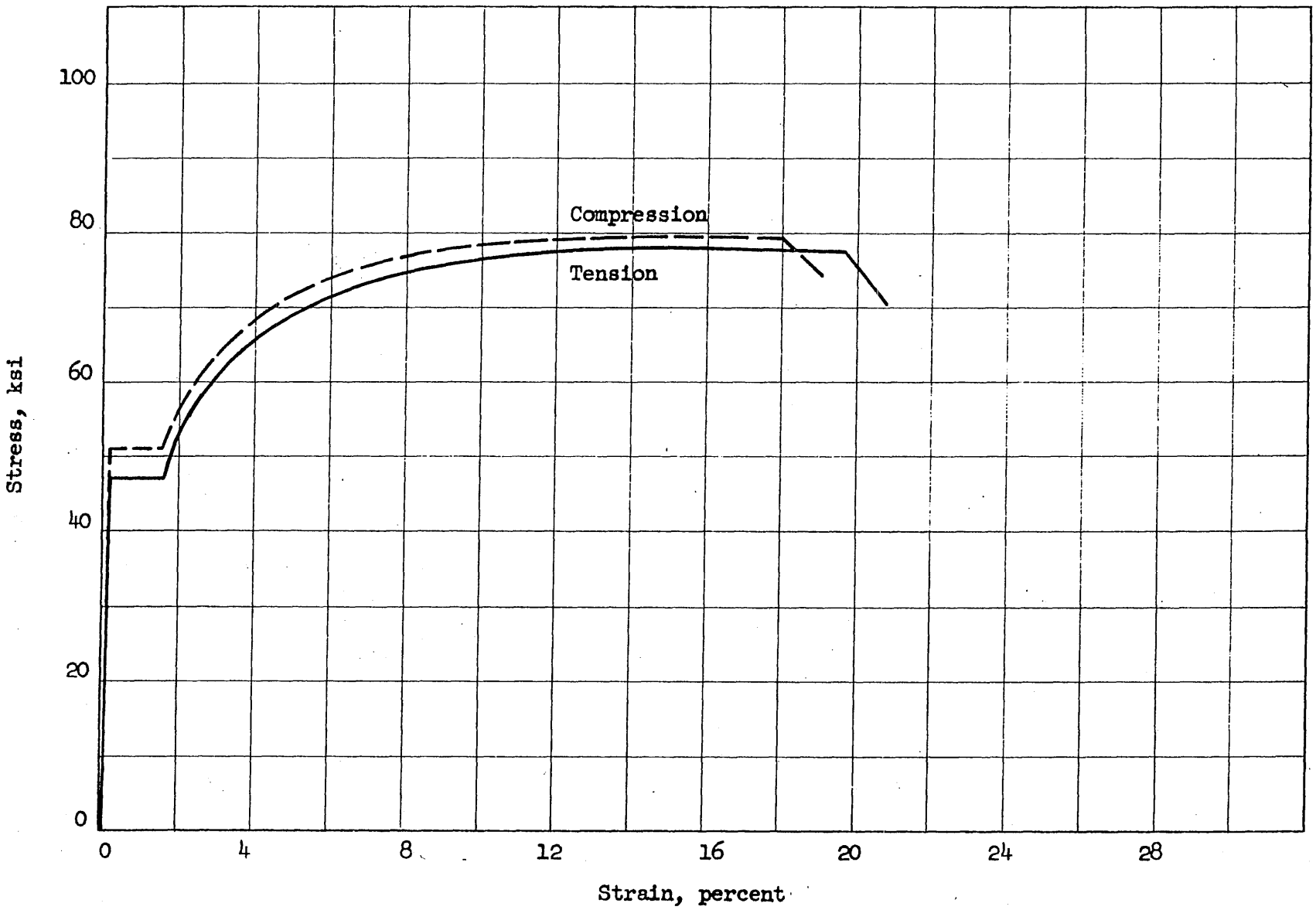

FIG. B.3 STRESS-STRAIN CURVES FOR REINFORCEMENT USED IN BEAMS OF SERIES G33S-11

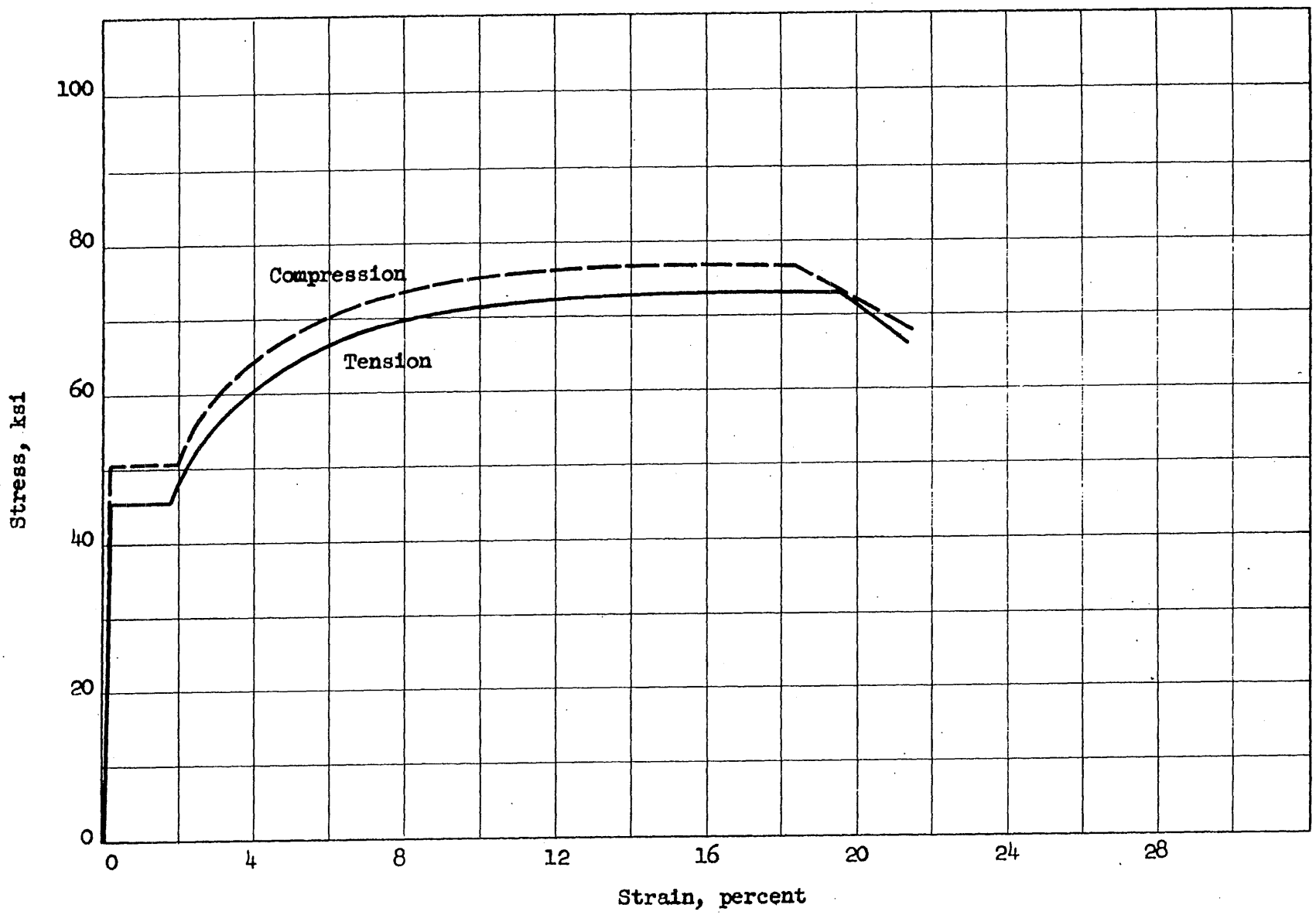

FIG. B.4 STRESS-STRAIN CURVES FOR REINFORCEMENT USED IN BEAMS OF SERIES G33S-21

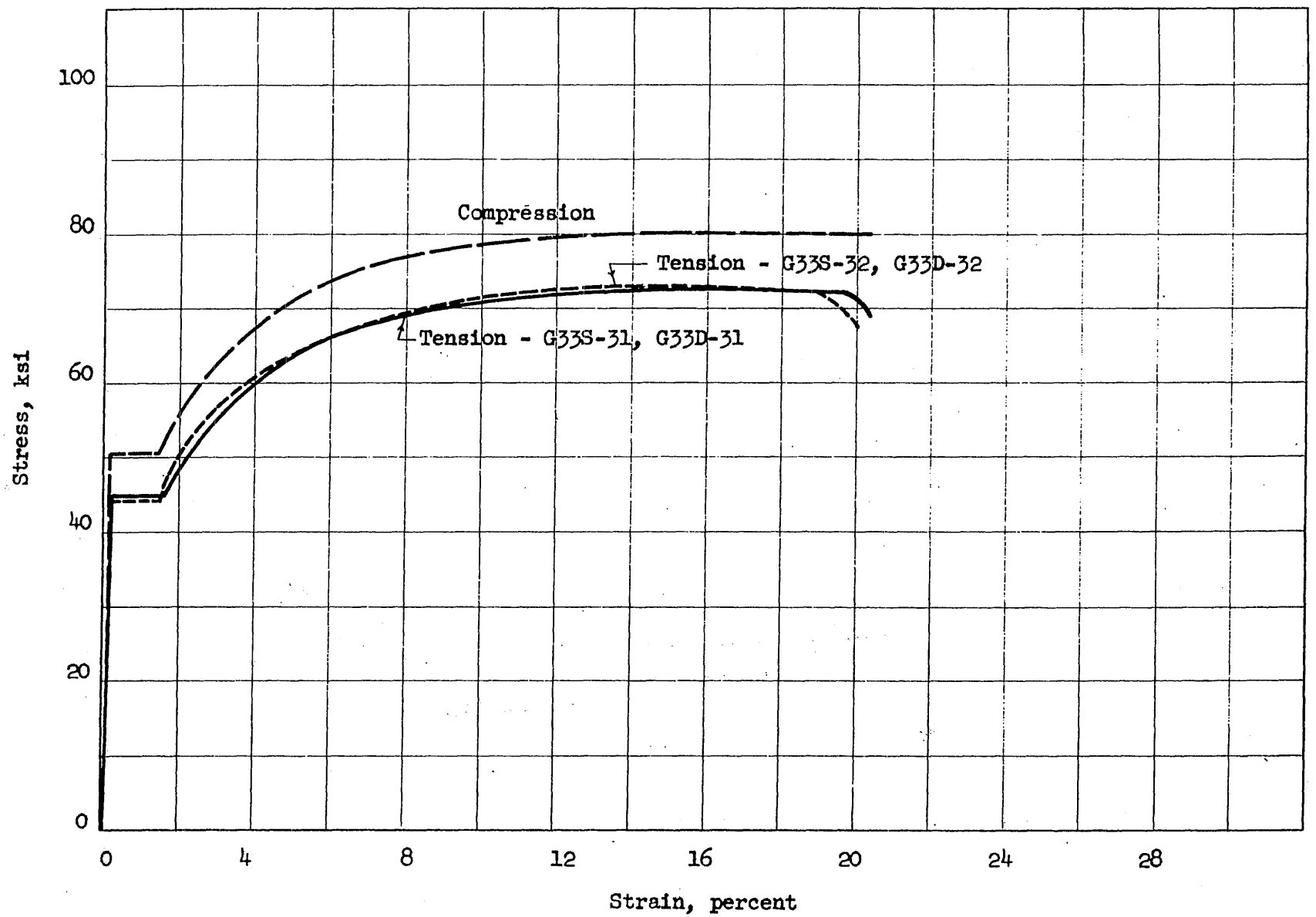

FIG. B.5 STRESS-STRAIN CURVES FOR REINFORCEMENT USED IN BEAMS OF SERIES G33S-31

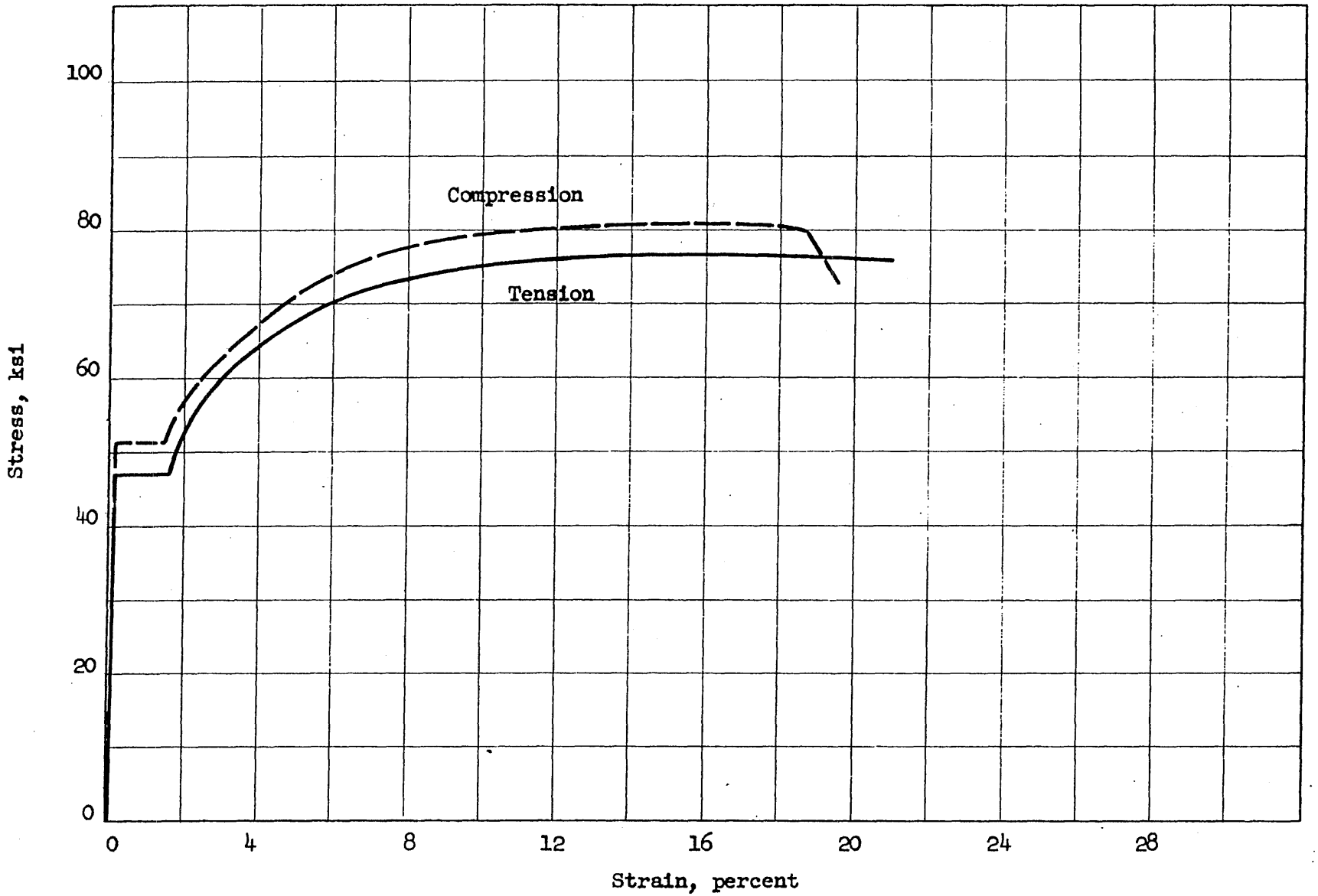

FIG. B.6 STRESS-STRAIN CURVES FOR REINFORCEMENT USED IN BEAMS OF SERIES G3$\frac{1}{4}$S-11

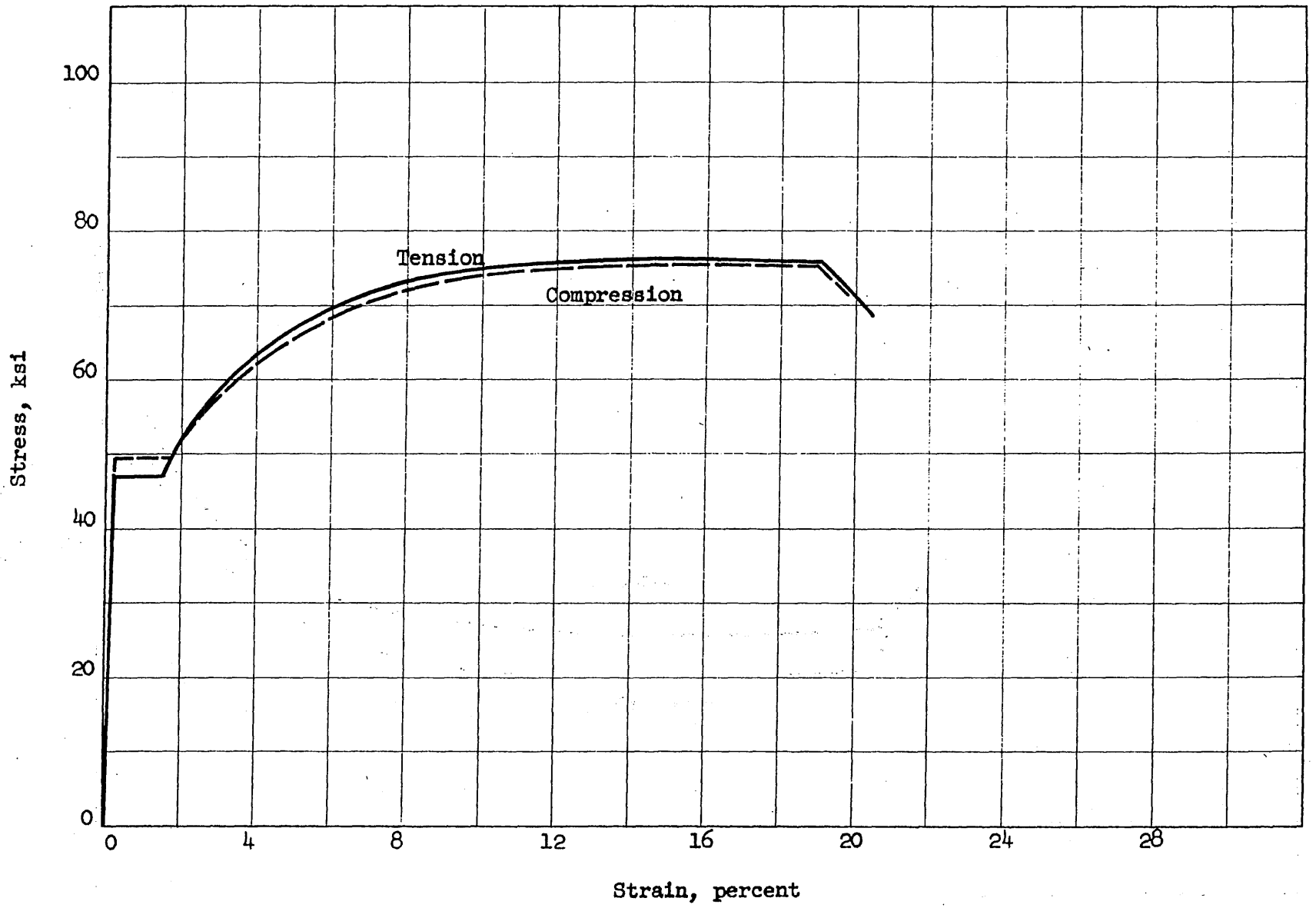

FIG. B.7 STRESS-STRAIN CURVES FOR REINFORCEMENT USED IN BEAMS OF SERIES G34S-21

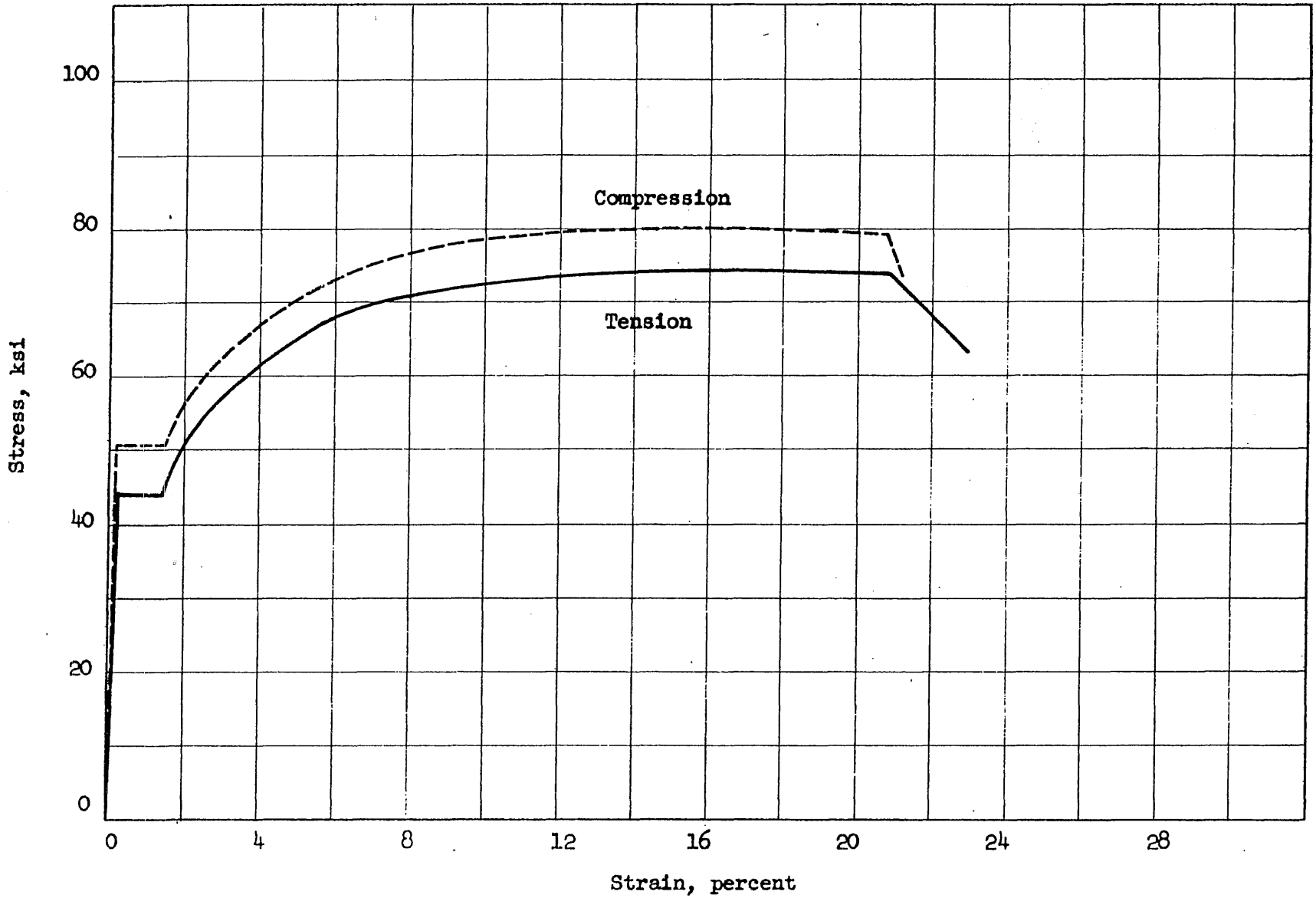

FIG. B.8 STRESS-STRAIN CURVES FOR REINFORCEMENT USED IN BEAMS OF SERIES G43S-11

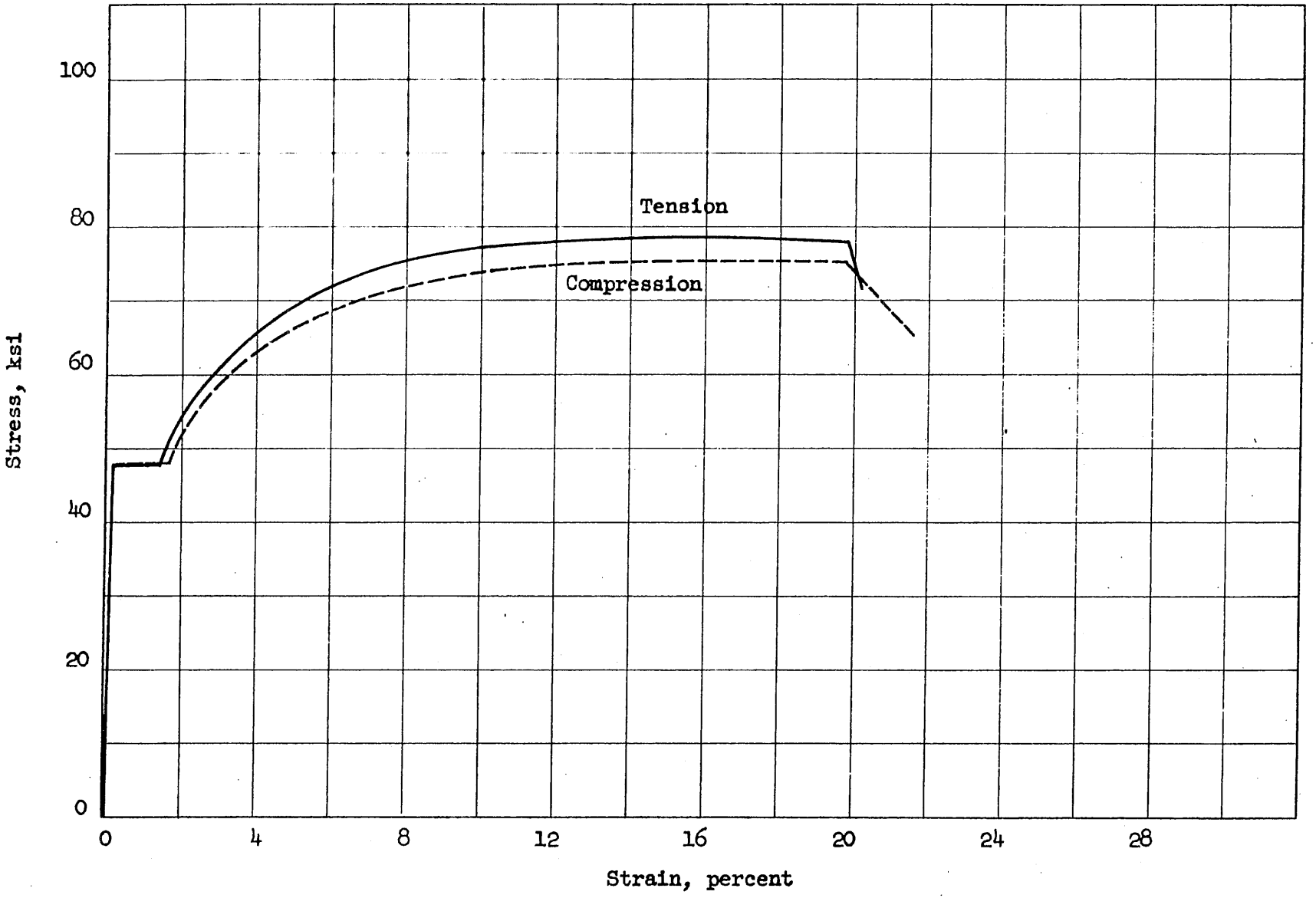

FIG. B.9 STRESS-STRAIN CURVES FOR REINFORCEMENT USED IN BEAMS OF SERIES G44S-11

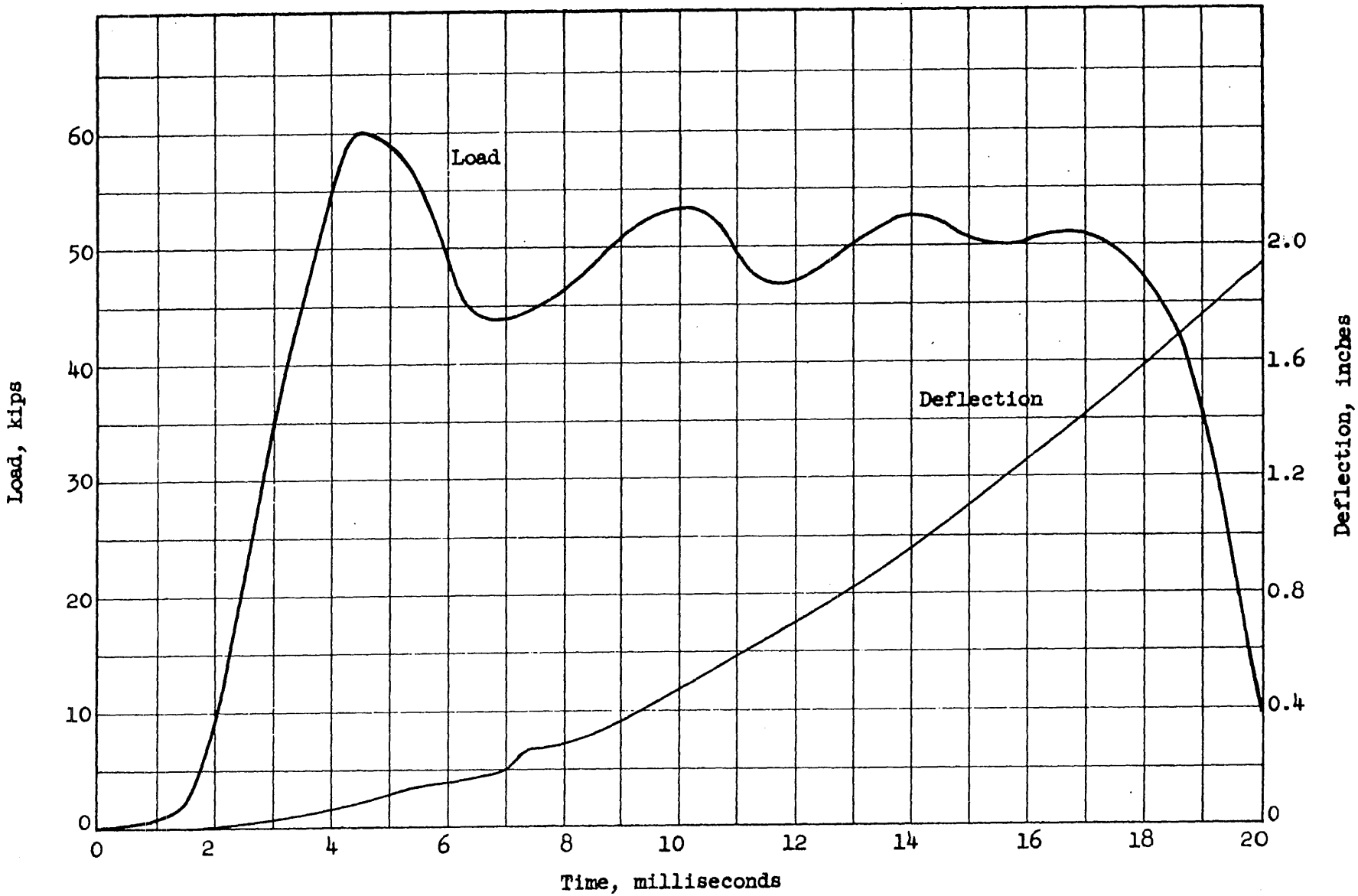

FIG. B.10 LOAD AND DEFLECTION VERSUS TIME FOR BEAM G23D-11

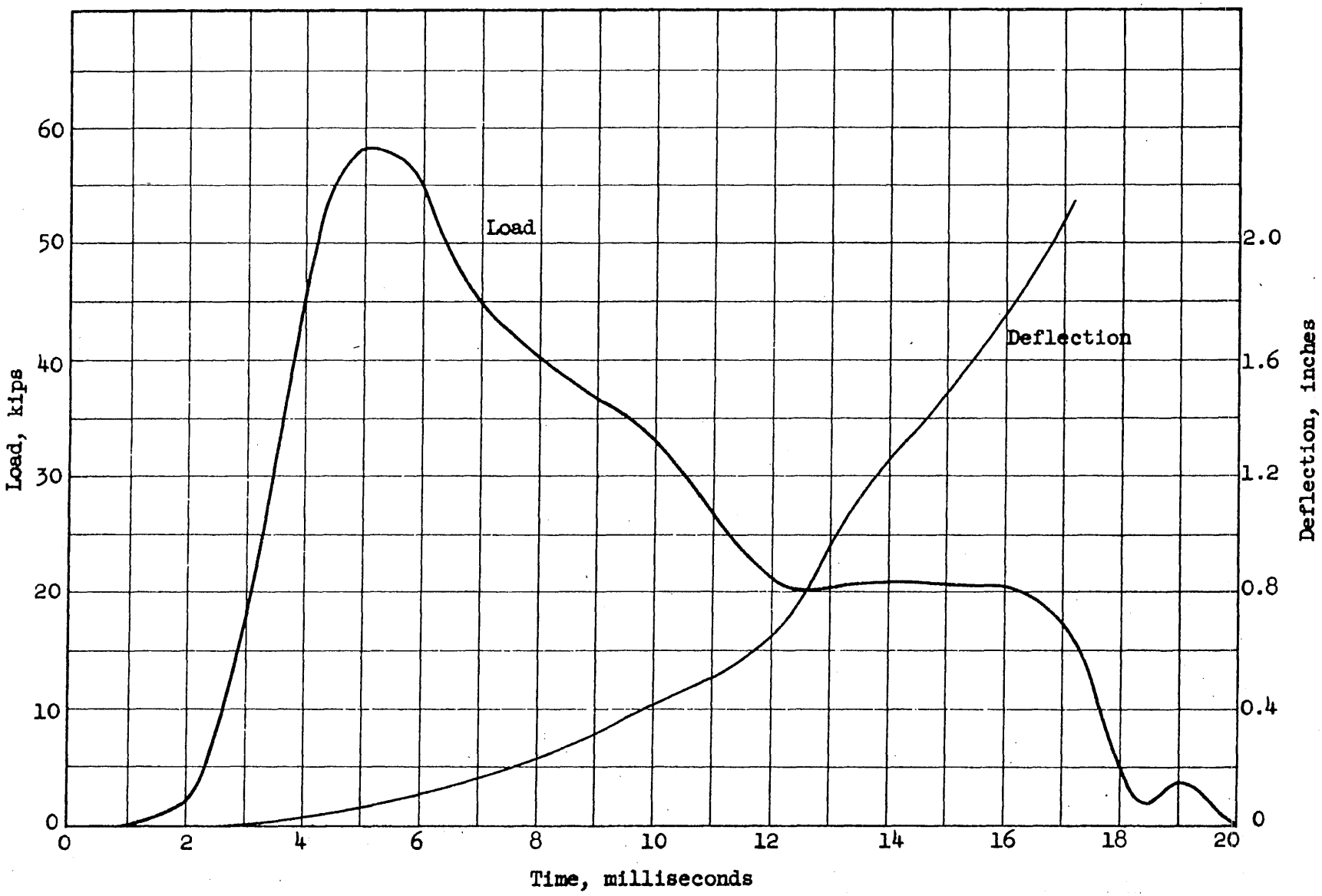

FIG. B-11 LOAD AND DEFLECTION VERSUS TIME FOR BEAM G23D-12

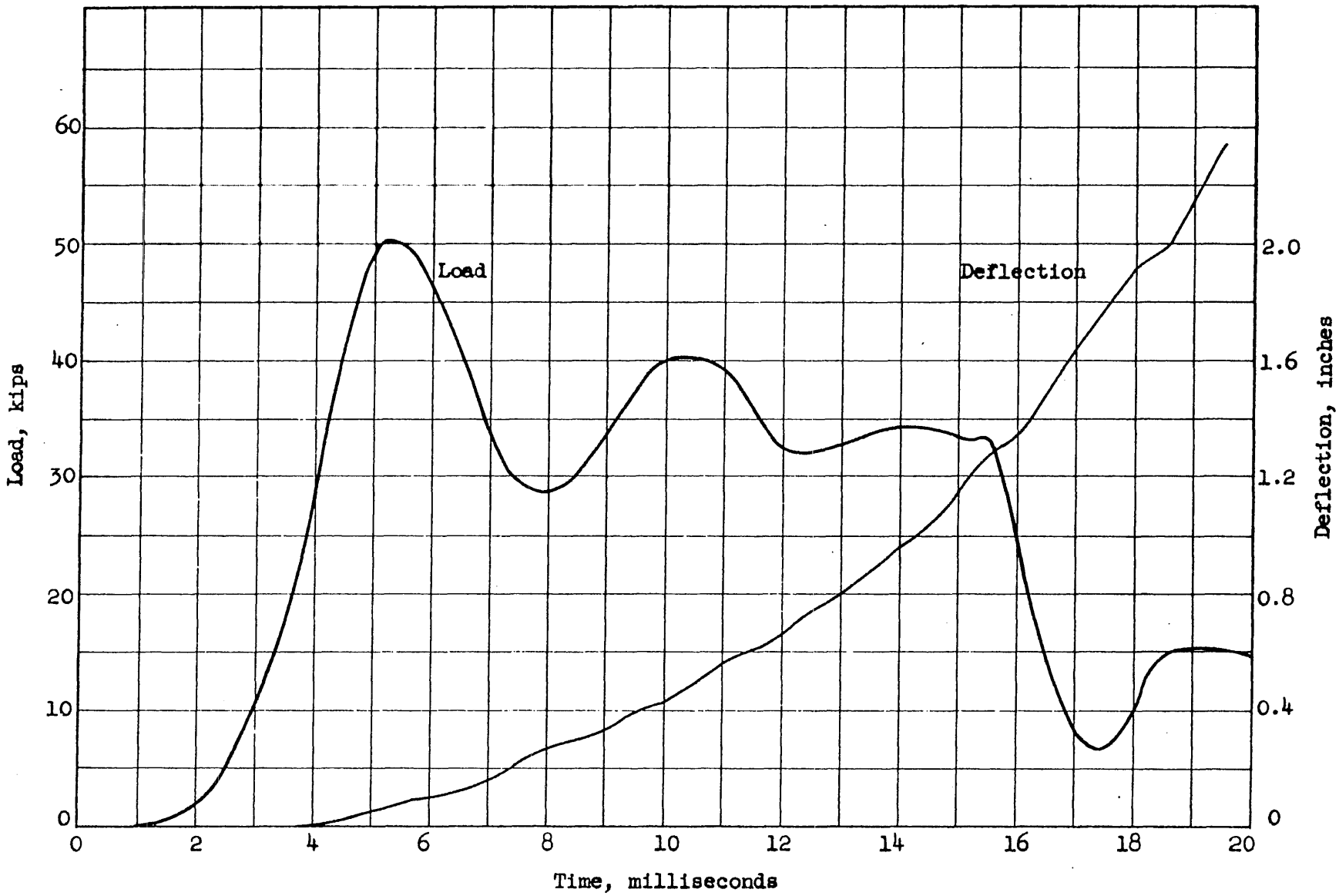

FIG. B.12 LOAD AND DEFLECTION VERSUS TIME FOR BEAM G23D-21

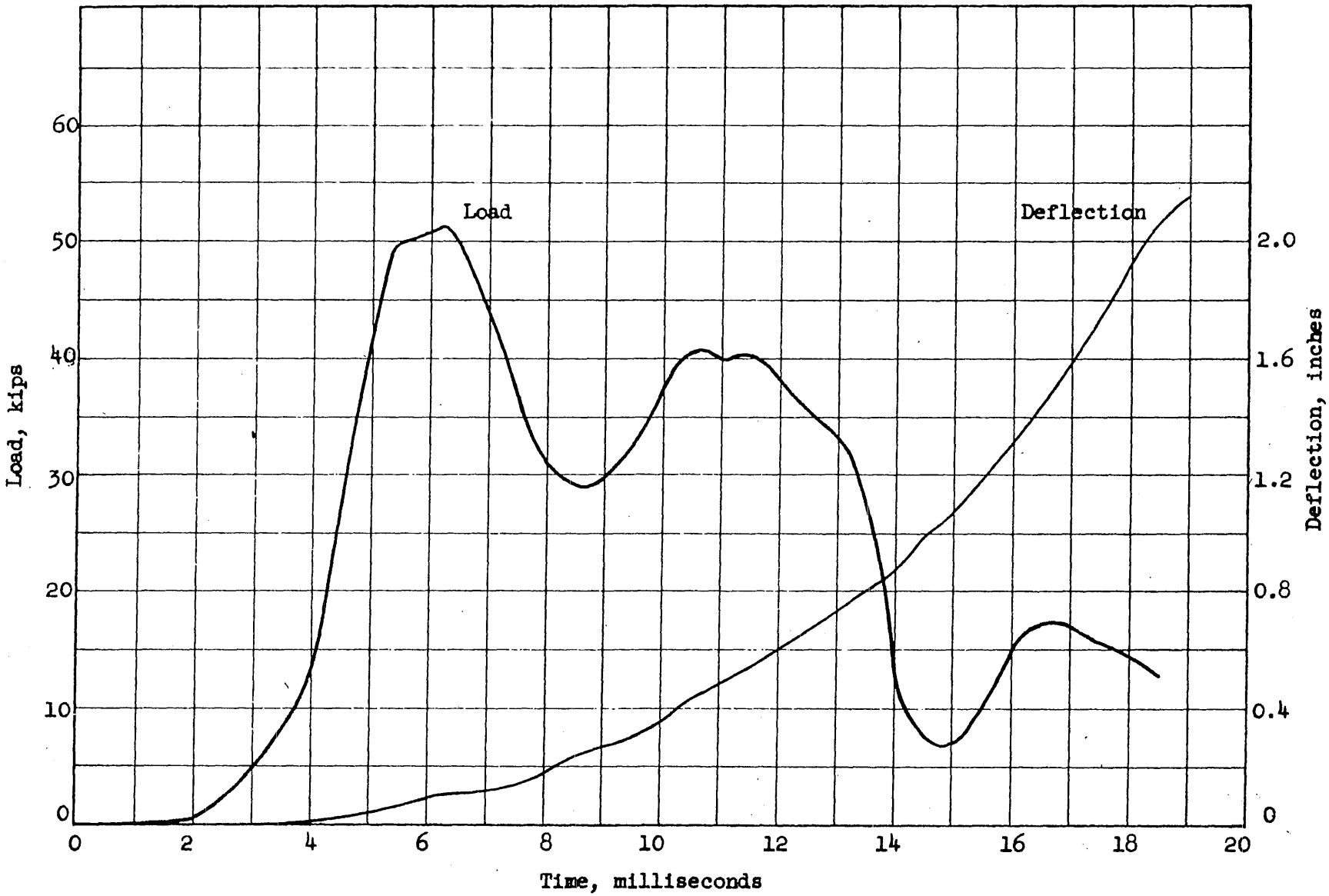

FIG. B.13 LOAD AND DEFLECTION VERSUS TIME FOR BEAM G23D-22

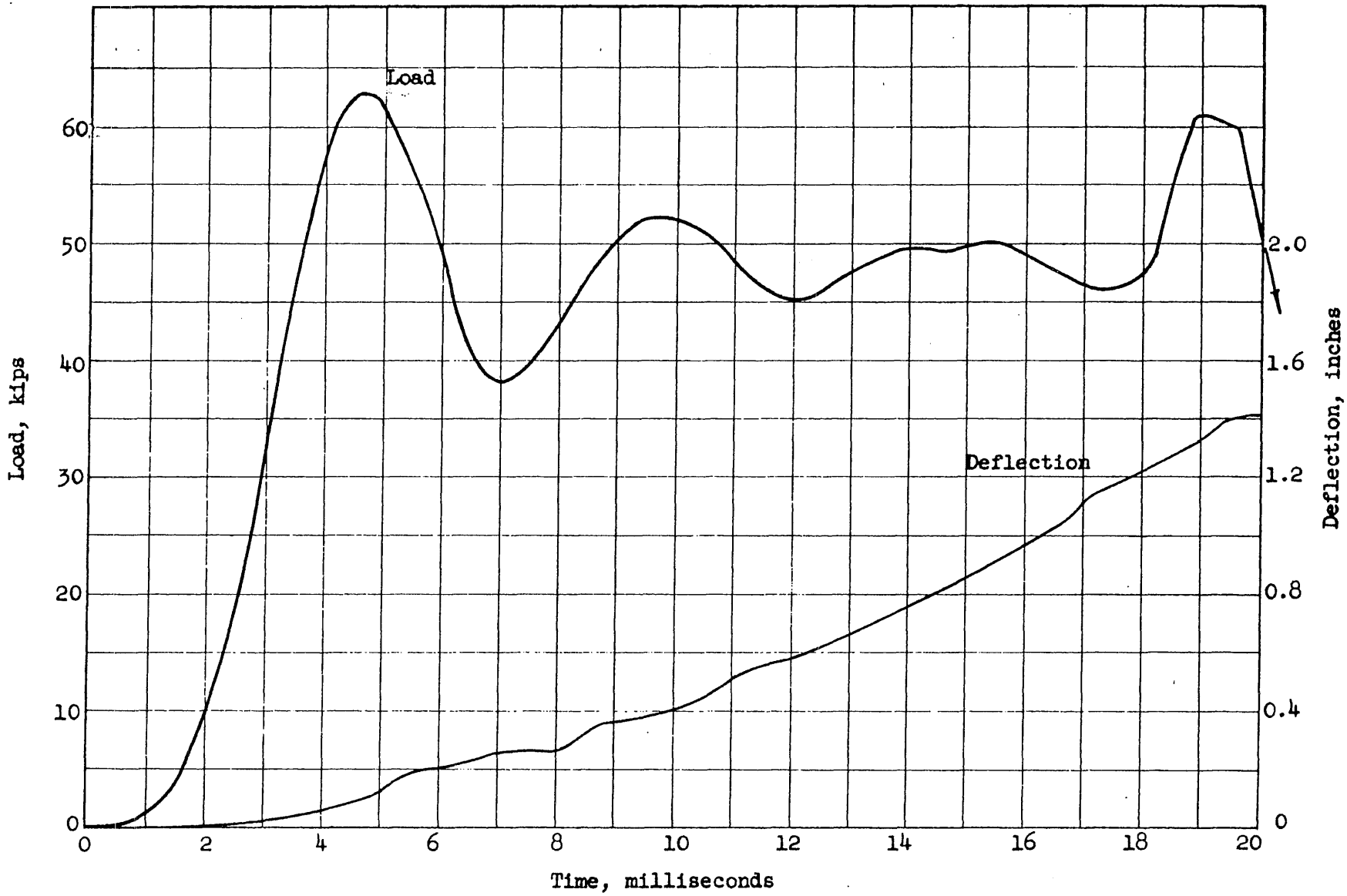

FIG. B.14 LOAD AND DEFLECTION VERSUS TIME FOR BEAM G24D-11

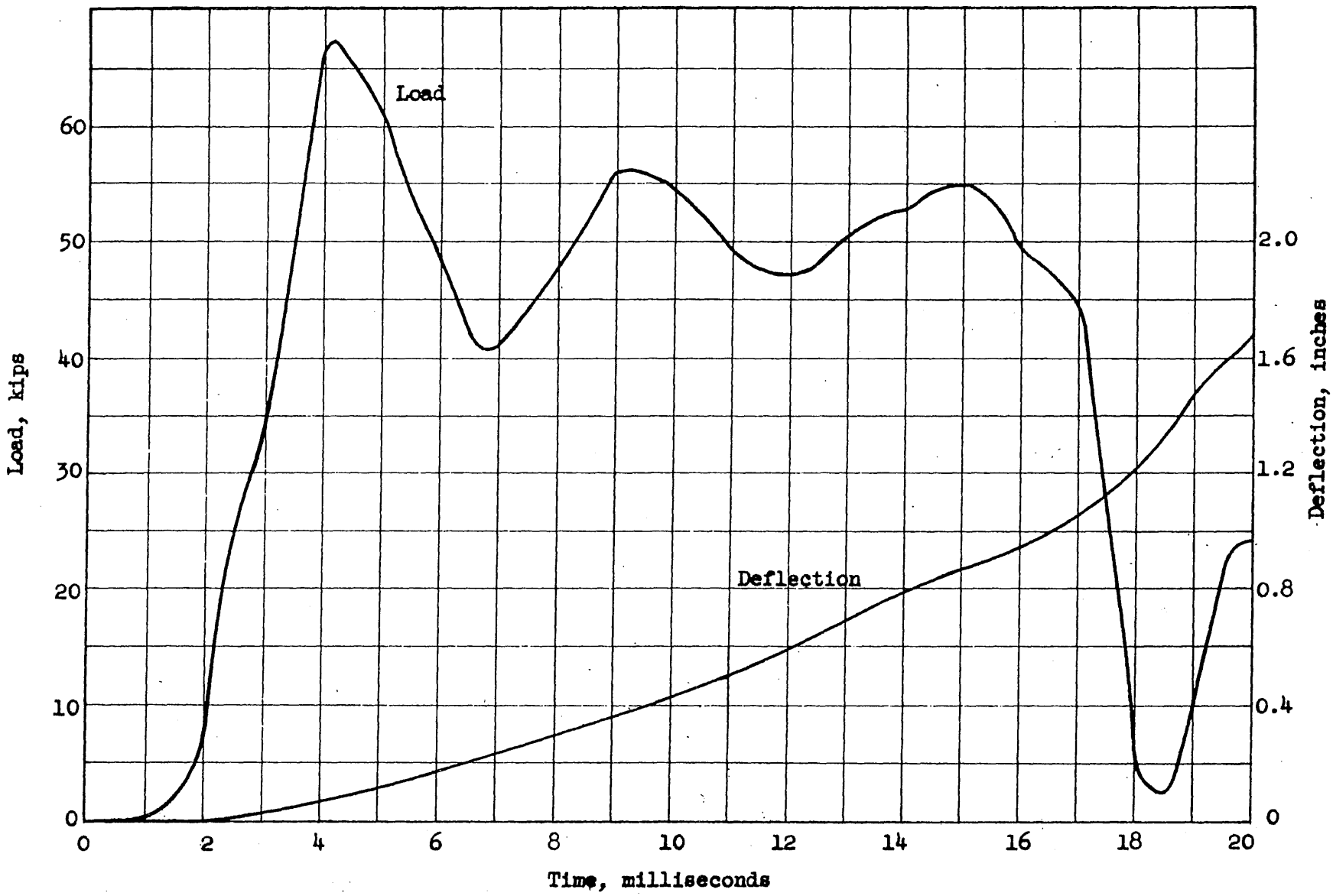

FIG. B.15 LOAD AND DEFLECTION VERSUS TIME FOR BEAM G24D-12

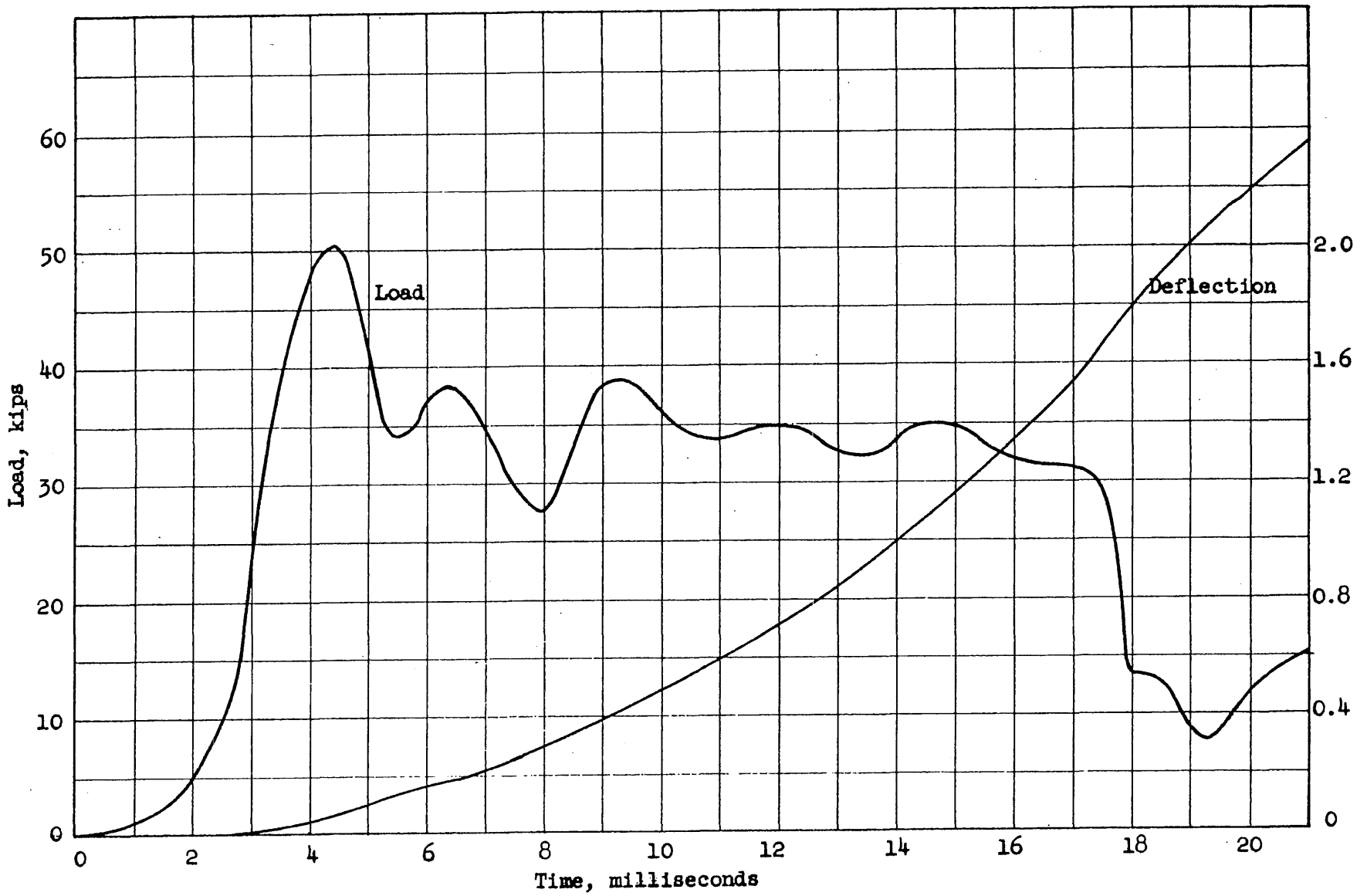

FIG. B.16 LOAD AND DEFLECTION VERSUS TIME FOR BEAM G24D-21

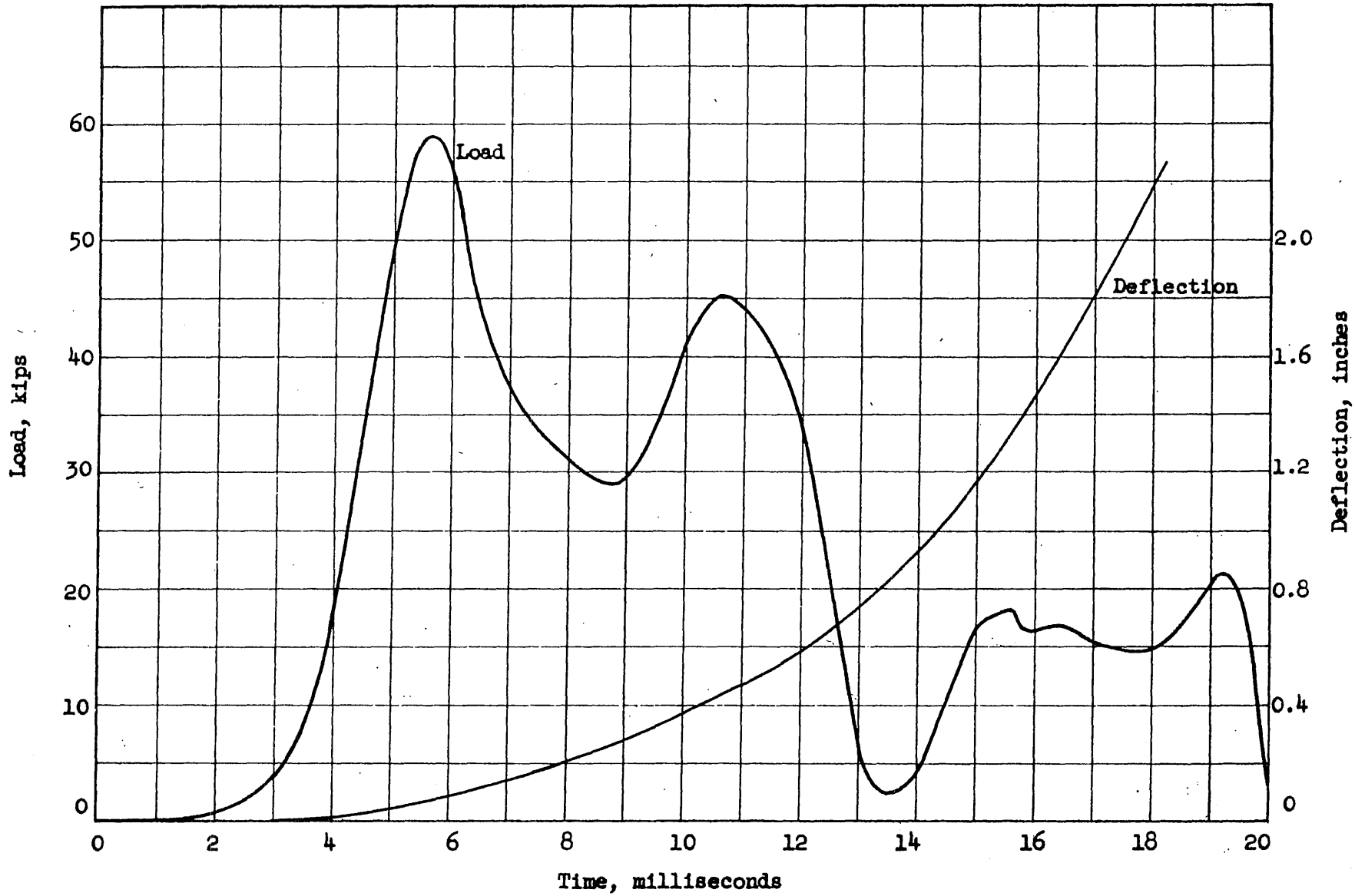

FIG. B.17 LOAD AND DEFLECTION VERSUS TIME FOR BEAM G24D-22

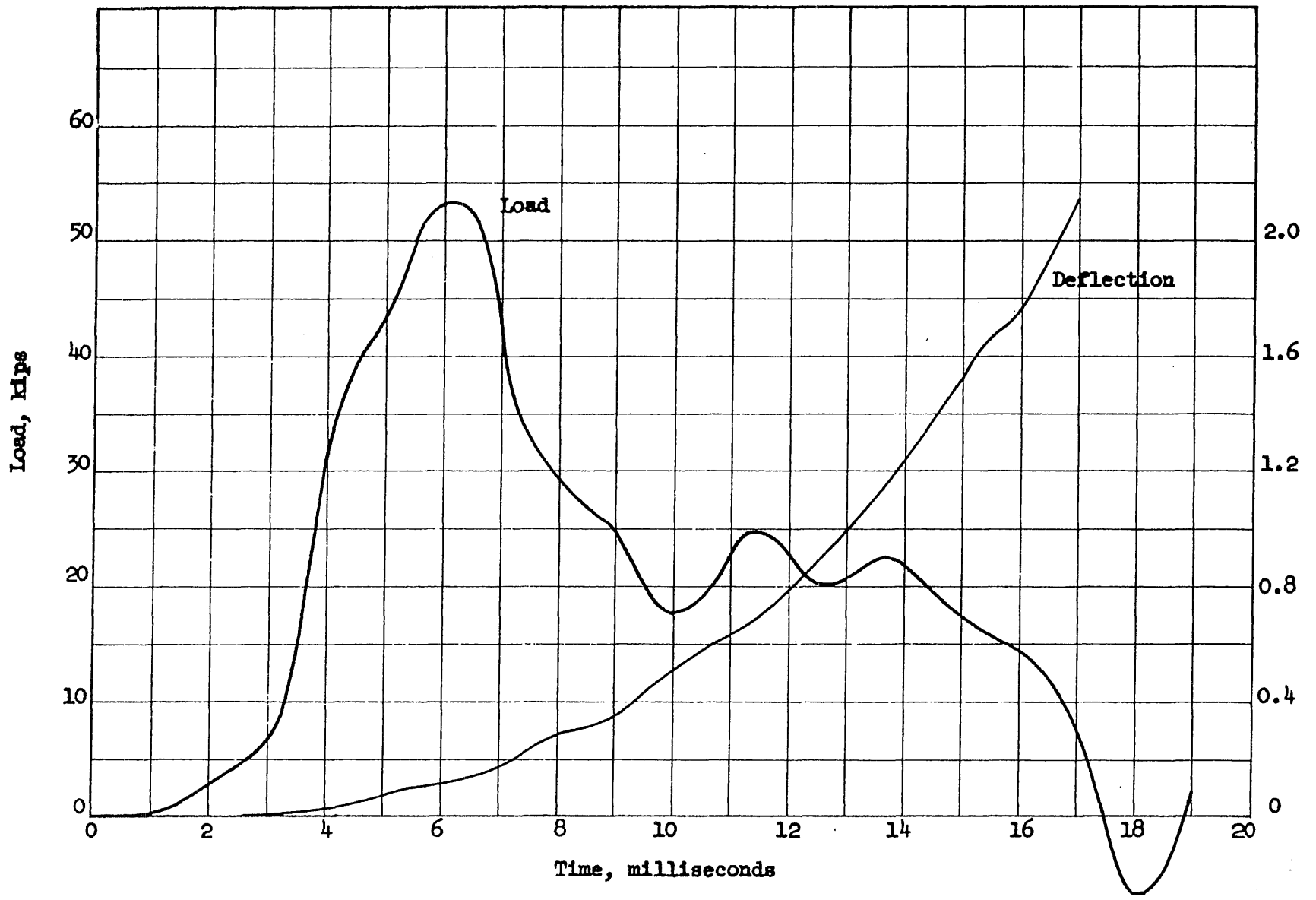

FIG. B.18 LOAD AND DEFLECTION VERSUS TIME FOR BEAM G33D-11

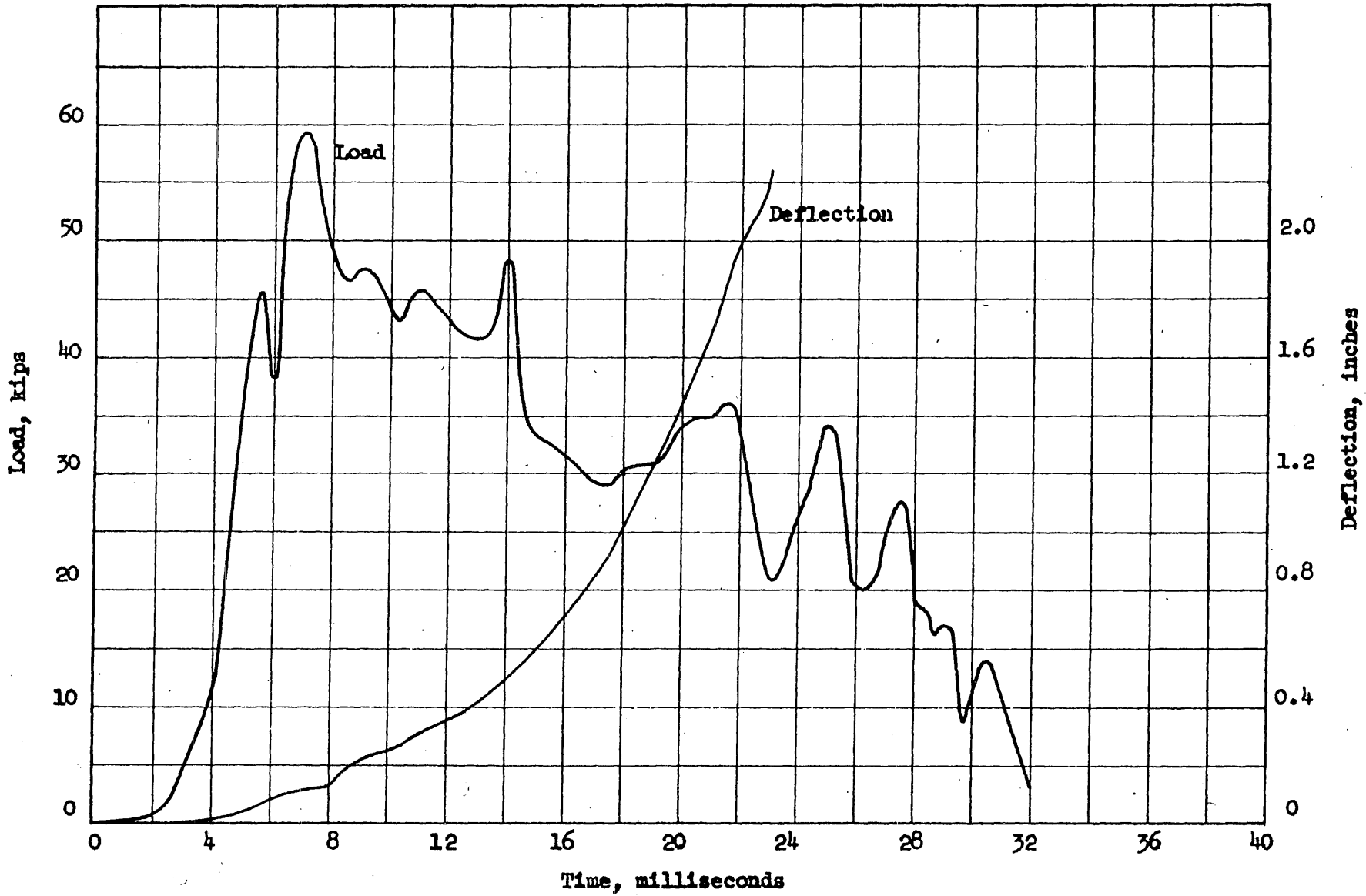

FIG. B.19 LOAD AND DEFLECTION VERSUS TIME FOR BEAM G33D-12

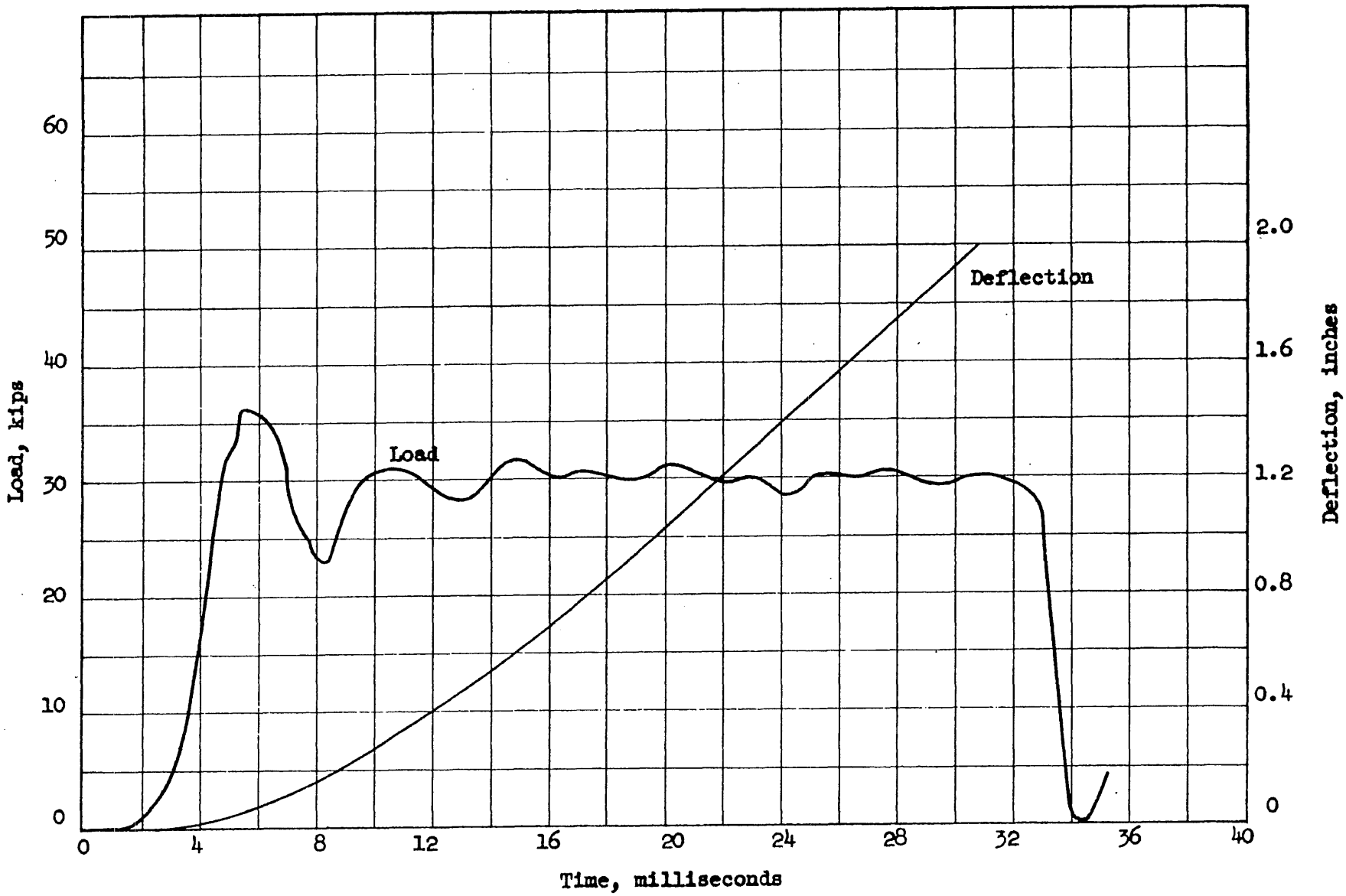

FIG. B.20 LOAD AND DEFLECTION VERSUS TIME FOR BEAM G33D-21

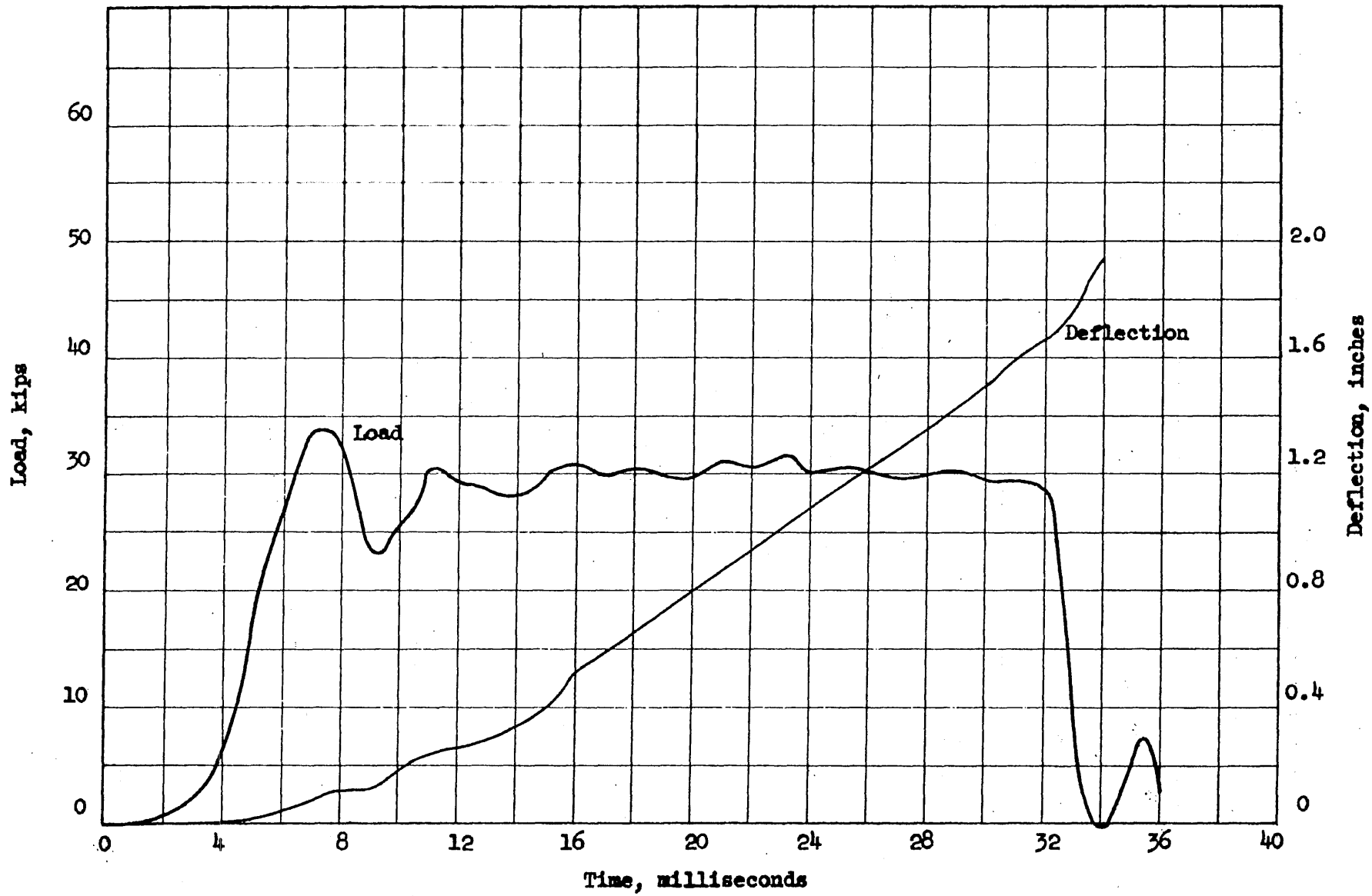

FIG. B.21 LOAD AND DEFLECTION VERSUS TIME FOR BEAM G33D-22

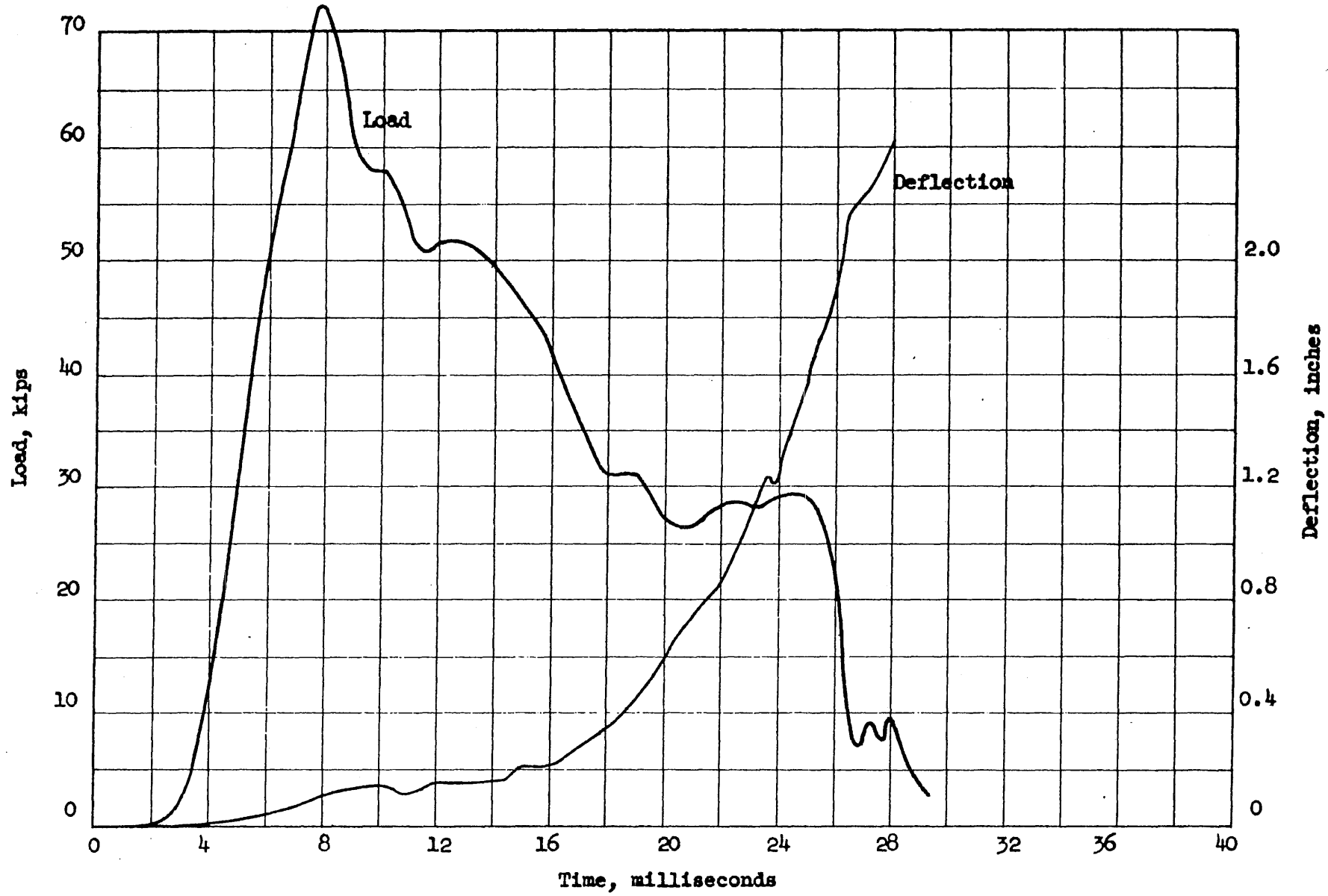

FIG. B.22 LOAD AND DEFLECTION VERSUS TIME FOR BEAM G33D-31

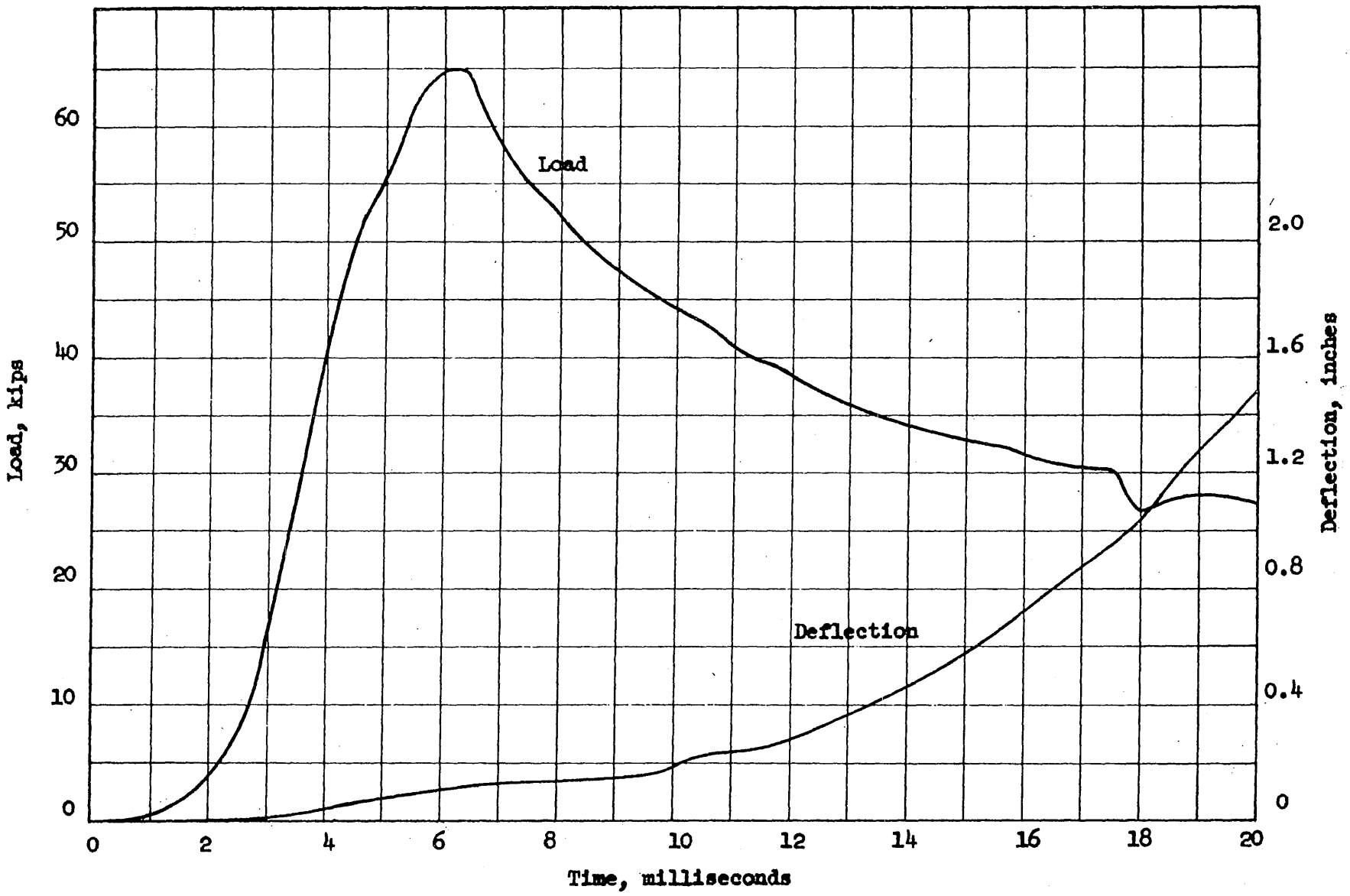

FIG. B.23 LOAD AND DEFLECTION VERSUS TIME FOR BEAM G33D-32

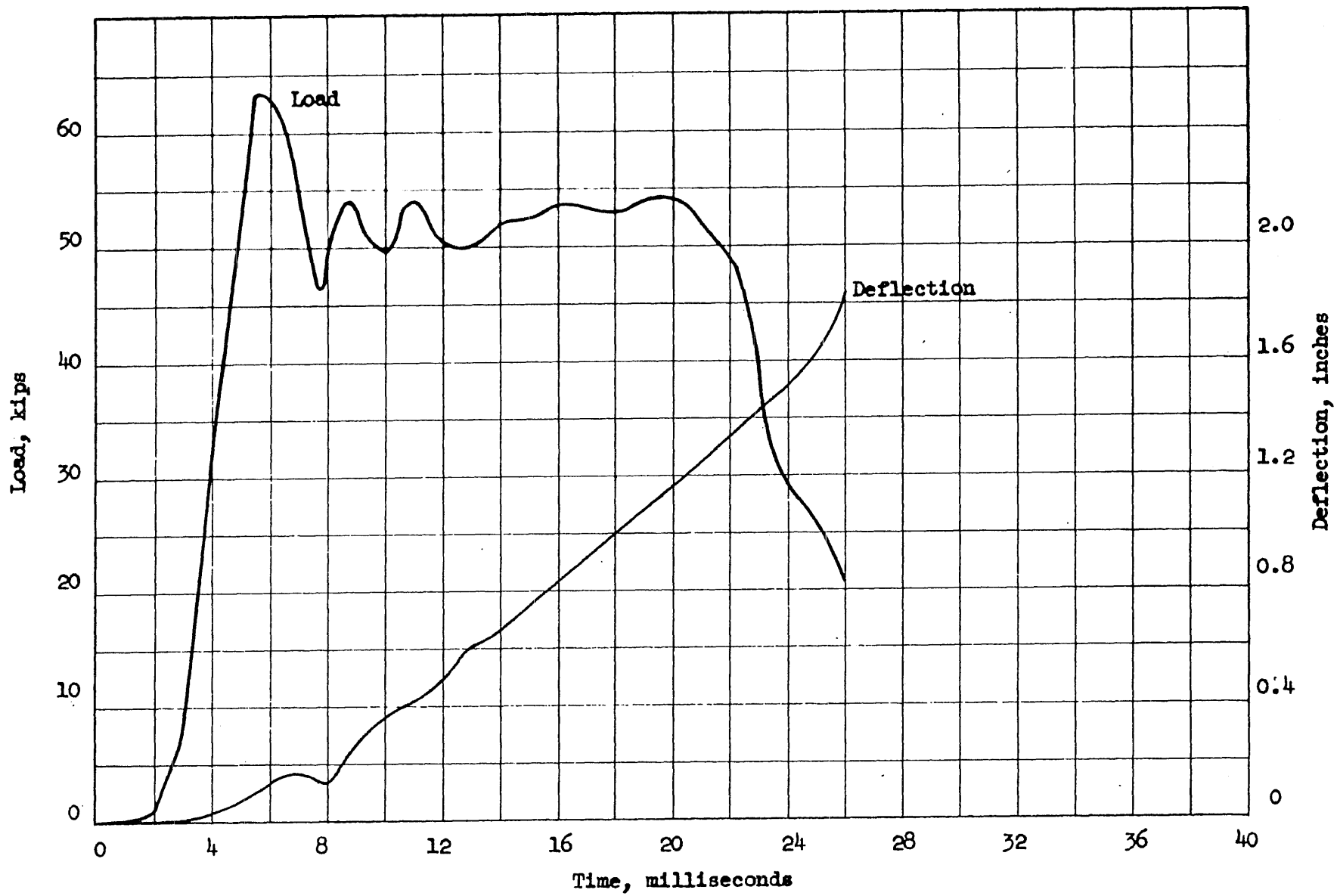

FIG. B.24 LOAD AND DEFLECTION VERSUS TIME FOR BEAM G34D-11

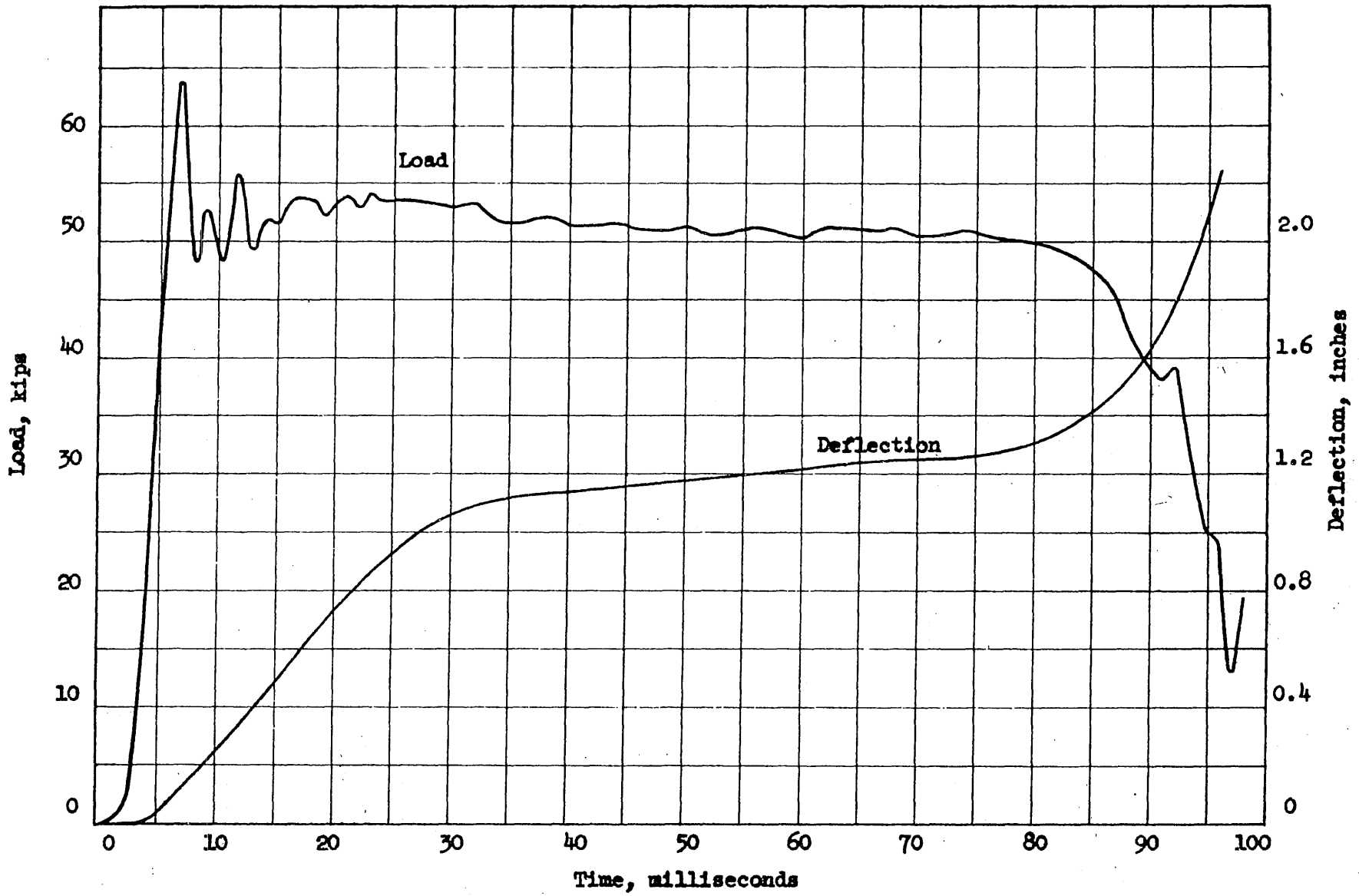

FIG. B.25 LOAD AND DEFLECTION VERSUS TIME FOR BEAM G34D-12

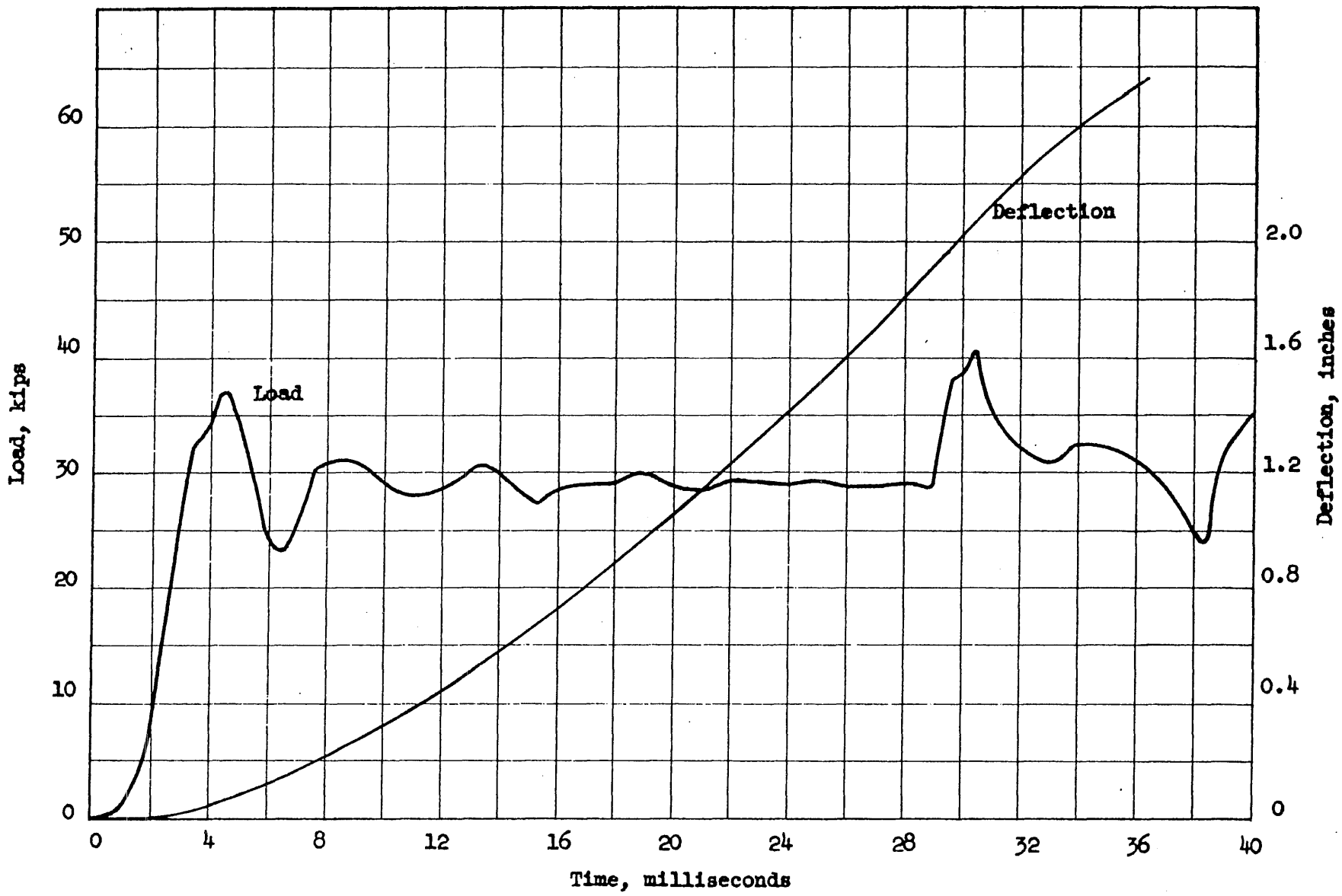

FIG. B.26 LOAD AND DEFLECTION VERSUS TIME FOR BEAM G34D-21

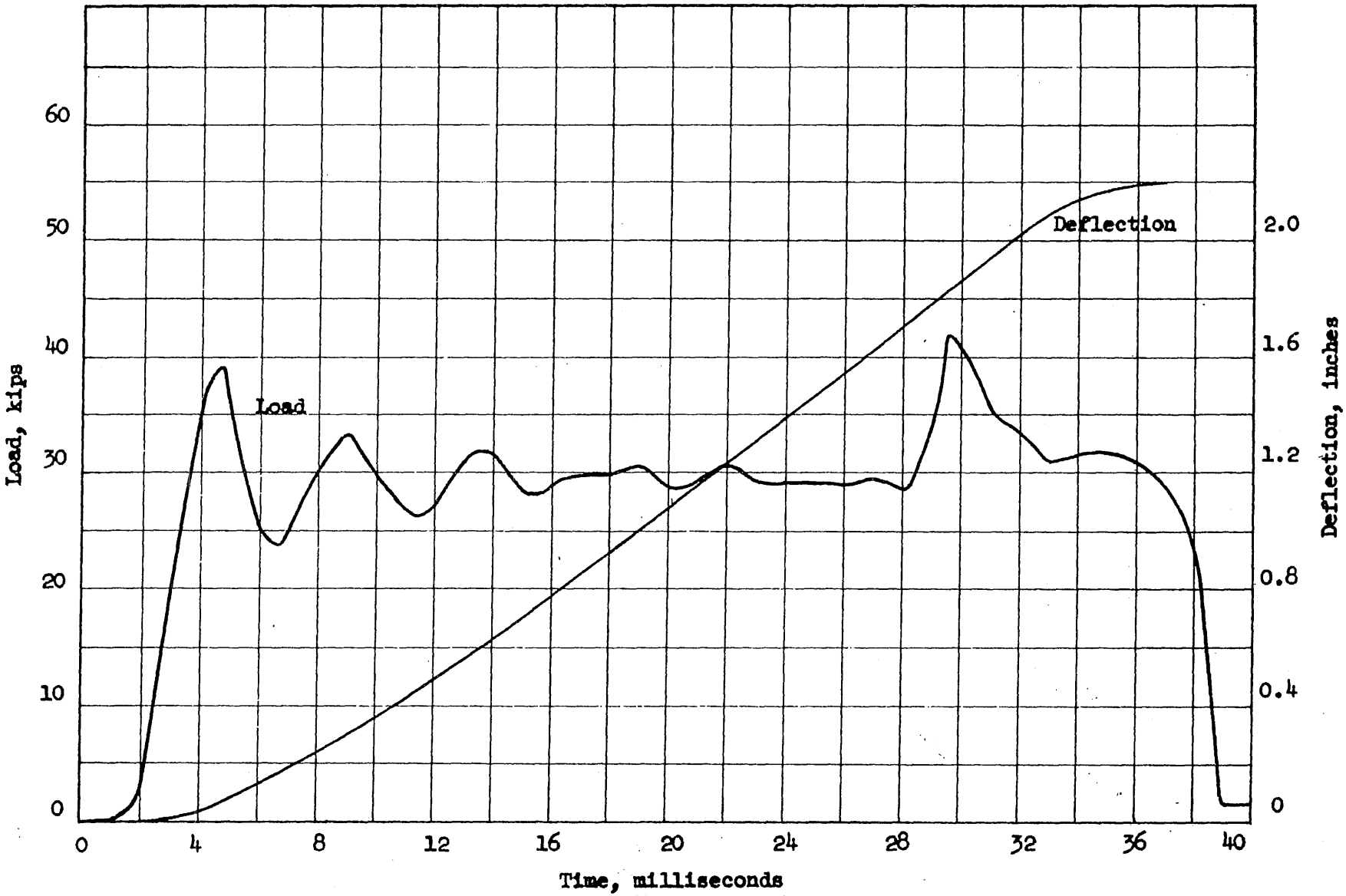

FIG. B.27 LOAD AND DEFLECTION VERSUS TIME FOR BEAM G34D-22

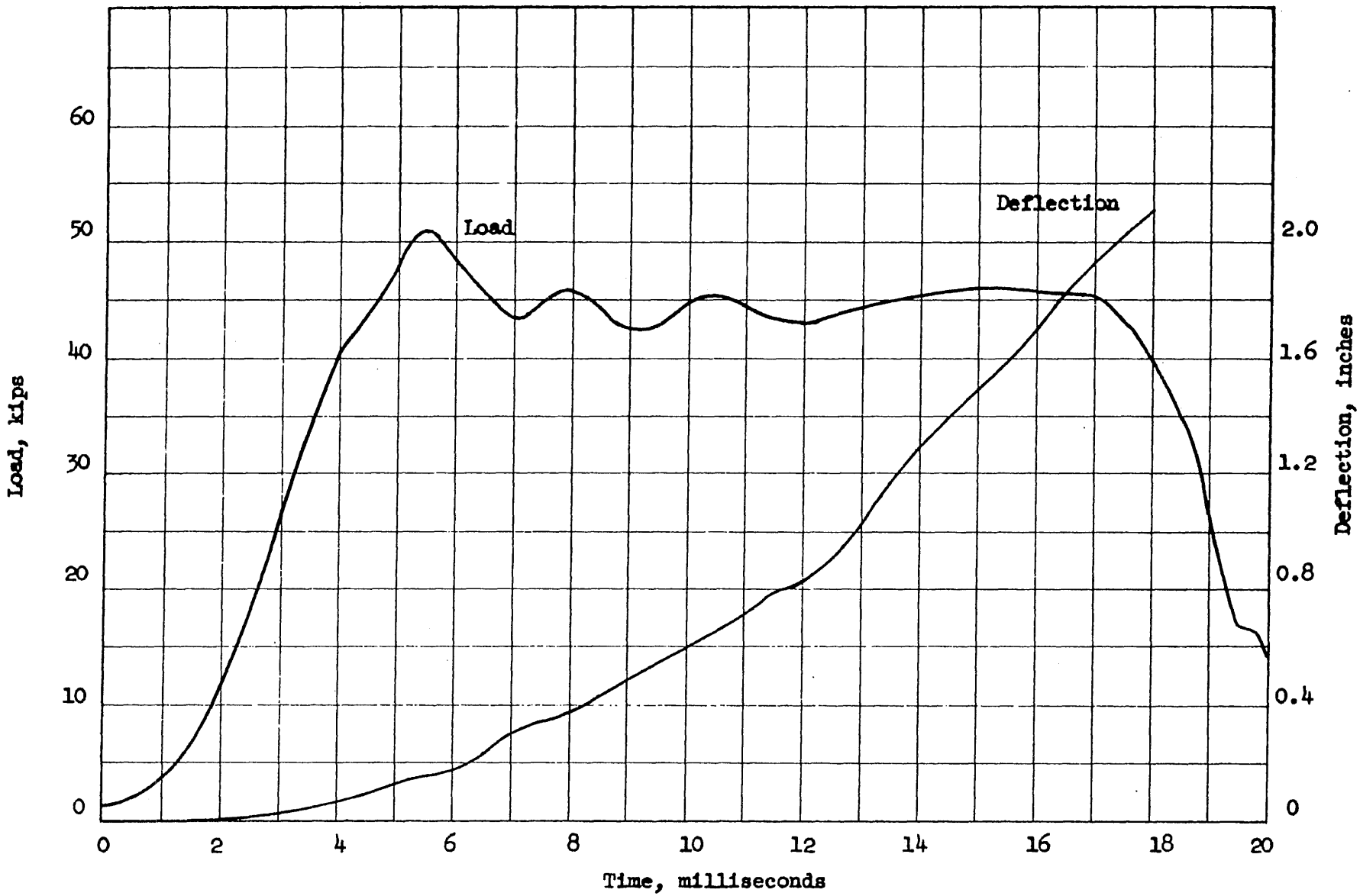

FIG. B.28 LOAD AND DEFLECTION VERSUS TIME FOR BEAM G43D-11

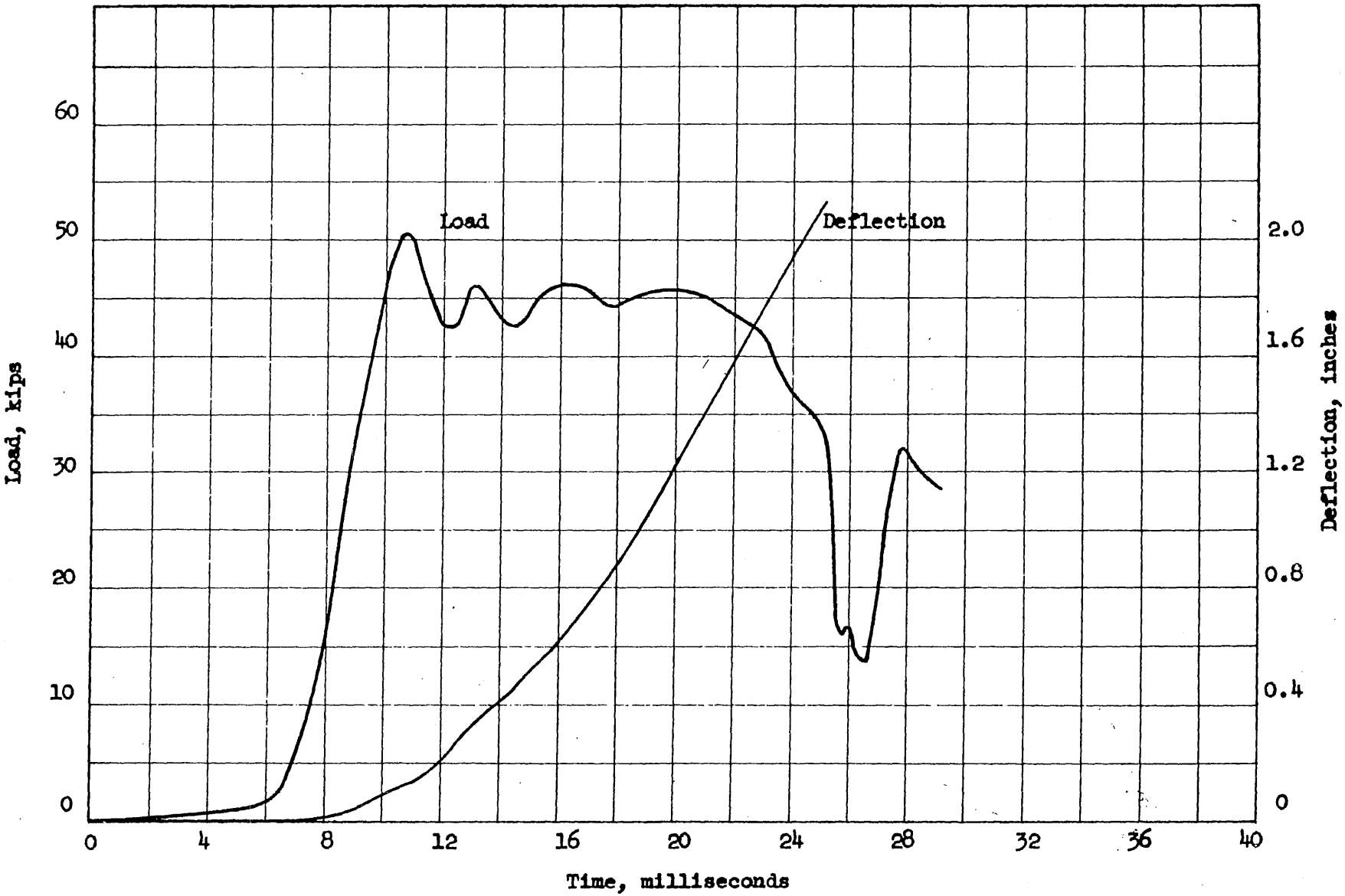

FIG. B.29 LOAD AND DEFLECTION VERSUS TIME FOR BEAM G43D-12

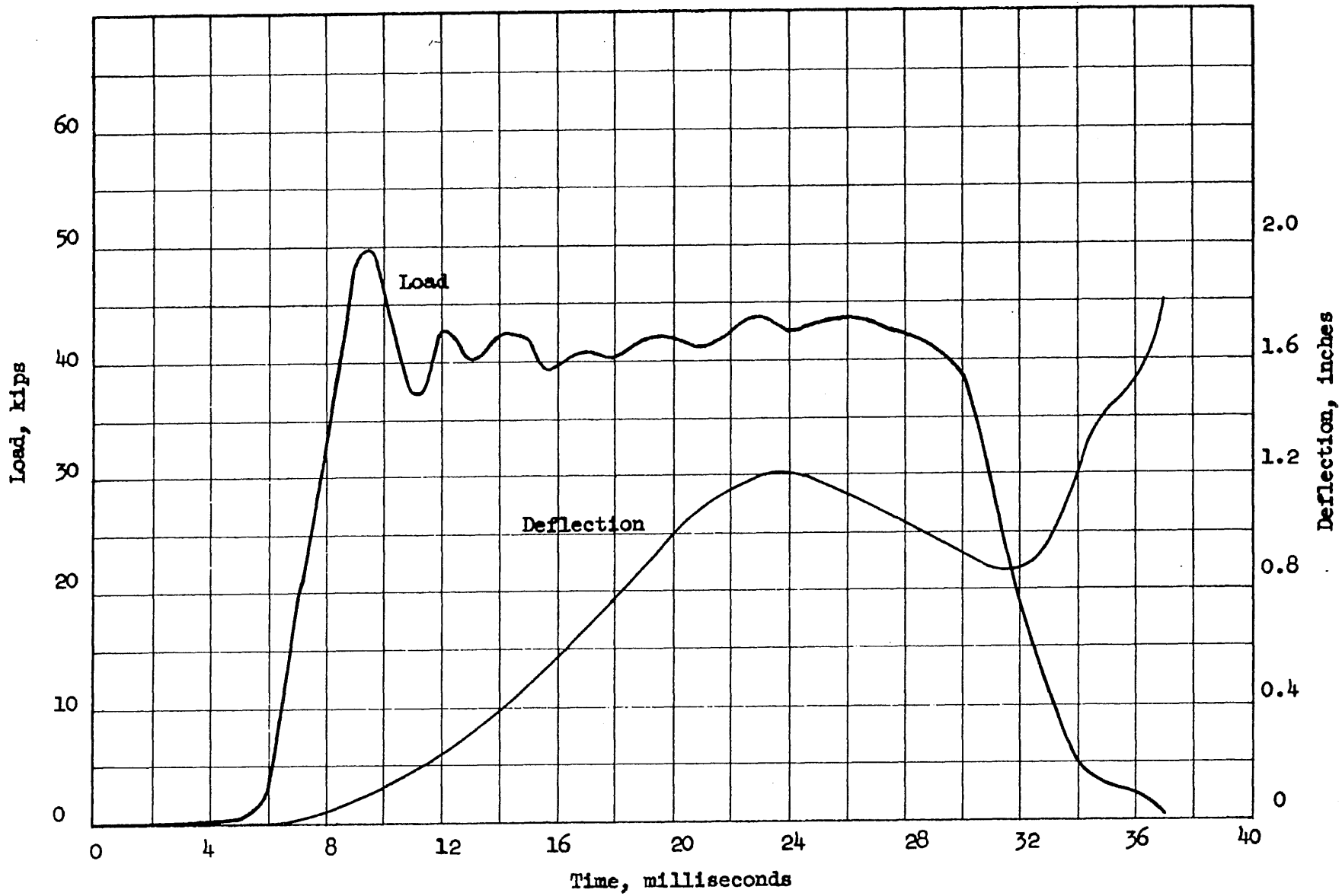

FIG. B.30 LOAD AND DEFLECTION VERSUS TIME FOR BEAM G44D-11

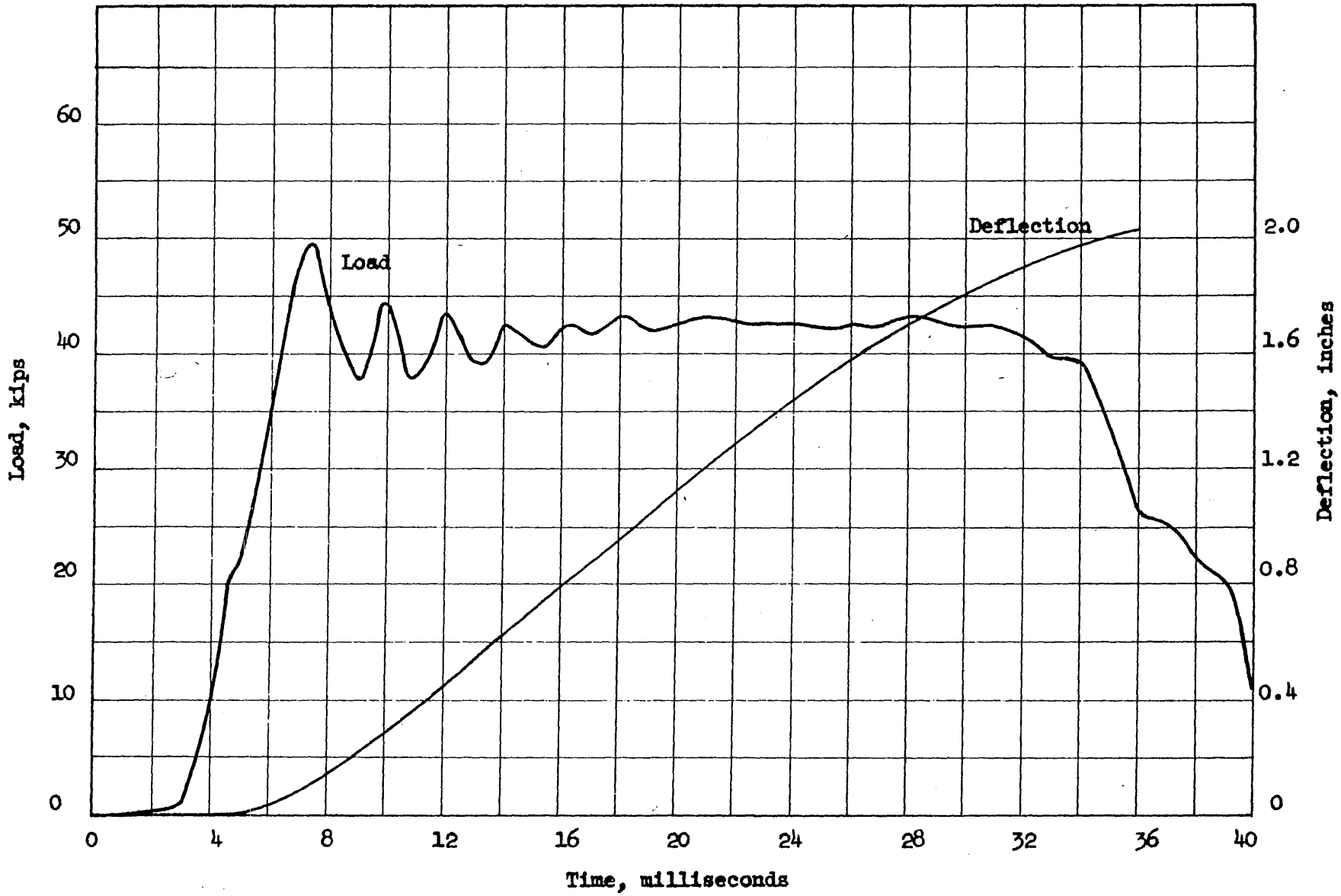

FIG. B.31 LOAD AND DEFLECTION VERSUS TIME FOR BEAM G44D-12

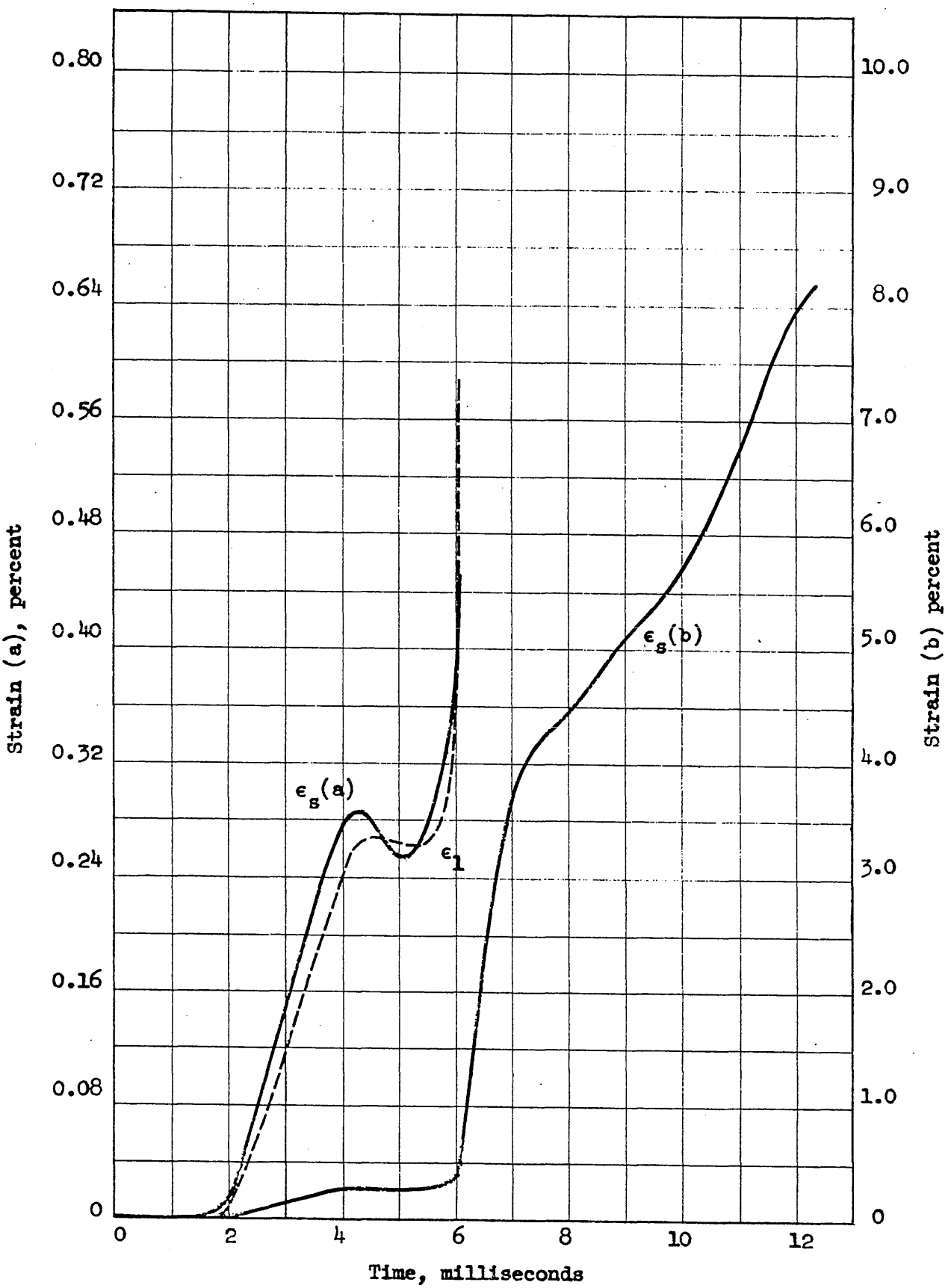

FIG. B.32 STEEL STRAIN VERSUS TIME FOR BEAM G23D-11

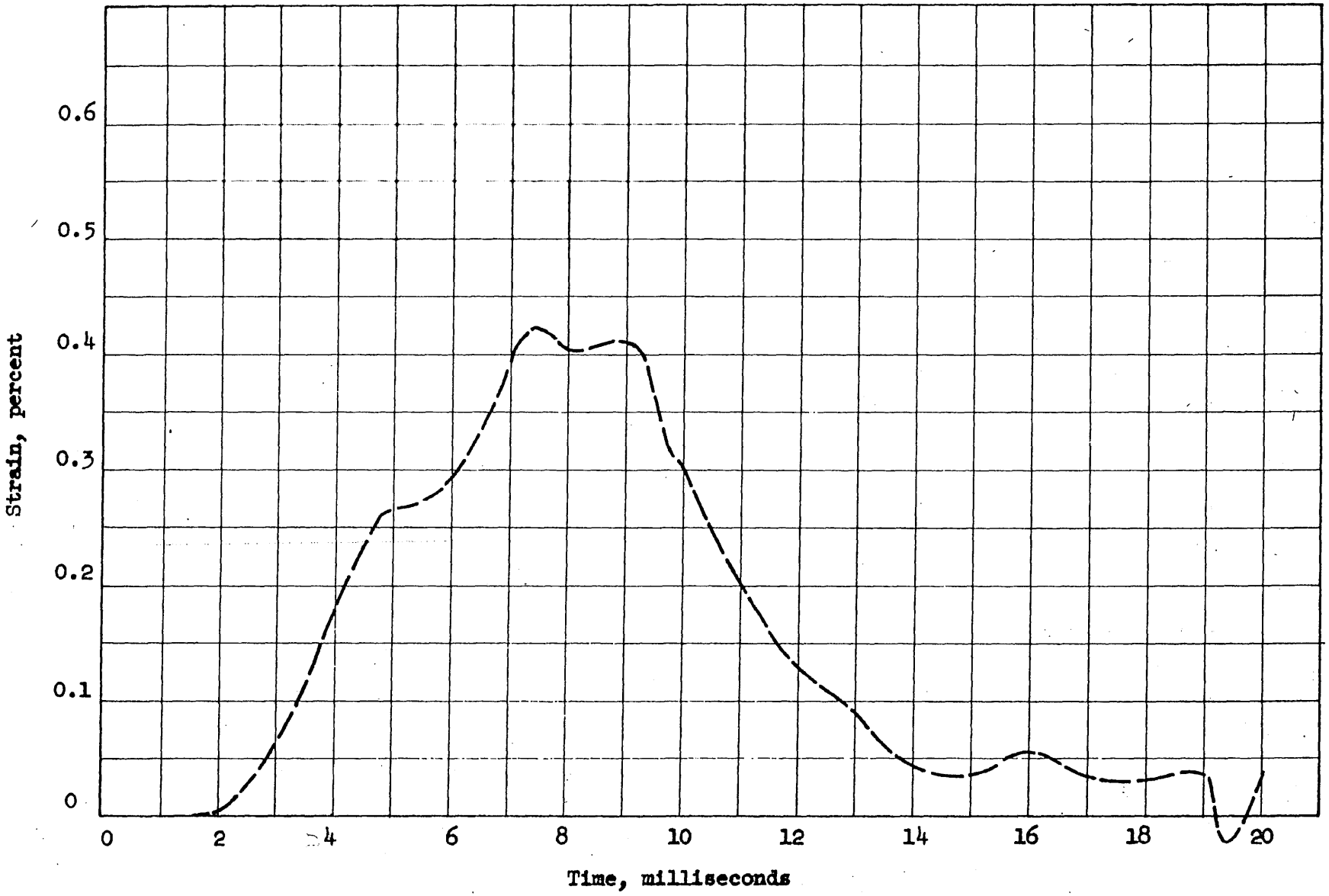

FIG. B.33 MIDSPAN CONCRETE STRAIN VERSUS TIME FOR BEAM G23D-11

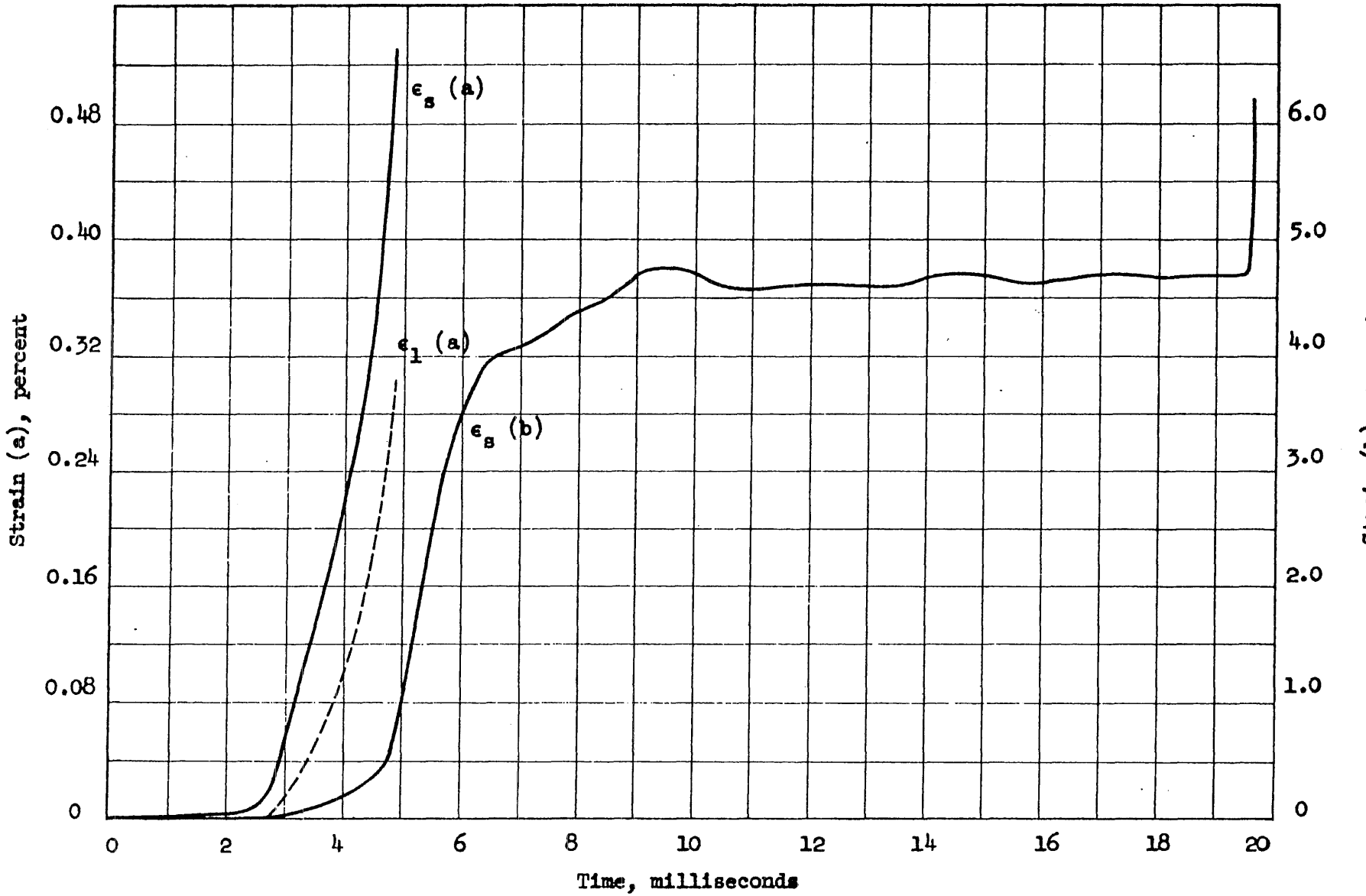

FIG. B.34 MIDSPAN STEEL STRAINS VERSUS TIME FOR BEAM G23D-12

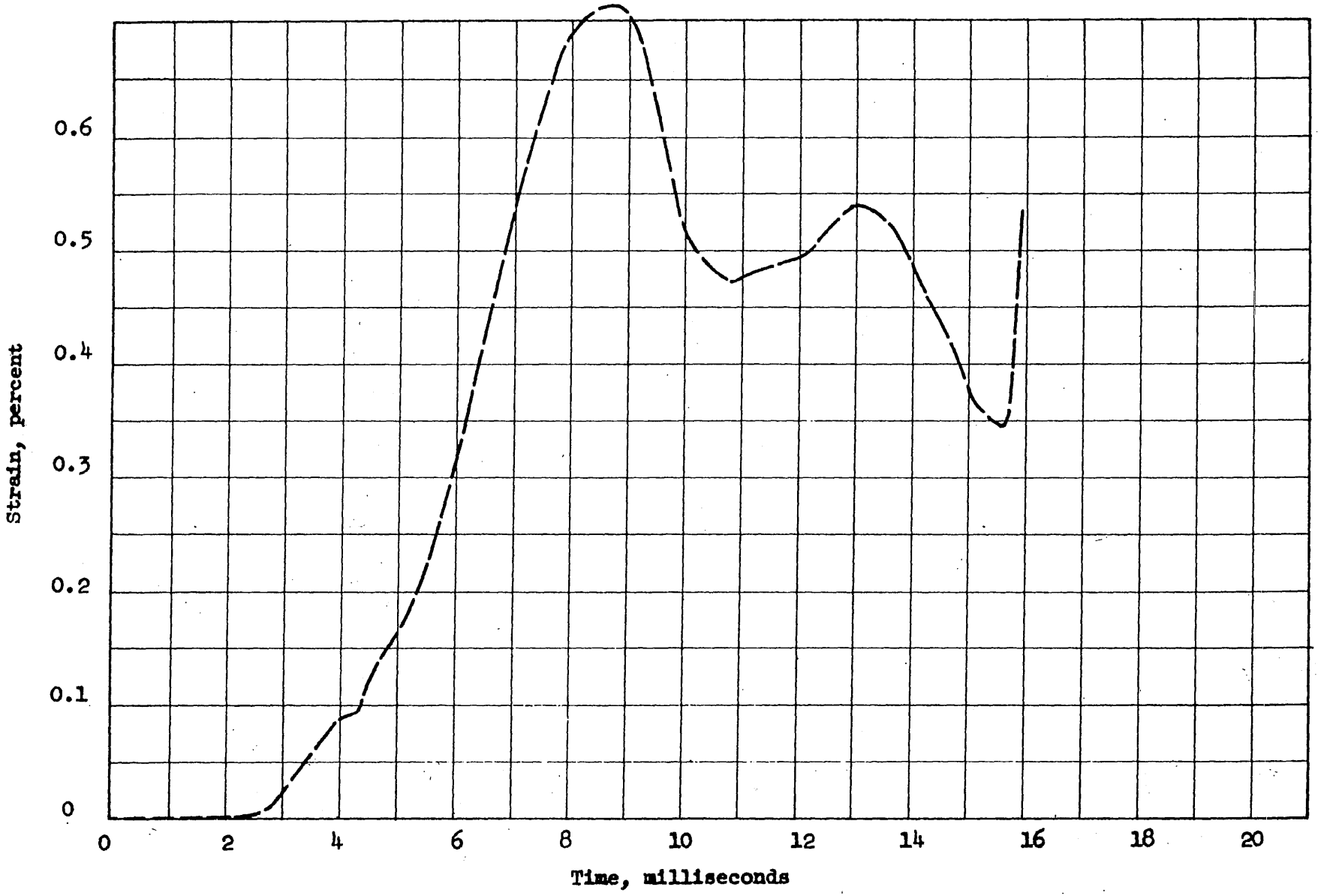

FIG. B.35 MIDSPAN CONCRETE STRAIN VERSUS TIME FOR BEAM G23D-12

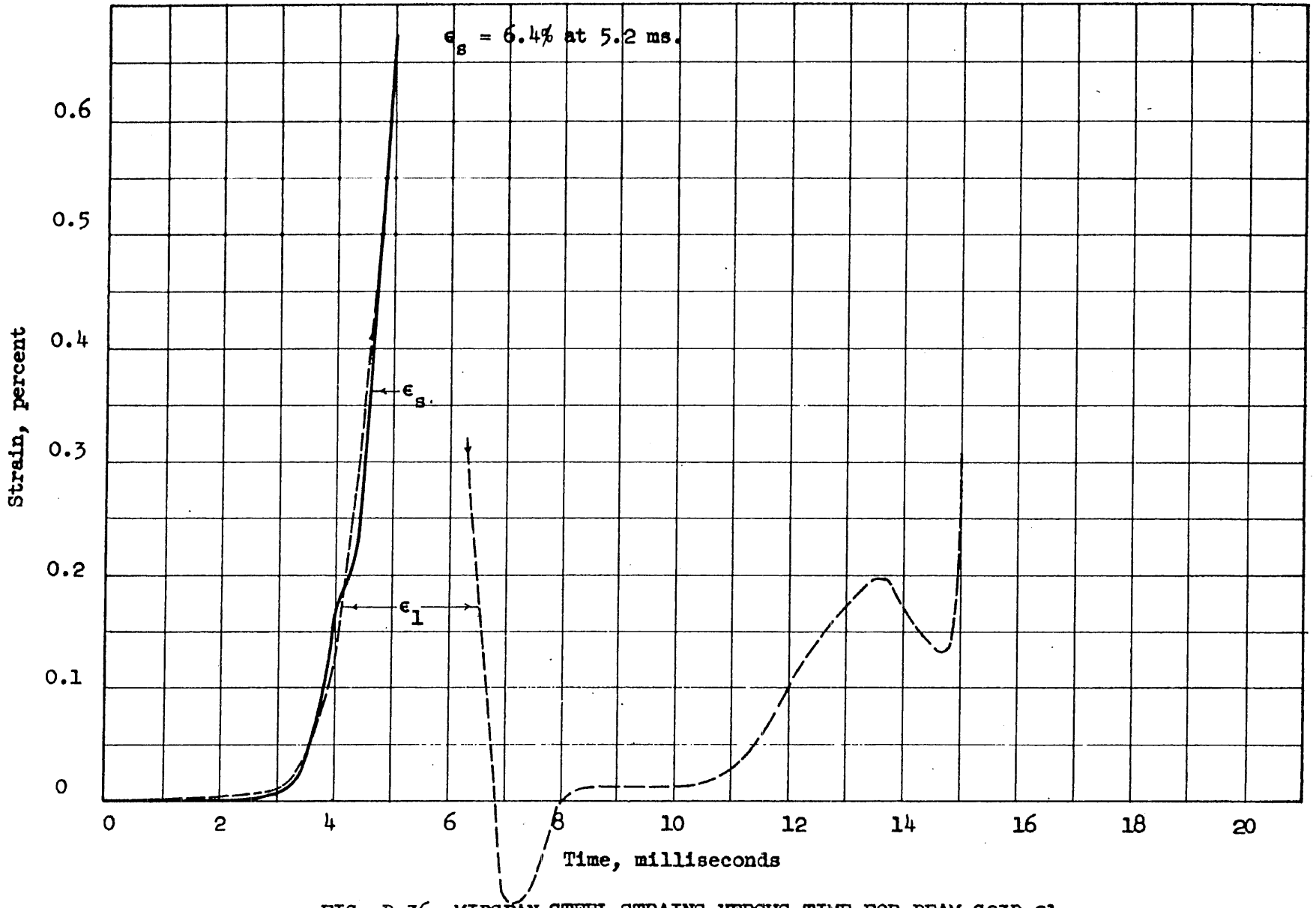

FIG. B.36 MIDSPAN STEEL STRAINS VERSUS TIME FOR BEAM G23D-21

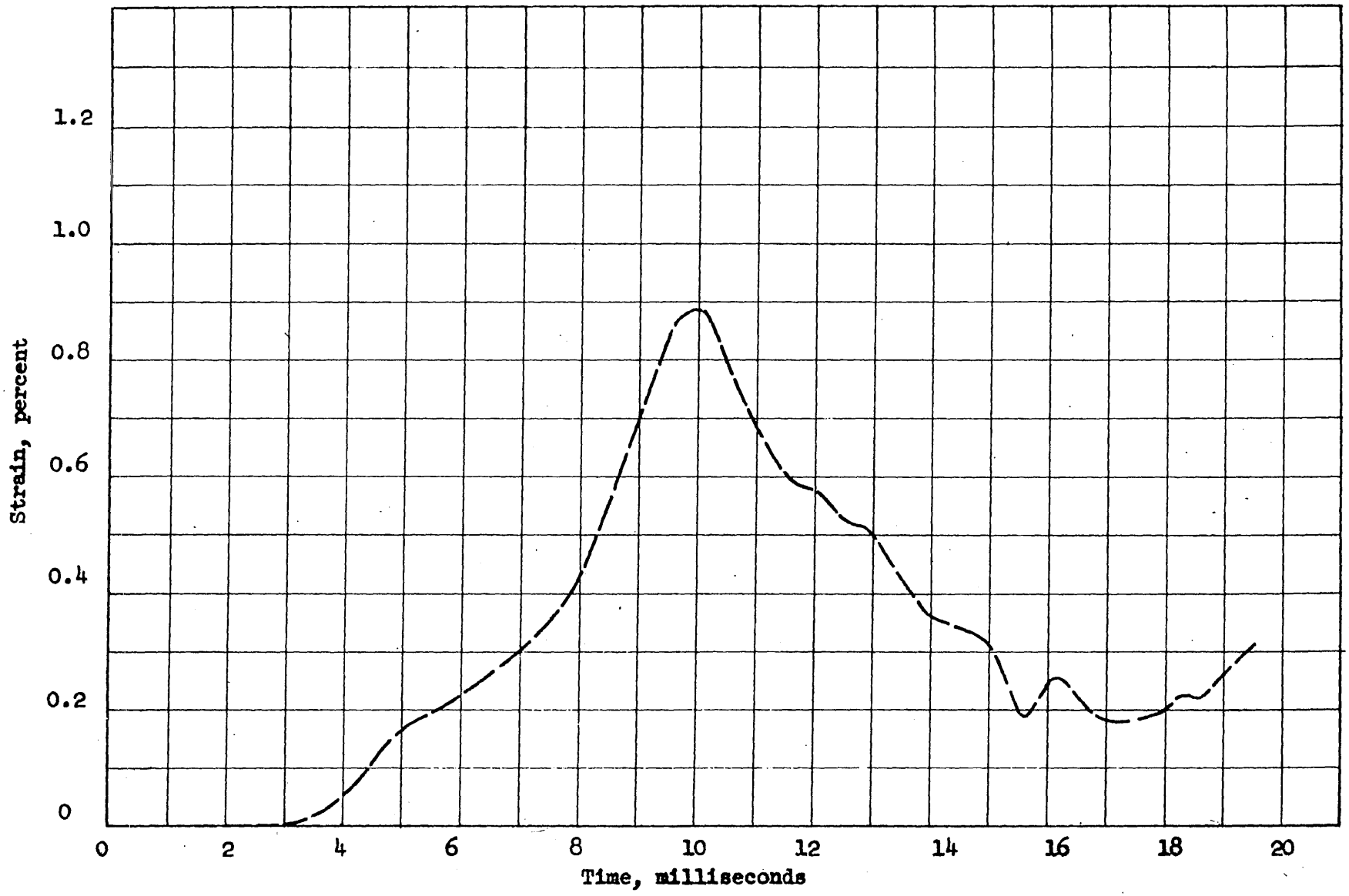

FIG. B.37 MIDSPAN CONCRETE STRAIN VERSUS TIME FOR BEAM G23D-21

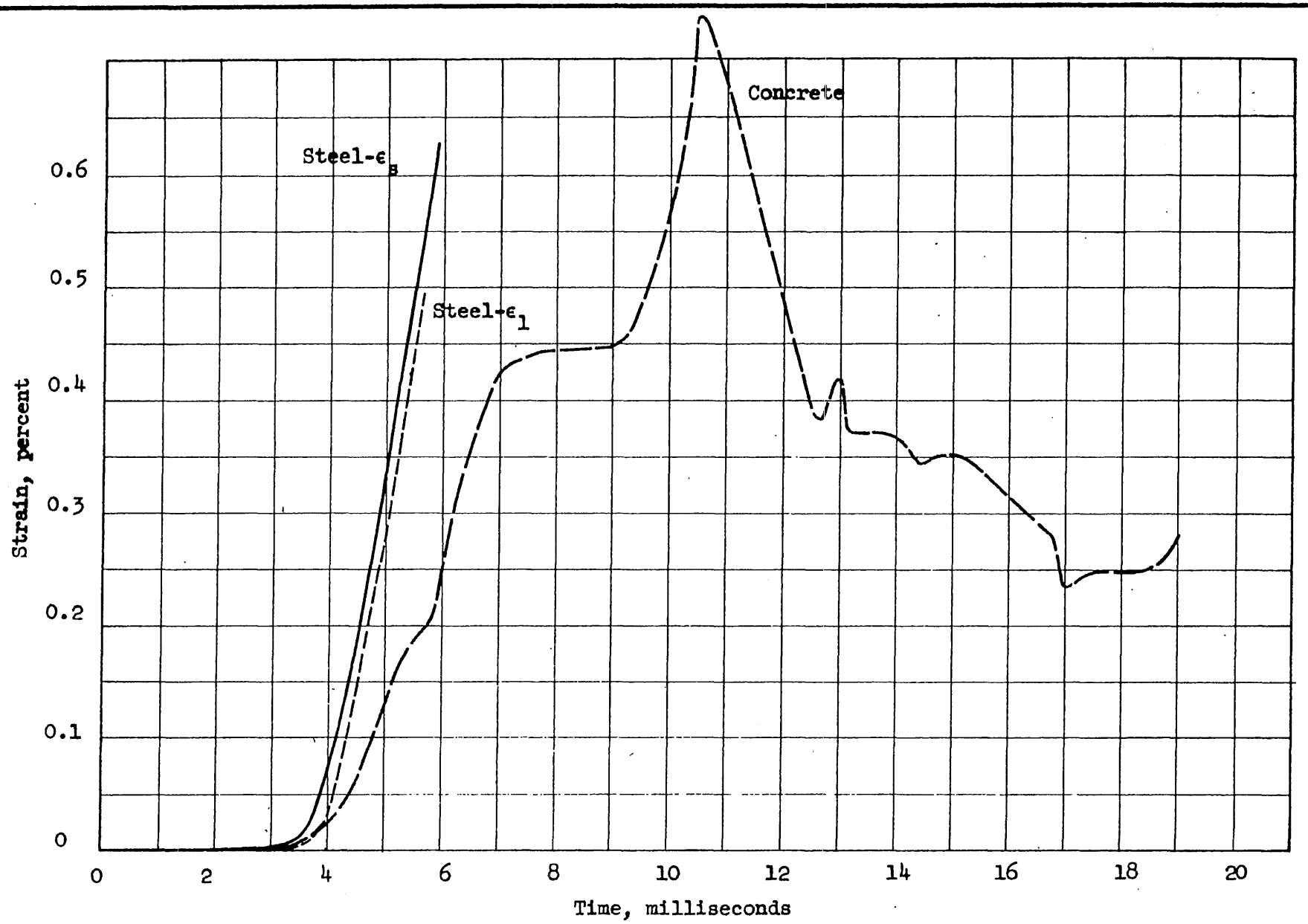

FIG. B.38 MIDSPAN STEEL AND CONCRETE STRAINS VERSUS TIME FOR BEAM G23D-22

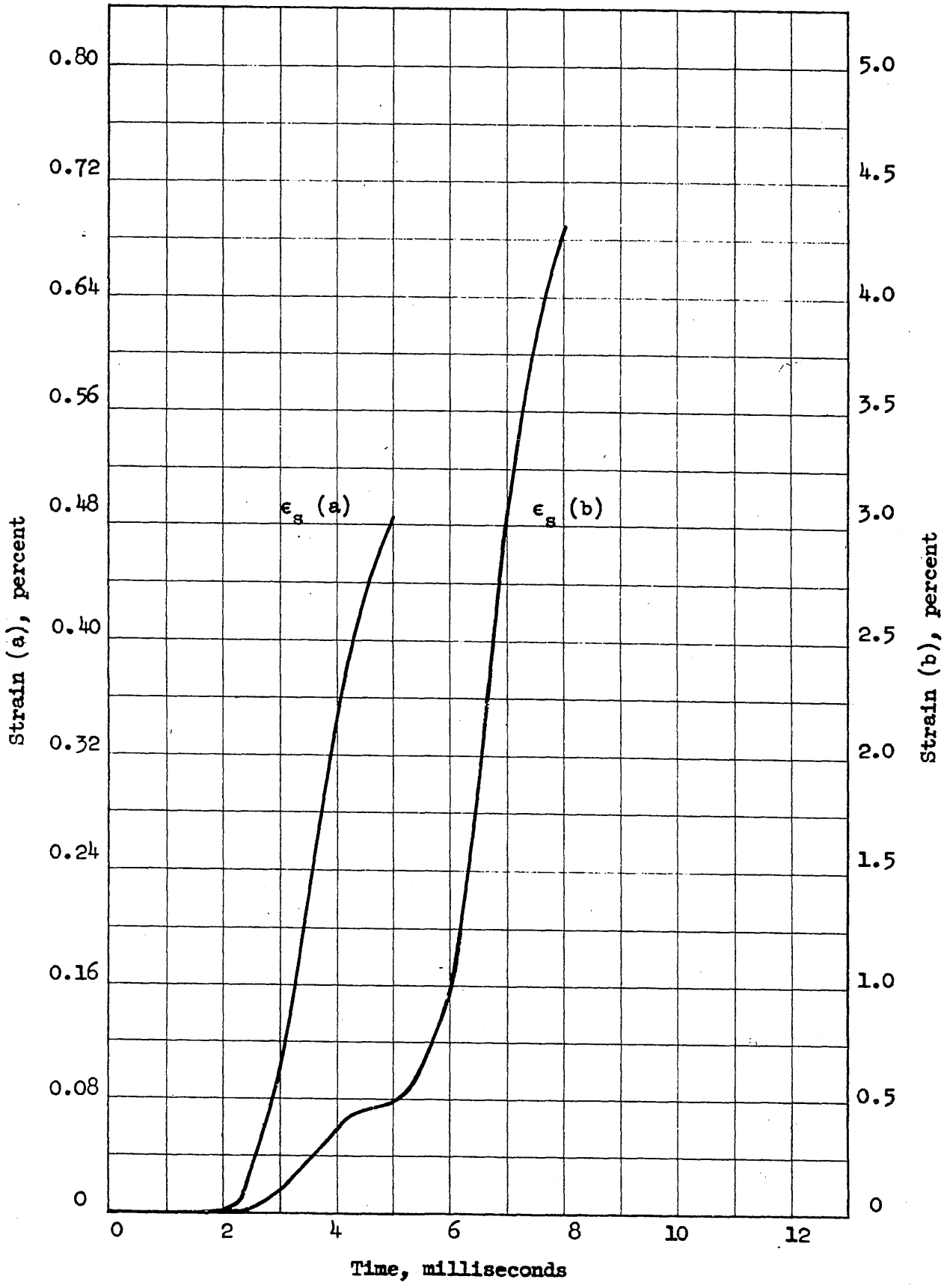

FIG. B.39 MIDSPAN STEEL STRAIN VERSUS TIME FOR BEAM G24D-11

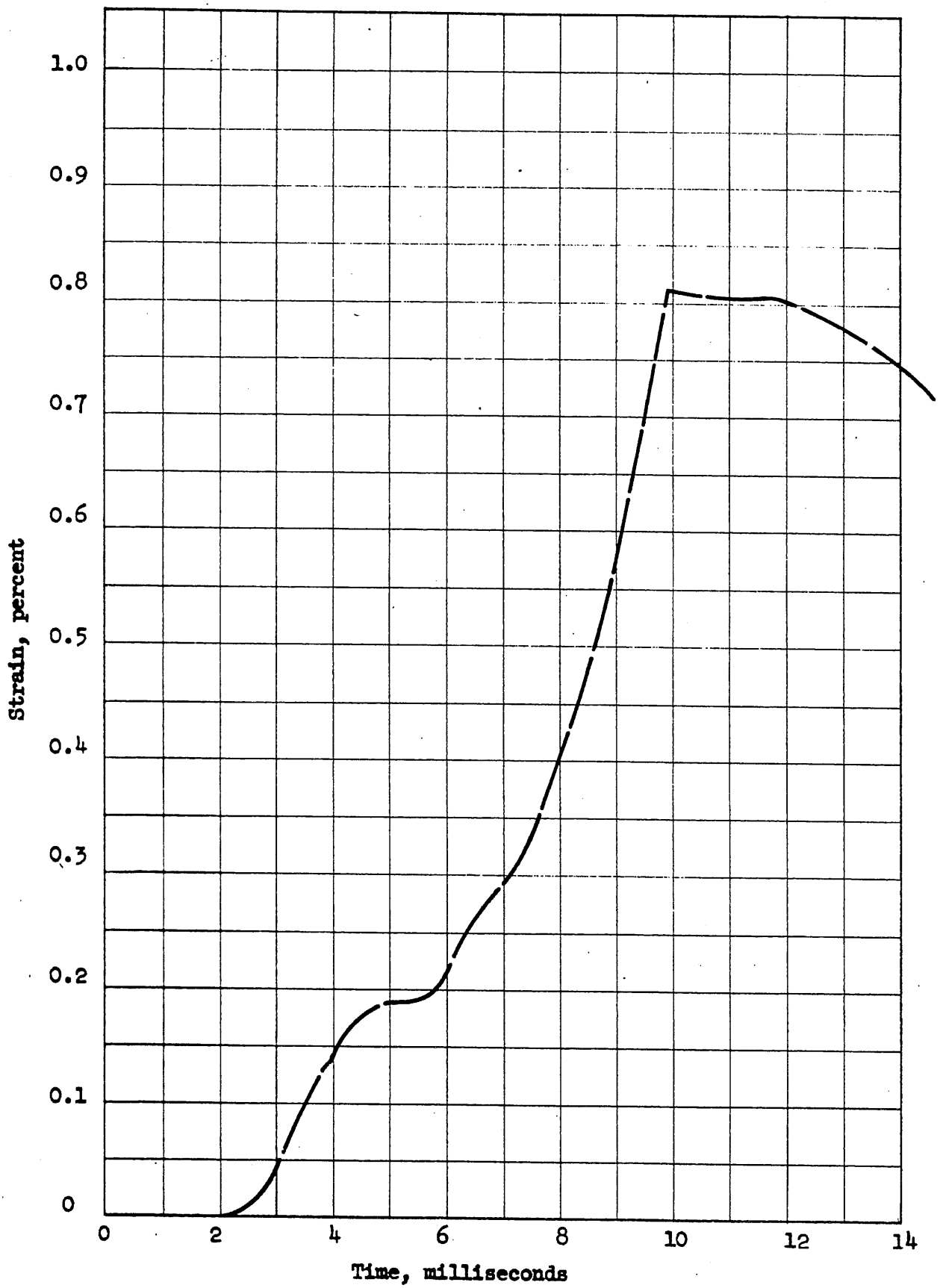

FIG. B.40 MIDSPAN CONCRETE STRAIN VERSUS TIME FOR BEAM G24D-11

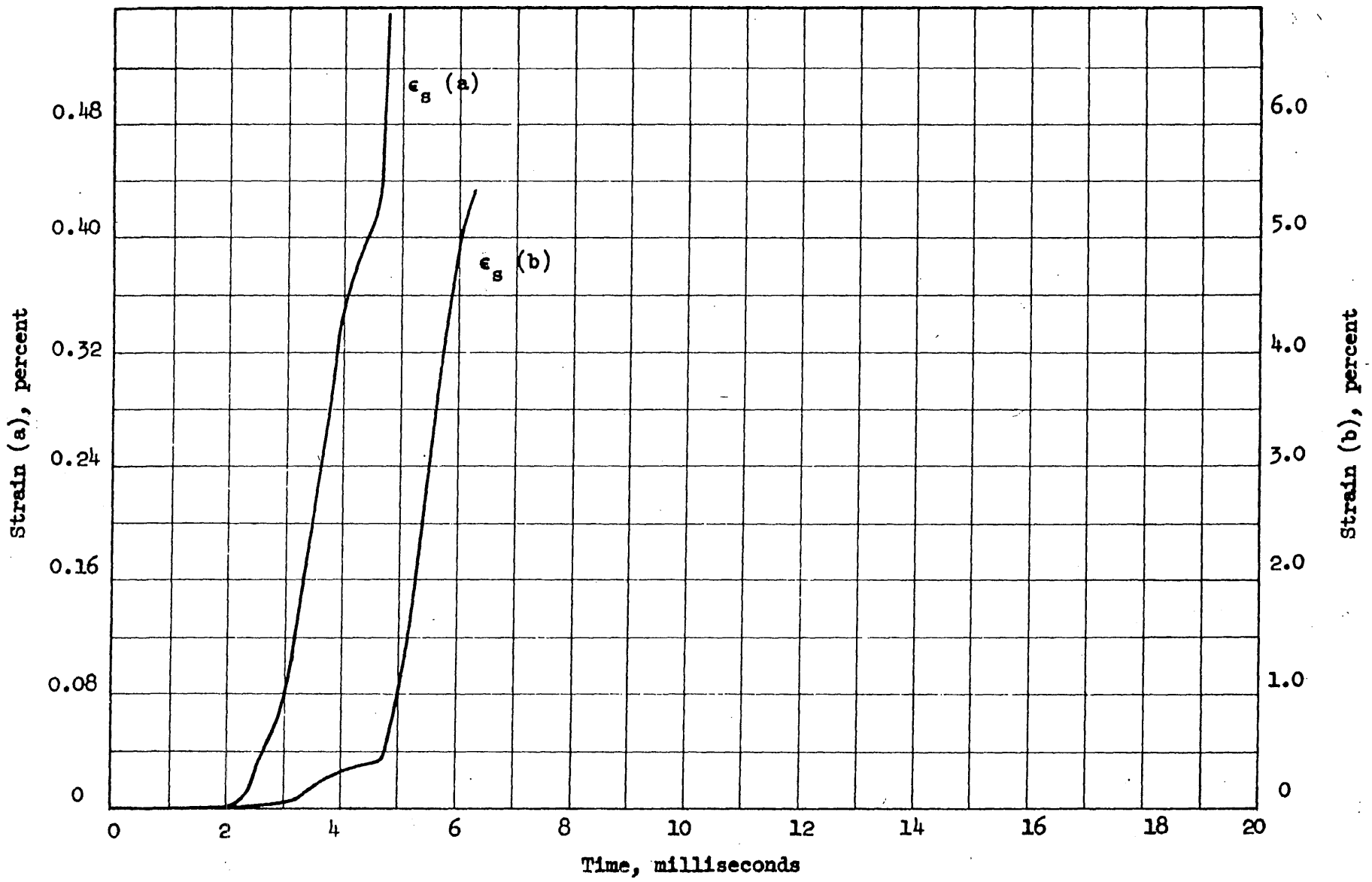

FIG. B.41 MIDSPAN STEEL STRAIN VERSUS TIME FOR BEAM G24D-12

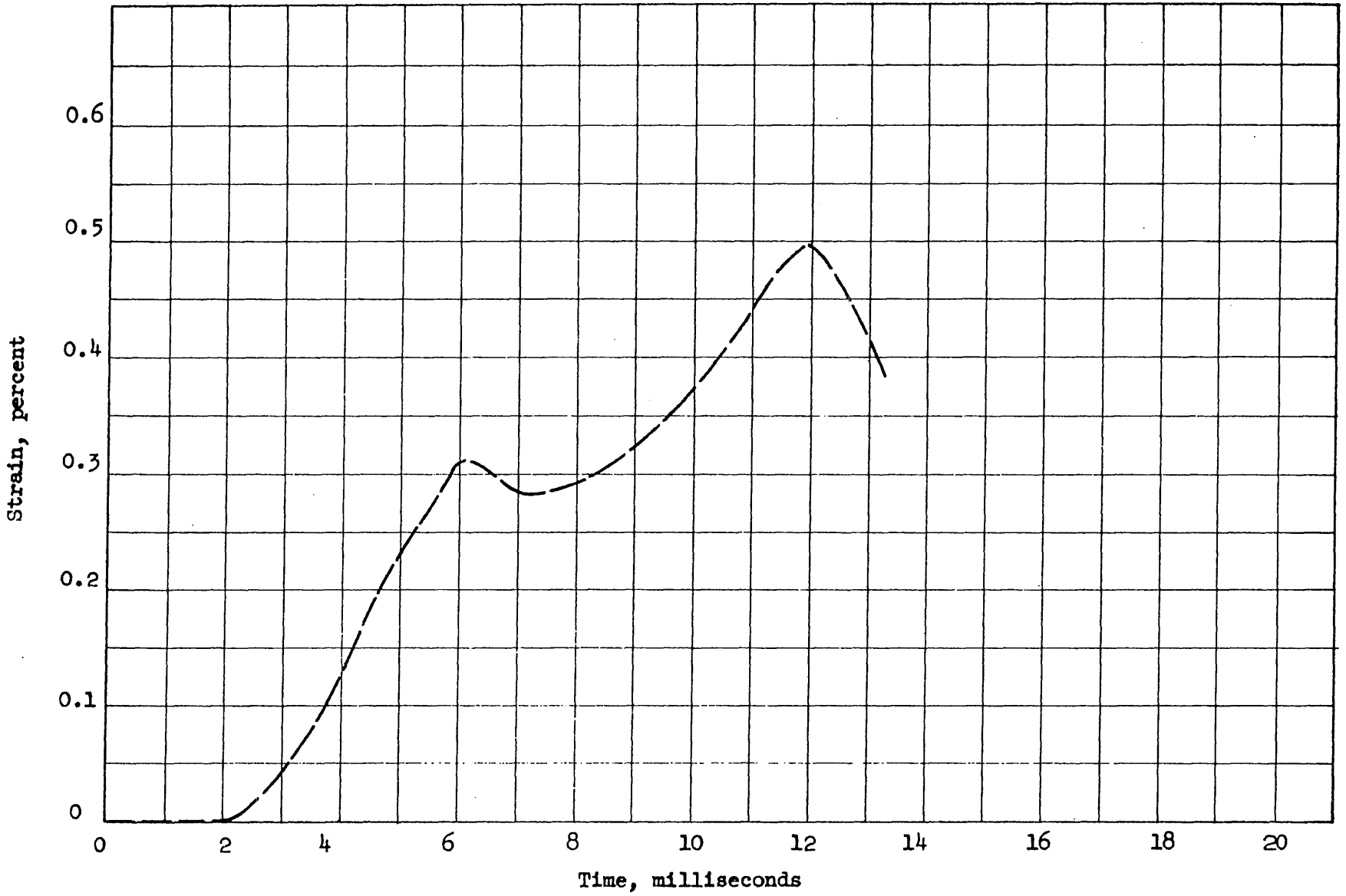

FIG. B.42 MIDSPAN CONCRETE STRAIN VERSUS TIME FOR BEAM G24D-12

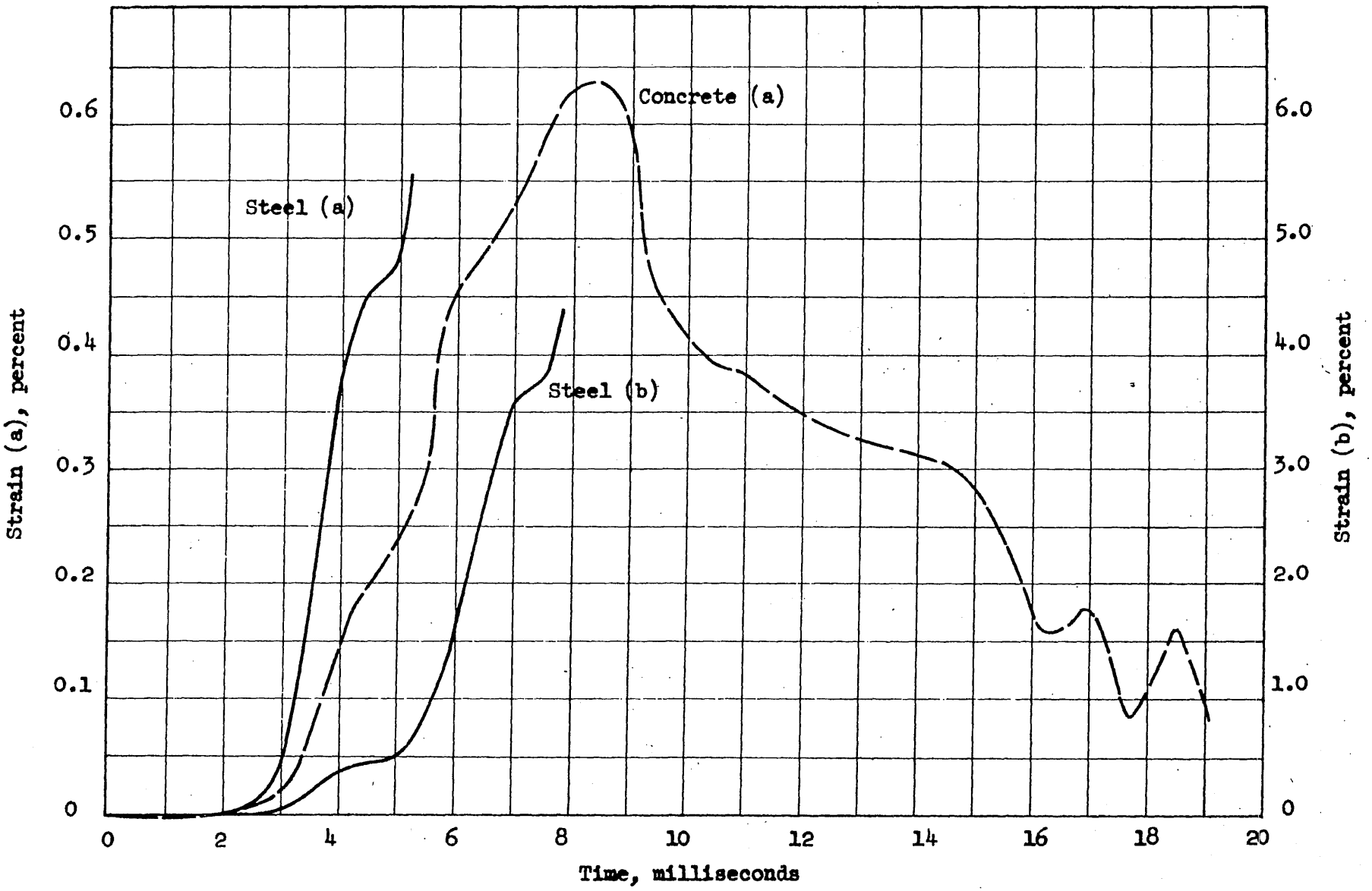

FIG. B.43 MIDSPAN STEEL AND CONCRETE STRAINS VERSUS TIME FOR BEAM G24D-21

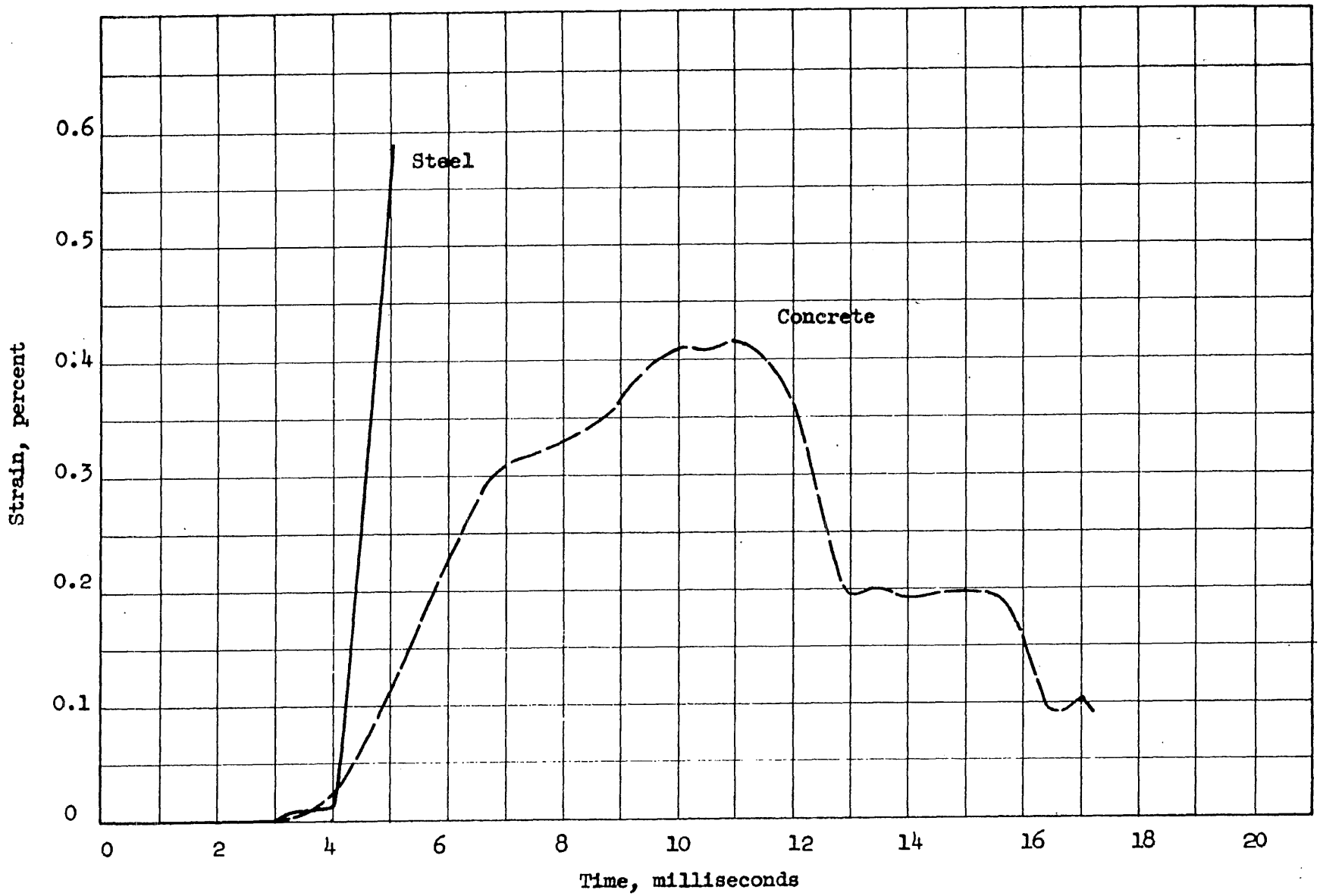

FIG. B.44 MIDSPAN STEEL AND CONCRETE STRAINS VERSUS TIME FOR BEAM G24D-22

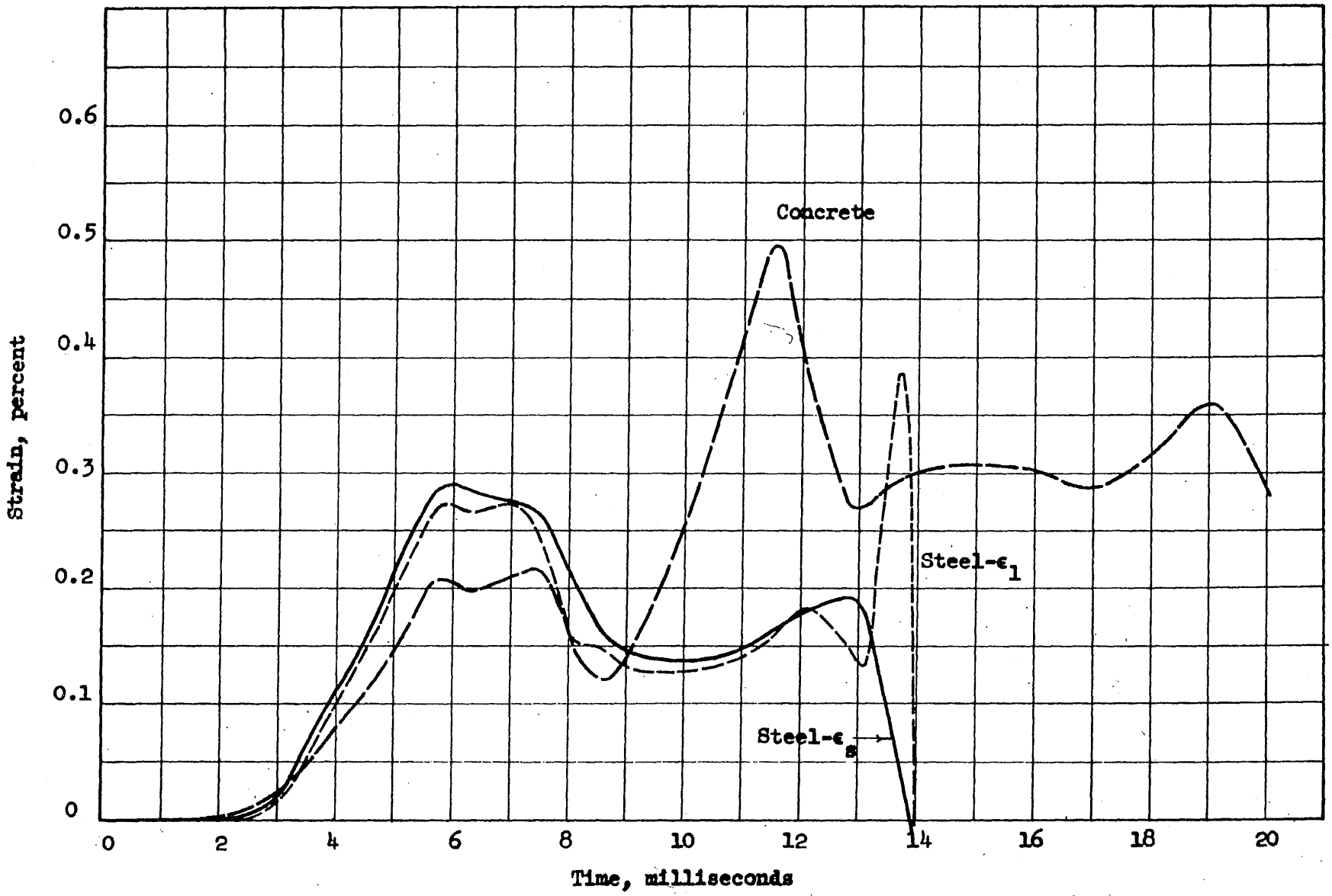

FIG. B.45 MIDSPAN STEEL AND CONCRETE STRAINS VERSUS TIME FOR BEAM G33D-11

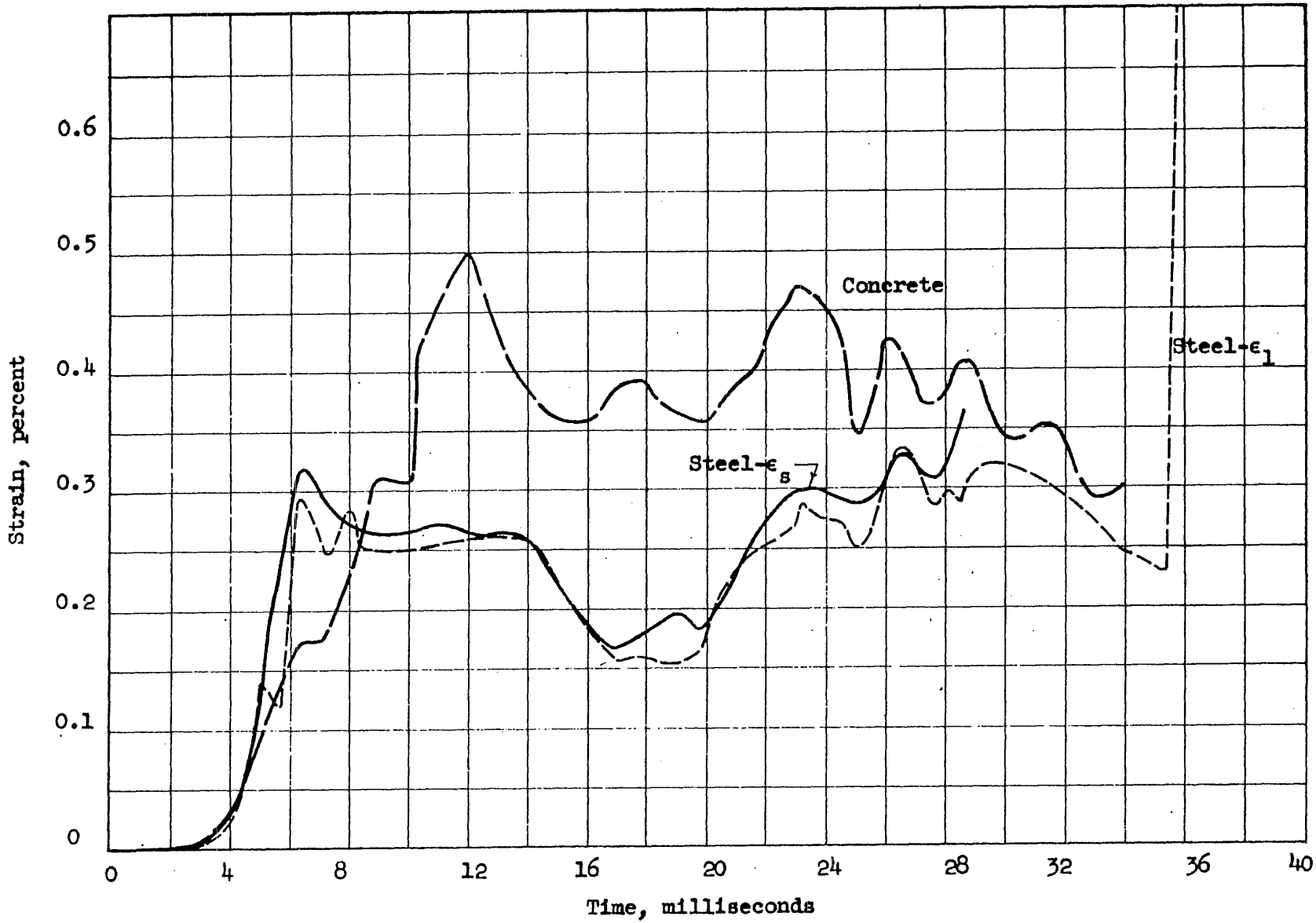

FIG. B.46 MIDSPAN STEEL AND CONCRETE STRAINS VERSUS TIME FOR BEAM G33D-12

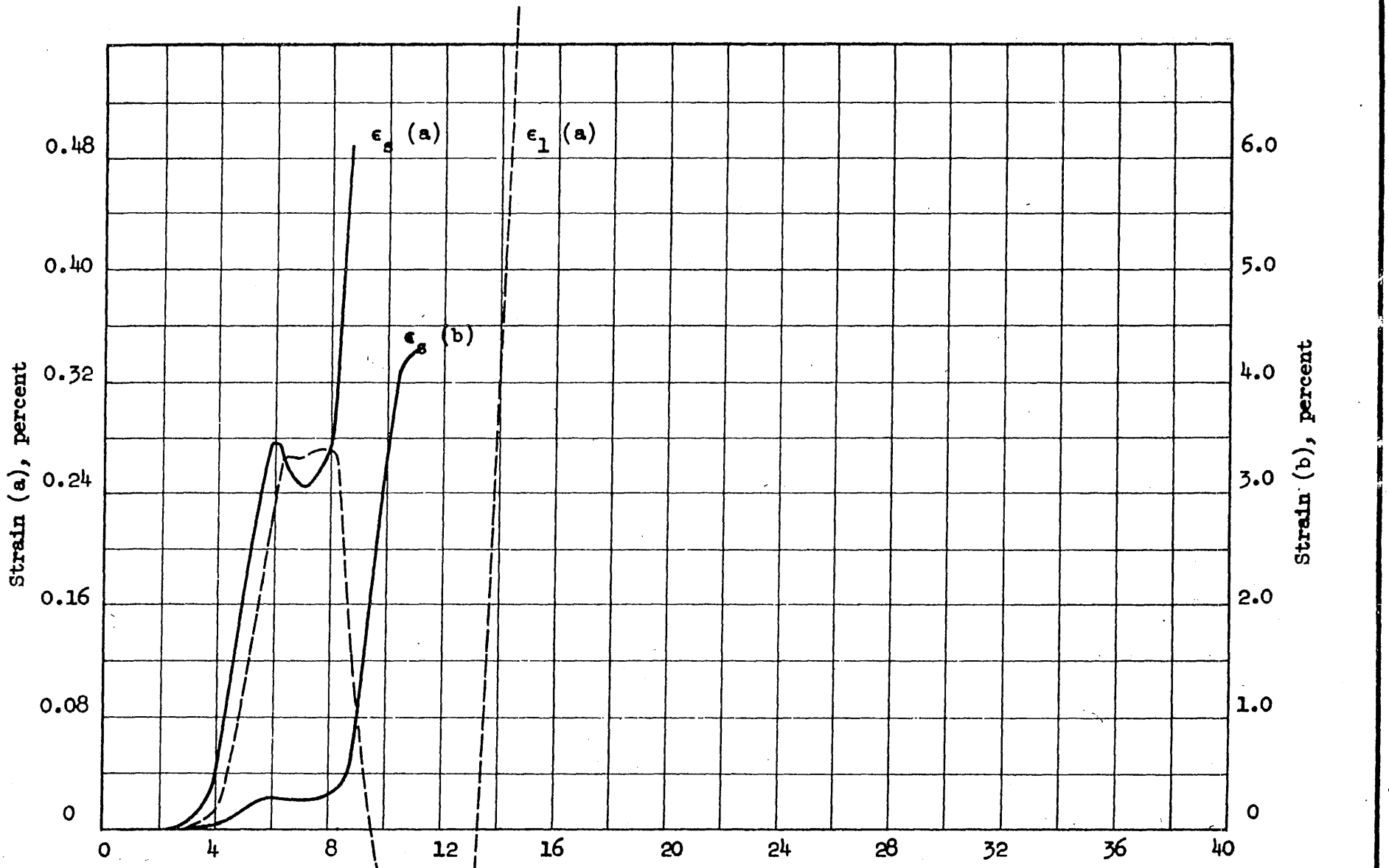

FIG. B.47 MIDSPAN STEEL STRAINS VERSUS TIME FOR BEAM G33D-21

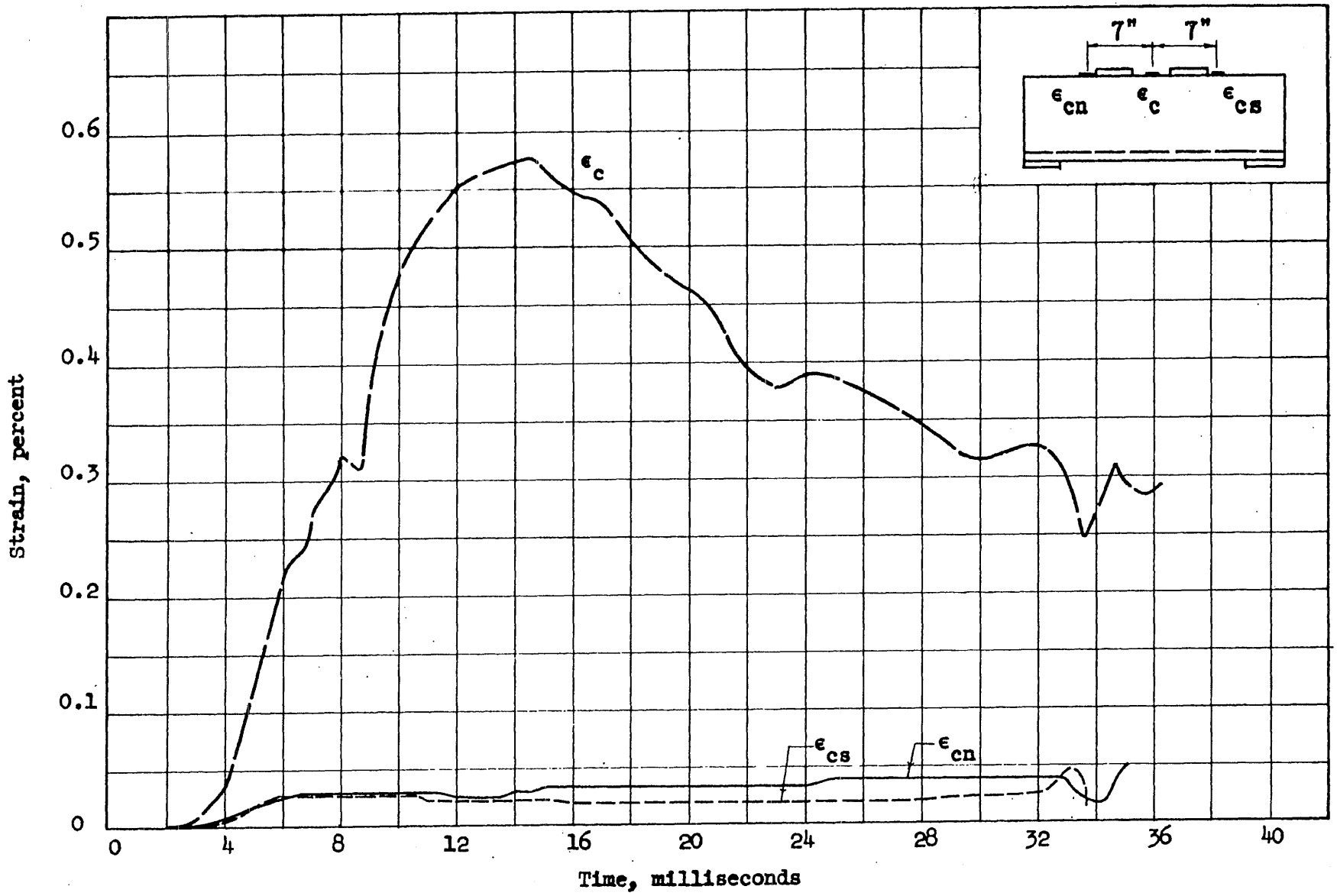

FIG. B.48 CONCRETE STRAINS VERSUS TIME FOR BEAM G33D-21

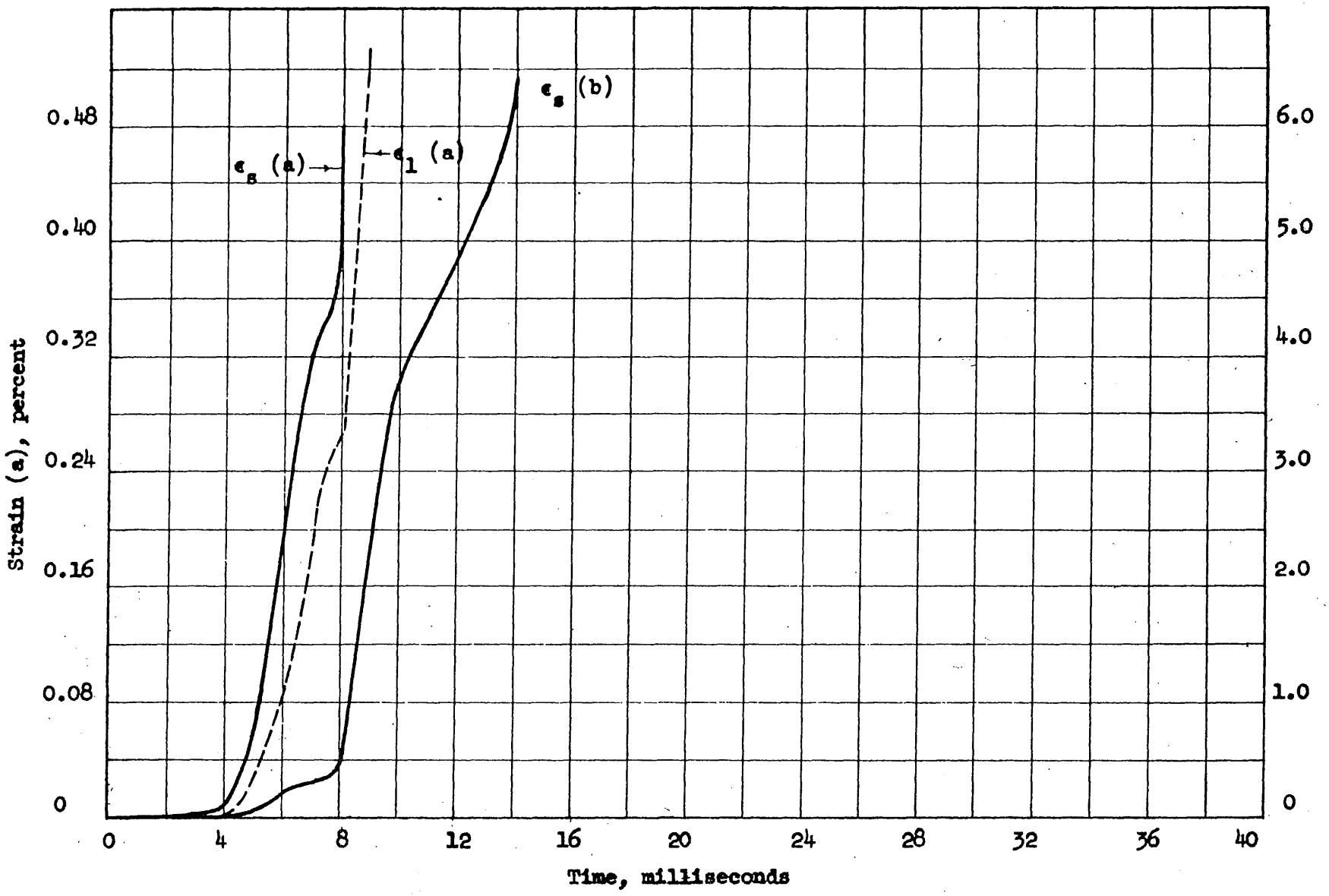

FIG. B.49 MIDSPAN STEEL STRAINS VERSUS TIME FOR BEAM G33D-22

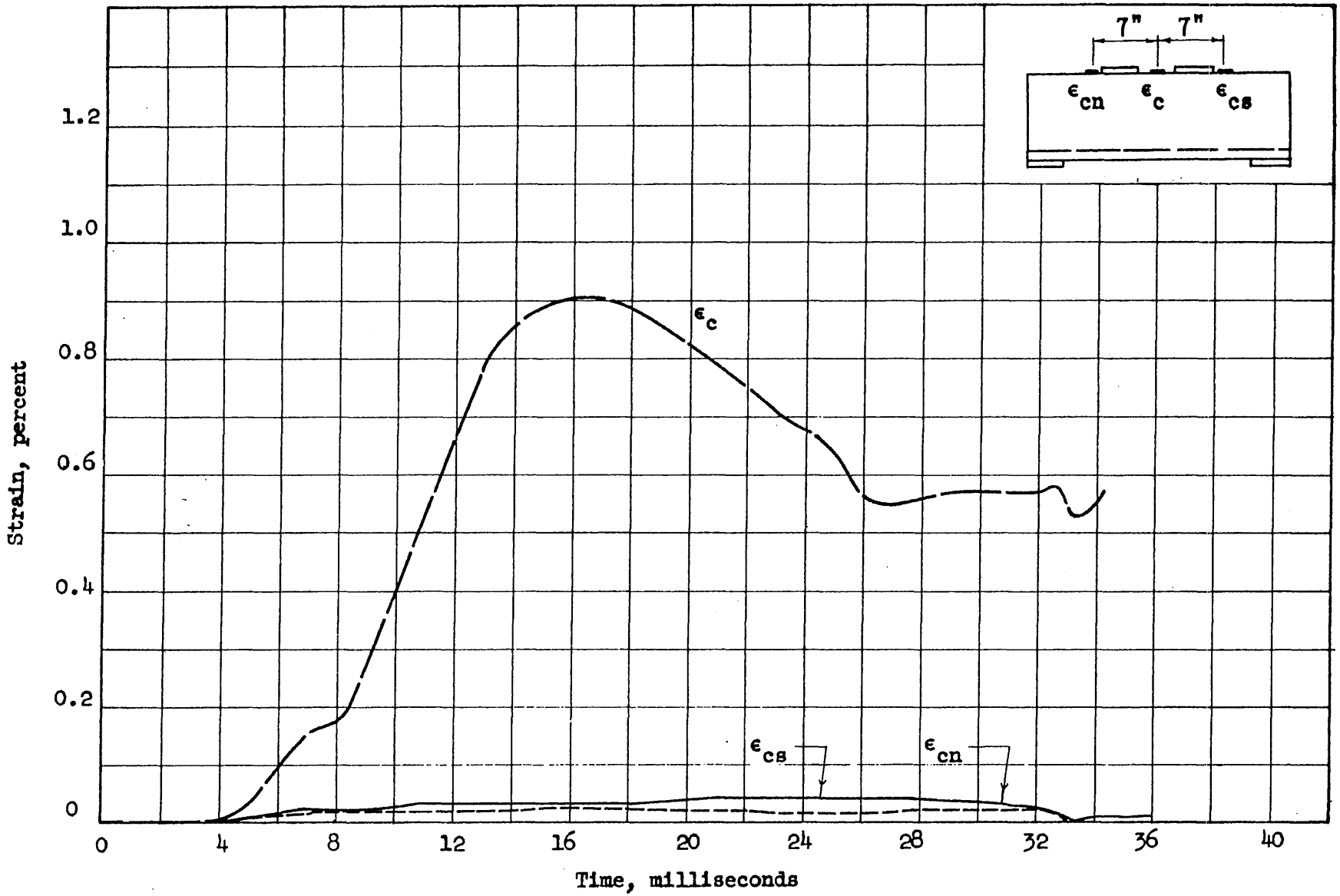

FIG. B.50 CONCRETE STRAINS VERSUS TIME FOR BEAM G33D-22

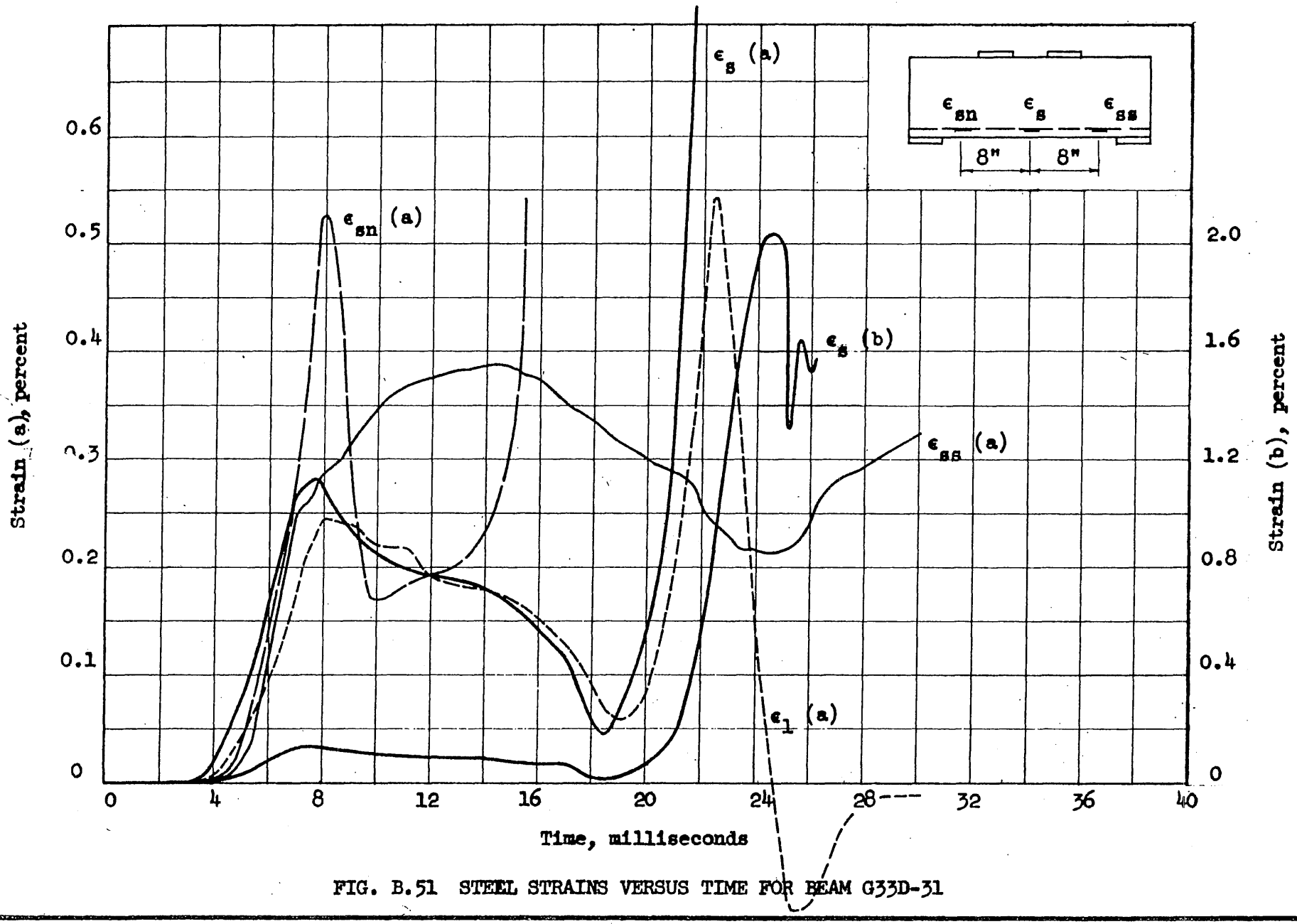

FIG. B.51 STEEL STRAINS VERSUS TIME FOR BEAM G33D-31

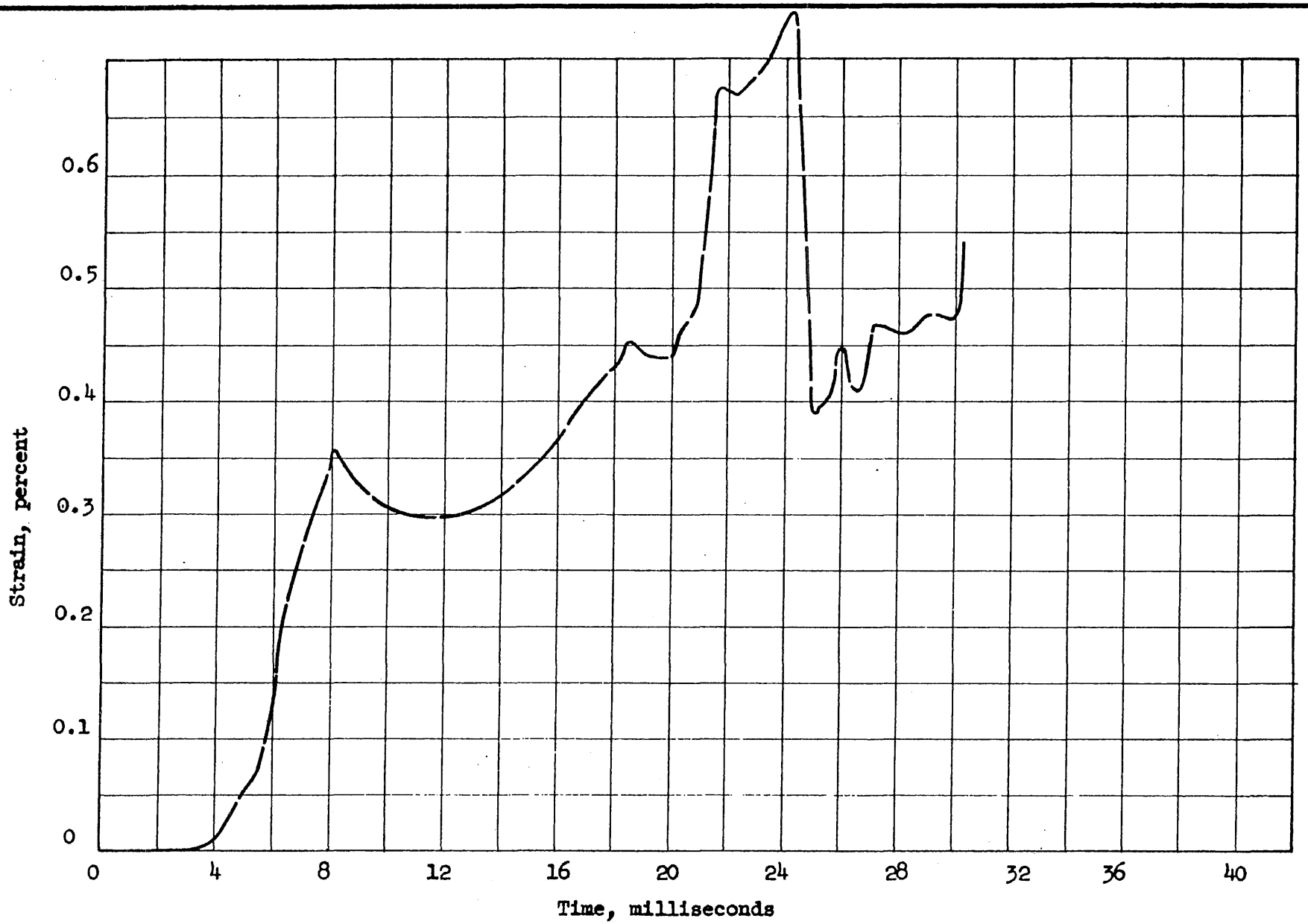

FIG. B.52 MIDSPAN CONCRETE STRAIN VERSUS TIME FOR BEAM G33D-31

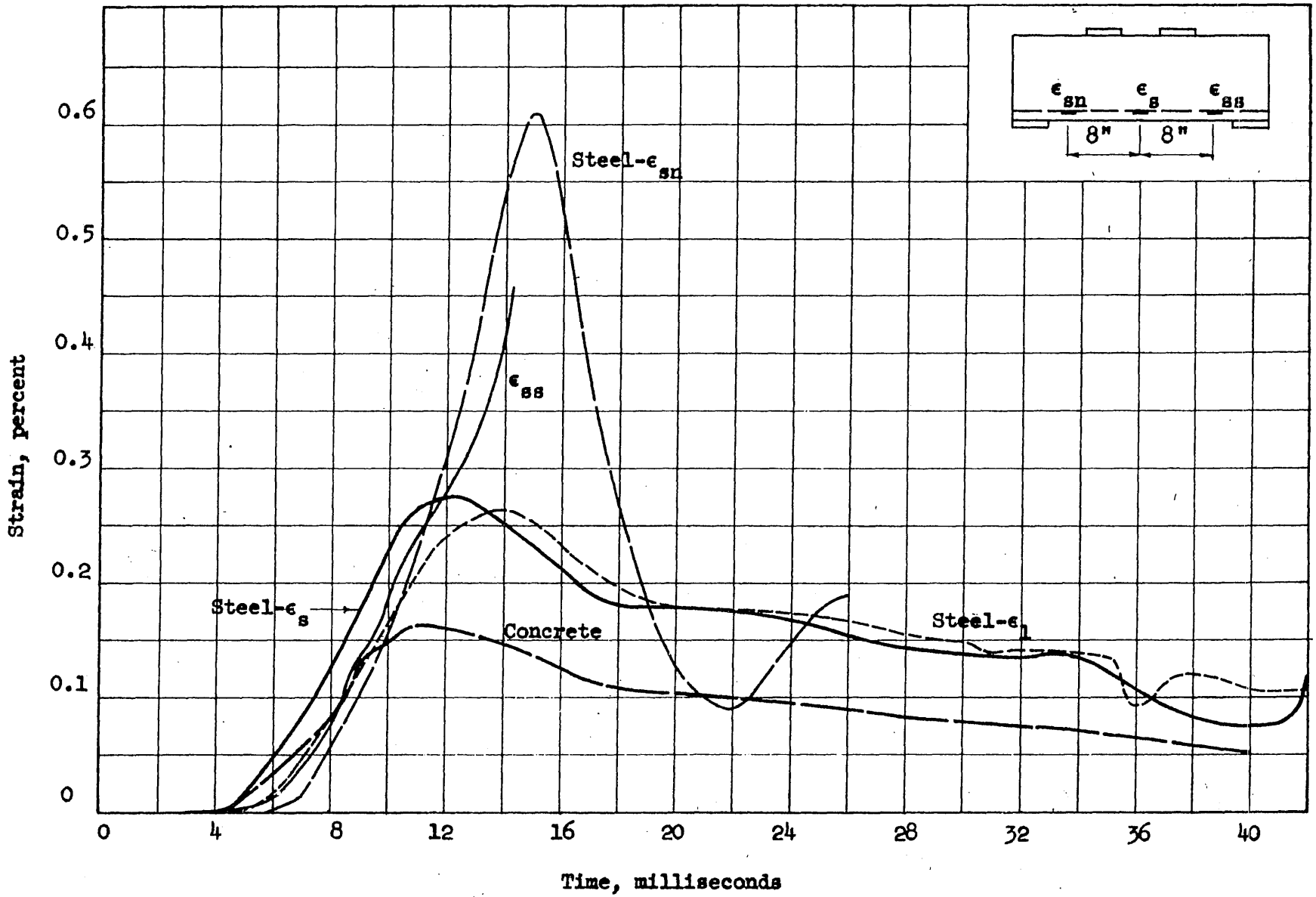

FIG. B.53 STEEL AND CONCRETE STRAINS VERSUS TIME FOR BEAM G33D-32

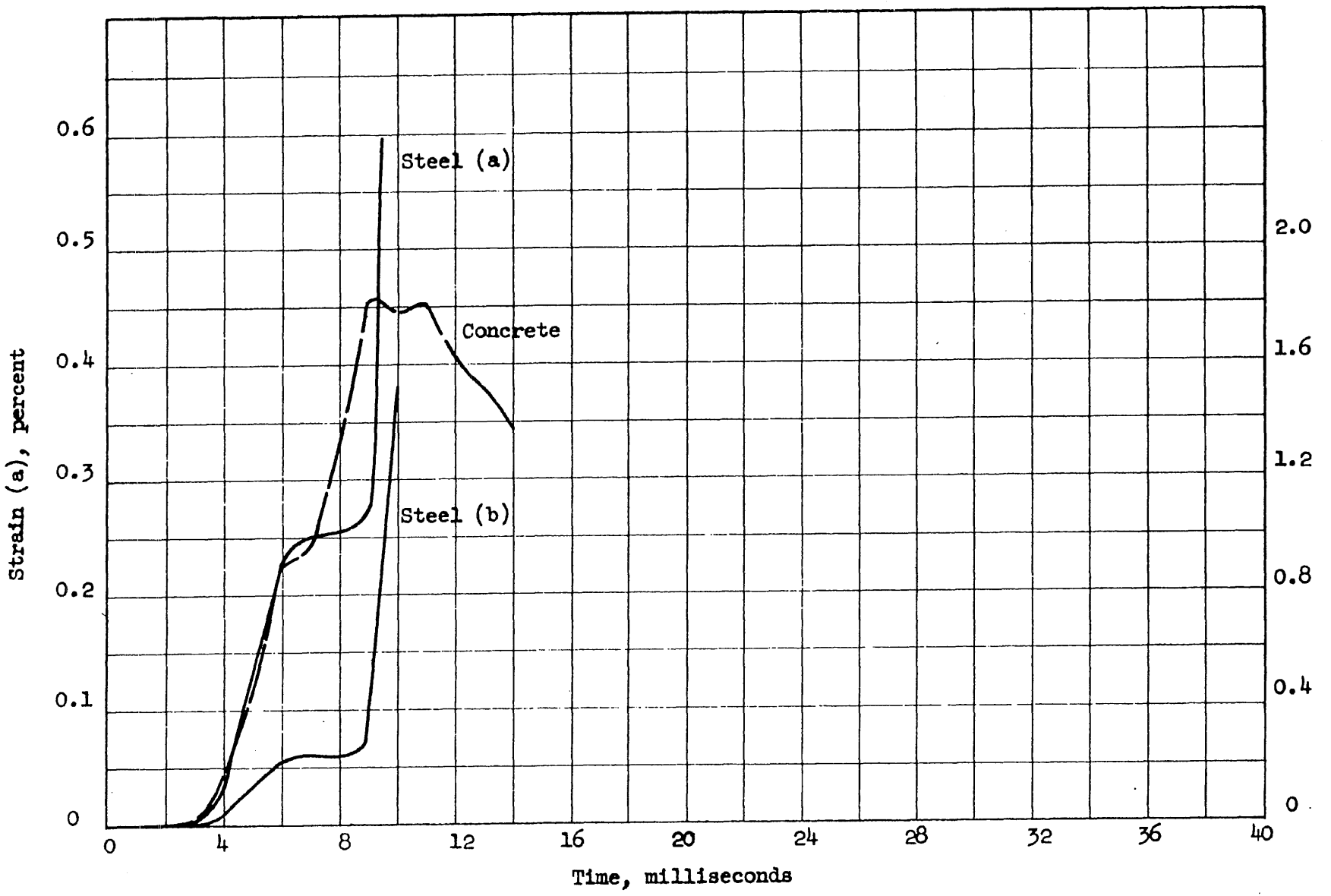

FIG. B.54 MIDSPAN STEEL AND CONCRETE STRAINS VERSUS TIME FOR BEAM G34D-11

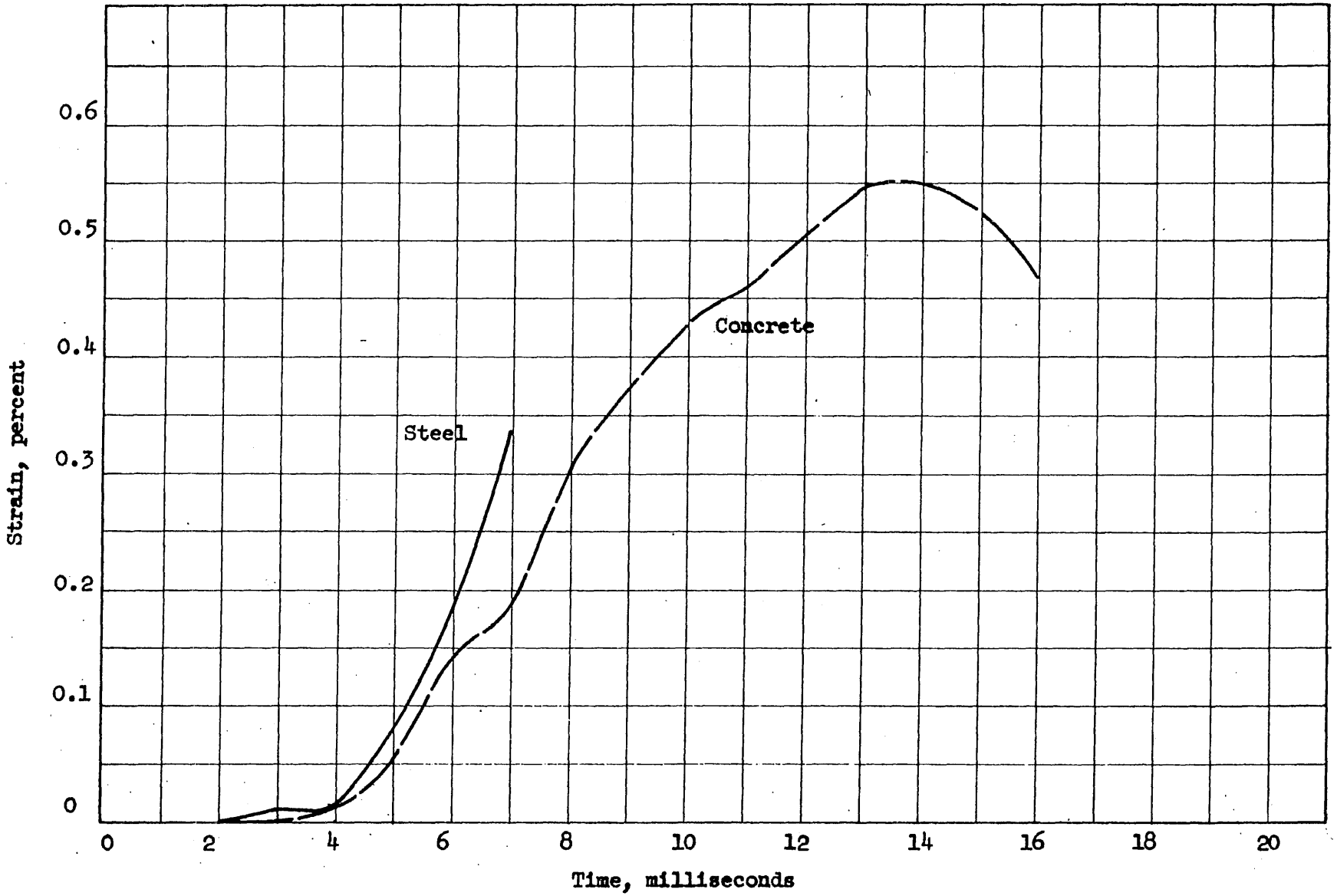

FIG. B.55 MIDSPAN STEEL AND CONCRETE STRAINS VERSUS TIME FOR BEAM G34D-12

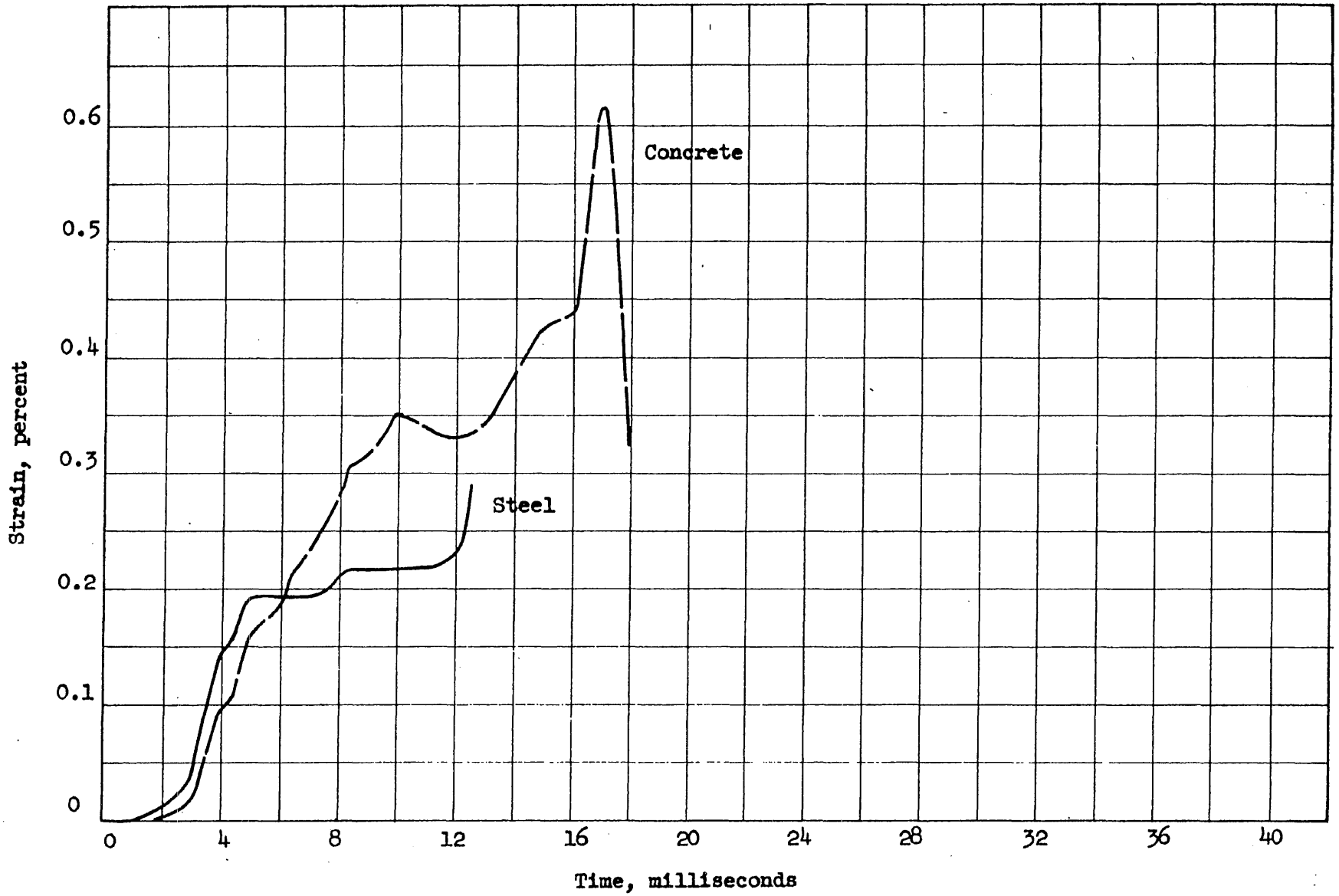

FIG. B.56 MIDSPAN STEEL AND CONCRETE STRAINS VERSUS TIME FOR BEAM G34D-21

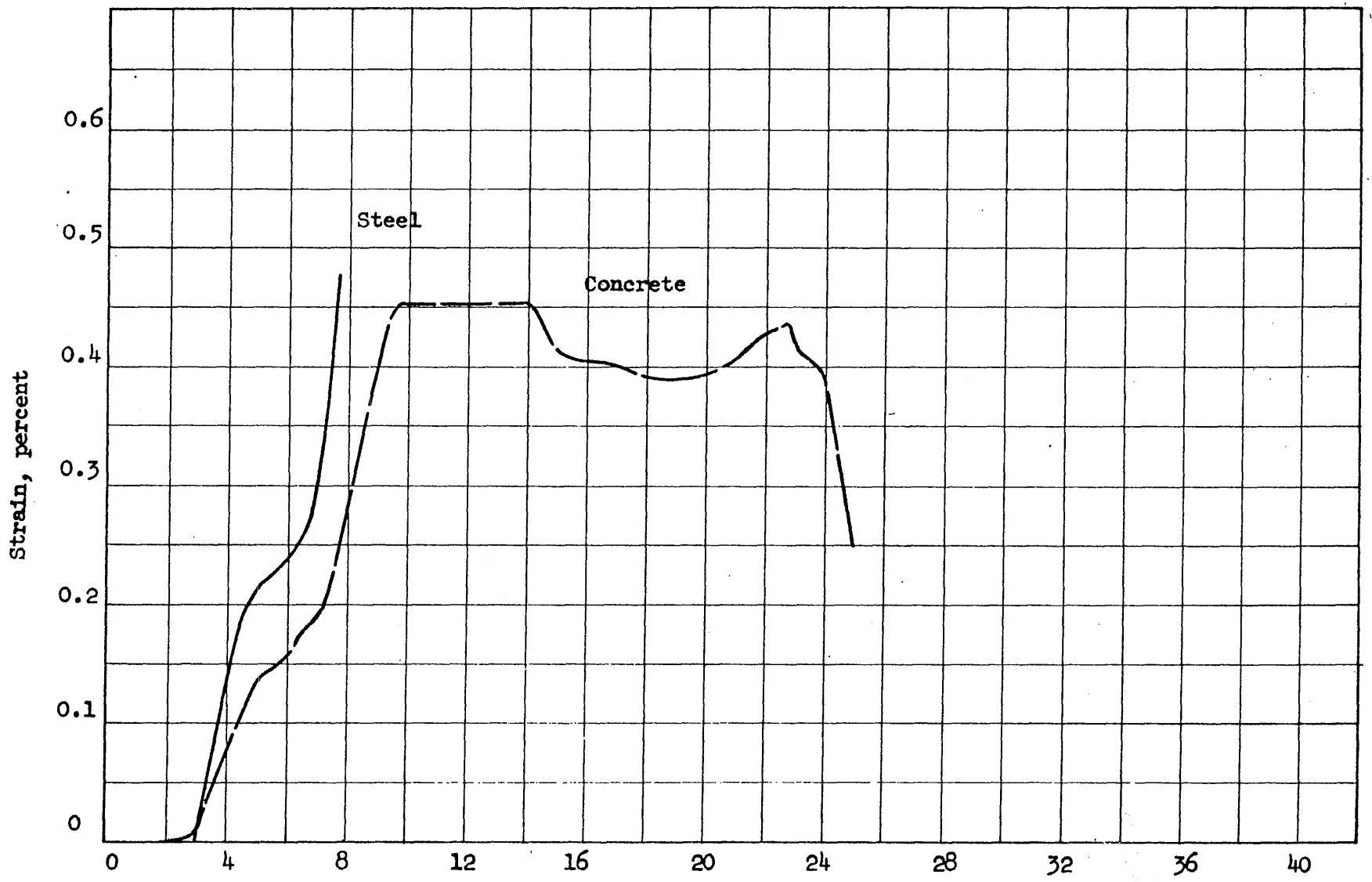

FIG. B.57 MIDSPAN STEEL AND CONCRETE STRAINS VERSUS TIME FOR BEAM G34D-22

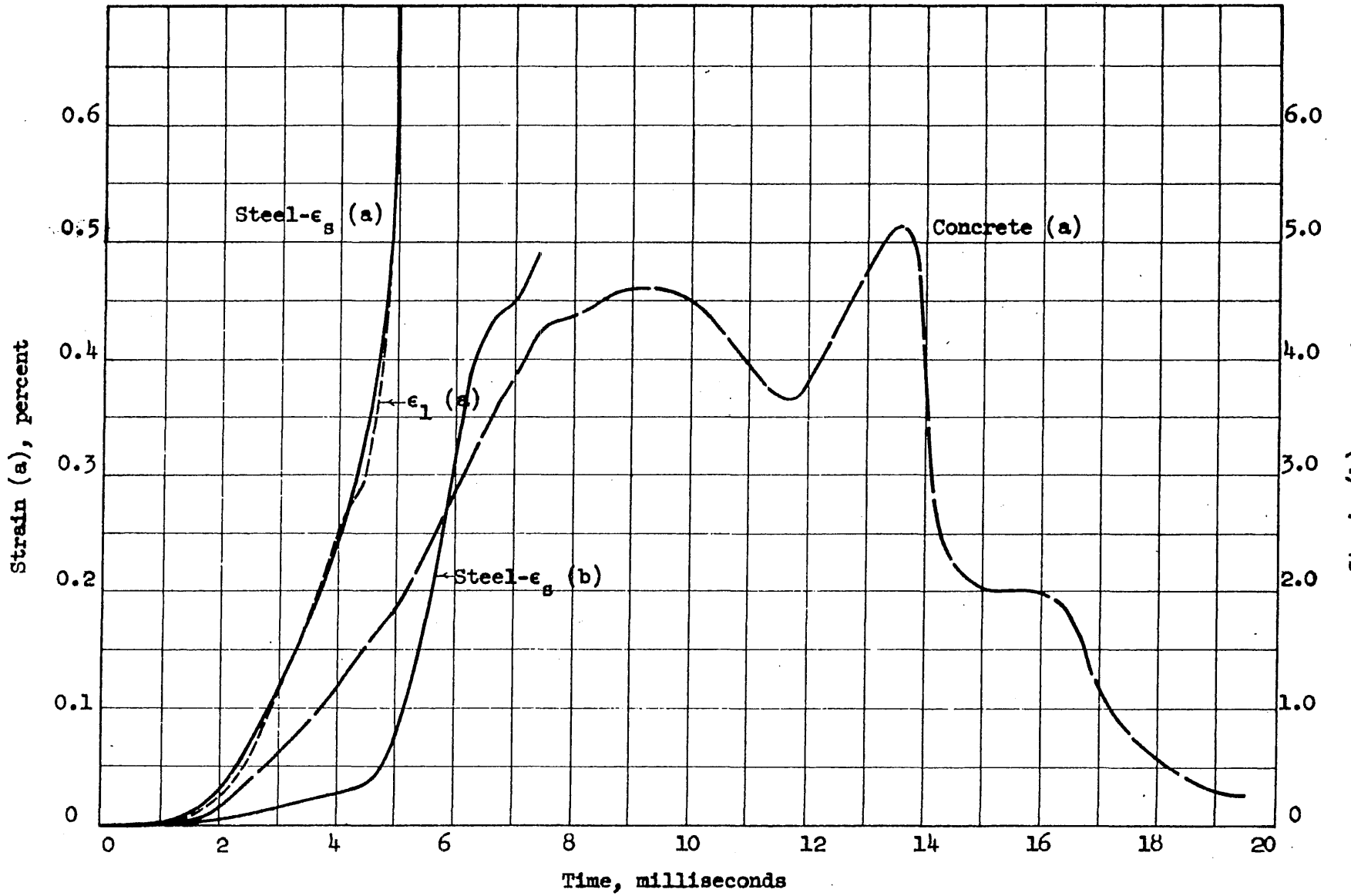

FIG. B.58 MIDSPAN STEEL AND CONCRETE STRAINS VERSUS TIME FOR BEAM G43D-11

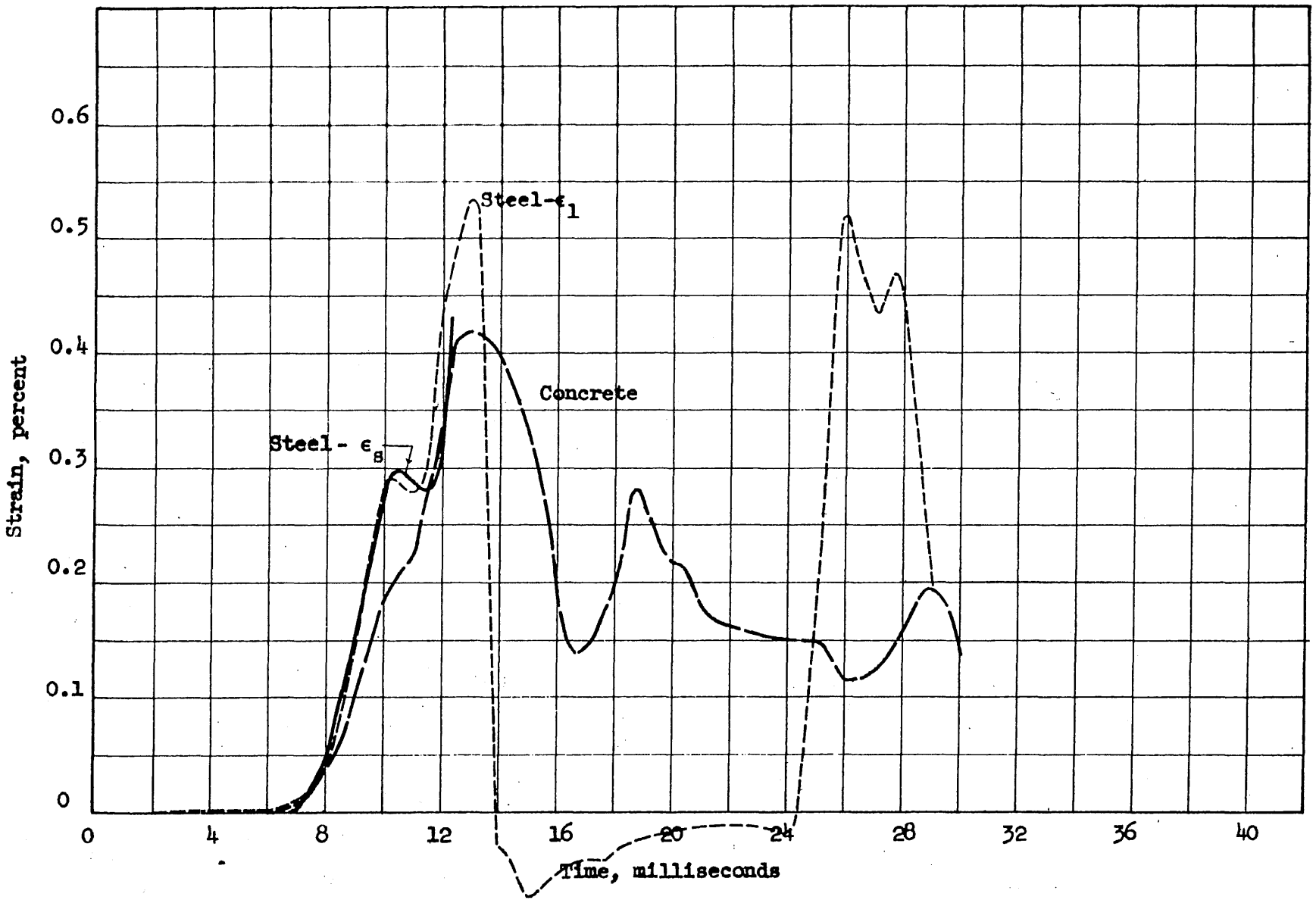

FIG. B.59 MIDSPAN STEEL AND CONCRETE STRAINS VERSUS TIME FOR BEAM G43D-12

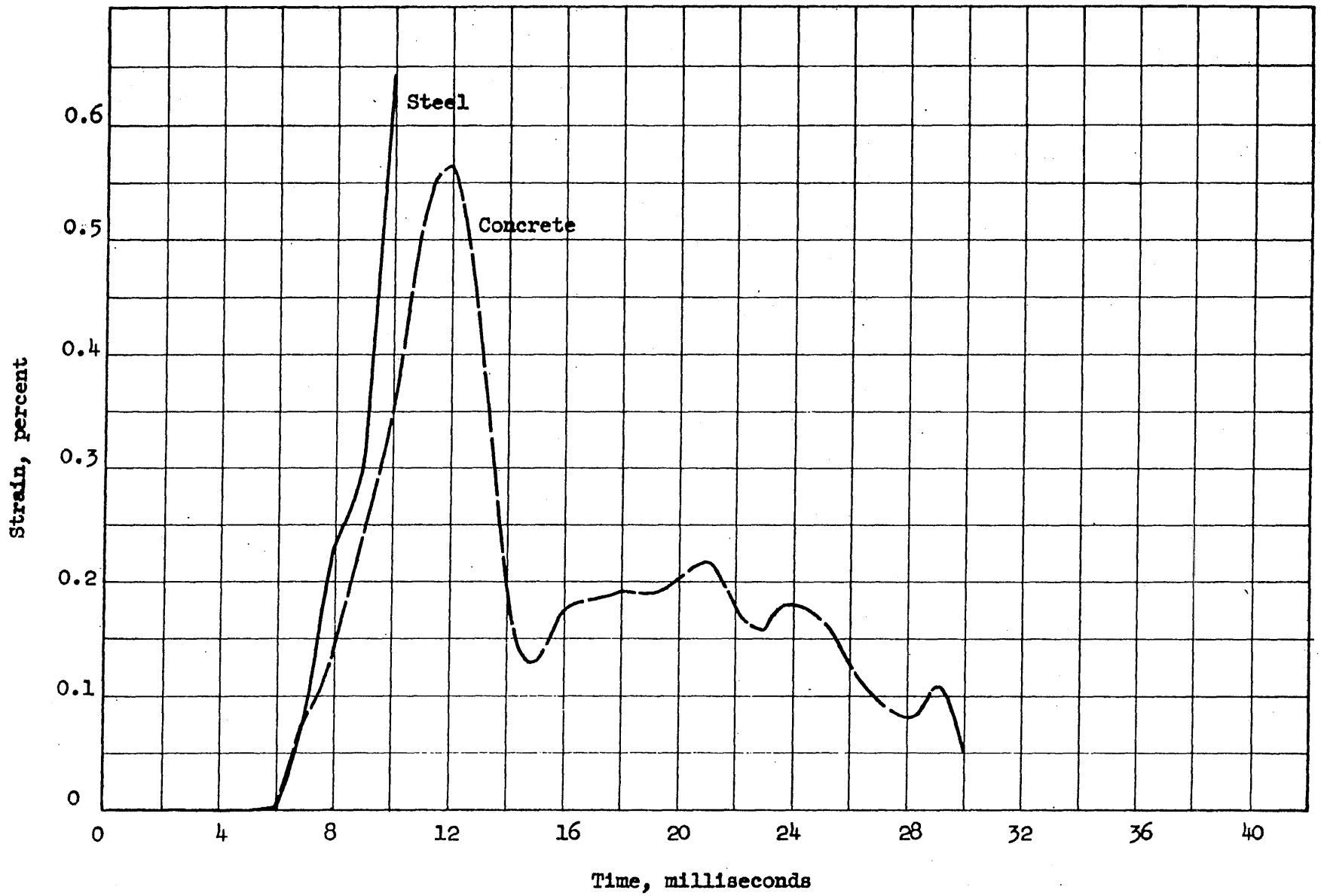

FIG. B.60 MIDSPAN STEEL AND CONCRETE STRAINS VERSUS TIME FOR BEAM G44D-11

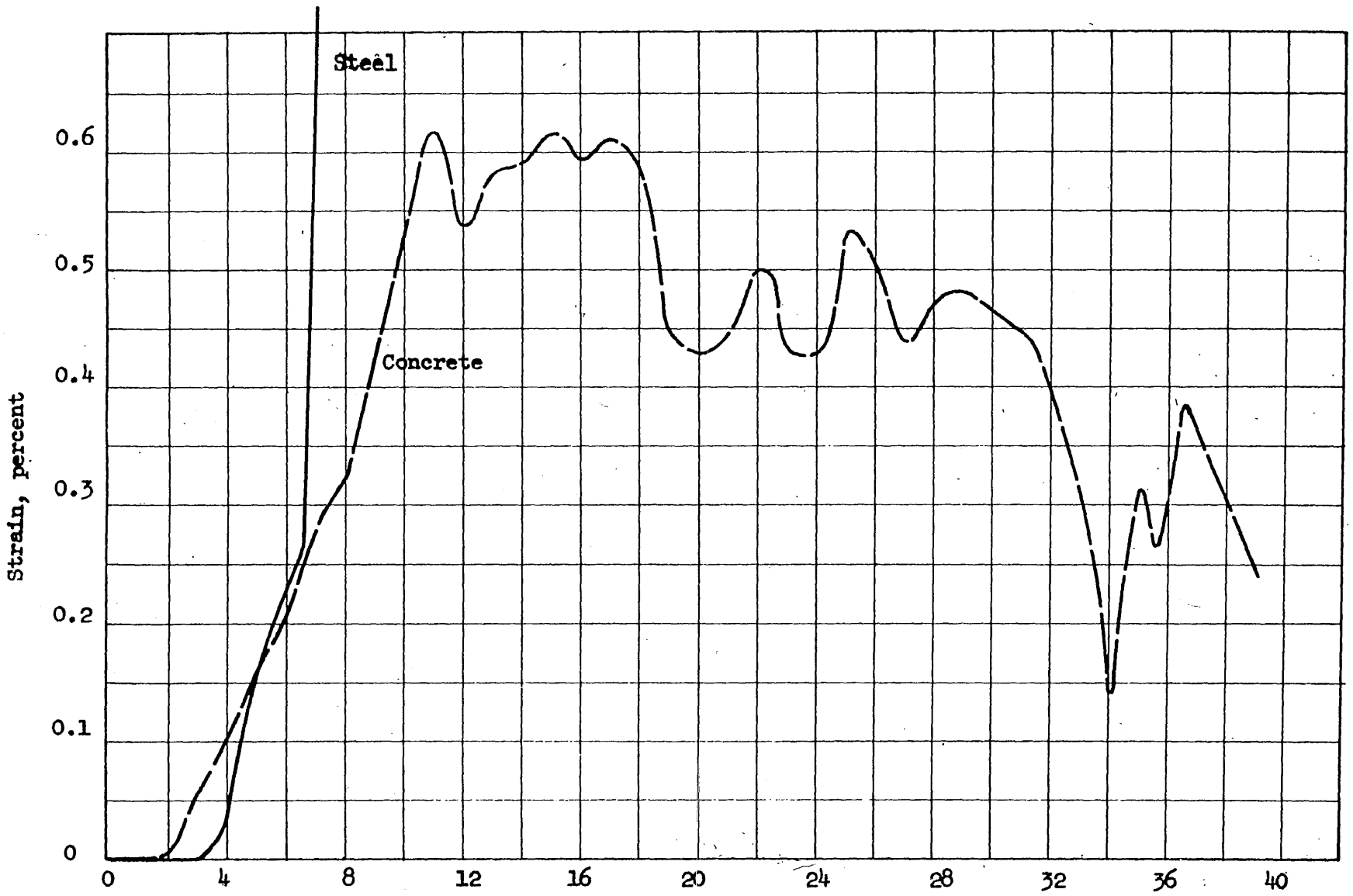

FIG. B.61 MIDSPAN STEEL AND CONCRETE STRAINS VERSUS TIME FOR BEAM G44D-12